

**Controls on rare earth element and neodymium
isotope distributions in the West Pacific:
local imprint vs. lateral transport**

Von der Fakultät V für Mathematik und Naturwissenschaften der
Carl von Ossietzky Universität Oldenburg zur
Erlangung des Grades und Titels einer
Doktorin der Naturwissenschaften

Dr. rer. nat.

angenommene Dissertation

von Frau Melanie Kirstin Behrens
geboren am 03.12.1985 in Lahr/Schwarzwald

Erstgutachterin: Dr. Katharina Pahnke

Zweitgutachter: Prof. Dr. Thorsten Dittmar

Tag der Disputation: 06.04.2017

Table of Contents

Table of Contents	I
Abstract	V
Kurzfassung	VII
1. Introduction	1
1.1. The importance of trace elements in the ocean	1
1.2. The distribution of trace elements in the ocean	2
1.3. Rare earth elements and Nd isotopes as tracers	4
1.3.1. Rare earth elements	4
1.3.2. Neodymium isotopes.....	5
1.4. Major advancements	8
1.5. Objectives and outline of this thesis	8
1.6. Author's contribution	12
2. Sources and processes affecting the distribution of dissolved Nd isotopes and concentrations in the West Pacific	14
Abstract	15
2.1. Introduction	16
2.2. Hydrography of the West Pacific	17
2.2.1. Surface waters	17
2.2.2. Subsurface waters.....	19
2.2.3. Intermediate waters	22
2.2.4. Deep waters	23
2.3. Materials and Methods	23
2.3.1. Samples and onboard procedures	23
2.3.2. Lab procedure.....	24
2.3.2.1. Neodymium isotopic composition	24
2.3.2.2. Neodymium concentrations	26
2.4. Results	28
2.4.1. Dissolved ϵ_{Nd} and [Nd] in the context of the hydrographic setting	31
2.4.1.1. Surface waters	31
2.4.1.2. Subsurface waters	31

2.4.1.3. Intermediate waters	32
2.4.1.4. Deep waters	32
2.5. Discussion	37
2.5.1. Continental input	37
2.5.2. Advection and modification of dissolved ϵ_{Nd} and [Nd]	37
2.5.2.1. Particle scavenging of dissolved Nd within the ECS	37
2.5.2.2. Tracing small-scale surface and subsurface circulation in the West Pacific with boundary exchange signatures from volcanic margins	39
2.5.2.3. Advection of dissolved Nd within subsurface water masses	41
2.5.2.4. Lateral transport vs. vertical cycling and modification of dissolved ϵ_{Nd} and Nd at intermediate to bottom water depth	42
2.6. Conclusions	44
2.7. Acknowledgments	45
3. Rare earth element distributions in the West Pacific: trace element sources and conservative vs. non-conservative behavior	46
Abstract	47
3.1. Introduction	48
3.2. Study area and circulation	49
3.3. Materials and Methods	52
3.3.1. Onboard procedures	52
3.3.2. Nutrient and REE analysis	52
3.3.4. Optimum Multiparameter Analysis (OMPA)	54
3.4. Results	55
3.4.1. Dissolved REE concentrations	55
3.4.2. Optimum Multiparameter Analysis: water mass mixing fractions	60
3.5. Discussion	61
3.5.1. Conservative vs. non-conservative processes and behavior	61
3.5.1.1. Trace element input to the West Pacific	61
3.5.1.2. Equatorial zonal trace element transport	63
3.5.1.3. REE transport within South and North Pacific Tropical Water	64
3.5.1.4. Antarctic Intermediate Water and North Pacific Intermediate Water	65
3.5.1.5. Deep to bottom waters	65
3.6. Conclusions	68
3.7. Acknowledgements	69
3.8. Supplementary Tables	70

4. Rapid and precise analysis of rare earth elements in small volumes of seawater - Method and intercomparison	77
Highlights	78
Abstract	78
4.1. Introduction	79
4.2. Materials and procedures	81
4.2.1. Sample locations and onboard procedure	81
4.2.2. Lab 1: Offline seaFAST pre-concentration of REEs and multi-element ID ICP-MS	81
4.2.2.1. Pre-concentration of REEs from seawater	81
4.2.2.2. REE determination by ID ICP-MS	84
4.2.3. Pre-concentration methods and mass spectrometry of labs participating in the intercomparison	88
4.3. Results and discussion	88
4.3.1. Lab 1: Offline seaFAST pre-concentration of REEs and multi-element ID ICP-MS	88
4.3.1.1. Blanks and detection limit	88
4.3.1.2. Accuracy and precision	89
4.3.2. Blanks and precision of participating labs	92
4.3.3. Dissolved REE concentrations at SAFe 3000 m (North Pacific): intercomparison	93
4.4. Conclusions	97
4.5. Acknowledgements	98
4.6. Supplementary material	99
4.6.1. Pre-concentration methods and mass spectrometry of participating labs	99
4.6.1.1. Lab 2, LDEO, Columbia University: Offline seaFAST pre-concentration and multi-element isotope dilution ICP-MS	99
4.6.1.2. Lab 3, CEOAS, Oregon State University: Offline seaFAST pre-concentration and external standards for REE quantification	101
4.6.1.3. Lab 4, LEGOS, University of Toulouse: Iron hydroxide co-precipitation and two-element isotope spike coupled with internal and external standards ..	102
4.6.2. Supplementary Tables	103
5. Conclusions and perspectives	106
5.1. Major Conclusions	106
5.2. Perspectives	108

6. References.....	111
7. Data handling.....	128
Acknowledgements	129
Curriculum vitae.....	130
Erklärung	132

Abstract

The ocean plays a crucial role in the Earth's climate system. Yet, the geochemical and physical processes in the ocean, their link and response to climate change are still not understood in detail. Dissolved oceanic trace elements (TEs) act as essential micronutrients and hence regulate marine ecosystems and carbon cycling, and as tracers and proxies of geochemical and physical processes in the present and past ocean. A comprehensive understanding of the ocean's role in climate change therefore requires a more precise knowledge of the distribution of TEs in the marine system.

The West Pacific is of particular interest with respect to the factors that control the distribution of TEs in the ocean, especially concerning the sources and processes that add and/or remove TEs to and/or from the ocean. This large oceanic region in the Pacific is a key study area to decipher locally and regionally important TE supply and small-scale and lateral transport. This is due to the fact that the West Pacific 1) lies in the influence of Asian rivers, 2) is surrounded by volcanic island margins that are thought to be a major source of TEs to the ocean, and 3) is connected to the important iron-limited high-nutrient, low-chlorophyll (HNLC) area in the East Pacific through a complex eastward flowing equatorial zonal current system that is thought to act as a conduit for key micronutrients to the east. Micronutrients limit primary productivity in HNLC areas and changes in their supply to these critical areas have a direct impact on phytoplankton growth and carbon fixation. Dissolved rare earth element concentrations ([REE]) and neodymium (Nd) isotopes (expressed as ϵ_{Nd}) in the ocean are not bioactive, and therefore trace the sources and processes that control REE (and other TE) distributions in the ocean. Yet, the dissolved [REE] and Nd isotope dataset in the West Pacific is still very rudimentary, and available stations sampled for at least three different water depths are sparse and scattered.

This thesis reports dissolved full water column [REE] and Nd isotope data from twelve stations along a NW-SE transect in the West Pacific at unprecedented vertical and lateral resolution for this area (chapters 2 and 3). Additionally, this thesis presents a new rapid and precise method for dissolved seawater [REE] analysis that was validated within an international intercomparison study (chapter 4). The major objectives of this thesis were 1) to investigate the sources and processes that control the distribution of dissolved [REE] and ϵ_{Nd} (and potentially other TEs) in the West Pacific, and 2) to provide a method that is easy to adopt by other laboratories and enables the extensive use of REEs in future marine studies. This approach opens the way to build a high-quality global ocean REE dataset, which will advance the understanding of REE distributions on a global scale.

The [REE] and ϵ_{Nd} results clearly indicate continental input to the surface in the East China Sea via South Korean and Chinese rivers. Elevated europium anomalies and radiogenic ϵ_{Nd} , characteristic for basaltic sources, further document imprints on surface and subsurface waters from volcanic island margins (the Philippine and Solomon Islands, Papua New Guinea, Fiji, and Samoa) and REE input into the tropical West Pacific from Papua New Guinea, and to a lesser extent from other volcanic islands. The REE and ϵ_{Nd} signals allow detailed tracing of zonal eastward transport of TEs within small-scale surface and subsurface currents to the HNLC area in the East Pacific. The data therefore highlight the importance of the tropical West Pacific as source region of micronutrients and other TEs to the iron-limited East Pacific. The [REE] data further indicate the dominant lateral control on REE distributions in North and South Pacific Tropical Water, Antarctic Intermediate Water, and Lower Circumpolar Deep Water, reflecting lateral transport of a preformed REE signal within these water masses in the Pacific, even at subsurface depth. The strong correlation of high-salinity with low-[REE] of South Pacific Tropical Water indicates advection of preformed low [REE] from its formation region in the oligotrophic South Pacific Subtropical Gyre to the tropical West Pacific, and hence explains the low subsurface [REE] previously found in this area. In contrast to the conservative behavior of REEs, Nd isotopes clearly demonstrate a non-conservative behavior, even in the deep ocean, indicating local radiogenic imprints through boundary exchange at volcanic island margins in the tropical West Pacific. With further distance to these radiogenic sources, mid-depth and deep water ϵ_{Nd} behave quasi-conservatively and trace water mass transport and mixing in the Northwest Pacific. In summary, preformed REE signals are transported laterally over substantial distances in the Pacific, while ϵ_{Nd} signatures are more quickly modified at volcanic island margins in the tropical West Pacific.

The new analytical method presents the first application of the automated seaFAST-pico system (Elemental Scientific Inc.) in offline mode for a robust and rapid pre-concentration and purification of dissolved REEs from small volumes of seawater (11-12 mL). It is combined with multi-element isotope dilution inductively coupled plasma mass spectrometry for routine analysis of low [REE] (picomolar level). To ensure high-quality data and to provide the first reference seawater REE standard in the Pacific for quality control of future REE studies, the method was verified in an international intercomparison with three other laboratories using seawater aliquots from the GEOTRACES intercalibration station SAFe (Sampling and Analysis of Iron) at 3000 m water depth in the North Pacific. The results obtained by the four laboratories show an excellent agreement of [REE] within 7% (2σ RSD).

Kurzfassung

Obwohl der Ozean eine entscheidende Rolle im Klimasystem der Erde spielt, sind seine geochemischen und physikalischen Prozesse sowie deren Einbindung in und ihre Auswirkung auf das Klimageschehen nicht im Detail bekannt. Im Meerwasser gelöste Spurenelemente dienen als essentielle Mikronährstoffe, die marine Ökosysteme sowie den Kohlenstoffkreislauf regulieren, und als Anzeiger und Stellvertreter für geochemische und physikalische Prozesse im heutigen und früheren Ozean. Ein detaillierterer Einblick in die Rolle des globalen Ozeans im Klimageschehen verlangt daher ein verbessertes Verständnis der Verteilung von Spurenelementen im marinen System.

Der Westpazifik ist von besonderem Interesse für die Faktoren, welche die Verteilung von Spurenelementen im Meer kontrollieren, insbesondere in Bezug auf die Quellen und Prozesse, die Spurenelemente in den Ozean eintragen und/oder aus ihm entfernen. Mehrere Faktoren machen den Westpazifik zu einem idealen Arbeitsgebiet für die Untersuchung lokaler und regionaler Spurenelementquellen sowie kleinskaliger lateraler Wassermassentransporte: Der Westpazifik liegt 1) im Einflussbereich von asiatischen Flüssen, ist 2) von vulkanischen Inselrändern umgeben, welche als eine Hauptquelle für Spurenelementeintrag in den Ozean angesehen werden, und ist 3) mit dem eisenlimitierten, nährstoffreichen und chlorophyllarmen Gebiet im Ostpazifik über ein komplexes ostwärts fließendes äquatoriales zonales Strömungssystem verbunden, das ein Transportmittel für entscheidende Mikronährstoffe in den Osten darstellt. Mikronährstoffe limitieren die Primärproduktivität in nährstoffreichen, chlorophyllarmen Gebieten. Änderungen in deren Eintrag in diese kritischen Gebiete haben direkte Auswirkungen auf das Phytoplankton-wachstum und somit auf die Bindung von Kohlenstoff (CO_2). Im Meerwasser gelöste Seltene Erdelementkonzentrationen ([SEE]) und Neodym (Nd) Isotope (ausgedrückt in ϵ_{Nd}) werden nicht biologisch umgesetzt und dienen daher als Anzeiger für Quellen und Prozesse, welche die Verteilung von SEE (und die anderer Spurenelemente) im Ozean kontrollieren. Dennoch ist der Datensatz an gelösten [SEE] und Nd Isotopen im Westpazifik immer noch sehr rudimentär und die verfügbaren Stationen, an denen mindestens drei verschiedene Wasser-tiefen beprobt wurden, sind spärlich und nicht zusammenhängend.

Diese Doktorarbeit befasst sich mit im Meerwasser gelösten [SEE] und Nd Isotopendaten an zwölf Stationen entlang eines NW-SO Transektes im Westpazifik in einer für diese Region noch nicht vorhandenen vertikalen und lateralen Auflösung der gesamten Wassersäule (Kapitel 2 und 3). Zusätzlich stellt diese Doktorarbeit eine neue, schnelle und präzise Methode für die Analyse von im Meerwasser gelösten [SEE] dar, welche in einer

internationalen Vergleichsstudie validiert wurde (Kapitel 4). Die Hauptziele dieser Doktorarbeit waren 1) die Untersuchung der Quellen und Prozesse, welche die Verteilung von gelösten [SEE] und ϵ_{Nd} (und die potentieller anderer Spurenelemente) im Westpazifik kontrollieren, und 2) eine Methode, die in anderen Laboren einfach nachzuvollziehen und umzusetzen ist, und die eine beträchtliche Anzahl an SEE Messungen in zukünftigen marinen Studien ermöglicht, zu entwickeln. Diese Herangehensweise ermöglicht den Aufbau eines präzisen SEE Datensatzes im globalen Ozean, welcher zu einem besseren Verständnis der globalen Verteilung von SEE beitragen wird.

Die [SEE] und ϵ_{Nd} Ergebnisse zeigen eindeutig einen kontinentalen Eintrag an der Oberfläche im Ostchinesischen Meer durch südkoreanische und chinesische Flüsse. Erhöhte Europium-Anomalien und radiogene ϵ_{Nd} Werte, welche charakteristisch für basaltische Quellen sind, zeigen weiterhin Überprägungen von vulkanischen Inselrändern (den Philippinen und Salomonen Inseln, Papua-Neuguinea, Fidschi und Samoa) im Oberflächenwasser und in der darunterliegenden Wassersäule an und weisen auf einen deutlichen Eintrag an SEE von Papua-Neuguinea und auf einen weniger deutlichen Eintrag von den anderen vulkanischen Inselrändern in den tropischen Westpazifik hin. Die SEE und ϵ_{Nd} Signale ermöglichen eine detaillierte Verfolgung von Spurenelementen, welche in zonalen, ostwärts fließenden, kleinskaligen Oberflächenströmungen und oberflächennahen Strömungen aus dem Westpazifik in den nährstoff- und chlorophyllarmen Ostpazifik transportiert werden. Die Daten heben daher die Wichtigkeit des tropischen Westpazifiks als Quellregion für Mikronährstoffe und andere Spurenelemente für den eisenlimitierten Ostpazifik hervor. Die [SEE] Daten zeigen ferner eine dominante laterale Kontrolle der SEE Verteilungen im Nord- und Südpazifischen Tropischen Wasser, im Antarktischen Zwischenwasser, und im unteren Zirkumpolarwasser auf, und verdeutlichen, sogar in oberflächennahen Wassermassen, den lateralen Transport eines bereits gebildeten SEE Signals entlang der Fließrichtungen dieser Wassermassen im Pazifik. Die gute Korrelation zwischen hoher Salinität und niedrigen [SEE] im Südpazifischen Tropischen Wasser weist auf den Transport von bereits gebildeten niedrig-[SEE] aus dem Herkunftsgebiet, dem oligotrophen südpazifischen subtropischen Wirbel, in den tropischen Westpazifik hin und erklärt somit die niedrigen oberflächennahen [SEE], welche bereits zuvor in anderen Studien in diesem Gebiet entdeckt wurden. Im Gegensatz zu dem konservativen Verhalten der SEE zeigen die Nd Isotopien eindeutig ein nicht-konservatives Verhalten auf, welches sogar im Tiefenwasser zu sehen ist und auf lokale radiogene Überprägungen durch 'boundary exchange' an vulkanischen Inselrändern im tropischen Westpazifik hindeutet. In größerer

Entfernung zu diesen radiogenen Quellen zeigen die ϵ_{Nd} Werte im Zwischen- und Tiefenwasser ein quasi-konservatives Verhalten auf und weisen auf Wassermassentransport und -mischung im Nordwestpazifik hin. Zusammenfassend zeigen die Ergebnisse, dass bereits gebildete SEE Signale lateral über eine sehr große Distanz im Pazifik transportiert werden, während ϵ_{Nd} Werte sehr viel schneller an vulkanischen Inselrändern im tropischen Westpazifik überprägt werden.

Die neue analytische Methode präsentiert die erste Anwendung des automatisierten seaFAST-pico Systems (Elemental Scientific Inc.) im offline Betrieb für eine robuste und schnelle Aufkonzentrierung und Abtrennung von gelösten SEE aus geringen Meerwasservolumina (11-12 mL). Die Methode beruht auf einer Isotopenverdünnungsmethode und einem Massenspektrometer mit induktiv gekoppeltem Plasma mit dem routinemäßige Analysen von gering konzentrierten SEE Proben (im pikomolaren Bereich) durchgeführt werden. Um sicherzustellen, dass mit dieser Methode präzise Daten produziert werden, und um den ersten SEE Meerwasserstandard im Pazifik zu liefern, welcher in zukünftigen SEE Studien als Vergleichsprobe dient, wurde die Methode in einer internationalen Vergleichsstudie mit drei weiteren Laboren überprüft. Dafür wurde Meerwasser von der GEOTRACES Interkalibrationsstation SAFe ('Sampling and Analysis of Iron') im Nordpazifik in 3000 m Wassertiefe als Vergleichsprobe ausgewählt und genutzt. Die Ergebnisse, welche von den vier Laboren erzielt wurden, zeigen eine exzellente Übereinstimmung der [SEE] innerhalb von 7% (2σ RSD).

1. Introduction

Chapter 1 describes the motivation for this thesis that focuses on identifying and characterizing trace element (TE) input and cycling using rare earth element (REE) and neodymium (Nd) isotope distributions in the West Pacific. The first section of this chapter provides an overview of the important roles of TEs in the ocean. The second section summarizes factors that may affect the distribution of TEs in the ocean, including major sources and processes that add and/or remove TEs to and/or from the ocean, and their internal cycling within the ocean. The following section introduces REEs and Nd isotopes as tracers. The last section of this chapter briefly introduces the major advancements in TE research.

1.1. The importance of trace elements in the ocean

Despite of the extremely low concentration of dissolved TEs in the ocean ($\mu\text{mol/kg}$ to fmol/kg , with most in the pmol/kg -range, e.g., Chester and Jickells, 2012), they play important roles as essential micronutrients and hence can regulate marine ecosystems and carbon cycling, and as tracers and proxies of geochemical and physical processes in the present and past ocean (e.g., SCOR Working Group, 2007). The ocean is an integral part of the Earth's climate system, yet, its geochemical and physical processes, their link and response to climate change are still not completely understood. A comprehensive understanding of the ocean's role in climate change therefore requires a more precise knowledge of the distribution of TEs in the global ocean. Certain TEs and their isotopes in seawater are tracers of processes that influence the distribution of TEs in the ocean, and thus can substantially advance the still incomplete knowledge about marine TE distributions on a regional and global scale (e.g., SCOR Working Group, 2007). In particular, dissolved seawater REE concentrations and Nd isotopes (with Nd belonging to the REEs) are not bioactive, and are therefore ideal to trace the sources and processes that add and/or remove REEs and potentially other TEs to and/or from the ocean, and that control their cycling within the ocean (e.g., Elderfield, 1988; Goldstein and Hemming, 2003) (chapters 2 and 3). In addition, Nd isotopes incorporated into authigenic minerals and fish teeth in marine sediments are used as proxy for the reconstruction of past ocean circulation (e.g., Frank, 2002; Pahnke et al., 2008). However, the utility of Nd isotopes as a water mass proxy depends on the knowledge of regional or local biogeochemical processes potentially overprinting the original water mass Nd isotope signature. The understanding of the distribution of Nd isotopes and the extent of regional and local biogeochemical overprints in the global ocean, and in particular in the Pacific Ocean, is so far largely incomplete.

Other TEs such as iron and zinc are critical for marine ecosystems and biological processes due to their function as essential micronutrients for phytoplankton (e.g., Morel et al., 2003). Thus, TEs serve and sustain the marine food web, and ultimately the nourishment of human populations depending on marine proteins (Séférian et al., 2014). In addition to the importance for the marine food web, iron plays a critical role in the ocean-atmosphere exchange of carbon dioxide (e.g., Coale et al., 1996), and hence in climate change. For example, iron, an essential micronutrient for phytoplankton growth, limits primary productivity in high-nutrient, low-chlorophyll (HNLC) areas such as the equatorial East Pacific (e.g., Ryan et al., 2006). Changes in iron supply to this critical area directly impact phytoplankton growth, and thus atmospheric carbon dioxide fixation (e.g., Ryan et al., 2006). The supply of micronutrients like iron from the equatorial West Pacific is thought to be a primary factor that controls phytoplankton growth in the equatorial East Pacific (e.g., Barber et al., 1996; Lacan and Jeandel, 2001; Slemons et al., 2010; Grenier et al., 2013). This potentially crucial role of the equatorial West Pacific in supplying the East Pacific with micronutrients highlights the importance for a detailed study on the sources and processes that may add TEs to the equatorial West Pacific and on their potential eastward transport within zonal currents (chapters 2 and 3).

1.2. The distribution of trace elements in the ocean

The distribution of TEs in the ocean is influenced by sources and processes that add and/or remove TEs to and/or from the ocean, and by their internal cycling within the ocean (e.g., Bruland and Lohan, 2003). Trace elements are added to the ocean via rivers, submarine groundwater discharge (SGD), or atmospheric dust deposition and dissolution (e.g., Frank, 2011) (Fig. 1.1). Sediment-seawater interactions at ocean margins and the seafloor (e.g., Lacan and Jeandel, 2001, 2005; Grenier et al., 2013) or hydrothermal systems at mid-ocean ridges can act as sources or sinks of TEs (e.g., German et al., 1990; Stichel et al., 2012a; Fitzsimmons et al., 2014; Measures et al., 2015; Resing et al., 2015) (Fig. 1.1). In the ocean, the distribution of TEs is subject to internal cycling through biological uptake (e.g., Hawco et al., 2016; Semeniuk et al., 2016) and/or geochemical and physical processes (e.g., Stichel et al., 2015; Osborne et al., 2015). Vertical geochemical processes in the water column include dissolved-particulate interactions such as adsorption and removal of TEs onto sinking particles (scavenging) and subsequent release from particles through desorption (e.g., Sholkovitz et al., 1994) (Fig. 1.1). Lateral physical water mass transport and mixing, governed by ocean circulation, lead to the redistribution of TEs within the ocean and separates them from their initial source regions (e.g., Zheng et al., 2016) (Fig. 1.1).

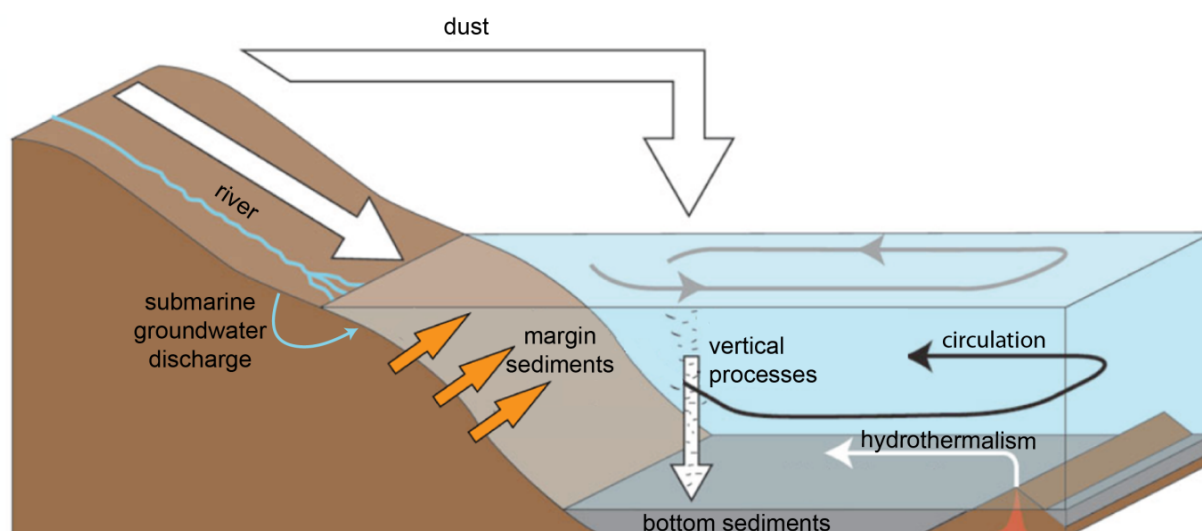


Fig. 1.1. Schematic illustration showing major sources and internal cycling of TEs in the ocean (modified after Frank, 2011).

The distribution of TEs in the ocean is grouped into three main categories showing either ‘conservative’-, ‘nutrient’-, or ‘scavenging’-type behavior based on their vertical profiles that are due to their oceanic residence times and the dominant vertical process affecting the respective TE (e.g., Bruland and Lohan, 2003; Chester and Jickells, 2012). ‘Conservative-type’ TEs such as molybdenum are characterized by weak dissolved-particulate interactions and have long oceanic residence times ($>10^5$ years), resulting in nearly constant concentrations with depth and geographical region (e.g., Bruland and Lohan, 2003). In contrast, ‘nutrient-type’ TEs (e.g., cadmium, zinc) have shorter oceanic residence times (tens of thousands of years) and are marked by low surface water and high deep water concentrations due to biological uptake at the surface and subsequent decomposition (remineralization) at depth (e.g., Chester and Jickells, 2012). ‘Scavenged-type’ TEs (e.g., manganese, aluminum, mercury) have shorter oceanic residence times (100-1000 years) than the global ocean mixing time (~ 1500 years, Broecker and Peng, 1982) and are characterized by strong dissolved-particulate interactions with enrichment at the surface from local inputs (e.g., dust, rivers, sediments) and decreasing concentrations with water depth indicating particle scavenging (e.g., Bruland and Lohan, 2003; Chester and Jickells, 2012).

Yet, the global distribution of TEs in the ocean is still not understood in detail. Thus, detailed studies on the sources as well as on the vertical and lateral processes that affect TE distributions in the ocean by using high-resolution vertical and spatial full water column profiles along transects is of crucial importance for TE research (chapters 2 and 3).

1.3. Rare earth elements and Nd isotopes as tracers

1.3.1. Rare earth elements

Rare earth elements are a coherent group of elements that form the series from lanthanum (La) to lutetium (Lu) and exist dominantly in the trivalent oxidation state (Elderfield and Greaves, 1982). Only cerium (Ce) and europium (Eu) can be oxidized to Ce(IV) or reduced to Eu(II) depending on the redox conditions (e.g., Elderfield, 1988). A chemical property of REEs is the decrease in ionic radii with increasing atomic number, which leads to an increase in the strength of complexation by carbonate ions from light REEs (LREE) to heavy REEs (HREE) in seawater (e.g., Byrne and Kim, 1990). Light REEs therefore have a higher particle affinity relative to HREEs and are therefore preferentially adsorbed onto particles, while HREEs remain longer in solution (e.g., Cantrell and Byrne, 1987; Byrne and Kim, 1990; Sholkovitz et al., 1994). As a result, dissolved seawater REE patterns show a typical HREE over LREE enrichment that represents their increasing oceanic residence times (LREE to HREE: 240 years to 2890 years, Nozaki, 2001) (e.g., Elderfield and Greaves, 1982). Dissolved seawater REE patterns are further characterized by a Ce-depletion, which reflects the short oceanic residence time of Ce (50 years, Nozaki, 2001) due to microbial controlled oxidation to insoluble Ce(IV) (e.g., Alibo and Nozaki, 1999; Moffett, 1990). In order to visualize relative changes in REE concentrations ([REE]), dissolved seawater [REE] are generally normalized to those of a reference material such as the Post Archean Australian Shale (PAAS) (Taylor and McLennan, 1985) or a reference water mass. Exploiting the systematic changes in the behavior of REEs, dissolved [REE] can be diagnostic of TE input into the ocean. For example, elevated [REE] in surface waters and a ‘flat’ REE pattern indicate local continental input to the ocean via rivers, SGD, margin sediments, or dust, while a strong HREE over LREE enrichment and hence ‘steep’ REE pattern may indicate enhanced scavenging by organic or inorganic particles (e.g., Greaves et al., 1999; Sholkovitz et al., 1999; Grenier et al., 2013; Hathorne et al., 2015; Osborne et al., 2015; Fröllje et al., 2016). PAAS-normalized positive Eu anomalies (i.e., an enrichment in Eu relative to its neighbors) are indicative of a volcanic source of the REEs added to the ocean (e.g., Grenier et al., 2013). In coastal surface waters near volcanic island margins in the southwestern equatorial Pacific, Grenier et al. (2013) used positive Eu anomalies to suggest TE input from Papua New Guinea and transport to the equatorial East Pacific.

In the past only spatially separated and few vertical REE profiles existed. Therefore, the vertical REE distributions in the water column with typically low surface water [REE] and increasing concentrations with depth were interpreted as indicating a dominance of vertical

processes (input, scavenging, release) (e.g., Elderfield and Greaves, 1982; Alibo and Nozaki, 1999). More recently however, observations from vertically and spatially high-resolution full water column profiles along transects with almost constant vertical Nd concentrations ([Nd]) in North Atlantic Deep Water (NADW) (Stichel et al., 2015; Lambelet et al., 2016) and high [Nd] shoaling upwards along the density surfaces in the southern South Pacific and Atlantic (Basak et al., 2015; Hathorne et al., 2015) indicated an additional lateral control on REE distributions. Further, using an optimum multiparameter analysis, Zheng et al. (2016) recently assessed quantitatively the conservative behavior of REEs in the South Atlantic, where dissolved deep water [REE] are dominantly controlled (>75%) by lateral water mass mixing. The high potential of REEs, in particular of HREEs, as water mass tracer becomes especially apparent when REE ratios are used. Zhang and Nozaki (1996) and Osborne et al. (2015) recognized the promising application of dysprosium (Dy), holmium (Ho), and erbium (Er) and their ratios as tracer of lateral water mass transport. Osborne et al. (2015) suggested that the distinctly low ratio of Dy over Er (Dy/Er) in Antarctic Intermediate Water (AAIW) in the tropical Atlantic may have been transported from its formation area in the Southern Ocean, and that Dy/Er may have the potential as a powerful tracer for AAIW, although the process that leads to the low Dy/Er signal was left unexplained. The depletion in the heaviest HREEs, expressed in the ratios of Er over ytterbium (Yb) and Er over Lu (Er/Yb and Er/Lu) in surface waters has previously been hypothesized to trace continental input (Hongo et al., 2006; Fröllje et al., 2016). In contrast, Takahashi et al. (2005, 2007) have shown that HREEs in seawater, especially thulium (Tm), Yb, and Lu are adsorbed onto bacteria cell walls leading to their preferential depletion in solution, and thus resulting in high dissolved Er/Yb and Er/Lu ratios in the surrounding seawater. Further investigations on the Er-Yb-Lu system in seawater are necessary in order to elucidate their potential use as tracer.

In summary, uncertainties remain about the conservative vs. non-conservative behavior of REEs and the sources (e.g., rivers, ocean margins) and processes (input, scavenging, release, lateral transport/mixing) that may affect seawater REE distributions (and by extension other TEs) in the West Pacific (chapter 3).

1.3.2. Neodymium isotopes

Neodymium has seven naturally occurring isotopes: ^{142}Nd , ^{143}Nd , ^{144}Nd , ^{145}Nd , ^{146}Nd , ^{148}Nd and ^{150}Nd . The Nd isotope ratio $^{143}\text{Nd}/^{144}\text{Nd}$ is expressed as $\epsilon_{\text{Nd}} = [({}^{143}\text{Nd}/{}^{144}\text{Nd}_{\text{sample}})/({}^{143}\text{Nd}/{}^{144}\text{Nd}_{\text{CHUR}}) - 1] \times 10^4$, where CHUR stands for Chondritic Uniform Reservoir with a value of ${}^{143}\text{Nd}/{}^{144}\text{Nd}_{\text{CHUR}} = 0.512638$ (Jacobsen and Wasserburg, 1980). The use of the Nd isotopes ($^{143}\text{Nd}/^{144}\text{Nd}$) as tracer stems from the fractionation of samarium (Sm)

and Nd between the Earth's mantle and the continental crust, and from the α -decay of ^{147}Sm to radiogenic ^{143}Nd with a half-life of 106 billion years. Although both Sm and Nd belong to the LREEs, Nd is slightly more incompatible than Sm, and is therefore preferentially enriched in crustal melts and consequently in crustal rocks, whereas Sm remains in the Earth's mantle. As a result, Sm/Nd ratios, and hence $^{143}\text{Nd}/^{144}\text{Nd}$ ratios, are lower in the old continental crust than in young mantle-derived volcanic rocks. This is expressed by more negative (i.e., 'unradiogenic') ϵ_{Nd} signatures of ~ -30 in old cratonic rocks surrounding the North Atlantic and by more positive (i.e., 'radiogenic') ϵ_{Nd} values of up to $+10$ in young mid-ocean ridge basalts located around the Pacific rim (e.g., Goldstein and Hemming, 2003; Jeandel et al., 2007) (Fig. 1.2). These variations of the Nd isotope ratio in different rock types with their systematic Sm/Nd ratios and ages leads to a heterogeneous ϵ_{Nd} distribution in rocks that is imprinted into the oceans through weathering inputs (e.g., Goldstein and Hemming, 2003; Jeandel et al., 2007). Due to the shorter residence time of Nd in the ocean (~ 300 to 1000 years, Tachikawa et al., 2003; Arsouze et al., 2009; Rempfer et al., 2011) compared to the ocean mixing time (~ 1500 years, Broecker and Peng, 1982) and since seawater ϵ_{Nd} signatures are set by Nd supply through weathering inputs of the surrounding source rocks (e.g., Goldstein and Hemming, 2003), different water masses carry distinct ϵ_{Nd} signatures of their source regions (e.g., Piepgras and Wasserburg, 1980). For instance, NADW has relatively unradiogenic ϵ_{Nd} values ($\epsilon_{\text{Nd}} = -13.5$, e.g., Piepgras and Wasserburg, 1987; Rickli et al., 2009) representing weathering inputs of old cratonic rocks such as from Greenland and the Canadian shield. On the other hand, North Pacific Deep Water (NPDW) has more radiogenic ϵ_{Nd} values ($\epsilon_{\text{Nd}} \sim -4$, e.g., Piepgras and Jacobsen, 1988; Amakawa et al., 2009; Pahnke et al., 2012) reflecting the surrounding young volcanic rocks of the Pacific rim (Fig. 1.2). The mixing of NADW and NPDW in the Southern Ocean, in addition to weathering inputs from Antarctica, results in ϵ_{Nd} signatures of -9 to -8 for Circumpolar Deep Water (e.g., Carter et al., 2012; Rickli et al., 2014; Basak et al., 2015) (Fig. 1.2). Consequently, variations and changes in dissolved seawater ϵ_{Nd} may be explained based on lateral water mass transport/mixing, and thus seawater ϵ_{Nd} has been considered as a quasi-conservative water mass tracer in the present and past deep open ocean (e.g., Piepgras and Wasserburg, 1980; Frank, 2002; Goldstein and Hemming, 2003). The high potential of seawater ϵ_{Nd} as water mass tracer is pointed out by the international GEOTRACES program (www.geotraces.org). Here, ϵ_{Nd} is one of the GEOTRACES key parameters that are investigated in order to better characterize the distribution of TEs in the global ocean.

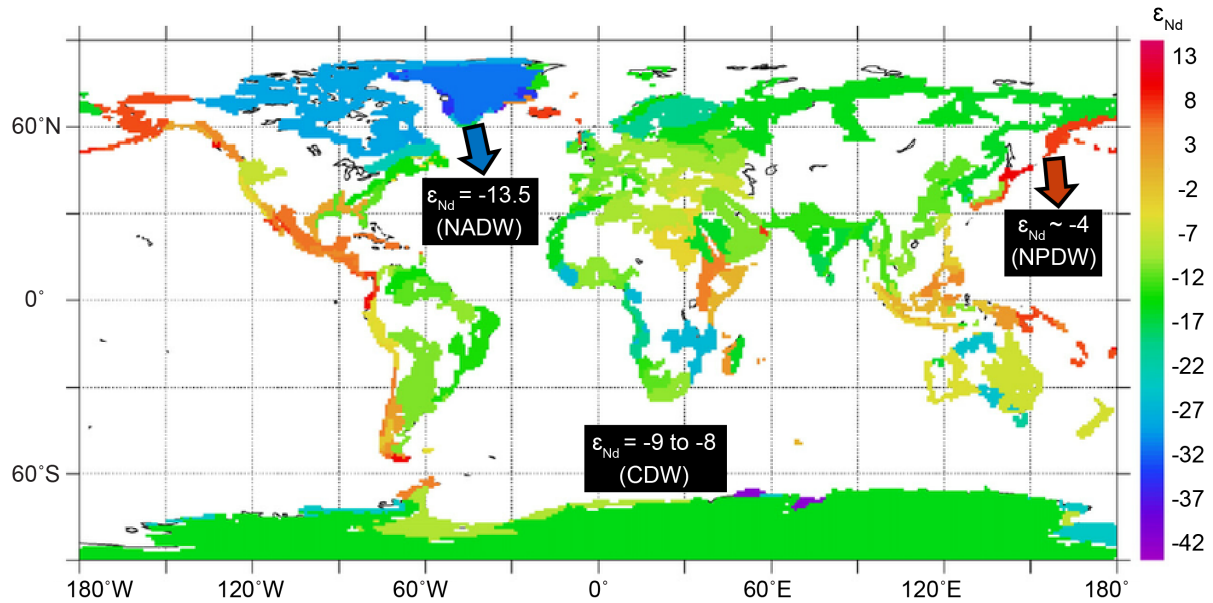


Fig. 1.2. Extrapolated map showing the heterogeneous ϵ_{Nd} distribution of rocks (in color) and typical dissolved seawater ϵ_{Nd} signatures of North Atlantic Deep Water (NADW), North Pacific Deep Water (NPDW) and Circumpolar Deep Water (CDW) (modified after Jeandel et al., 2007).

Seawater ϵ_{Nd} is widely used to trace water mass transport in the different oceans apart from continental inputs (e.g., Andersson et al., 2008; Amakawa et al., 2009; Singh et al., 2012; Stichel et al., 2015). Nevertheless, the understanding of the sources (e.g., rivers, ocean margins) and processes that may affect seawater ϵ_{Nd} in the different oceans, and their impact on the potential use of ϵ_{Nd} as quasi-conservative water mass tracer is still incomplete. A poorly understood process is ‘boundary exchange’ at ocean margins, a mechanism that couples isotopic exchange with continental input (source) and removal (sink) of Nd to and from the ocean, and thus modifies seawater ϵ_{Nd} without significantly affecting [Nd] (Lacan and Jeandel, 2001, 2005; Arsouze et al., 2007). The West Pacific is of particular interest with respect to ‘boundary exchange’ as this area is surrounded by volcanic island margins.

While seawater ϵ_{Nd} is thought to trace local imprints and lateral water mass transport/mixing, the [Nd] in the open ocean is interpreted to dominantly reflect vertical cycling (input, scavenging, release) rather than lateral water mass transport/mixing (Piepgras and Wasserburg, 1980; Goldstein and Hemming, 2003). This apparent discrepancy between seawater ϵ_{Nd} and [Nd] is termed the ‘Nd paradox’ (Goldstein and Hemming, 2003). Because in the past only spatially separated and few vertical ϵ_{Nd} and [Nd] profiles existed, the concept of the ‘Nd paradox’ had been related to ‘reversible scavenging’, a vertical process linking continuous isotopic exchange with removal/release of Nd through/from sinking particles (Siddall et al., 2008). In contrast, recent studies using observations from vertically and spatially high-resolution transects highlighted the dominance of lateral rather than vertical

control on seawater [Nd] in different oceanic regions and settings (Basak et al., 2015; Hathorne et al., 2015; Stichel et al., 2015; Lambelet et al., 2016, Zheng et al., 2016).

In summary, open questions remain with respect to the relative importance and impact of different sources (e.g., rivers, ocean margins) and processes (input, scavenging, release, lateral water mass transport/mixing, boundary exchange) that may affect dissolved seawater ϵ_{Nd} and/or [Nd], and therefore on the use of ϵ_{Nd} as a quasi-conservative water mass tracer in the West Pacific (chapter 2).

1.4. Major advancements

The low ($\mu\text{mol/kg}$ to fmol/kg) concentrations of dissolved TEs in the ocean, the limited sensitivity of analytical instruments, and the lack of strict quality control procedures resulted in low-quality marine TE data until the 1970s (e.g., Bruland et al., 1979) and hindered their extensive use in marine studies. This has changed due to major technical advancements and specific marine TE research over the last few decades, including the Geochemical Ocean Sections Study (GEOSECS) of the 1970s that produced the first precise seawater concentration profiles of TEs (Broecker and Peng, 1982). As a result, and mostly through the progress of the ongoing GEOTRACES program, researchers have recognized the importance of TEs for marine ecosystems, the carbon cycle, and climate change (e.g., SCOR Working Group, 2007). Within the framework of the GEOTRACES program, new clean shipboard sampling techniques, approved sampling protocols and new methods for sample processing and analysis, as well as quality control procedures were initialized (e.g., Bruland et al., 2005; Cutter and Bruland, 2012; Pahnke et al., 2012; van de Flierdt et al., 2012).

These major advancements opened the way for a global study of TE distributions along vertically and spatially high-resolution transects within the GEOTRACES program, which is providing a continuously growing high-quality dataset of global TE distributions. The study presented in this thesis adds to the GEOTRACES dataset and is recognized as a GEOTRACES Process Study (GPpr04).

1.5. Objectives and outline of this thesis

As pointed out in the previous sections, despite the importance in advancing our understanding of TEs in the ocean and thus in exploiting the high potential of [REE] and Nd isotopes as tracers, many open questions remain, especially in the Pacific. This is due to an insufficient vertical and spatial coverage of dissolved seawater REE and Nd isotope data, and the fact that major advancements in sampling, processing, analysis, and validation only recently opened the way to a growing high-quality global ocean dataset.

In the Pacific, the REE and Nd isotope dataset is still very rudimentary, as the available stations sampled for at least three different water depths are sparse, scattered, and were mainly sampled for only REE or only Nd isotope data (Fig. 1.3).

This thesis presents the first vertically and spatially high-resolution full water column profiles of dissolved ϵ_{Nd} and [REE] from twelve stations along a NW-SE transect in the West Pacific from South Korea to Fiji (R/V *Sonne* cruise SO223T, GEOTRACES Process Study GPpr04) (Fig. 1.3). The set of stations almost doubles the number of currently available stations sampled for at least three water depths and for both ϵ_{Nd} and REE data in the West Pacific.

The major objective of this thesis was to investigate a high-resolution transect that enables to exploit the high potential of Nd isotopes in combination with [Nd] (chapter 2), as well as of [REE] (chapter 3) as tracers of sources and processes that control their distributions (and by extension other TEs) in the West Pacific. The data of this thesis provide an essential part of the international effort of the GEOTRACES program in depicting a comprehensive picture of TE distributions in the global ocean to completely decipher the important roles of TEs. Consequently, the data will be included in the GEOTRACES Intermediate Data Product 2017 (IDP2017). In addition, this thesis presents a new robust and rapid method for the routine pre-concentration, purification, and analysis of dissolved [REE] from small seawater volumes, and further includes an international intercomparison study by four laboratories using seawater from the GEOTRACES reference sampling station SAFe (Sampling and Analysis of Iron) in the North Pacific for quality control (chapter 4). This REE method is easy to adopt, and therefore opens the way for a fast growing high-quality global ocean REE dataset that will substantially contribute to a better understanding of the factors that control global REE distributions.

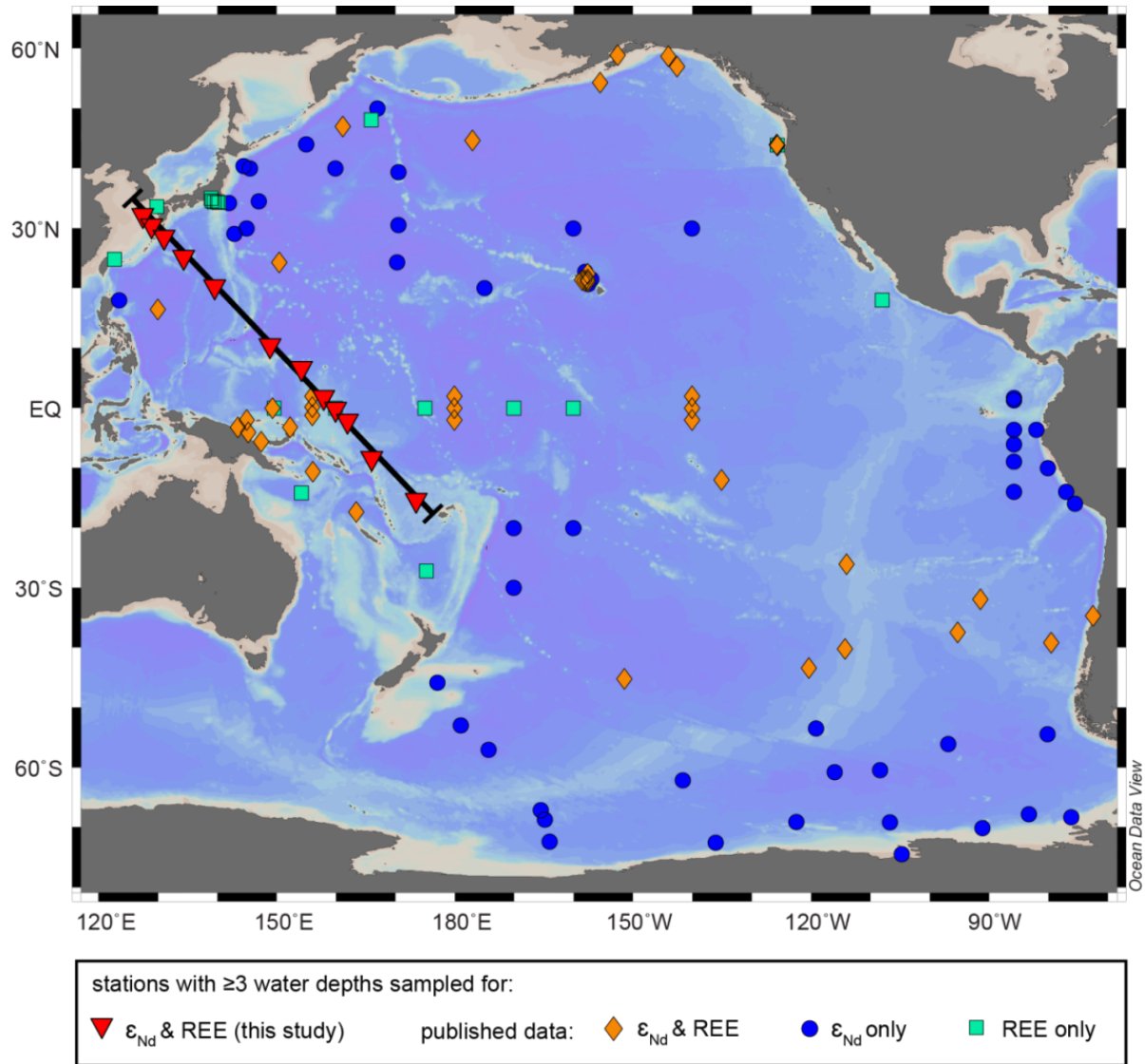


Fig. 1.3. Map showing the locations of all stations sampled for at least three water depths for seawater REE concentrations and/or Nd isotopes in the Pacific, with stations from this study (red triangles) and published data (Piepgras and Wasserburg, 1980; de Baar et al., 1985; Piepgras and Jacobsen, 1988; Tanaka et al., 1990; Piepgras and Jacobsen, 1992; Shimizu et al., 1994; Zhang and Nozaki, 1996, 1998; Alibo and Nozaki, 1999; Lacan and Jeandel, 2001; Amakawa et al., 2004a; Vance et al., 2004; Hara et al., 2009; Hongo et al., 2007; Wang and Yamada, 2007; Amakawa et al., 2009; Zimmermann et al., 2009; Carter et al., 2012; Grasse et al., 2012; Pahnke et al., 2012; Amakawa et al., 2013; Grenier et al., 2013; Jeandel et al., 2013; Molina-Kescher et al., 2014; Haley et al., 2014; Rickli et al., 2014; Abbott et al., 2015a, b; Basak et al., 2015; Wu et al., 2015; Fröllje et al., 2016).

Below, the major objectives of this thesis are outlined:

- Identification of sources of REEs (and by extension other TEs) to the West Pacific, using ϵ_{Nd} and [REE], and processes controlling their distributions: characterization of coastal input near South Korea and volcanic islands in the tropical West Pacific, evaluation of the conservative vs. non-conservative behavior of REEs, and verification of the integrity of ϵ_{Nd} as water mass tracer
- Assessment of TE input to the tropical West Pacific and eastward transport within equatorial zonal currents
- Development of a new REE method that is easy to adopt and allows a rapid and precise analysis of dissolved [REE] from small volumes of seawater (~11-12 mL) to open the way for a global high-quality seawater REE dataset
- Realization of an international intercomparison of dissolved seawater [REE] to validate the new REE method and to establish the first reference seawater REE standard for quality control of future marine REE studies in the Pacific

Chapter 2 describes the dynamic setting and hydrographic properties of major Pacific water masses in the context of the dissolved ϵ_{Nd} and [Nd] found in the West Pacific along a transect from South Korea to Fiji. The study in this chapter aims to clarify the relative importance and impact of the different sources (e.g., rivers, volcanic island margins) and processes on seawater ϵ_{Nd} and [Nd], and to assess the integrity of seawater ϵ_{Nd} as quasi-conservative water mass tracer in the West Pacific. The investigation of ϵ_{Nd} and [Nd] along the transect points out the significance of vertical processes and lateral water mass transport on their distribution.

The focus of chapter 3 is on dissolved [REE] in the West Pacific along the same transect as in the study presented in chapter 2 and provides a detailed characterization of the sources and processes that control seawater REE (and potentially other TE) distributions in the West Pacific. This chapter highlights the small-scale equatorial zonal eastward transport of surface and subsurface water REE inputs, and hence supports the previous hypothesis on TE inputs to the tropical West Pacific and their transport to the iron-limited HNLC area of the East Pacific.

Chapter 4 presents the first application of the automated seaFAST-pico system (Elemental Scientific Inc.) in offline mode using multi-element isotope dilution inductively coupled plasma-mass spectrometry for the robust and rapid pre-concentration, purification, and analysis of dissolved [REE] from small volumes of seawater (11-12 mL). The method

described in this chapter is easy to adopt and enables the extensive use of seawater [REE] in marine studies, ultimately opening the way to build a global seawater REE dataset. In addition, the study provides the first international intercomparison of REE values for the GEOTRACES intercalibration station SAFe in the North Pacific at 3000 m water depth, and establishes this station and depth as first reference seawater REE standard for quality control of future marine REE studies in the Pacific.

Finally, chapter 5 provides an overview of the major conclusions of this thesis and presents an outlook of future studies and projects.

1.6. Author's contribution

This thesis includes chapters that are prepared for submission to *Geochimica et Cosmochimica Acta* (chapter 2) and *Earth and Planetary Science Letters* (chapter 3), and one chapter that is published in *Marine Chemistry* (chapter 4). The content of the published manuscript is not changed, but its format is adapted to that of this thesis. A complete list of references is given in chapter 6. In the following, the author's contribution to each chapter is outlined.

Chapter 2: Sources and processes affecting the distribution of dissolved Nd isotopes and concentrations in the West Pacific (prepared for *Geochimica et Cosmochimica Acta*)

Melanie K. Behrens, Katharina Pahnke, Bernhard Schnetger, Hans-Jürgen Brumsack

Chapter 3: Rare earth element distributions in the West Pacific: trace element sources and conservative vs. non-conservative behavior (prepared for *Earth and Planetary Science Letters*)

Melanie K. Behrens, Katharina Pahnke, Ronja Paffrath, Bernhard Schnetger, Hans-Jürgen Brumsack

The project in chapters 2 and 3 was designed and initiated by Katharina Pahnke. The packing and planning for the R/V *Sonne* cruise SO223T was coordinated by Katharina Pahnke with help from Melanie Behrens and Lene Meiners (lab technician). The seawater samples were collected and processed onboard by Melanie Behrens, Katharina Pahnke, and Lene Meiners. The CTD data were processed by Melanie Behrens under the supervision of Katharina Pahnke. Melanie Behrens further processed all seawater samples in the home laboratory and analyzed all samples for dissolved Nd isotopes and REE concentrations at the University of Oldenburg. Melanie Behrens intercalibrated the home laboratory at the University of Oldenburg for dissolved Nd isotopes using seawater standards from the

GEOTRACES intercalibration stations BATS (Bermuda Atlantic Time Series) and SAFe (chapter 2). All authors contributed to the manuscripts with data interpretation and discussion. Ronja Paffrath conducted the optimum multiparameter analysis using an openly available MATLAB code (chapter 3). Bernhard Schnetger provided technical assistance with the ICP-MS for REE analysis (chapter 3). Melanie Behrens wrote the manuscripts with contributions from all co-authors.

Chapter 4: Rapid and precise analysis of rare earth elements in small volumes of seawater: method and intercomparison (published manuscript)

Melanie K. Behrens, Jesse Muratli, Catherine Pradoux, Yingzhe Wu, Philipp Böning, Hans-Jürgen Brumsack, Steven L. Goldstein, Brian Haley, Catherine Jeandel, Ronja Paffrath, Leopoldo D. Pena, Bernhard Schnetger, Katharina Pahnke

published in *Marine Chemistry* 186, 110-120, doi.10.1016/j.marchem.2016.08.006 (2016)

This study was designed and initiated by Katharina Pahnke and Melanie Behrens. Melanie Behrens, supervised by Katharina Pahnke, developed and validated the new method, with help from Philipp Böning, Bernhard Schnetger, and Ronja Paffrath. Melanie Behrens coordinated the international intercalibration between the four laboratories, advised by Katharina Pahnke. Data analysis within the intercomparison study was done by Melanie Behrens (Lab 1, University of Oldenburg), Jesse Muratli (Lab 3, Oregon State University), Catherine Pradoux (Lab 4, University of Toulouse), and Yingzhe Wu (Lab 2, Columbia University). Melanie Behrens intercalibrated the home laboratory at the University of Oldenburg for dissolved REE concentrations using seawater standards from the GEOTRACES intercalibration stations BATS and SAFe. All authors contributed to data interpretation and discussion. Melanie Behrens wrote the manuscript with contributions from all co-authors. The supplementary material including the different methods used by the participating laboratories was written by the participants and by Melanie Behrens with input from the participants.

2. Sources and processes affecting the distribution of dissolved Nd isotopes and concentrations in the West Pacific

Melanie K. Behrens^a, Katharina Pahnke^a, Bernhard Schmetger^b, Hans-Jürgen Brumsack^b

manuscript prepared for

Geochimica et Cosmochimica Acta

^aMax Planck Research Group for Marine Isotope Geochemistry, Institute for Chemistry and Biology of the Marine Environment (ICBM), University of Oldenburg, Carl-von-Ossietzky-Str. 9-11, 26129 Oldenburg, Germany

^bMicrobiogeochemistry, Institute for Chemistry and Biology of the Marine Environment (ICBM), University of Oldenburg, Carl-von-Ossietzky-Str. 9-11, 26129 Oldenburg, Germany

Abstract

The dissolved neodymium (Nd) isotopic composition (ϵ_{Nd}) of seawater is widely used as a quasi-conservative water mass tracer in the present and past ocean. However, our knowledge of the sources and processes that control Nd cycling in the Pacific and their influence on the potential use of ϵ_{Nd} as water mass tracer there is still incomplete. The West Pacific is of particular interest as this key area lies in the influence of Asian rivers, is surrounded by volcanic island margins, has a complex surface to subsurface current system, and a sluggish deep water circulation. Here we present the first high-resolution vertical and spatial full water column profiles of dissolved ϵ_{Nd} and Nd concentrations ([Nd]) from twelve stations along a transect in the West Pacific between South Korea and Fiji. Our data show continental input via freshwater discharge to South Korean surface water, as indicated by low salinity, unradiogenic ϵ_{Nd} (-7.3), and elevated [Nd] (15.30 pmol/kg). Net removal of Nd and isotopic exchange with unradiogenic continent-derived particles controls both Nd and ϵ_{Nd} distributions below the surface in the East China Sea. Boundary exchange at volcanic island margins in the tropical West Pacific imprint a radiogenic ϵ_{Nd} signature (up to +0.7) on surface and subsurface waters that acts as a fingerprint for the origin and small-scale eastward transport within the equatorial zonal current system. Our data further demonstrate the dominant control of lateral water mass transport on the [Nd] distribution within North and South Pacific Tropical Water (NPTW and SPTW), Antarctic Intermediate Water, and Lower Circumpolar Deep Water (LCDW). Advection of low-[Nd], high-salinity SPTW into our study area explains the low subsurface [Nd] previously observed in this area. Antarctic Intermediate Water can be traced northward to up to 10°N based on its low [Nd], while its ϵ_{Nd} signature is modified through boundary exchange at volcanic island margins. Similarly, LCDW can be traced to ~25°N based on low and vertically constant [Nd], but its ϵ_{Nd} is more radiogenic by 3.5-4.4 ϵ_{Nd} units than in the Southern Ocean when it enters our study area and is modified mainly during transit through the Samoan Passage. Upper Circumpolar Deep Water/Pacific Deep Water (UCDW/PDW) along the transect is controlled by upwelling of high-[Nd] in the Philippine Sea and Nd release from sinking lithogenic particles, while its ϵ_{Nd} shows constant values around -3.1, consistent with previous data from the North Pacific and indicative of conservative behavior of ϵ_{Nd} within UCDW/PDW in the Northwest Pacific. Overall, our data clearly show a dominant conservative component in the distribution of [Nd] in the West Pacific and the strong non-conservative behavior of ϵ_{Nd} due to boundary exchange at volcanic margins and ridges. The latter however facilitates small-scale tracing of the complex zonal current system in the equatorial Pacific. Moreover, while non-conservative

behavior of ϵ_{Nd} is due to boundary exchange, deviations from conservative behavior of $[\text{Nd}]$ are due to vertical overprints through Nd release from organic (intermediate depth) or lithogenic (UCDW/PDW) particles.

2.1. Introduction

The dissolved neodymium (Nd) isotope ratio ($^{143}\text{Nd}/^{144}\text{Nd}$, expressed as ϵ_{Nd}) of seawater is widely used as water mass tracer in the different ocean basins (e.g., Andersson et al., 2008; Amakawa et al., 2009; Singh et al., 2012; Basak et al., 2015; Stichel et al., 2015; Lambelet et al., 2016). Nevertheless, our understanding of the sources and processes that control seawater Nd cycling in the different oceans, and their impact on the potential use of ϵ_{Nd} as water mass tracer is not yet complete. For example, uncertainties remain about the impact and relative importance of river inputs (e.g., Osborne et al., 2014; Rousseau et al., 2015) and submarine groundwater discharge (SGD) (e.g., Johannesson and Burdige, 2007; Kim and Kim, 2014). Moreover, a poorly understood process is boundary exchange near continental or volcanic islands margins that couples continental input (source) and removal (sink) of Nd to and from the ocean and can modify seawater ϵ_{Nd} without affecting dissolved Nd concentrations ($[\text{Nd}]$) (Lacan and Jeandel, 2001, 2005). Additionally, a still ongoing debate is the ‘Nd paradox’, the apparent discrepancy between seawater ϵ_{Nd} and $[\text{Nd}]$, which, in contrast to ϵ_{Nd} , tends to increase with water depth following vertical nutrient-like patterns rather than lateral water mass advection (e.g., Goldstein and Hemming, 2003). This has been related to reversible scavenging, a vertical process linking continuous isotopic exchange with removal/release of Nd through/from sinking particles (e.g., Siddall et al., 2008). Based on increasing $[\text{Nd}]$ with increasing apparent oxygen utilization (AOU) (i.e., decreasing oxygen concentration due to its consumption by the decomposition (reminerzalization) of organic matter), recent studies observed a vertical nutrient-like pattern of Nd reflecting its adsorption and removal (scavenging) onto particles in the (sub)surface and subsequent release from organic particles due to the onset of remineralization (e.g., Stichel et al., 2015; Lambelet et al., 2016). However, seawater Nd cycling can also be controlled by lateral water mass transport in different oceanic regions and settings (e.g., Basak et al., 2015; Stichel et al., 2015; Osborne et al., 2015; Lambelet et al., 2016; Zheng et al., 2016).

The dissolved Nd isotope ratio ($^{143}\text{Nd}/^{144}\text{Nd}$) is expressed as $\epsilon_{\text{Nd}} = [(\text{}^{143}\text{Nd}/\text{}^{144}\text{Nd}_{\text{sample}})/(\text{}^{143}\text{Nd}/\text{}^{144}\text{Nd}_{\text{CHUR}})-1]\times 10^4$, where CHUR stands for Chondritic Uniform Reservoir with a value of $^{143}\text{Nd}/^{144}\text{Nd}_{\text{CHUR}} = 0.512638$ (Jacobsen and Wasserburg, 1980). Seawater ϵ_{Nd} signatures are set by continental Nd supply through weathering of surrounding

source rocks of different ages and lithology, and since the residence time of Nd (~ 300 to 1000 years, Tachikawa et al., 2003; Arsouze et al., 2009; Rempfer et al., 2011) in the ocean is shorter than the ocean mixing time (~ 1500 years, Broecker and Peng, 1982), different water masses carry distinct ϵ_{Nd} values of their source region (e.g., Goldstein and Hemming, 2003). In the modern ocean, North Atlantic Deep Water has relatively unradiogenic ϵ_{Nd} values ($\epsilon_{\text{Nd}} = -13.5$, e.g., Piepgras and Wasserburg, 1987; Rickli et al., 2009) representing weathering inputs from old continental rocks. In contrast, North Pacific Deep Water has more radiogenic ϵ_{Nd} signatures ($\epsilon_{\text{Nd}} \sim -4$, e.g., Piepgras and Jacobsen, 1988; Amakawa et al., 2009; Pahnke et al., 2012) resulting from weathering contributions of mantle derived young volcanic rocks located around the Pacific rim. These two water masses mix in the Southern Ocean, and along with weathering inputs from Antarctica result in an ϵ_{Nd} signature of -9 to -8 for Circumpolar Deep Water (e.g., Carter et al., 2012; Rickli et al., 2014; Basak et al., 2015). Consequently, changes in the expected seawater ϵ_{Nd} signatures may be explained based on water mass mixing, and thus seawater ϵ_{Nd} has been considered as a quasi-conservative water mass tracer in the deep open ocean (e.g., Piepgras and Wasserburg, 1980).

Here we present the first high-resolution vertical and spatial full water column profiles of dissolved ϵ_{Nd} and $[\text{Nd}]$ from the West Pacific between South Korea and Fiji (Fig. 2.1a). Our study aims to clarify the impact and relative importance of different Nd sources (river, SGD, volcanic islands margins) and processes on dissolved ϵ_{Nd} and $[\text{Nd}]$ distributions in the West Pacific, and to assess the integrity of seawater ϵ_{Nd} as water mass tracer in this area. Using dissolved $[\text{Nd}]$ along the transect, we evaluate the relative importance of vertical processes and lateral water mass transport on the Nd distribution.

2.2. Hydrography of the West Pacific

2.2.1. Surface waters

The study area lies in the West Pacific and extends along a NW-SE transect from South Korea to Fiji (Fig. 2.1a). We divide the transect into two sections for ease of reference, a South Korea to open ocean section (SKO) including stations GeoB17001 to GeoB17005 (referred to as stations 01 to 05), and a tropical West Pacific (TWP) section including stations GeoB17011 to GeoB17019 (referred to as stations 11 to 19) (Figs. 2.1a, b). In the following, we describe the dynamic setting (Figs. 2.1a, b) and hydrographic properties of water masses (Figs. 2.2a, b, Table 2.1a) found in our study area.

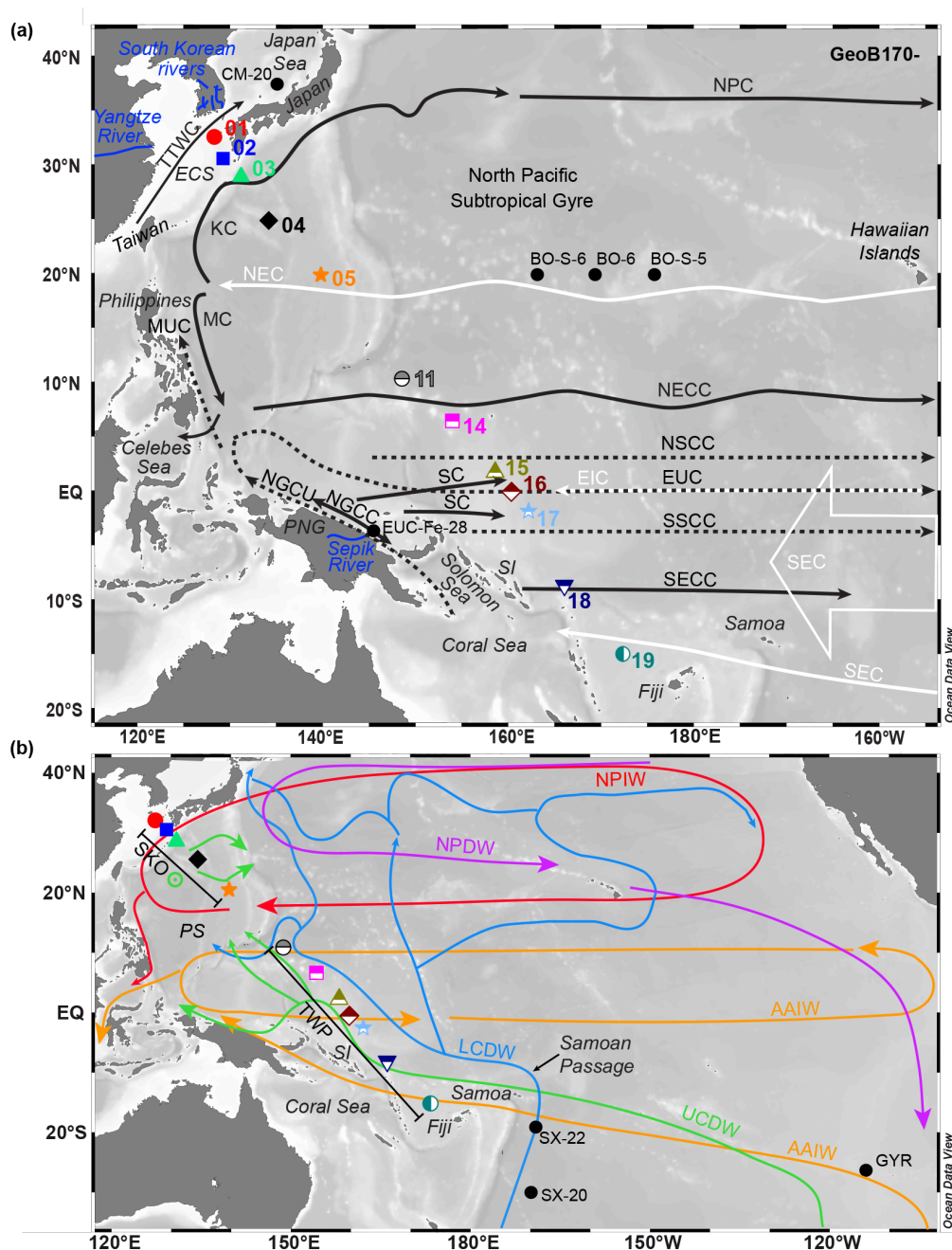


Fig. 2.1. Maps showing the locations of all seawater profiles sampled in the West Pacific along the SO223T transect, with stations (GeoB170-) 01-05 and 11-19 from the SKO (South Korea - open ocean) and TWP (tropical West Pacific) sections together with published stations (black dots) discussed in the text. CM-20, BO-S-6, BO-6, BO-S-5 (Amakawa et al., 2004b); SX-20, SX-22 (Amakawa et al., 2013); EUC-Fe-28 (Grenier et al., 2013); GYR (Jeandel et al., 2013). (a) West Pacific schematic major surface (solid arrows) and subsurface (dashed arrows) westward (white) and eastward (black) currents of the study area (after e.g., Nitani, 1972; Wyrski and Kilonsky, 1984; Fine et al., 1994; Tomczak and Godfrey, 1994; Reid, 1997; Isobe, 1999; Grenier et al., 2011; Talley et al., 2011; and determined from real time ocean surface current analyses corresponding to the SO223T cruise period, <http://www.oscar.noaa.gov/>). (b) Schematic West Pacific intermediate and deep water circulation (after Kawabe and Fujio, 2010). Green circle with a center point indicates upwelling of UCDW to the surface/intermediate layer (Kawabe and Fujio, 2010). Abbreviations used for water masses, currents, islands, and seas are listed in Tables 2.1a, b. Four major South Korean rivers after Lan et al. (1995). Map was created using Ocean Data View (Schlitzer, 2014).

The surface circulation in the study area of the SKO section is dominated by currents of the North Pacific Subtropical Gyre (stations 03-05): the North Equatorial Current (NEC) flowing westward at $\sim 20^\circ\text{N}$ that feeds the northeastward flowing Kuroshio Current (KC) (e.g., Nitani, 1972; Tomczak and Godfrey, 1994; Reid, 1997) (Fig. 2.1a). Stations 01 and 02 of the SKO section are located near South Korea in the East China Sea (ECS), and were sampled in September when the seasonally changing Taiwan-Tsushima Warm Current (TTWC) originates from near Taiwan and flows northward into the ECS and through the Korea Strait (stations 01 and 02) towards the Japan Sea (Isobe, 1999) (Fig. 2.1a).

In the TWP section, the surface circulation is dominated by currents of the equatorial zonal current system (Fig. 2.1a). The northern TWP stations 11 and 14 are located within the eastward flowing North Equatorial Countercurrent (NECC) that is fed by the Mindanao Current (MC), a western boundary current that flows equatorward near the Philippines (e.g., Nitani, 1972; Lukas et al., 1991) (Fig. 2.1a). The equatorial stations 15-17 lie in the flow path of eastward flowing surface currents (SC) that transport surface waters of the New Guinea Coastal Current (NGCC), a current that flows along the coast of Papua New Guinea (PNG) (e.g., Fine et al., 1994) (Fig. 2.1a). In the southern TWP, stations 18 and 19 near the Solomon Islands (SI) and Fiji are located within the South Equatorial Countercurrent (SECC) (e.g., Reid, 1959) and the South Equatorial Current (SEC) (e.g., Wyrтки and Kilonsky, 1984), respectively (Fig. 2.1a).

2.2.2. Subsurface waters

Subsurface waters sampled in our study area below ~ 60 m water depth (w. d. in the following) are North and South Pacific Tropical Water (NPTW and SPTW), North Pacific Subtropical Mode Water (STMW), East China Sea Subsurface Water (ECSSUW), and Western North and South Pacific Central Water (WNPCW and WSPCW).

The NPTW is formed by subduction of high salinity surface water (Suga et al., 2000) through evaporation in the subtropical central North Pacific (Cannon, 1966; Fine et al., 1994). It is transported from the subtropical central North Pacific near Hawaii westwards into our study area by the NEC (station 05, 61-101 m w. d.) towards the coast of the Philippines (e.g., Fine et al., 1994; Kashino et al., 1996), where it splits into the KC (stations 03 and 04, NPTW at 62-250 m w. d.) (e.g., Qu et al., 1999; Suga et al., 2000) and the MC, that ultimately feeds the NECC (stations 11 and 14, NPTW at 121-142 m w. d.) (e.g., Nitani, 1972; Fine et al., 1994; Kashino et al., 1996). The STMW is formed on the southern side of the KC in winter (e.g., Masuzawa, 1969; Bingham, 1992). It is found in our study area below the depth of

NPTW within the NEC (station 05) and KC (stations 03 and 04) at depths between 201 m and 303 m (e.g., Masuzawa, 1969; Bingham, 1992). The NPTW and STMW can be distinguished from the ECSSUW that is observed at stations 01 and 02 (100-150 m w. d.) by their characteristic subsurface salinity maximum (NPTW, e.g., Qu et al., 1999) and slightly higher potential density range (STMW, Suga et al., 2004) (Fig. 2.2a, Table 2.1a).

The Southern Hemisphere counterpart of NPTW, the SPTW, is formed by subduction of high salinity surface water within the oligotrophic South Pacific Subtropical Gyre (e.g., O'Connor et al., 2005; Qu et al., 2013). The SPTW is transported from its formation region westward within the South Equatorial Current (SEC) into our study area (stations 17-19, 120-200 m w. d.), and the majority continues within the New Guinea Coastal Undercurrent (NGCU) along the PNG coast and then contributes to the eastward flowing Equatorial Undercurrent (EUC) (stations 15 and 16, 101-150 m w. d.) (e.g., Tsuchiya et al., 1989; Fine et al., 1994; Grenier et al., 2011). In our study area, at stations 15-19 of the TWP section, SPTW is observed by its higher and clearly pronounced subsurface salinity maximum compared to that of NPTW (e.g., Qu et al., 1999) (Fig. 2.2a).

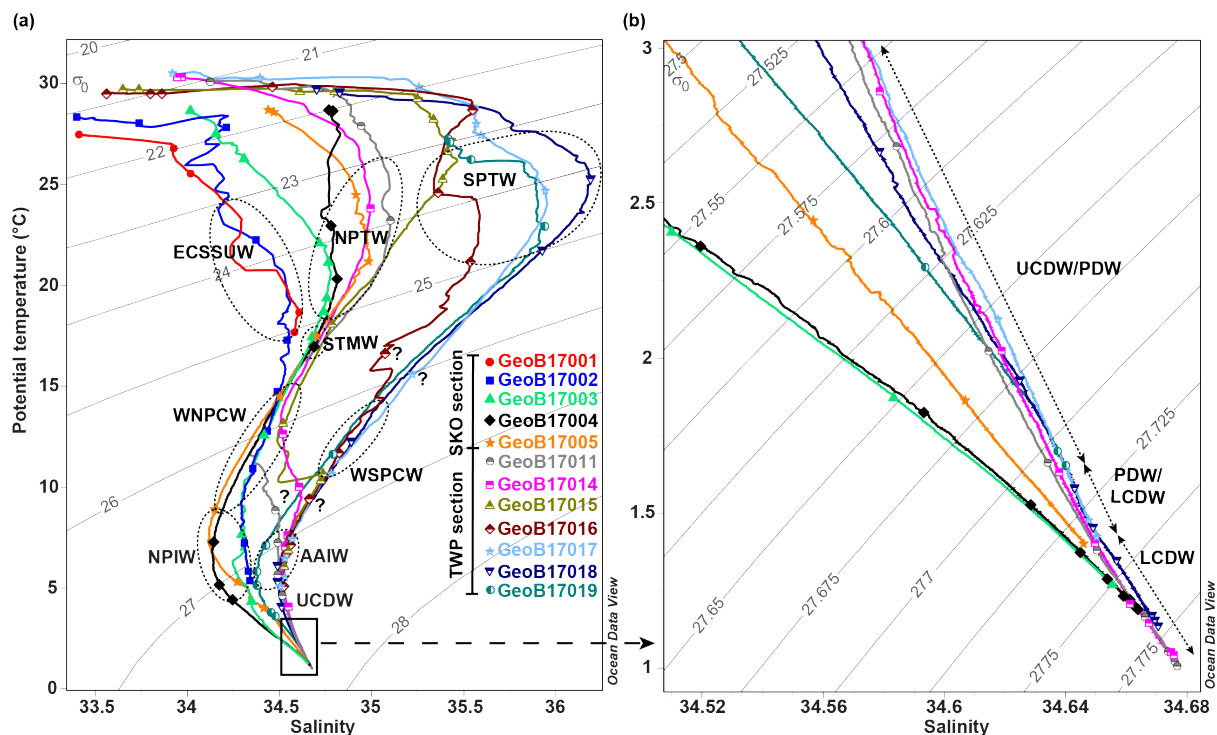


Fig. 2.2. Hydrographic properties of sampled stations along the transect as indicated in Fig. 2.1. (a) Full range potential temperature (°C) vs. salinity plot. Black rectangle outlines the area of deep water samples illustrated in panel (b). Stippled black circles in (a) and stippled black arrows in (b) refer to water mass characteristics as presented in Tables 2.1a and 2.3. For abbreviations of water masses see Table 2.1a. Sampled water depths are marked by symbols. Potential density (kg/m^3) contours are shown in solid grey. Plots produced with Ocean Data View (Schlitzer, 2014).

Table 2.1a: Abbreviations used for water masses and hydrographic water mass properties.

Abbreviation	Water masses	Salinity	Pot. Density (kg/m ³)	Neutral Density (kg/m ³)	References
AAIW	Antarctic Intermediate Water	34.4-34.6	27.1-27.3	27.0 < γ_n ≤ 27.4	Bingham and Lukas, 1995; Sloyan and Rintoul, 2001; Zenk et al., 2005
ECSSUW	East China Sea Subsurface Water	≤34.6	23.0-25.0		this study
LCDW	Lower Circumpolar Deep Water			28.0 < γ_n < 28.27	Orsi et al., 1995; Whitworth et al., 1998
NPIW	North Pacific Intermediate Water	34.0-34.3	26.6-27.4	26.5-27.4	You et al., 2003; Yasuda, 2004; Talley et al., 2011
(N)PDW	(North) Pacific Deep Water			27.70-28.01	Macdonald et al., 2009; Talley et al., 2011
STMW	North Pacific Subtropical Mode Water	34.6-34.8	25.0 < σ_θ < 25.6		Nakamura, 1996; Suga et al., 2004
NPTW	North Pacific Tropical Water	<35.25	23.0-25.0		Qu et al., 1999, 2013
SPTW	South Pacific Tropical Water	>35.25	23.5-25.0		Qu et al., 1999, 2013
UCDW	Upper Circumpolar Deep Water			27.55 < γ_n < 28.0	Garabato et al., 2002
WNPCW	Western North Pacific Central Water	33.5-34.5	25.2-26.4		Pickard and Emery, 1990; Tomczak and Godfrey, 2003; Talley et al., 2011
WSPCW	Western South Pacific Central Water	34.8-35.5	26.23-26.65		Tsuchiya, 1981; Tomczak and Godfrey, 2003; Qu et al., 2009

Table 2.1b: Abbreviations used for currents, islands, and seas.

Abbreviation	Currents	Abbreviation	Currents
EIC	Equatorial Intermediate Current	NGCU	New Guinea Coastal Undercurrent
EUC	Equatorial Undercurrent	NPC	North Pacific Current
KC	Kuroshio Current	NSCC	North Subsurface Countercurrents
MC	Mindanao Current	SC	Surface Currents
MUC	Mindanao Undercurrent	SEC	South Equatorial Current
NEC	North Equatorial Current	SECC	South Equatorial Countercurrents
NECC	North Equatorial Countercurrents	SSCC	South Subsurface Countercurrents
NGCC	New Guinea Coastal Current	TTWC	Taiwan-Tsushima Warm Current
Abbreviation	Islands	Abbreviation	Seas
PNG	Papua New Guinea	ECS	East China Sea
SI	Solomon Islands	PS	Philippine Sea

The depth below NPTW, ECSSUW, and STMW is occupied by WNPCW that is formed and subducted at the northern subtropical convergence (e.g., Tomczak and Godfrey, 2003). The WNPCW extends from the western part of the North Pacific Subtropical Gyre (Tomczak and Godfrey, 2003) southward to the North and South Subsurface Countercurrents (N/SSCC) (e.g., Rowe et al., 2000; Grenier et al., 2013) and is marked by its characteristic low-salinity and potential density (e.g., Pickard and Emery, 1990; Tomczak and Godfrey, 2003; Talley et al., 2011) (Fig. 2.2a, Table 2.1a).

Its Southern Hemisphere counterpart, the WSPCW, is subducted at the southern subtropical convergence between Tasmania and New Zealand and contributes to the equatorial 13°C water (e.g., Tsuchiya, 1981; Qu et al., 2009). It circulates in the South Pacific Subtropical Gyre and reaches our study area within the SEC (Qu and Lindstrom, 2002). The

WNPCW and WSPCW are recognized at stations 02-15 (200-496 m w. d.) and 15-19 (241-410 m w. d.) respectively, and differ from each other by a higher salinity of WSPCW (Fig. 2.2a, Table 2.1a).

2.2.3. Intermediate waters

North Pacific Intermediate Water (NPIW) is formed east of Japan by mixing of fresh subpolar Oyashio water that contains NPIW source water from the Okhotsk Sea, with more saline subtropical water of the KC (e.g., Yasuda et al., 1996; Yasuda, 2004). The NPIW is then advected eastward along the North Pacific Subtropical Gyre (Sverdrup et al., 1942; Reid 1965; You et al., 2000) (Fig. 2.1b). It reaches the Philippine Sea (PS) by westward transport in the NEC (station 05, 751 m w. d.) (Qu et al., 1999), and flows northeastward in the KC near the Philippine coast (stations 03 and 04, 645-1004 m w. d.) and southward in the MC (Kaneko et al., 2001) (Figs. 2.1a, b). The main part of the NPIW is transported from the MC through the Indonesian Throughflow into the Celebes Sea (Fine et al., 1994; Bingham and Lukas, 1995; Kaneko et al., 2001) (Figs. 2.1a, b). In addition to its characteristic potential and neutral densities, the NPIW is characterized by a salinity minimum of 34.0-34.3 (e.g., You et al., 2003) (Fig. 2.2a, Table 2.1a) and low oxygen concentrations of 50-150 $\mu\text{mol/kg}$ (Bostock et al., 2010).

The Equatorial Pacific Intermediate Water (EqPIW) and Antarctic Intermediate Water (AAIW) are grouped under the overall term 'AAIW' in the following, since EqPIW is mainly a mixture of AAIW and upwelled Pacific Deep Water (PDW) (Bostock et al., 2010). The AAIW is mainly formed in the Southeast Pacific (McCartney, 1982) with additional sources southeast of New Zealand (Slyoan and Rintoul, 2001). It is entrained into the South Pacific Subtropical Gyre and transported as a tongue of high-oxygen and low-salinity westward within the SEC into our study area (stations 18 and 19, 550-800 m w. d.) (Reid, 1965, 1997; Talley, 1999) (Figs. 2.1a, b). The AAIW is carried within the NGCU from the Solomon Sea to the equatorial TWP (stations 15-17, 501-893 m w. d.) (Reid, 1965; Tsuchiya, 1991; Zenk et al., 2005). A part of the AAIW flows from the equator northward along the Philippine coast within the Mindanao Undercurrent (MUC) (e.g., Qu et al., 1998) towards $\sim 12\text{-}15^\circ\text{N}$ (e.g., Lukas et al. 1991; Tsuchiya, 1991; Talley, 1993; Qu et al., 1999; Qu and Lindstrom, 2004). The other part of the AAIW is transported within the equatorial eastward flowing Northern and Southern Intermediate Countercurrents (NICC and SICC, respectively) (Firing et al., 1998; Stramma et al., 2010) or alternatively within alternating eastward and westward mid-depth (~ 1000 m) and deep (~ 1500 m) zonal jets between 10°N - 10°S (Cravatte et al., 2012). In

the East Pacific, a return-flow transports AAIW westwards (e.g., Kawabe and Fujio, 2010) to the northern TWP (stations 11 and 14, 502-799 m w. d.) and the Indonesian Throughflow (e.g., Gordon, 1986). Along our transect, AAIW is confined to the TWP section and differs from NPIW by its higher salinity (Fig. 2.2a).

2.2.4. Deep waters

Pacific Deep Water originates from the upwelling of Southern Ocean sourced Circumpolar Deep Water in the North Pacific which is divided into Upper and Lower Circumpolar Deep Water (UCDW and LCDW, respectively) (e.g., Talley, 2008). The UCDW is transported from the Southern Ocean northwestward by an anticyclonic flow around the South Pacific Subtropical Gyre, reaches our study area in the TWP, and flows into the PS (e.g., Kawabe et al., 2003, 2009; Kawabe and Fujio, 2010) (Fig. 2.1b). In the PS (stations 03-05), part of the UCDW upwells from ~3000 m w. d. to the surface/intermediate layer, while the remaining part of the UCDW flows out at the northern PS (Kawabe and Fujio, 2010) (Fig. 2.1b). It is characterized by a neutral density of $27.55 \text{ kg/m}^3 < \gamma_n < 28.0 \text{ kg/m}^3$ (Garabato et al., 2002) and hence lies approximately in the same density range as PDW ($\gamma_n = 27.70\text{-}28.01 \text{ kg/m}^3$, Macdonald et al., 2009; Talley et al., 2011) (Fig. 2.2b). UCDW is further marked by an oxygen minimum that is inherited from PDW and Indian Deep Water (Callahan, 1972). In our study area, the low-oxygen UCDW, and UCDW/PDW, is observed at all of our deep stations (~1000-3000 m w. d.) based on its neutral density and characteristic high salinity (Figs. 2.2a, b).

The LCDW enters the Southwest Pacific basin with the Deep Western Boundary Current (e.g., Kawano et al., 2006) and spreads into the North Pacific, with a branch flowing into our study area in the PS (Johnson and Toole, 1993; Kawabe et al., 2003; Kawano et al., 2006; Kawabe and Fujio, 2010) (Fig. 2.1b). The LCDW north of 20°S is marked by high oxygen concentrations (up to 158 $\mu\text{mol/kg}$) and a neutral density of $28.0 \text{ kg/m}^3 < \gamma_n < 28.27 \text{ kg/m}^3$ (Orsi et al., 1995; Whitworth et al., 1998). Along our transect, LCDW is found at all deep stations at ≥ 3000 m w. d. (stations 03-14, 17, 18) (Fig. 2.2b).

2.3. Materials and Methods

2.3.1. Samples and onboard procedures

Seawater samples were collected along the cruise transect of SO223T (TransGeoBioOc, R/V *Sonne*, GEOTRACES Process Study GPpr04, September-October 2012) from Busan (South Korea) to Suva (Fiji) at twelve stations and up to 17 depths per

station (Fig. 2.1a). Seawater was sampled from 24 non-metallic free-flushing 12 L Niskin bottles (Ocean Test Equipment Inc.) with PVC sampler body, internal springs made of latex tubing, and Delrin® drain valve with NBR70 (Acrylnitril-Butadien-Kautschuk) O-rings. The Niskin bottles were mounted on a frame equipped with an SBE 9plus CTD profiler (Sea-Bird Electronics Inc.). The CTD data were processed using the Sea-Bird software after McTaggart et al. (2010). Surface water was collected using the ship's contamination-free seawater intake (5 m w. d.). The samples were filtered directly from Niskin bottles (or the seawater tap in the lab) through AcroPak500 (0.8/0.2 μm pore size) filter cartridges into previously acid-cleaned LDPE containers (5-15 L for Nd isotopes) and bottles (250 mL for [Nd]) using Teflon-lined Tygon tubing and PP fittings (for detail see Pahnke et al., 2012). The AcroPak500 filter cartridges were flushed with seawater prior to sample collection and re-used for the same w. d. at each station. For sample processing onboard, we extended a laminar flow bench to create a low particle environment. Most of the samples for Nd isotope analyses were pre-concentrated onboard using a method modified after Shabani et al. (1992) and Jeandel et al. (1998): Samples were acidified to pH of 3.5 using 6 N HCl (optima quality, Fisher Chemical) and passed through SepPak® C₁₈ cartridges (Waters Inc., one cartridge per 5 L) using a peristaltic pump at 20 mL/min. The cartridges were preloaded with 300 mg of 2-ethylhexyl phosphate (Merck). Samples for [Nd] and remaining samples for Nd isotopes were acidified to pH ≤ 2 for further processing in the home laboratory.

For total procedural onboard blanks of Nd isotopes and [Nd], 5 L containers and 250 mL bottles were filled with (1) onboard MilliQ water (18.2 M Ω cm), (2) MilliQ water brought onto the ship from a Millipore system at the ICBM (Institute for Chemistry and Biology of the Marine Environment), and (3) MilliQ water half-and-half from onboard and ICBM, and were treated the same way as the samples excluding filtration.

2.3.2. Lab procedure

2.3.2.1. Neodymium isotopic composition

In the home lab (ICBM), we used 0.01 N HCl to remove remaining Ba from C₁₈ SepPak® cartridges (5 mL for one cartridge, 10 mL for 2-3 cartridges). The rare earth elements (REE) were eluted from C₁₈ SepPak® cartridges with 6 N HCl (35 mL for one cartridge, 50 mL for 2-3 cartridges, modified after Jeandel et al., 1998). Neodymium was separated by two-step column chemistry (Pin and Zalduegui, 1997). The Eichrom® cation exchange resin (TRU-Spec resin, 100-150 μm mesh-size, 0.1 mL resin bed) was used to separate REEs from major element cations. Neodymium was further purified from other REEs

using TrisKem[®] LN-Spec resin (50-100 mesh-size, 0.25 mL resin bed). In preparation for analysis, the Nd cut was treated with a 1:1 mixture of concentrated HNO₃ and H₂O₂ (30%), dried, and then re-dissolved in 2% HNO₃. All chemicals used were of optima quality (Fisher Chemical).

Total procedural onboard and column chemistry blanks were processed the same way as the samples and subsequently spiked with a ¹⁴⁶Nd spike for quantification. The total procedural blanks ranged from 80-85 pg (n = 2) up to 120 pg Nd (n = 1) for onboard and ICBM MilliQ water, which was <3.5% of the minimum concentration (3.5 ng, two samples) and <1.2% of the concentration of typical samples (10 ng Nd). The column chemistry blanks were lower than 1.5 pg Nd (n = 6).

At the ICBM, dissolved Nd isotope ratios were analyzed on a Thermo Scientific Neptune Plus multicollector-inductively coupled plasma-mass spectrometer (MC-ICP-MS) that was coupled to an autosampler (CETAC ASX-112FR) and a desolvation introduction system (CETAC Aridus 2). The measured ¹⁴³Nd/¹⁴⁴Nd ratios were corrected for instrumental mass fractionation using an exponential law and ¹⁴⁶Nd/¹⁴⁴Nd = 0.7219 (O'Nions et al., 1977). The measured and mass bias-corrected ¹⁴³Nd/¹⁴⁴Nd ratios were normalized to 0.512115, the accepted value for the JNdi-1 standard (Tanaka et al., 2000). The JNdi-1 standard and an in-house Nd standard were typically measured at the beginning and end of a session and after every third sample. The external long-term reproducibility derived from 5-20 ppb JNdi-1 measurements of all sessions used for this study was ± 0.000011 (± 0.2 ε_{Nd}, 2σ SD, n = 285). For individual samples, the 2σ standard deviation of the JNdi-1 measurements of the respective session is provided as external reproducibility. Standards and samples were run at the same concentrations. Two samples (GeoB17015-1-2, GeoB17015-1-9+10) with the lowest [Nd] of 3.5 ng Nd were corrected after Vance and Thirlwall (2002) resulting in an external reproducibility of ¹⁴³Nd/¹⁴⁴Nd of ± 0.000011 (± 0.2 ε_{Nd}, 2σ SD, n = 7) that was comparable to the reported external long-term reproducibility of this study.

GEOTRACES intercalibration seawater standards BATS 15 m and 2000 m, and SAFe 3000 m were passed through SepPak[®] C₁₈ cartridges and processed the same way as the samples. Our measured ε_{Nd} values of GEOTRACES intercalibration seawater standards BATS 15 m and 2000 m (n = 2 for each depth) and SAFe 3000 m (n = 3, one re-analyzed sample) were comparable within the uncertainty of the measurements to the GEOTRACES intercalibration values (van de Flierdt et al., 2012) (Table 2.2).

Table 2.2: Dissolved Nd isotope ratios of GEOTRACES intercalibration standards BATS (15 m, 2000 m) and SAFe 3000 m compared to published values of van de Flierdt et al. (2012).

station and sample ID	$^{143}\text{Nd}/^{144}\text{Nd}$ measured	$^{143}\text{Nd}/^{144}\text{Nd}$ normalized ^a	ϵ_{Nd}	$2\sigma^{\text{b}}$
BATS 15 m				
KN193-6-Nd-523_run1	0.512064	0.512189	-8.8	0.2
KN193-6-Nd-523_run2	0.512040	0.512182	-8.9	0.2
average of this study (n = 2)			-8.8	
2 σ SD			0.2	
GEOTRACES intercalibration value (van de Flierdt et al., 2012)			-9.2	
2 σ SD			0.6	
BATS 2000 m				
KN193-6-Nd-320_run1	0.511817	0.511994	-12.6	0.3
KN193-6-Nd-320_run2	0.511833	0.512004	-12.4	0.2
average of this study (n = 2)			-12.5	
2 σ SD			0.3	
GEOTRACES intercalibration value (van de Flierdt et al., 2012)			-13.1	
2 σ SD			0.6	
SAFe 3000 m				
KN195-8-Nd-2151_run1	0.512378	0.512505	-2.6	0.2
KN195-8-Nd-2151_run1 ^c	0.512374	0.512499	-2.7	0.3
KN195-8-Nd-2151_run2	0.512397	0.512522	-2.3	0.2
average of this study (n = 3)			-2.5	
2 σ SD			0.5	
GEOTRACES intercalibration value (van de Flierdt et al., 2012)			-3.2	
2 σ SD			0.5	

^aNormalized to a JNdi-1 value of $^{143}\text{Nd}/^{144}\text{Nd}=0.512115$ of Tanaka et al. (2000).

^bPropagated error is calculated from internal and external errors (2 σ), with external errors deriving from repeated measurements of JNdi-1 standards during each analytical session.

^cRe-analyzed sample.

Total procedural replicates from different stations and w. d. ≥ 696 m (onboard pre-concentration, n = 6) and re-analyzed samples (n = 8) had consistent ϵ_{Nd} values within the analytical uncertainty (Table 2.3). Note that one flagged value of ϵ_{Nd} (sample GeoB17004-1-19+20) is excluded due to a high propagated error (Table 2.3). Lacking a real crossover station, we compared our results from station 15 to those of nearby station EUC-Fe-21 (Grenier et al., 2013; apart by 2°Long., 0°Lat.; samples from 25-355 m w. d.) and found the ϵ_{Nd} values at ≥ 200 m w. d. to be within the analytical uncertainty, except for two shallower depths due to the fact that the samples were taken during different years in an area of very dynamic surface and subsurface circulation.

2.3.2.2. Neodymium concentrations

We used the commercially available automated seaFAST-pico system (Elemental Scientific Inc.) in offline mode for the pre-concentration and purification of Nd (and other REEs) from seawater, and isotope dilution (ID) analysis for the quantification of [Nd] as described in Behrens et al. (2016). Briefly, depending on the expected [Nd], seawater samples

(pH ≤ 2) of ~ 11 mL, or ~ 21 mL for low-concentration samples, were processed once, or up to six times through the seaFAST column and elution fractions were combined for analysis. The samples were weighed into pre-cleaned PFA tubes or HDPE bottles and spiked with a multi-element isotope spike enriched, among others, in ^{145}Nd . The sample-spike mixture was equilibrated for at least 48 hours prior to processing by the seaFAST system. Samples were automatically loaded onto the seaFAST column that is packed with a REE-complexing resin consisting of ethylenediaminetriacetic acid and iminodiacetic acid functional groups (<http://www.icpms.com/pdf/seaFAST-seawater-analysis.pdf>). Each sample was loaded together with MilliQ water and buffer solution (pH = 6.0 ± 0.2) onto the column to ensure a pH of 6. The buffer was prepared from MilliQ water, glacial acetic acid (optima quality, Fisher Chemical), and ammonium hydroxide (ultra-quality, Carl Roth). The column was then rinsed with the buffer solution-MilliQ water mix to remove the seawater matrix. The Nd (and other REE) was eluted with 500 μL of 1.5 N HNO_3 (optima quality, Fisher Chemical) each time resulting in combined elution volumes of up to 3000 μL for low-concentration samples. The samples were collected in pre-cleaned PFA micro vials and manually diluted with MilliQ water (or dried) to volumes of ~ 0.7 -1.2 mL in preparation for analysis. During each seaFAST session, at least three seawater samples of GEOTRACES standards BATS 15 m, 2000 m and/or SAFe 3000 m were processed the same way as the samples (Behrens et al., 2016). At least three procedural lab blanks of 2% HNO_3 (optima quality, Fisher Chemical) were processed during each seaFAST session and subsequently spiked with the multi-element isotope spike for quantification.

Dissolved [Nd] were determined using a Thermo Finnigan Element 2 sector field inductively coupled plasma-mass spectrometer (ICP-MS) at the ICBM that was coupled to an autosampler (CETAC ASX-100) and a desolvation introduction system (CETAC Aridus 2). Oxide formation was monitored with a 100 ng/L tune solution and was always 0.01-0.03% for Ce and Ba. For details on the ID-ICP-MS method see Behrens et al. (2016).

Acid blanks of 2% HNO_3 were measured routinely before each sample and standard to check the instrumental blank. We corrected the sample and standard raw counts for instrumental blanks, which accounted for $\leq 0.9\%$ of the measured sample and standard intensities for Nd, except for two samples (1.1-1.4%).

The accuracy and external long-term reproducibility of our method were assessed from multiple processed and analyzed GEOTRACES seawater standards BATS 15 m and 2000 m, and SAFe 3000 m, respectively (Behrens et al., 2016). Our mean [Nd] of BATS 15 m and 2000 m (13.98 ± 0.44 pmol/kg and 17.26 ± 0.80 pmol/kg, 2σ SD, respectively, Behrens et

al., 2016) agreed well within the uncertainty of the published intercalibration Nd values (14.1 ± 1.2 pmol/kg and 17.3 ± 1.2 pmol/kg, 2σ SD, respectively, van de Flierdt et al., 2012). The external long-term reproducibility of our [Nd] analyses based on replicates of GEOTRACES standard SAFe 3000 m was 2.4% (2σ RSD, $n = 16$, Behrens et al., 2016). If the internal error of a sample was higher than the external error, the internal error is reported (Table 2.3). Our mean [Nd] of SAFe 3000 m (46.4 ± 1.1 pmol/kg, 2σ SD) was within the [Nd] measured on the same sample by three other labs as part of an international intercomparison study (45.9 ± 2.9 pmol/kg, 2σ SD pmol/kg, Behrens et al., 2016) and was comparable to published [Nd] previously analyzed by two other labs (44.4 ± 1.0 pmol/kg, 2σ SD, and 44.4 ± 2.5 pmol/kg, 2σ SE, Pahnke et al., 2012).

Total procedural replicates from different stations and w. d. ≥ 696 m ($n = 6$) and re-processed and re-analyzed samples ($n = 3$) agreed within the external long-term reproducibility of SAFe 3000 m [Nd], except for one re-processed and re-analyzed sample (GeoB17004-1-21+22, Table 2.3). Note that flagged [Nd] are excluded (samples GeoB17004-1-21+22, GeoB17019-1-22+23). These data are considered contaminated because of 2 and 1.4 times higher [Nd] than above and below that depth (Table 2.3). Our [Nd] from station 15 at ≥ 200 m w. d. were within analytical error to those of nearby station EUC-Fe-21 (Grenier et al., 2013).

The average total procedural blank ranged between 0.35 pmol/kg Nd ($n = 2$, onboard blank) and 0.04 pmol/kg Nd ($n = 2$, onboard blank including one re-processed and re-analyzed blank), which is 2.7% and 0.3% of the mean [Nd] of all samples from this study, respectively, and 12.6% and 1.4% of the minimum concentration of the samples (2.77 pmol/kg Nd), respectively. The average procedural lab blank of 2% HNO₃ ($n = 25$) was 0.06 pmol/kg Nd, which is 0.5% of the average [Nd] of all samples from this study, and 2.2% of the minimum concentration of the samples.

2.4. Results

Dissolved ϵ_{Nd} and [Nd] are presented in Figs. 2.3-2.4 and Table 2.3 along with hydrographic properties that were used to identify the sampled water masses (Fig. 2.2). All data are also available on Pangaea (www.pangaea.de) under doi:10.1594/PANGAEA.869418 and the GEOTRACES data center (www.bodc.ac.uk/geotraces). In the following, we describe the dissolved ϵ_{Nd} and [Nd] in the context of the hydrographic setting in our study area. All errors mentioned are 2σ standard deviations (SD).

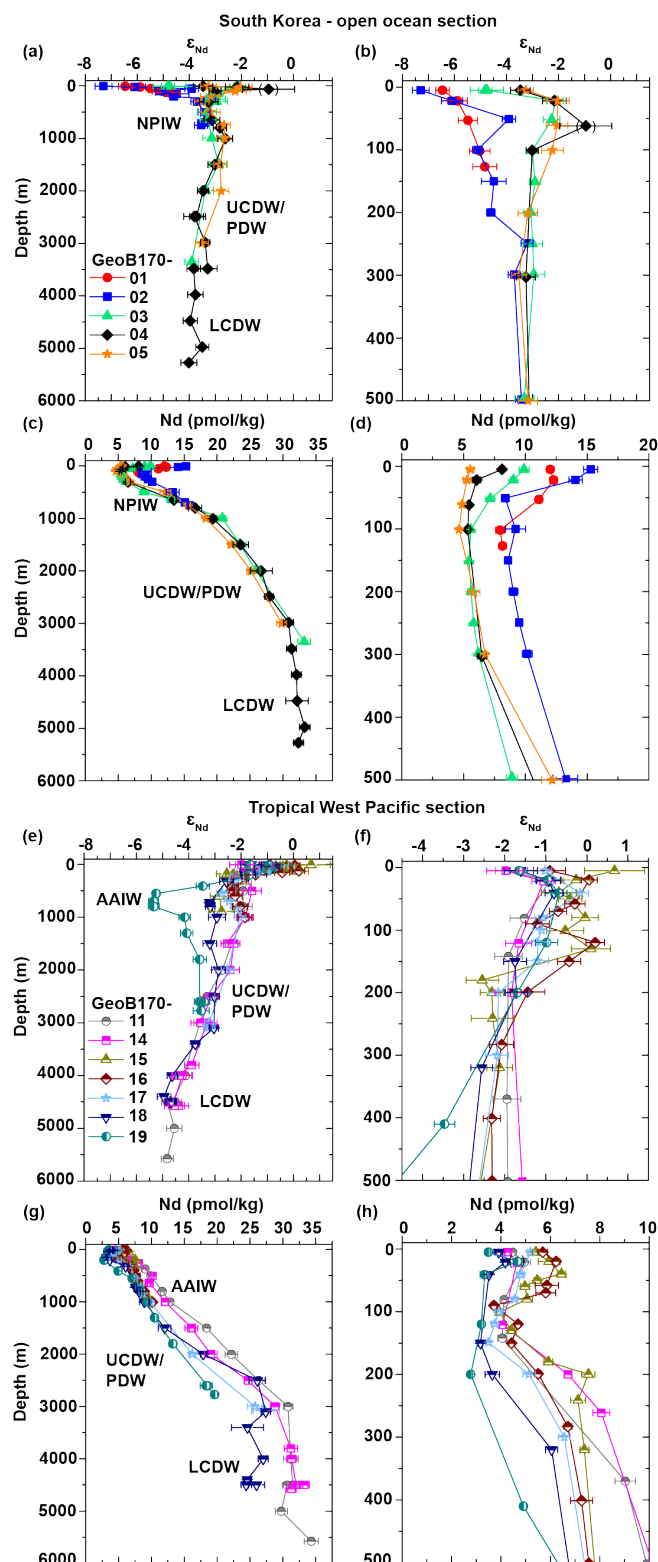


Fig. 2.3. Vertical full water (left panels) and upper water column profiles (right panels) showing the distribution of (a, b, e, f) ϵ_{Nd} and (c, d, g, h) Nd concentration (pmol/kg) of stations from the SKO (01-05) and TWP (11-19) sections, respectively. Error bars denote propagated ϵ_{Nd} error that is calculated from internal and external errors (2σ), with external errors deriving from repeated measurements of JNdi-1 standards during each analytical session, and external error (2σ SD) of Nd concentration that is derived from independently processed GEOTRACES seawater standard SAFe 3000 m (Table 2.3). For abbreviations of water masses see Table 2.1a. Note that bracketed data points are excluded from interpretation (see Method section).

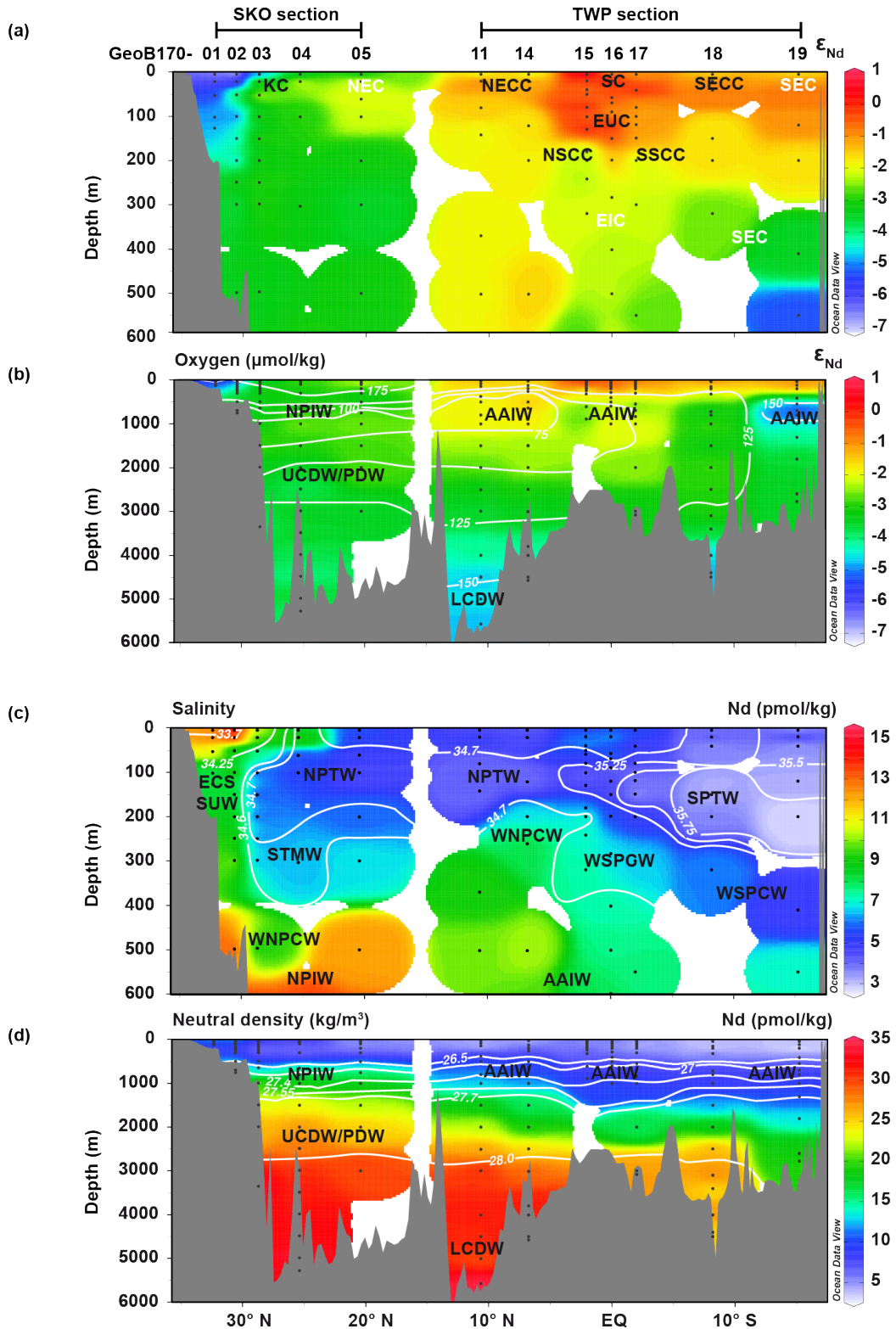


Fig. 2.4. Sections of upper water column (a, c) and full water column (b, d) showing the distribution of (a, b) ϵ_{Nd} and (c, d) Nd concentration (pmol/kg) of stations from the SKO (01-05) and TWP (11-19) sections, respectively. (a) Equatorial westward (white) and eastward (black) flowing surface and subsurface currents (for references see Fig. 2.1). (b, c, d) Oxygen, salinity, and neutral density (kg/m^3) contours are shown in solid white. For abbreviations of currents and water masses see Tables 2.1a, b. Note that flagged data are excluded (see Method section). Sections produced with Ocean Data View (Schlitzer, 2014).

2.4.1. Dissolved ϵ_{Nd} and [Nd] in the context of the hydrographic setting

2.4.1.1. Surface waters

Along the SKO section (stations 01-05), surface waters (upper 50 m w. d.) show a wide range in salinities (33.4-34.8), ϵ_{Nd} (-7.3 to -2.0), and [Nd] (5.27-15.30 pmol/kg) (Figs. 2.2a, 2.3b, d, 2.4a, c). Surface waters change from lowest salinity (33.4-34.2), most unradiogenic ϵ_{Nd} (-5.9 ± 1.1 , $n = 6$), and highest [Nd] (12.19 ± 2.41 pmol/kg, $n = 6$) of this study at stations 01 and 02 near South Korea to high salinity (≥ 34.4 -34.8), more radiogenic ϵ_{Nd} (-4.8 to -2.0), and lower [Nd] (5.27-9.90 pmol/kg) at stations 03-05 in the open ocean. The lowest salinity (33.4) coinciding with the lowest ϵ_{Nd} values (-7.3 and -6.5), and the highest [Nd] (12.01 and 15.30 pmol/kg) of all surface waters in this study are observed at the surface near South Korea (stations 01 and 02), respectively.

Surface waters (upper 50 m w. d.) of the TWP section have high ϵ_{Nd} values of -2.0 to +0.7 and [Nd] of 3.34-6.45 pmol/kg, with low [Nd] at stations 11, 14, 18, and 19 (3.34-4.95 pmol/kg). Surface waters in the equatorial TWP (stations 15-17) show the most radiogenic ϵ_{Nd} values of -1.0 to +0.7 along with highest [Nd] of 4.80-6.45 pmol/kg of the TWP section.

2.4.1.2. Subsurface waters

NPTW and STMW are present at stations 03-14 and 03-05 (61-303 m w. d.), and are marked by a subsurface salinity maximum (34.6-34.7 and 34.7-35.1) and [Nd] minimum (4.06-5.81 pmol/kg), respectively. These waters are clearly distinguishable from ECSSUW and WNPCW at stations 01-02 and 02-15 (100-150 m and 200-496 m w. d.), which show lower salinity (34.4 to 34.6 and 34.5), a higher [Nd] (7.96-9.21 pmol/kg and 6.71-10.15 pmol/kg) and lower ϵ_{Nd} (-5.1 to -4.5 and -3.7 to -1.8), respectively, than NPTW and STMW (Figs. 2.2a, 2.4a, c, Table 2.2). NPTW transported by the KC (101-250 m w. d., stations 03 and 04) has an ϵ_{Nd} signature of -3.0 ± 0.1 ($n = 5$). On the contrary, NPTW flowing within the NEC (61-101 m w. d., station 05) and NECC (142 m w. d., station 11, and 121 m w. d., station 14) shows higher ϵ_{Nd} signatures of -2.2 to -2.1 and -1.9 to -1.7, respectively (Fig. 2.4a). STMW has a homogenous ϵ_{Nd} signature of -3.2 ± 0.3 ($n = 3$) (Table 2.2).

In contrast to NPTW, SPTW is marked by high salinity, low [Nd], and high ϵ_{Nd} ([Nd] = 2.77-4.69 pmol/kg, $\epsilon_{\text{Nd}} = -1.7$ to +0.2). Most extreme salinity and [Nd] are found at the southern stations 17-19 within the SEC (120-200 m w. d.) with values of 35.5-36.2 and 2.77-3.66 pmol/kg, respectively, that go along with the lowest ϵ_{Nd} of SPTW (-1.7 to -1.0). SPTW flowing within the EUC (stations 15: 101-130 m w. d., station 16: 120-150 m w. d.), on the

other hand, has less extreme salinity and [Nd] values and more positive ϵ_{Nd} (salinity = 35.4-35.5, [Nd] = 3.95-4.69 pmol/kg, ϵ_{Nd} = -0.5 to +0.2) (Figs. 2.4a, c).

Below SPTW, the WSPCW is present at stations 15-19 (241-410 m w. d.) and differs from WNPCW by a slightly higher salinity of 34.7-34.9 along with lower [Nd] (4.91-7.12 pmol/kg instead of 6.71-10.15 pmol/kg) (Figs. 2.2a, 2.4c). WSPCW has ϵ_{Nd} values of -3.5 to -2.1 (Fig. 2.4 a).

2.4.1.3. Intermediate waters

NPIW is present at stations 02-05 at 498-1004 m w. d. and differs from AAIW and the overlying subsurface waters by its characteristic salinity minimum of 34.1-34.3 (Fig. 2.2a). It is further characterized by low oxygen concentrations (\sim 53-120 $\mu\text{mol/kg}$), an ϵ_{Nd} signature of -3.5 to -2.6, and [Nd] of 13.10-19.38 pmol/kg (Figs. 2.3a, c, 2.4b, d).

The low salinity (34.4-34.5) and high oxygen concentrations of AAIW (up to 163 $\mu\text{mol/kg}$) coincide with the lowest ϵ_{Nd} (-5.3, $n = 3$) along the entire section and with low mid-depth [Nd] (7.05-8.55 pmol/kg, 550-800 m w. d., station 19) (Figs. 2.2a, 2.3e, g, 2.4b, d). These signatures are quickly eroded towards the equatorial TWP (stations 15-18) reaching lower oxygen concentrations (78-115 $\mu\text{mol/kg}$), and higher ϵ_{Nd} (-3.2 to -2.0), while [Nd] remains low to station 11 (7.56-11.63 pmol/kg). The lowest oxygen concentrations and highest ϵ_{Nd} (-1.9 to -1.6) of AAIW are found in the northern TWP (stations 11 and 14).

2.4.1.4. Deep waters

UCDW/PDW is sampled at \sim 1000-3000 m w. d. with ϵ_{Nd} values of -4.2 to -1.8 that increase towards the north, and [Nd] increasing with depth and from the south to the north

(Figs. 2.4b, d). The mean ϵ_{Nd} of UCDW/PDW is -3.1 ± 0.8 ($n = 8$, stations 03-05) in the SKO section. Near Fiji (station 19), UCDW/PDW has an ϵ_{Nd} of -4.2 to -3.4, while the other stations of the TWP (stations 18, 17, 16, 14, 11) show higher ϵ_{Nd} (-3.3 to -1.8).

LCDW is present at stations 03-14, 17, and 18 at \geq 3000 m w. d. and has constant [Nd] with depth and higher [Nd] in the north than in the south (Figs. 2.3c, g, 2.4d). Oxygen concentrations and ϵ_{Nd} (-4.9 to -3.3) respectively increase and decrease with depth (Figs. 2.3e, 2.4b).

Table 2.3: Hydrographic data, dissolved Nd isotope ratios and Nd concentrations (pmol/kg) for all samples of this study.

Sample ID	Water depth ^a (m)	S ^a	θ ^a (°C)	σ _θ ^a (kg/m ³)	γ _n ^b (kg/m ³)	O ₂ ^a (μmol/kg)	AOU (μmol/kg)	ε _{Nd}	2σ ^c	QF ^d	[Nd]	2σ RSD % ^e	QF ^d	Water mass
<i>Station GeoB17001- (32.3332°N 127.4995°E; MLD: 7-8 m; bottom: 129 m)</i>														
1-surf	5	33.47	27.41	21.433	21.437	182.9	16	-6.5	0.3	1	12.01	2.4	1	SW
1-8	22	33.92	26.83	21.958	21.965	187.3	13	-5.9	0.4	1	12.29	2.4	1	SW
1-6	53	34.02	25.62	22.411	22.419	189.0	16	-5.5	0.4	1	11.09	2.4	1	SW
1-4	102	34.60	18.69	24.791	24.817	153.2	78	-5.0	0.4	1	7.96	4.7	1	ECSSUW
1-1	127	34.58	17.68	25.024	25.052	152.2	83	-4.8	0.5	1	8.15	3.6	1	ECSSUW
<i>Station GeoB17002- (30.5830°N 129.0004°E; MLD: 10-11 m; bottom: 749 m)</i>														
1-surf	5	33.41	28.38	21.073	21.077	181.1	15	-7.3	0.3	1	15.30	3.7	1	SW
1-18+19	22	33.74	28.02	21.440	21.445	180.9	16	-6.1	0.4	1	14.06	3.8	1	SW
1-16+17	51	34.22	27.82	21.865	21.871	179.0	18	-3.9	0.3	1	8.37	3.8	1	SW
1-14+15	100	34.39	22.01	23.749	23.766	159.6	58	-5.1	0.2	1	9.21	8.9	1	ECSSUW
1-12+13	150	34.53	17.30	25.084	25.113	158.0	79	-4.5	0.5	1	8.60	3.0	1	ECSSUW
1-10+11	200							-4.6	0.2	1	9.03	4.1	1	
	201	34.50	14.66	25.657	25.693	155.5	95							
1-8+9	249	34.43	12.64	26.023	26.071	143.7	117	-3.2	0.2	1	9.50	2.4	1	WNPCW
1-7	299	34.35	10.94	26.275	26.337	137.6	133	-3.7	0.2	1	10.15	4.0	1	WNPCW
1-6	498	34.30	7.56	26.787	26.889	99.6	192	-3.4	0.2	1	13.25	7.5	1	NPIW
1-5	696	34.34	5.74	27.060	27.195	79.1	225	-3.4	0.3	1	15.11	2.4	1	NPIW
1-4 ^f	696							-3.4	0.3	1	15.15	3.2	1	
1-1	748	34.35	5.25	27.13	27.28	74.1	234	-3.5	0.3	1	15.81	2.4	1	NPIW
<i>Station GeoB17003- (28.7163°N 131.0852°E; MLD: 11-12 m; bottom: 3357 m)</i>														
1-surf	5	34.02	28.63	21.454	21.460			-4.8	0.3	1	9.90	4.1	1	SW
1-surf ^e	5							-4.8	0.6	1				
	6					180.0	15							
1-22+23	22	34.16	27.56	21.903	21.911	184.0	14	-2.1	0.3	1	9.03	2.4	1	SW
1-20+21	52	34.32	26.13	22.483	22.491	185.5	17	-2.3	0.3	1	7.16	4.8	1	SW
1-18+19	101	34.72	22.06	23.988	24.005	177.3	40	-3.0	0.2	1	5.57	2.4	1	NPTW
1-16+17	151	34.77	20.93	24.338	24.358	172.7	49	-2.9	0.2	1	5.44	2.4	1	NPTW
1-14+15	200	34.75	19.34	24.746	24.770	173.0	55	-3.1	0.3	1	5.62	4.8	1	NPTW
1-12+13	250	34.73	18.67	24.901	24.926	170.2	61	-3.0	0.4	1	5.81	2.4	1	NPTW
1-10+11	298	34.69	17.50	25.154	25.181	171.0	65	-3.0	0.4	1	6.20	2.4	1	STMW
1-9	496	34.42	12.45	26.053	26.104	146.5	115	-3.3	0.4	1	8.91	5.2	1	WNPCW
1-7	645	34.30	8.22	26.691	26.784	109.5	178	-3.3	0.3	1	13.10	3.4	1	NPIW
1-5	993	34.39	3.48	27.356	27.541	57.8	264	-3.1	0.3	1	20.80	2.4	1	NPIW/UCDW
1-4	1490	34.51	2.40	27.548	27.771	72.9	257	-2.9	0.3	1	23.44	4.1	1	UCDW, PDW
1-3	1988	34.58	1.87	27.648	27.900	97.8	237	-3.4	0.3	1	25.88	2.4	1	UCDW, PDW
1-1	3350	34.66	1.27	27.750	28.048	134.1	205	-3.9	0.3	1	33.22	2.9	1	LCDW
<i>Station GeoB17004- (25.3782°N 134.3756°E; MLD: 27-28 m; bottom: 5339 m)</i>														
1-surf	5	34.78	28.65	22.015	22.02	178.7	15	-3.5	0.4	1	8.10	2.4	1	SW
1-21+22	22	34.77	28.65	22.006	22.014	177.6	16	-2.2	0.5	1	6.06	5.4	1	SW
1-21+22 ^h	22										12.1	11	3	
1-19+20	62	34.78	23.01	23.765	23.780	209.5	4	-0.9	1.0	3	5.44	2.4	1	NPTW
1-17+18	101	34.81	20.19	24.570	24.590	196.9	27	-3.0	0.2	1	5.33	3.8	1	NPTW
1-15+16	303	34.68	16.91	25.289	25.318	187.0	52	-3.3	0.4	1	6.48	5.9	1	STMW
1-14	651	34.15	7.59	26.665	26.768	119.5	172	-3.1	0.3	1	13.46	2.4	1	NPIW
1-13	800	34.17	5.26	26.987	27.132	77.5	231	-2.8	0.3	1	16.7	6.1	1	NPIW
1-12	1004	34.33	3.74	27.280	27.459	52.5	267	-2.6	0.3	1	19.38	2.4	1	NPIW
1-11	1501	34.52	2.36	27.558	27.783	74.7	256	-3.0	0.3	1	23.6	5.0	1	UCDW, PDW
1-10	2000	34.59	1.83	27.659	27.914	102.3	233	-3.5	0.2	1	26.7	6.3	1	UCDW, PDW
1-9	2487	34.63	1.53	27.709	27.986	119.0	218	-3.7	0.3	1	27.89	2.4	1	UCDW, PDW
1-9g	2487							-3.8	0.4	1				
1-8	2985	34.64	1.37	27.734	28.024	128.3	210	-3.4	0.2	1	30.85	2.4	1	PDW/LCDW
1-7	3483	34.65	1.28	27.748	28.046	133.8	206	-3.3	0.4	1	31.29	2.4	1	LCDW

Table 2.3 (continued)

Sample ID	Water depth ^a (m)	S ^a	θ ^a (°C)	σ _θ ^a (kg/m ³)	γ _n ^b (kg/m ³)	O ₂ ^a (μmol/kg)	AOU (μmol/kg)	ε _{Nd}	2σ ^c	QF ^d	[Nd]	2σ RSD % ^e	QF ^d	Water mass
1-7 ^e	3483							-3.8	0.3	1				
1-6	3980	34.66	1.23	27.756	28.059	137.2	203	-3.8	0.3	1	32.06	2.4	1	LCDW
1-5	4479	34.66	1.21	27.759	28.065	139.7	200	-4.0	0.3	1	32.14	5.3	1	LCDW
1-4	4977	34.66	1.20	27.760	28.068	140.3	199	-3.5	0.2	1	33.29	2.4	1	LCDW
1-1	5276	34.66	1.20	27.760	28.068	144.0	196	-4.0	0.3	1	32.35	2.4	1	LCDW
<i>Station GeoB17005- (20.4323°N 139.6161°E; MLD: 35-36 m; bottom: 6315 m)</i>														
1-surf	5	34.44	28.71	21.740	21.748			-3.3	0.3	1	5.55	5.0	1	SW
	6					179.7	14							
1-21+22	22	34.45	28.64	21.768	21.776	179.1	15	-2.0	0.4	1	5.27	5.7	1	SW
1-19+20	61	34.92	24.50	23.430	23.441	203.3	4	-2.1	0.4	1	4.88	2.4	1	NPTW
1-13+14	101	34.98	21.10	24.448	24.465	174.1	46	-2.2	0.4	1	4.64	3.4	1	NPTW
1-11+12	201	34.69	17.42	25.180	25.206	179.5	57	-3.2	0.4	1	5.85	8.1	1	STMW
1-9+10	300	34.50	14.56	25.683	25.721	172.2	78	-3.5	0.3	1	6.74	2.4	1	WNPCW
1-8	500	34.13	8.45	26.525	26.615	133.5	153	-3.2	0.4	1	12.16	6.9	1	WNPCW/NPIW
1-7	751	34.30	5.13	27.109	27.256	52.8	256	-2.7	0.3	1	15.59	2.4	1	NPIW
1-6	998	34.45	3.79	27.374	27.550	63.7	255	-2.6	0.3	1	18.30	2.4	1	UCDW
1-5	1500	34.56	2.44	27.580	27.802	86.0	244	-2.8	0.2	1	22.20	2.4	1	UCDW, PDW
1-4	2002	34.61	1.86	27.667	27.920	104.2	230	-2.8	0.3	1	25.14	2.4	1	UCDW, PDW
1-1	3000	34.65	1.40	27.733	28.021	125.9	212	-3.5	0.3	1	29.81	2.4	1	LCDW
<i>Station GeoB17011- (10.6342°N 148.9010°E; MLD: 41-42 m; bottom: 5667 m)</i>														
1-surf	5	34.15	30.11	21.050	21.057			-2.0	0.3	1	4.47	2.4	1	SW
	6					173.4	17							
1-21+22	21	34.14	30.09	21.053	21.061	173.3	17	-0.9	0.3	1	4.95	5.1	1	SW
1-19+20	81	34.96	27.86	22.407	22.414	188.2	8	-1.5	0.3	1	4.12	2.4	1	
1-17+18	142	35.10	23.29	23.923	23.935	165.5	46	-1.9	0.3	1	4.06	4.6	1	NPTW
1-15+16	370	34.48	8.90	26.729	26.817	55.2	228	-1.9	0.3	1	9.03	4.6	1	
1-14	502	34.49	7.21	26.988	27.102	67.2	227	-1.9	0.3	1	9.89	2.4	1	AAIW
1-13	799	34.51	5.27	27.253	27.397	68.2	239	-1.9	0.4	1	11.63	2.4	1	AAIW
1-12	1001	34.53	4.45	27.361	27.520	70.8	243	-1.9	0.3	1	12.84	2.4	1	AAIW/UCDW
1-11	1500	34.58	2.68	27.582	27.794	87.6	240	-2.4	0.2	1	18.39	2.4	1	UCDW, PDW
1-10	2002	34.61	2.02	27.661	27.905	100.6	233	-2.7	0.2	1	22.16	4.3	1	UCDW, PDW
1-9	2502	34.63	1.67	27.704	27.971	110.6	226	-3.3	0.3	1	26.30	3.7	1	UCDW, PDW
1-8	3000	34.65	1.39	27.737	28.025	123.3	215	-3.6	0.2	1	30.79	2.4	1	LCDW
1-7	4002	34.67	1.17	27.766	28.075	139.9	201	-4.2	0.3	1	31.22	3.6	1	LCDW
1-7 ^e	4002							-4.1	0.3	1				
1-6	4502	34.67	1.08	27.776	28.095	148.4	193	-4.6	0.2	1	31.51	2.4	1	LCDW
1-6 ^e	4502							-4.7	0.3	1				
1-5 ^f	4502							-4.8	0.2	1	30.65	2.4	1	
1-4	5001	34.68	1.03	27.783	28.108	155.3	186	-4.6	0.3	1	29.74	3.1	1	LCDW
	5573					157.7	184							
1-1	5574	34.68	1.01	27.786	28.114			-4.8	0.2	1	34.32	3.1	1	LCDW
<i>Station GeoB17014- (6.7842°N 154.1982°E; MLD: 30-31 m; bottom: 4583 m)</i>														
1-surf	5	33.96	30.28		20.858			-2.0	0.5	1	4.27	2.4	1	SW
	6			20.857		174.0	16							
1-21+22	22	34.00	30.25	20.889	20.894	174.9	15	-1.1	0.3	1	4.64	2.4	1	SW
1-19+20	121	34.99	23.48	23.787	23.798	157.2	54	-1.7	0.3	1	4.07	3.0	1	NPTW
1-16+17	200	34.51	12.69	26.076	26.127	80.2	180	-1.8	0.4	1	6.71	2.4	1	WNPCW
1-15	261	34.61	9.97	26.652	26.730	44.2	232				8.06	4.2	1	
1-14	502	34.56	7.80	26.956	27.060	61.4	228	-1.6	0.3	1	10.15	2.4	1	AAIW
1-13	641	34.52	6.65	27.089	27.211	56.4	241				9.61	2.4	1	AAIW
1-13 ^h	641										9.74	3.5	1	
1-12	1002	34.54	4.27	27.390	27.553	70.6	245	-1.8	0.3	1	12.06	4.2	1	UCDW
1-11	1501	34.58	2.87	27.561	27.767	85.1	241	-2.5	0.2	1	16.13	2.4	1	UCDW, PDW
1-10 ^f	1501							-2.3	0.2	1	16.07	6.1	1	

Table 2.3 (continued)

Sample ID	Water depth ^a (m)	S ^a	θ^a (°C)	σ_θ^a (kg/m ³)	γ_n^b (kg/m ³)	O ₂ ^a (μmol/kg)	AOU (μmol/kg)	ϵ_{Nd}	2 σ^c	QF ^d	[Nd]	2 σ RSD % ^e	QF ^d	Water mass
1-9	2001	34.62	2.02	27.665	27.908	99.5	234	-2.4	0.4	1	19.07	4.9	1	UCDW, PDW
1-8	2501	34.64	1.62	27.711	27.980	112.9	224	-3.1	0.3	1	24.71	2.4	1	UCDW, PDW
1-7	3001	34.65	1.41	27.736	28.022	124.0	214	-3.5	0.4	1	28.83	2.4	1	LCDW
1-7 ^e	3001							-3.3	0.4					
1-6	3800	34.66	1.20	27.761	28.065	138.2	202	-3.9	0.3	1	31.21	3.3	1	LCDW
1-5	4001	34.67	1.14	27.768	28.079	142.5	198	-4.4	0.2	1	31.32	2.4	1	LCDW
1-5 ^e	4001							-4.3	0.4					
1-4	4500	34.67	1.05	27.780	28.101	151.6	190	-4.6	0.3	1	32.02	3.2	1	LCDW
1-4 ^h	4500										33.26	2.4	1	
1-3	4573	34.67	1.05	27.780	28.102	152.8	189	-4.4	0.4	1	31.29	2.4	1	LCDW
1-3 ^e	4573							-4.5	0.4	1				
<i>Station GeoB17015- (2.0046°N 157.9976°E; MLD: 19-20 m; bottom: 2695 m)</i>														
1-surf	5	33.65	29.87	20.757	20.758	175.9	15	0.7	0.7	1	5.42	2.4	1	SW
1-23+24	20	33.74	29.66	20.895	20.897	178.5	13	-0.3	0.4	1	5.94	7.2	1	SW
1-21+22	40	34.61	29.58	21.574	21.582	179.1	12	-0.7	0.4	1	6.45	2.4	1	SW
1-19+20	50	34.80	29.62	21.707	21.714	179.2	12	-0.4	0.3	1	5.46	2.4	1	SW
1-17+18	60	35.25	29.32	22.145	22.151	177.8	13				4.97	3.5	1	
1-15+16	80	35.34	28.25	22.569	22.575	143.5	51	0.0	0.3	1	5.06	4.3	1	
1-13+14	101	35.42	26.88	23.075	23.082	133.5	65	-0.5	0.4	1	3.95	3.5	1	SPTW?
1-11+12	130	35.39	25.08	23.608	23.616	125.3	80	0.1	0.5	1	4.42	2.9	1	SPTW
1-9+10	180	34.78	18.04	25.097	25.122	128.5	105	-2.5	0.4	1	5.92	3.0	1	NPTW?
1-7+8	200	34.51	13.05	26.003	26.052	115.3	143	-2.3	0.3	1	7.54	3.5	1	WNPCW
1-5+6	241	34.74	10.68	26.630	26.702	119.7	152	-2.3	0.5	1	7.12	4.2	1	WSPCW
1-3+4	320	34.73	10.34	26.681	26.757	106.8	167	-2.1	0.3	1	7.38	2.4	1	WSPCW?
1-2	602	34.54	6.65	27.101	27.223	81.1	217	-2.8	0.4	1	8.02	2.4	1	AAIW
1-1	893	34.52	5.13	27.275	27.422	93.4	215	-2.7	0.5	1	9.31	4.0	1	AAIW
<i>Station GeoB17016- (0.0001°N 160.0003°E; MLD: 16-17 m; bottom: 2837 m)</i>														
1-surf	5	33.56	29.48	20.821	20.822	177.6	15	-0.9	0.4	1	5.69	3.4	1	SW
1-23+24	20	33.79	29.50	20.985	20.988	178.6	14	0.1	0.2	1	6.23	2.4	1	SW
1-21+22	58	33.89	29.50	21.060	21.064	177.5	15	-0.3	0.2	1	5.86	8.1	1	
1-19+20	70	34.45	29.89	21.349	21.355	178.9	12	-0.7	0.2	1	5.82	6.9	1	
1-17+18	90	35.56	28.71	22.581	22.587	166.7	26	-1.2	0.3	1	3.71	3.2	1	
1-15+16	120	35.36	24.49	23.767	23.775	123.6	84	0.2	0.2	1	4.69	2.4	1	SPTW
1-13+14	150	35.53	21.10	24.872	24.888	121.3	98	-0.4	0.3	1	4.43	2.4	1	SPTW
1-11+12	199	35.09	16.88	25.615	25.646	125.3	113	-1.4	0.4	1	5.50	2.4	1	
1-9+10	283	34.82	11.80	26.490	26.553	127.4	138	-2.1	0.3	1	6.71	2.4	1	WSPCW
1-7+8	401	34.66	9.34	26.796	26.883	95.6	184	-2.3	0.2	1	7.26	6.2	1	
1-5+6	501	34.56	7.63	26.981	27.089	114.3	177	-2.3	0.2	1	7.56	9.3	1	AAIW
1-3+4	599	34.55	6.98	27.066	27.183	77.6	218	-2.2	0.3	1	7.86	2.9	1	AAIW
1-2	799	34.51	5.38	27.246	27.389	90.8	216	-2.0	0.3	1	8.88	2.4	1	AAIW
1-1	1003	34.53	4.46	27.363	27.521	86.0	228	-1.9	0.3	1	10.15	4.4	1	AAIW/UCDW
<i>Station GeoB17017- (2.0021°S 161.9998°E; MLD: 11-12 m; bottom: 3162 m)</i>														
1-surf	5	33.94	30.45	20.774	20.779	173.2	16	-1.0	0.2	1	5.20	2.4	1	SW
1-23+24	41	34.40	30.27	21.182	21.189	176.7	13	-0.2	0.2	1	4.80	3.2	1	SW
1-21+22	80	35.25	29.84	21.970	21.976	178.0	12	-1.1	0.2	1	4.56	2.4	1	
1-19+20	100	35.57	27.92	22.848	22.853	156.9	38	-1.1	0.2	1	3.92	3.9	1	
1-17+18	119	35.57	27.53	22.976	22.981	148.0	49	-1.2	0.3	1	3.75	3.7	1	
1-15+16	149	35.95	24.62	24.172	24.179	122.0	84	-1.2	0.3	1	3.49	2.4	1	SPTW
1-13+14	200	35.21	15.45	26.035	26.074	99.1	146	-2.2	0.2	1	5.14	4.9	1	SPTW/WSPCW?
1-11+12	300	34.76	10.64	26.651	26.725	124.3	147	-2.2	0.3	1	6.57	3.6	1	WSPCW
1-9+10	550	34.54	6.89	27.068	27.187	97.7	198	-2.7	0.2	1	7.59	2.4	1	AAIW
1-7+8	701	34.51	6.11	27.155	27.287	98.0	203	-2.5	0.2	1	8.15	3.3	1	AAIW
1-6	840	34.50	5.22	27.256	27.401	106.9	201	-2.2	0.2	1	8.72	2.4	1	AAIW
1-5	1004	34.51	4.59	27.337	27.493	103.3	209	-2.0	0.2	1	9.81	3.1	1	AAIW/UCDW

Table 2.3 (continued)

Sample ID	Water depth ^a (m)	S ^a	θ ^a (°C)	σ _θ ^a (kg/m ³)	γ _n ^b (kg/m ³)	O ₂ ^a (μmol/kg)	AOU (μmol/kg)	ε _{Nd}	2σ ^c	QF ^d	[Nd]	2σ RSD % ^e	QF ^d	Water mass
1-4	2000	34.62	2.13	27.655	27.893	104.8	227	-2.5	0.2	1	16.22	3.2	1	UCDW, PDW
1-3	2998	34.65	1.48	27.729	28.009	120.9	217	-3.2	0.2	1	25.73	4.5	1	PDW/LCDW
1-2	3082	34.65	1.43	27.734	28.018	122.9	215	-3.3	0.2	1	27.4	7.8	1	LCDW
1-1 ^f	3082							-3.2	0.2	1	27.0	5.8	1	
<i>Station GeoB17018- (8.2019°S 166.0826°E; MLD: 43-44 m; bottom: 4623 m)</i>														
1-surf	5	34.73	29.74	21.614	21.622			-1.6	0.4	1	3.91	3.9	1	SW
	6					174.8	16							
1-23+24	21	34.73	29.71	21.624	21.632	173.4	17	-0.9	0.3	1	4.18	2.4	1	SW
1-21+22	41	34.78	29.59	21.702	21.710	176.1	15	-0.8	0.2	1	3.52	2.4	1	SW
1-19+20	150	36.19	25.30	24.147	24.152	133.2	70	-1.7	0.3	1	3.17	3.2	1	SPTW
1-17+18	200	35.91	21.62	25.018	25.031	127.4	90	-1.7	0.3	1	3.66	8.0	1	SPTW
1-15+16	320	34.89	12.22	26.463	26.524	89.5	173	-2.6	0.3	1	6.05	4.1	1	WSPCW
1-13+14	720	34.49	5.40	27.224	27.368	113.1	194	-3.2	0.2	1	7.57	2.4	1	AAIW
1-11+12	800	34.49	5.02	27.272	27.422	115.4	194	-3.2	0.2	1	8.10	2.4	1	AAIW
1-10	1002	34.52	4.13	27.388	27.555	111.3	205	-2.9	0.3	1	8.92	7.9	1	UCDW
1-9	1502	34.58	2.67	27.578	27.795	118.5	209	-3.2	0.3	1	12.00	8.1	1	UCDW, PDW
1-8	2000	34.62	1.93	27.676	27.925	120.5	213	-2.9	0.3	1	17.89	2.4	1	UCDW, PDW
1-7	2501	34.64	1.59	27.717	27.988	123.0	214	-3.0	0.2	1	26.1	4.8	1	PDW/LCDW
1-6	3100	34.65	1.46	27.731	28.013	126.1	212	-3.0	0.2	1	27.42	2.4	1	PDW/LCDW
1-5	3403	34.66	1.34	27.747	28.038	133.4	206	-3.7	0.1	1	24.6	10	1	LCDW
1-4	4002	34.67	1.17	27.768	28.075	146.7	194	-4.6	0.2	1	27.00	2.8	1	LCDW
1-3	4400	34.67	1.14	27.770	28.080	149.1	192	-4.9	0.3	1	24.59	2.4	1	LCDW
	4498	34.7	1.14	27.771	28.081	148.7	192							LCDW
1-2	4500							-4.7	0.2	1	26.0	4.7	1	
1-1 ^f	4500							-4.7	0.2	1	24.41	3.2	1	
<i>Station GeoB17019- (15.2179°S 173.5187°E; MLD: 103 m; bottom: 2784 m)</i>														
1-surf	5	35.41	27.20	22.959	22.964	182.7	15	-1.7	0.2	1	3.49	2.4	1	SW
1-22+23	20	35.42	27.19	22.971	22.977	182.9	15	-1.0	0.3	1	4.67	3.6	3	SW
1-20+21	41	35.42	27.19	22.970	22.976	183.1	15	-0.7	0.2	1	3.34	5.6	1	SW
1-18+19	120	35.54	26.19	23.382	23.387	176.4	25	-1.0	0.3	1	3.21	2.4	1	SPTW?
1-16+17	200	35.94	22.97	24.653	24.662	143.5	68	-1.7	0.3	1	2.77	2.4	1	SPTW
1-14+15	410	34.79	11.72	26.479	26.545	120.7	145	-3.5	0.3	1	4.91	2.4	1	WSPCW
1-12+13	550	34.48	8.03	26.862	26.966	161.4	127	-5.3	0.1	1	7.05	2.4	1	AAIW
1-10+11	700	34.38	5.70	27.102	27.240	163.2	141	-5.3	0.2	1	7.96	2.4	1	AAIW
1-8+9	800	34.39	4.88	27.207	27.363	156.4	154	-5.3	0.2	1	8.55	2.4	1	AAIW
1-7	1002	34.47	3.70	27.392	27.573	142.8	177	-4.2	0.2	1	9.30	2.4	1	UCDW
1-6	1302	34.53	3.01	27.512	27.721	133.9	191	-4.1	0.2	1	10.47	3.6	1	UCDW
1-5	1802	34.59	2.29	27.623	27.854	131.3	200	-3.6	0.3	1	13.25	4.3	1	UCDW, PDW
1-4	2600	34.64	1.70	27.705	27.968	132.4	203	-3.6	0.2	1	18.48	2.4	1	UCDW, PDW
1-3 ^f	2600							-3.4	0.2	1	18.33	5.1	1	
	2771					132.0	204							
1-2	2772	34.64	1.65	27.710	27.977			-3.5	0.3	1	19.61	2.4	1	UCDW, PDW

Abbreviations used for water masses are listed in Table 2.1a.

MLD: mixed layer depth related to 0.125 kg/m³ density offset from surface (Miller, 1976).

^aHydrographic data (S: Salinity, θ: Pot. temperature, σ_θ: Pot. Density, O₂: Oxygen) measured onboard R/V *Sonne* (cruise SO223T).

^bγ_n: Neutral density derived by Ocean Data View (Schlitzer, 2014).

^cPropagated error is calculated from internal and external errors (2σ), with external errors deriving from repeated measurements of JNdi-1 standards during each analytical session.

^dQF: Quality Flag Scheme after IODE: 1 = good data, 3 = questionable/suspect data

(http://www.iode.org/index.php?option=com_oe&task=viewDocumentRecord&docID=10762).

^eexternal error is derived from independently processed GEOTRACES seawater standard SAFe 3000 m (n = 16), if the internal error of a sample was higher than the external error, the internal error is reported.

^ftotal procedural onboard duplicate for ε_{Nd} and [Nd].

^gε_{Nd} re-analyzed.

^htotal procedural lab duplicate for [Nd].

2.5. Discussion

2.5.1. Continental input

The coincidence of lowest salinity (33.4) with least radiogenic ϵ_{Nd} (as low as -7.3) and highest [Nd] (up to 15.30 pmol/kg) of the entire transect in surface waters near South Korea (stations 01, 02), implies continental Nd input through freshwater discharge. The major freshwater sources in the ECS are river discharge, precipitation, and the TTWC transporting low-salinity water from the South China Sea (Chang and Isobe, 2003). The discharge rate of the South Korean Nakdong River is $\sim 63 \times 10^9 \text{ m}^3/\text{year}$ (Park and Chu, 1991). The Yangtze River, the world's fifth largest river in terms of discharge that drains into the ECS has an annual mean discharge rate of $946 \times 10^9 \text{ m}^3/\text{year}$ (Beardsley et al., 1985). Rare earth element input through SGD from Jeju Island off the southern coast of South Korea has been shown to be comparable to REE fluxes from large rivers ($120 \pm 60 \text{ mol Nd/d}$) (Kim and Kim, 2014). Sediments from South Korean rivers ($\epsilon_{\text{Nd}} \sim -18$ to -13 , Lan et al., 1995) and the Yangtze River ($\epsilon_{\text{Nd}} \sim -11$, Goldstein et al., 1984) are very unradiogenic, suggesting that rivers and SGD (Kim and Kim, 2014) are the source of unradiogenic ϵ_{Nd} and elevated [Nd] in surface waters near South Korea. Amakawa et al. (2004b) also found low surface water salinity along with unradiogenic ϵ_{Nd} (-8.9) and elevated [Nd] (31.5 pmol/kg) in the Japan Sea (station CM-20, Fig. 2.1a) and suggested freshwater input from South Korea and the Yangtze River. The even lower ϵ_{Nd} and higher [Nd] found by Amakawa et al. (2004b) (sampled in July-Aug. 1998) compared to our surface values closest to South Korea (-7.3, 15.30 pmol/kg, sampled in Sept. 2012), may indicate seasonal and interannual changes in river input with a peak discharge of the Yangtze River in June-Aug. (Beardsley et al., 1985). Additionally, variable surface circulation could account for differences in seawater ϵ_{Nd} and [Nd] in this very dynamic area.

2.5.2. Advection and modification of dissolved ϵ_{Nd} and [Nd]

2.5.2.1. Particle scavenging of dissolved Nd within the ECS

At the northernmost stations in the ECS, the rapid vertical decrease in [Nd] in the upper 50-100 m w. d. by up to 4.33 pmol/kg at station 01 and 6.92 pmol/kg at station 02 suggests scavenging of Nd onto suspended particles (Figs. 2.3d, 2.4c). The Yangtze River plume is the world's fourth largest river in terms of solid discharge ($4.86 \times 10^8 \text{ tons/year}$) (e.g., Tian et al., 1993) including a significant discharge of particulate organic carbon ($4.4 \times 10^6 \text{ tons/year}$) (e.g., Milliman and Meade, 1983; Dagg et al., 2004). Hence, this plume is the main source of suspended particles in the ECS (e.g., Hoshika et al., 2003) making it a likely agent

for enhanced scavenging of Nd in this region. The plot of [Nd] as a function of AOU (i.e., a measure of oxygen utilization through the remineralization of organic matter) further visualizes the processes that control the vertical Nd distribution (Fig. 2.5). In Fig. 5, arrow A clearly reflects scavenging of Nd onto organic and inorganic particles with a decrease of [Nd] by up to 6.92 pmol/kg at constant AOU from the surface to the subsurface at the northernmost stations (01 and 02). Coupling [Nd] (7.96-9.21 pmol/kg) to ϵ_{Nd} values of subsurface waters in the ECS (ECSSUW, -5.1 to -4.5) indicates that reversible scavenging with net removal of Nd and isotopic exchange with unradiogenic continent-derived particles (see 5.1.) is the process that controls both [Nd] and ϵ_{Nd} distributions below the surface in the ECS (Figs. 2.3b, d).

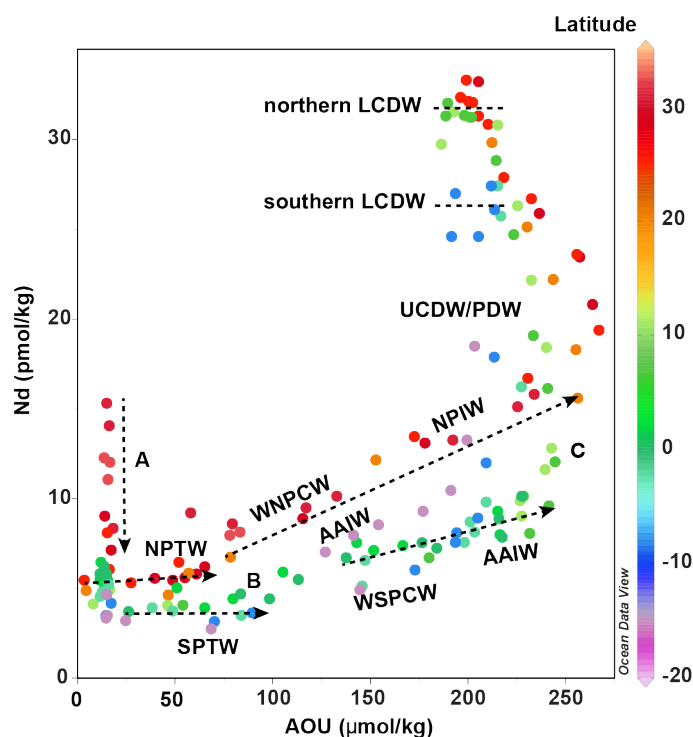


Fig. 2.5. Neodymium concentration vs. apparent oxygen utilization (AOU) for all samples of this study. Colors represent latitude. Behavior of Nd in the water column is (A) scavenging of surface Nd inputs (stations 01, 02); (B) flat trend in NPTW and SPTW with increasing AOU at rather constant [Nd], indicating no Nd release from particles, neither from organic particles through remineralization, nor by desorption from inorganic particles; (C) [Nd] increase along with increasing AOU, suggesting Nd release from organic particles in the upper and intermediate water column through remineralization. Upper and lower arrows follow the trend of individual stations rather than representing the average slope of the respective data. UCDW/PDW: [Nd] increase along with slightly decreasing AOU, indicating Nd release from inorganic particles. Northern and southern LCDW: constant [Nd] along with lower AOU than for UCDW/PDW, suggesting no Nd release from particles. AOU calculated using ODV (Schlitzer, 2014) (see Table 2.3). For abbreviations of water masses see Table 2.1a. Plot produced with Ocean Data View (Schlitzer, 2014).

2.5.2.2. *Tracing small-scale surface and subsurface circulation in the West Pacific with boundary exchange signatures from volcanic margins*

The most conspicuous feature of the ϵ_{Nd} distribution in our study area is the high surface and subsurface water ϵ_{Nd} signature (-2.0 to +0.7) in the TWP (Fig. 2.4a). This signature is more radiogenic than open Pacific surface waters outside the tropical area and indicates regional radiogenic ϵ_{Nd} imprints from basaltic volcanic islands and eastward transport in the equatorial zonal current system (e.g., Grenier et al., 2013). The most radiogenic ϵ_{Nd} (-1.0 to +0.7) and highest [Nd] (4.80-6.45 pmol/kg) of the equatorial surface water at stations 15-17 must be derived from PNG, given that the surface water at these sites is transported within the NGCC along PNG and directly eastward by surface currents (SC, Fig. 2.1a) towards our stations 15-17. These surface currents are marked by the highest surface current velocity found in this area (up to ~0.8 m/s) determined from real time ocean surface current analyses corresponding to the SO223T cruise period (www.oscar.noaa.gov). Less radiogenic ϵ_{Nd} values (-2.0 to -0.7) along with lower [Nd] (3.34-4.95 pmol/kg) are detected in surface waters dominated by the eastward flowing NECC (stations 11, 14), SECC (station 18), and the westward flowing SEC (station 19). The latter flows along Fiji and must pick up the signal there, while the SECC and NECC get their signal from the SI and the Philippine Islands. Similar to surface waters, SPTW at subsurface depth that flows eastward within the EUC (stations 15, 16), carries a radiogenic ϵ_{Nd} signature and elevated [Nd] ($\epsilon_{\text{Nd}} = -0.5$ to +0.2, [Nd] = 3.95-4.69 pmol/kg (Fig. 2.4a). In contrast, SPTW within the westward flowing SEC (stations 17-19) or NPTW in the flow path of the eastward flowing NECC (stations 11, 14), are both marked by less radiogenic ϵ_{Nd} values along with slightly lower [Nd], acquiring their radiogenic imprints from the SI, Fiji, Samoa, or the Philippine Islands ($\epsilon_{\text{Nd}} = -1.7$ to -1.0, [Nd] = 2.77-3.66 pmol/kg and $\epsilon_{\text{Nd}} = -1.9$ to -1.7, [Nd] = 4.06-4.07, respectively) (Figs. 2.1a, 2.4a). These differences in the modified radiogenic ϵ_{Nd} signatures in surface and subsurface waters of the TWP section reflect the larger distance of stations 11 and 14 from the Philippine Islands (Fig. 2.1a), and the higher importance of PNG relative to other volcanic islands such as the SI, Fiji, and Samoa in adding [Nd] and other trace elements (e.g., Radic et al., 2011; Labatut et al., 2014), and modifying ϵ_{Nd} of surface and subsurface waters. This is supported by the study of Grenier et al. (2013), who reported the most radiogenic ϵ_{Nd} (+2.3) and highest [Nd] (8.3 pmol/kg) of all samples from the southwestern equatorial Pacific, close to the coast of PNG near the Sepik River mouth (station EUC-Fe-28, Fig. 2.1a). For the process and source of trace element input to the equatorial TWP, Sholkovitz et al. (1999) suggested the Sepik River as major source based on middle-REE enrichments in the river

water and equatorial surface water. This was however discounted as major source for the central equatorial surface water due to the lack of middle-REE anomalies there and an isotopic composition of Sepik river water that is not radiogenic enough ($\epsilon_{Nd} = -3.1$, Sholkovitz, personal communication, cited in Lacan and Jeandel, 2001). Grenier et al. (2013) therefore suggested that the middle-REE anomalies in surface and subsurface waters of the southwestern equatorial Pacific are caused by submarine weathering of basaltic margin sediments, and that [Nd] coupled to ϵ_{Nd} values indicate boundary exchange. This study and that of Lacan and Jeandel (2001) hypothesized that boundary exchange at volcanic island margins is the main process that controls the distribution of both REE and ϵ_{Nd} in the southwestern and central equatorial Pacific. Boundary exchange occurs at the sediment-ocean interface and links isotopic exchange with dissolved Nd supply (source) and removal (sink) to and from the ocean (Lacan and Jeandel, 2005). Our very radiogenic and only slightly elevated [Nd] data in both surface and subsurface waters support the dominance of boundary exchange over river discharge in this area. Additionally, our data highlight the radiogenic ϵ_{Nd} signal within the eastward flowing currents of the equatorial zonal current system that allows detailed tracing of small-scale circulation in this area (Fig. 2.4a).

Below SPTW, the ϵ_{Nd} signature (-3.5 to -2.1) of WSPCW in the TWP (stations 15-19) may be derived from westward transport of Eastern Equatorial Central Water within the EIC and SEC (Figs. 2.1a, 2.4a) (e.g., Grenier et al., 2013). This water mass acquires its modification through boundary exchange at the Peruvian margin and/or exchange with volcanic particles in the East Pacific ($\epsilon_{Nd} = -3.5$ to -2.2 , $1^{\circ}40'N$ to $6^{\circ}S$, Grasse et al., 2012). In contrast to the ϵ_{Nd} of WNPCW below NPTW at stations 02-05 ($\epsilon_{Nd} = -3.7$ to -3.2), its modified ϵ_{Nd} values of -2.3 to -1.8 within the flow path of the NECC (station 14) and NSCC (station 15) in the TWP suggest a radiogenic fingerprint from the Philippine Islands (Figs. 2.1a, 2.4a). Our data indicate the large spatial extent of radiogenic signatures arising from boundary exchange along the volcanic islands margins in the West and lateral transport of the boundary exchange signature.

In contrast to the low ϵ_{Nd} in surface waters of the SKO section near South Korea (stations 01 and 02), higher ϵ_{Nd} values (up to -2.0) in the upper 50 m at the open ocean stations 03-05 indicate an imprint of a radiogenic ϵ_{Nd} source (Figs. 2.3b, 2.4a). We suggest that surface waters within the NEC are modified near Hawaii and transported westwards into our study area, where the NEC feeds the KC (Figs. 2.1a, 2.4a). Coastal Hawaiian surface waters have ϵ_{Nd} values of up to $+1.4$ (Fröllje et al., 2016). Downstream from Hawaii, surface waters in the NEC are characterized by ϵ_{Nd} values of -1.7 to -1.6 (stations BO-S-5, BO-6, BO-

S-6, Amakawa et al., 2004b) indicating mixing with open ocean Pacific waters. At our station 05, directly in the westward flow path of the NEC, ϵ_{Nd} values (~ -2) are slightly less radiogenic than further upstream (stations BO-S-5 and -6, BO-6 of Amakawa et al., 2004b), and are further mixed with unradiogenic surface waters from the ECS (see stations 01, 02) as the KC, fed by the NEC, flows northeastward towards station 03 ($\epsilon_{Nd} \sim -3$, Figs. 2.1a, 2.4a). This modification in ϵ_{Nd} of the surface waters along the flow path of the NEC and KC is also seen in the underlying NPTW. This water mass within the NEC shows an ϵ_{Nd} of -2.2 to -2.1 (station 05) and reaches ϵ_{Nd} values of -3.0 ± 0.1 ($n = 5$) at stations 03 and 04 within the KC due to mixing with unradiogenic ECSSUW (stations 01, 02, $\epsilon_{Nd} = -5.1$ to -4.5).

2.5.2.3. Advection of dissolved Nd within subsurface water masses

The most striking feature of the [Nd] distribution in the upper 600 m of our transect is the strong correlation of very low [Nd] (2.77-4.69 pmol/kg) with the characteristic high salinity of SPTW (>35.25) in the TWP (Fig. 2.4c). This clearly indicates lateral advection of preformed low [Nd] of SPTW that originates from the oligotrophic South Pacific Subtropical Gyre, where surface water [Nd] is extremely low due to the absence of atmospheric or coastal input (Jeandel et al., 2013). SPTW is transported within the SEC westwards (stations 17-19, [Nd] = 2.77-3.66 pmol/kg) and is fed via the NGCU into the eastward flowing EUC (stations 15, 16, [Nd] = 3.95-4.69 pmol/kg) (Figs. 2.1a, 2.4a, c). Along its way past PNG, SPTW is modified towards the most radiogenic subsurface ϵ_{Nd} values of our study area (up to $\epsilon_{Nd} = +0.2$ to +0.1 at stations 15, 16) and higher [Nd] (0.9-1.2 pmol/kg Nd addition from station 17 to 16). The NGCU was suggested previously as major pathway for waters feeding the EUC (e.g., Tsuchiya et al. 1989; Fine et al., 1994; Grenier et al., 2011). Our data now clearly depict the SPTW as source water and as transport agent of trace elements from PNG into the EUC and hence the equatorial Pacific. Moreover, our data identify the source of the low [Nd] found in subsurface waters in the equatorial West Pacific, that has previously been observed but was left unexplained.

The constant [Nd] of SPTW with depth despite an increase in AOU (i.e., the onset of remineralization, Fig. 2.5, lower arrow B) suggests that [Nd] is unaffected by remineralization and hence release from decomposing organic particles. Instead, this supports the notion of lateral advection of preformed [Nd] by SPTW into our transect. Similarly, NPTW found at stations 03 to 14 shows constant but slightly higher [Nd] than SPTW (Fig. 2.5, upper arrow B). This, and the fact that the [Nd] distribution of NPTW correlates with the characteristic high salinity of NPTW (>34.7) along its flow path (Fig. 2.4c), supports lateral advection of

Nd within NPTW. Moreover, the association of the high salinity of STMW (stations 03-05) with constant [Nd] (5.58-6.48 pmol/kg) and homogenous ϵ_{Nd} indicates transport of both [Nd] and ϵ_{Nd} with STMW ($\epsilon_{\text{Nd}} = -3.2 \pm 0.3$, $n = 3$) (Figs. 2.4a, c).

2.5.2.4. Lateral transport vs. vertical cycling and modification of dissolved ϵ_{Nd} and Nd at intermediate to bottom water depth

In Fig. 2.5, the gradual increase in [Nd] along with an increase in AOU at the depths of WNPCW and NPIW (stations 02-05, upper arrow C) indicates Nd release from sinking organic particles through remineralization and hence a dominant vertical control on Nd cycling within these water masses. The ϵ_{Nd} of WNPCW (-3.7 to -3.2) and NPIW (-3.5 to -2.6) at stations 02-05, however, is typical for these water masses in the North Pacific (Piepgras and Jacobsen, 1992; Amakawa et al., 2009), suggesting no modification by vertical processes. This decoupling is explained by reversible scavenging that leads to a strong vertical change in [Nd], but no or only a slight change in ϵ_{Nd} as particles continuously exchange their isotopic composition with the surrounding seawater (Siddall et al., 2008; Stichel et al., 2015). AAIW and directly overlying WSPCW show low [Nd] (4.91-11.63 pmol/kg) extending from the southern end of our section to at least 10°N and 2°N (stations 11 and 15), respectively. AAIW has low [Nd] due to intense scavenging in the opal belt of the Southern Ocean just south of the formation region of AAIW (Stichel et al., 2012b). In Fig. 2.5, [Nd] within AAIW and WSPCW only increases slightly with increasing AOU resulting in a flat slope (lower arrow C). This suggests reduced influence of remineralization on [Nd] and a dominant lateral control. The low [Nd] of AAIW within the TWP (7.05-11.63 pmol/kg, 501-893 w. d., stations 11-19) is similar to the [Nd] of AAIW just downstream of its formation region in the Southeast Pacific (8.8 pmol/kg, 700 m w. d., station GYR, Jeandel et al., 2013) and thus constant over a large spatial area (Fig. 2.1b). In contrast, the ϵ_{Nd} of AAIW at our southernmost station 19 ($\epsilon_{\text{Nd}} = -5.3$) has been clearly modified from its original signature in the Southern Ocean ($\epsilon_{\text{Nd}} = -8.4$ to -6.6 , Stichel et al., 2012b; Basak et al., 2015), most likely through boundary exchange at volcanic margins. This modification of ϵ_{Nd} must occur in the Fiji-Samoa area, as AAIW just downstream of its formation region (station GYR, Jeandel et al., 2013) and southeast of our southernmost station 19 (station SX-22, Amakawa et al., 2013) has an ϵ_{Nd} of -6.9, some 1.6 ϵ_{Nd} units lower than at station 19 ($\epsilon_{\text{Nd}} = -5.3$) (Figs. 2.1b, 2.3e). Additional ϵ_{Nd} modification of AAIW occurs along its northward flow path, reaching values of -3.2 (station 18) and -2.5 (station 17), indicating boundary exchange at the volcanic island margins of SI and PNG (e.g., Lacan and Jeandel, 2001; Grenier et al., 2013). This modified

equatorial AAIW is carried eastward within the equatorial zonal current system (Fig. 2.1b) and becomes less oxygenated and more radiogenic at the Peruvian shelf ($\epsilon_{\text{Nd}} = -1.6$ at $1^{\circ}40'N$, Grasse et al., 2012). The westward return-flow (Kawabe and Fujio, 2010) of this modified AAIW thus may explain the lowest oxygen concentrations and highest ϵ_{Nd} (-1.9 to -1.6) of AAIW at stations 11 and 14 (Figs. 2.1b, 2.4b).

At UCDW/PDW depth, Fig. 2.5 demonstrates a strong release of [Nd] from sinking lithogenic particles, as [Nd] increases without a change in AOU. In addition to this vertical increase of [Nd] with depth, [Nd] of UCDW/PDW (~ 1000 - 3000 m w. d.) also increase from the south to the north (Fig. 2.4d), reflecting the sluggish deep water circulation and water mass ageing (Talley, 2008). In addition, as part of the UCDW upwells from ~ 3000 m w. d. to the surface/intermediate layer within the PS (stations 03-05) (Kawabe and Fujio, 2010), upwelling of high [Nd] deep water can explain the higher [Nd] of PDW at the northern stations 03-05 at shallower depths (~ 1000 m). We therefore suggest that Nd cycling within UCDW/PDW along the section is controlled by Nd release from lithogenic particles and upwelling in the PS.

The ϵ_{Nd} of UCDW/PDW (~ 1000 - 3000 m w. d.) in the TWP section is modified in its ϵ_{Nd} towards more radiogenic values (-4.2 to -1.8) relative to UCDW near its origin ($\epsilon_{\text{Nd}} = \sim -8$, e.g., Basak et al., 2015). Potential sources of radiogenic ϵ_{Nd} for UCDW at station 19 (-4.2 to -3.4) are the Tonga and Lau Ridges, and active hydrothermal venting in this area (e.g., Lupton et al., 2004, 2015) that has the potential to change the seawater ϵ_{Nd} slightly through exchange with hydrothermal particles (Stichel et al., 2012a; Jeandel et al., 2013). The continuing increase in ϵ_{Nd} of UCDW/PDW towards the north along the TWP section (stations 18-11, Figs. 2.1b, 2.4b) indicates additional boundary exchange at the tropical volcanic island margins (Grenier et al., 2013). With further distance to these volcanic island margins, ϵ_{Nd} of UCDW/PDW (-3.1 ± 0.8 , $n = 8$, stations 03-05) in the SKO section becomes more similar to the ϵ_{Nd} of central and eastern NPDW through mixing (-3.5 ± 0.5 , $n = 15$, Fröllje et al., 2016).

The striking vertical constancy of [Nd] below 3000 m w. d. at all deep stations of our transect (stations 03-14, 17, 18) coincides with the density range and elevated oxygen concentrations of LCDW (see section 2.4.1.4., Figs. 2.3c, g, 2.4b, d). The [Nd] at our southernmost deep station 18 (25.7 ± 2.7 pmol/kg, $n = 6$), is similar to the [Nd] of LCDW in the Southwest Pacific (25.9 pmol/kg, Basak et al., 2015). The AOU decreases with depth within LCDW (Fig. 2.5). The small latitudinal increase in [Nd] within LCDW of 6.6 pmol/kg (station 18 to 04) is therefore likely due to mixing with high-[Nd] UCDW/PDW in the north.

That is, the [Nd] distribution within LCDW along our section is dominantly controlled by lateral advection and water mass mixing, confirming previous results of a clear dominance of advection over vertical cycling of REE in the deep South Atlantic (Zheng et al., 2016).

The ϵ_{Nd} of LCDW is lower than overlying UCDW/PDW and decreases with depth, with lowest values in the deepest samples at stations 18 and 11 of $\epsilon_{\text{Nd}} = -4.9$ to -4.7 (Figs. 2.3e, 2.4b). This isotopic composition is however higher than LCDW in the Southern Ocean ($\epsilon_{\text{Nd}} = -9.1$ to -8.4 , Basak et al., 2015) and at stations SX-20 and -22 ($\epsilon_{\text{Nd}} = -9.2$ to -8.6 , Amakawa et al., 2013) just southeast of our transect (Fig. 2.1b). Hence, substantial boundary exchange with basaltic rocks must occur as LCDW passes through the Samoan Passage (Fig. 2.1b). Towards station 04, ϵ_{Nd} of LCDW shows an increase by ~ 1 ϵ_{Nd} unit, suggesting boundary exchange along the flow path of LCDW to the PS. While [Nd] largely shows conservative behavior at LCDW depth, ϵ_{Nd} is modified along the northward flow path of LCDW.

2.6. Conclusions

We presented dissolved Nd isotopes and concentrations from twelve stations (168 samples) along SO223T (GEOTRACES Process Study GPpr04) in the West Pacific at unprecedented vertical and lateral resolution for this area. The results allow a detailed assessment of the Nd sources and the conservative and non-conservative components of ϵ_{Nd} and Nd concentrations ([Nd]) in the major water masses of the West Pacific.

In detail, we showed that the ECS south of Korea is strongly influenced by trace element input via South Korean and Chinese rivers. This surface input is rapidly scavenged with depth by continent-derived particles. Reversible scavenging with net removal of Nd and isotopic exchange with unradiogenic continent-derived particles is the process that controls both Nd and ϵ_{Nd} distributions below the surface in the ECS.

In the northern West Pacific, modified surface and subsurface water ϵ_{Nd} demonstrates the radiogenic imprint from the Hawaiian Islands upstream and allows tracing their transport within the NEC and KC.

In the tropical West Pacific, boundary exchange at volcanic island margins (the Philippine and Solomon Islands, Papua New Guinea, Fiji, and Samoa) imprints a radiogenic ϵ_{Nd} signature on surface and subsurface waters that act as a fingerprint for the origin and small-scale eastward transport within the equatorial zonal current system. The strong correlation of salinity with [Nd] of SPTW clearly indicates advection of preformed low [Nd] from its formation region in the oligotrophic South Pacific Subtropical Gyre to the tropical West Pacific, while ϵ_{Nd} is modified towards more radiogenic values. This explains the low

subsurface [Nd] found in the tropical West Pacific, and supports the earlier notion of the NGCU as major pathway for SPTW feeding the eastward flowing EUC.

Constant low [Nd] within the flow path of AAIW, from the subtropical Southeast Pacific to the northern tropical West Pacific, indicates the northward advection of preformed low-[Nd] AAIW. The ϵ_{Nd} of AAIW, on the other hand, is modified through boundary exchange at volcanic margins. In contrast, distinct ϵ_{Nd} values of NPIW trace its lateral advection, while [Nd] at NPIW depth shows a clear remineralization signature, suggesting a dominant vertical addition of Nd. Similarly, ϵ_{Nd} at UCDW/PDW depth is indicative of conservative behavior of ϵ_{Nd} within UCDW/PDW in the Northwest Pacific, whereas in the tropical West Pacific, ϵ_{Nd} of UCDW/PDW is modified through boundary exchange at volcanic margins. At UCDW/PDW depth, [Nd] suggests a dominant vertical control, and an increase in [Nd] from south to north due to the sluggish circulation and water mass ageing. At the depth of LCDW (≥ 3000 m w. d.), constant vertical and lateral [Nd] from the southern to northern West Pacific (10°S to 25°N) indicates advection of [Nd] within LCDW and hence conservative behavior of [Nd]. Again, while ϵ_{Nd} of LCDW is clearly less radiogenic than overlying waters, consistent with its source in the Southern Ocean, it is modified towards more radiogenic ϵ_{Nd} in the Samoan Passage and towards the Philippine Sea.

In summary, our results clearly show a dominant conservative component in the distribution of [Nd] in the West Pacific and the strong non-conservative behavior of ϵ_{Nd} due to boundary exchange at volcanic margins. The latter however facilitates small-scale tracing of the complex zonal current system in the equatorial Pacific. Further, our data demonstrate that non-conservative behavior of [Nd] (e.g., in UCDW/PDW and WNPCW, NPIW) is due to vertical overprints through Nd release from organic (intermediate depth, WNPCW, NPIW) and lithogenic (deep depth, UCDW/PDW) particles, while boundary exchange has little effect on [Nd].

2.7. Acknowledgments

We thank the scientific party, particularly the chief scientist Mahyar Mohtadi, the captain, and crew of R/V *Sonne* cruise SO223T. We thank all members of the Max Planck Research Group for Marine Isotope Geochemistry (University of Oldenburg), particularly M. Schulz and P. Böning for their help in the lab. Financial support came from the German Research Foundation (DFG, PA2411/1-1), the Institute for Chemistry and Biology of the Marine Environment (ICBM), and the Max Planck Institute for Marine Microbiology.

3. Rare earth element distributions in the West Pacific: trace element sources and conservative vs. non-conservative behavior

Melanie K. Behrens^a, Katharina Pahnke^a, Ronja Paffrath^a, Bernhard Schnetger^b, Hans-Jürgen Brumsack^b

manuscript prepared for

Earth and Planetary Science Letters

^aMax Planck Research Group for Marine Isotope Geochemistry, Institute for Chemistry and Biology of the Marine Environment (ICBM), University of Oldenburg, Carl-von-Ossietzky-Str. 9-11, 26129 Oldenburg, Germany

^bMicrobiogeochemistry, Institute for Chemistry and Biology of the Marine Environment (ICBM), University of Oldenburg, Carl-von-Ossietzky-Str. 9-11, 26129 Oldenburg, Germany

Abstract

Systematic variations in dissolved seawater rare earth element (REE) patterns and vertical concentration profiles trace sources and processes associated with trace element (TE) input and transport to and within the ocean. Here we report the first vertical and spatial high-resolution profiles of dissolved REE concentrations ([REE]) from twelve stations along a NW-SE transect in the West Pacific. Surface water REE patterns reveal sources of TE input near South Korea and in the tropical equatorial West Pacific via river discharge and exchange at ocean margins, respectively. Positive europium anomalies and middle REE enrichments in surface and subsurface water REE patterns are indicative of TE input from volcanic rocks and fingerprint in detail their small-scale equatorial zonal eastward transport to the iron-limited tropical East Pacific. The low [REE] of North and South Pacific Tropical Waters and Antarctic Intermediate Water are a preformed lateral advected signal, whereas increasing [REE] with depth within North Pacific Intermediate Water result from release of particles. Optimum multiparameter analysis of deep to bottom waters indicates a dominant control of particle fluxes on [REE] in deep water (1500-3000 m water depth) of the tropical West Pacific. At the depth of Lower Circumpolar Deep Water [REE] (≥ 3000 m water depth), on the other hand, are dominated by lateral transport and hence show conservative behavior (73-100%), allowing the northward tracing of LCDW to $\sim 28^\circ\text{N}$ in the Northwest Pacific.

3.1. Introduction

Dissolved rare earth element concentrations ([REE]) in seawater are used to trace sources of micronutrients and other trace elements (TE) to the ocean by exploiting systematic changes and differences in their behavior (e.g. Lacan and Jeandel, 2001; Grenier et al., 2013). The chemically coherent group of REEs shows a characteristic light (LREE) over heavy (HREE) REE fractionation in seawater that is due to preferential adsorption of LREE onto particles and stronger complexation of HREE by carbonate ions (e.g., Cantrell and Byrne, 1987; Elderfield, 1988; Byrne and Kim, 1990; Quinn et al., 2006). Elevated surface water [REE] are typical for local continental input of TEs to the ocean via margin sediments, dust, or rivers (e.g., Greaves et al., 1999; Sholkovitz et al., 1999; Jeandel et al., 2013; Grenier et al., 2013; Osborne et al., 2015; Fröllje et al., 2016). Post Archean Australian Shale (PAAS) normalized positive europium (Eu) anomalies in seawater have been shown to be indicative of input or exchange with basaltic rocks or sediments (e.g., Grenier et al., 2013). Pore fluids from bottom sediments have recently been hypothesized as REE source to deep waters in some areas of the ocean (Haley et al., 2004; Abbott et al., 2015a) but not in others (Yang and Haley, 2016). The long-standing interpretation of the distribution of REEs in seawater, with generally low concentrations at the surface and increasing concentrations with depth, is therefore the dominance of vertical processes (input, scavenging, release) (e.g., Elderfield and Greaves, 1982; Alibo and Nozaki, 1999). Several recent studies using high-resolution transects of [REE] through the ocean, have suggested an additional lateral control on REE distributions. The evidence came from nearly constant vertical neodymium concentrations ([Nd]) at the depth of vigorously flowing North Atlantic Deep Water (Stichel et al., 2015; Lambelet et al., 2016), and high [Nd] shoaling upwards with the density surfaces in the southern South Pacific and Atlantic (Basak et al., 2015; Hathorne et al., 2015). Using a zonal [REE] section in the South Atlantic, Zheng et al. (2016) provided evidence for a dominance of water mass mixing on REE distributions. Due to the potential of dissolved seawater [REE] to identify sources and processes associated with TE input, scavenging, and transport, REEs are a diagnostic tool to better understand TE cycling in the ocean (e.g., Lacan and Jeandel, 2001; Grenier et al., 2013; Hathorne et al., 2015; Osborne et al., 2015).

Trace element cycling in West Pacific is of particular interest as this key study area is 1) surrounded by volcanic island margins that are thought to be an important source of micronutrients and other TEs to the ocean, and 2) connected to the iron-limited high-nutrient, low-chlorophyll (HNLC) area in the East Pacific through the equatorial zonal current system

that may act as a conduit of micronutrients and other TEs from the tropical West Pacific to the HNLC area in the East Pacific (e.g., Lacan and Jeandel, 2001, Slemons et al., 2010; Radic et al., 2011; Grenier et al., 2013).

Here, we present the first vertically and spatially high-resolution transect of dissolved [REE] from the West Pacific between South Korea and Fiji (Fig. 3.1a). We provide a detailed characterization of the relative importance of the different sources and processes that control the seawater REE cycling in the West Pacific and highlight the clear depiction of the small-scale equatorial zonal transport in REE distributions.

3.2. Study area and circulation

The study area and circulation are presented in detail in Behrens et al. (in prep.). Briefly, the NW-SE transect from South Korea to Fiji comprises twelve full water column stations that were sampled during cruise SO223T (TransGeoBioOc) with R/V *Sonne* (GEOTRACES Process Study GPpr04) from September to October 2012. For ease of reference to the different stations, we divide the transect into two sections: the South Korea to open ocean section (SKO) that includes stations GeoB17001 to GeoB17005 (GeoB17001 to GeoB17005 referred to as stations 01-05), and the tropical West Pacific section (TWP) that includes stations GeoB17011 to GeoB17019 (GeoB17011 to GeoB17019 referred to as stations 11-19) (Figs. 3.1a, b).

The surface (upper 50 m water depth, w. d. in the following) and subsurface circulation is dominated by the North Equatorial Current (NEC) and the Kuroshio Current (KC) in the study area of the SKO section (stations 03-05), and by currents of the complex equatorial zonal current system in the TWP (stations 15-19): the North Equatorial Countercurrent (NECC), surface currents (SC), the Equatorial Undercurrent (EUC), the Equatorial Intermediate Current (EIC), the South Equatorial Countercurrent (SECC), and the South Equatorial Current (SEC) (e.g., Wyrтки and Kilonsky, 1984; Fine et al., 1994; Reid, 1997; Tomczak and Godfrey, 2003; Grenier et al., 2011; Talley et al., 2011; SC: determined from real time ocean surface current analyses for the time of the SO223T cruise, <http://www.oscar.noaa.gov/>) (Fig. 3.1a).

Subsurface waters are North and South Pacific Tropical Water (NPTW and SPTW) at 61-250 m and 101-200 m w. d. in our study area, respectively. NPTW differs from SPTW by its less pronounced subsurface salinity maximum (e.g., Qu et al., 1999). It originates in the central subtropical North Pacific (Cannon, 1966) and is transported by the NEC and the KC towards stations 03-05 (e.g., Fine et al., 1994; Qu et al., 1999; Suga et al., 2000) and the

Mindanao Current (MC), that feeds the NECC, towards stations 11 and 14 (e.g., Fine et al., 1994; Kashino et al., 1996). SPTW originates in the oligotrophic South Pacific Subtropical Gyre (e.g., O'Connor et al., 2005; Qu et al., 2013). It flows from its formation region westwards within the SEC into our study area (stations 17-19), and further within the New Guinea Coastal Undercurrent (NGCU) along the coast of PNG and finally turns eastward within the EUC (stations 15 and 16) (e.g., Tsuchiya et al., 1989; Fine et al., 1994; Grenier et al., 2011).

North Pacific Intermediate Water (NPIW) flows along the North Pacific Subtropical Gyre (Sverdrup et al., 1942; Reid, 1965; You et al., 2000) and is found within the NEC and the KC (stations 03-05, at 645-1004 m w. d.) in our study area (e.g., Qu et al., 1999) (Figs. 3.1a, b). Antarctic Intermediate Water (AAIW), originating in the Southeast Pacific, is entrained into the South Pacific Subtropical Gyre and flows within the SEC into our study area (stations 18 and 19, at 501-893 m w. d.) (McCartney, 1982), where it reaches the equatorial TWP via the NGCU (stations 15-17) (e.g., Tsuchiya, 1991; Zenk et al., 2005) (Figs. 3.1a, b). In the equatorial TWP, AAIW is transported eastward and then returns westwards to the northern TWP (stations 11 and 14) (e.g., Kawabe and Fujio, 2010) (Fig. 3.1b).

The deep water circulation in our study area is marked by the northward flow of Southern Ocean sourced Upper and Lower Circumpolar Deep Water (UCDW and LCDW, respectively) and the southward flow of North Pacific Deep Water (NPDW) (e.g., Kawabe and Fujio, 2010) (Fig. 3.1b).

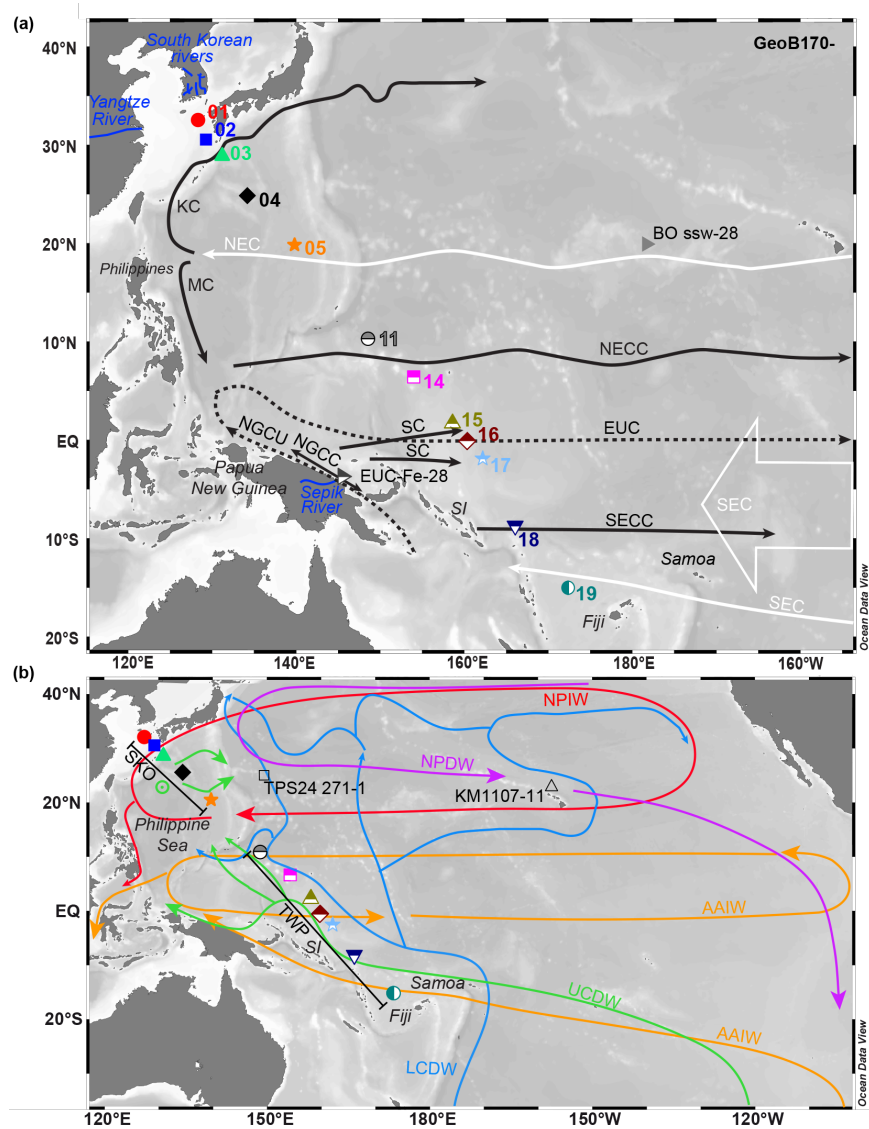


Fig. 3.1. Maps modified from Behrens et al. (in prep.) showing stations 01-05 and 11-19 from the SKO (South Korea - open ocean) and TWP (tropical West Pacific) sections along with published stations discussed in the text. TPS24 271-1 (Piepgras and Jacobsen, 1992); BO ssw-28 (Hongo et al., 2006); EUC-Fe-28 (Grenier et al., 2013); KM1107-11 (Fröllje et al., 2016). (a) Schematic major surface (solid arrows) and subsurface (dashed arrows) westward (white) and eastward (black) currents of the study area (e.g., Wyrтки and Kilonsky, 1984; Fine et al., 1994; Reid, 1997; Tomczak and Godfrey, 2003; Grenier et al., 2011; Talley et al., 2011; and determined from real time ocean surface current analyses corresponding to the SO223T cruise period, <http://www.oscar.noaa.gov/>). (b) Schematic West Pacific intermediate and deep water circulation (after Kawabe and Fujio, 2010). Antarctic Intermediate Water (AAIW), North Pacific Deep Water (NPDW), North Pacific Intermediate Water (NPIW), Lower Circumpolar Deep Water (LCDW), Upper Circumpolar Deep Water (UCDW). Green circle with a center point indicates upwelling of UCDW to the surface/intermediate layer (Kawabe and Fujio, 2010). Equatorial Intermediate Current (EIC), Equatorial Undercurrent (EUC), Kuroshio Current (KC), Mindanao Current (MC), New Guinea Coastal Current (NGCC), New Guinea Coastal Undercurrent (NGCU), North Equatorial Current (NEC), North and South Equatorial Countercurrents (NECC and SECC), Surface Currents (SC), South Equatorial Current (SEC). Solomon Islands (SI). Four major South Korean rivers after Lan et al. (1995). Map was produced using Ocean Data View (Schlitzer, 2014).

3.3. Materials and Methods

3.3.1. Onboard procedures

Seawater was sampled for the determination of dissolved nutrient (phosphate, nitrate, silicate) and REE concentrations at twelve full water column stations. Details of onboard seawater sampling followed established GEOTRACES protocols (for details see Pahnke et al., 2012; <http://www.geotraces.org/images/stories/documents/intercalibration/Cookbook.pdf>) and are described in Behrens et al. (in prep.). Briefly, seawater samples were filtered directly from Niskin bottles (or the ship's contamination-free seawater intake in the lab for the collection of surface water) through AcroPak500 (0.8/0.2 μm pore size) filter cartridges into previously acid-cleaned 20 mL HDPE bottles (for nutrient analysis) or 250 mL LDPE bottles (for REE analysis) using Teflon-lined Tygon tubing and PP fittings. Seawater samples were poisoned with 3.5% mercury chloride for nutrient analysis or acidified to $\text{pH} \leq 2$ using 6 N HCl (optima quality, Fisher Chemical) for REE analysis. All samples were stored onboard for further processing in the home laboratory at the ICBM (Institute for Chemistry and Biology of the Marine Environment). Total procedural onboard blanks of (1) onboard MilliQ water (18.2 $\text{M}\Omega \text{ cm}$), (2) MilliQ water brought onto the ship from a Millipore system at the ICBM, and (3) MilliQ water half-and-half from onboard and ICBM were also acidified to $\text{pH} \leq 2$ using 6 N HCl and stored onboard.

3.3.2. Nutrient and REE analysis

At the ICBM, nutrients were measured photometrically using a Multiscan GO Microplate Spectrophotometer (Thermo Scientific) and an EasyChem Plus discrete analyzer (AMS-SYSTEAM). Nitrate (NO_3^-) was determined from nitrite and NO_x^- , following the method described by Schnetger and Lehnert (2014). Reference solutions of known concentrations were used to check for precision and accuracy (<10%).

Seawater REEs were pre-concentrated and purified using the automated seaFAST-pico system in offline mode (Elemental Scientific Inc., Nebraska, USA) and quantified by isotope dilution (ID) analysis as described in Behrens et al. (2016). Briefly, depending on the expected [REE], seawater samples ($\text{pH} \leq 2$) of ~11 mL, or ~21 mL for low-concentration samples, were processed once, or up to 6 times through the seaFAST column and elution fractions were combined for analysis. The samples were weighed into pre-cleaned PFA tubes or HDPE bottles and spiked with a multi-element spike. After equilibration for at least 48 hours, the sample-spike mixture was placed into the seaFAST autosampler and automatically mixed with a buffer solution ($\text{pH} = 6$) and MilliQ water and passed through the seaFAST

column (REE-complexing resin of ethylenediaminetriacetic acid and iminodiacetic acid functional groups). The buffer solution ($\text{pH} = 6.0 \pm 0.2$) was prepared from MilliQ water, glacial acetic acid (optima quality, Fisher Chemical), and ammonium hydroxide (ultra-quality, Carl Roth). The seawater matrix was washed off the column with a buffer solution-high purity water mix before the REEs were eluted with 500 μL of 1.5 N HNO_3 (optima quality, Fisher Chemical) each time resulting in combined elution volumes of up to 3000 μL for low-concentration samples. The REE fractions were collected in pre-cleaned PFA micro vials and manually diluted with MilliQ water (or dried) to volumes of ~ 0.7 -1.2 mL in preparation for the measurement.

GEOTRACES seawater standards (BATS 15 m, 2000 m, and SAFe 3000 m) (Pahnke et al., 2012; van de Flierdt et al., 2012; Behrens et al., 2016) were processed the same way as the samples. Procedural lab blanks of 2% HNO_3 (optima quality, Fisher Chemical) were processed during each session and subsequently spiked with a diluted multi-element REE spike for quantification.

At the ICBM, the dissolved [REE] were measured using a Thermo Finnigan Element 2 sector field inductively coupled plasma-mass spectrometer (ICP-MS) (Behrens et al., 2016). The instrument was coupled to an autosampler (CETAC ASX-100) and a desolvation introduction system (CETAC Aridus 2) that used a nitrogen-argon gas mixture to reduce oxide formation rates to a negligible level (always 0.01-0.03% for cerium (Ce) and barium (Ba)). Instrumental blanks of 2% HNO_3 were measured and subtracted for each sample. The accuracy and external long-term precision of our method were assessed by repeated processing and analysis of GEOTRACES seawater standards BATS (15 m, 2000 m) and SAFe 3000 m, respectively (Behrens et al., 2016). The average [REE] obtained for BATS 15 m and 2000 m showed agreement within the 2σ SD confidence interval of the published GEOTRACES intercalibration (van de Flierdt et al., 2012). The external long-term precision of our [REE] analyses based on replicates of SAFe 3000 m was $\leq 3.9\%$ for all REEs, except for Ce (39%) and Gd (6.2%) (2σ RSD, $n = 16$) (Behrens et al., 2016). Total procedural replicates from different stations and water depths (≥ 696 m, $n = 6$) and re-processed and re-analyzed samples ($n = 3$) had [REE] that agreed within the external long-term precision of SAFe (3000 m), except for one re-processed and re-analyzed sample (GeoB17004-1-21+22), which is probably due to contamination in the laboratory (supplementary Table S3.2).

The average total procedural onboard blank was $\leq 3.3\%$ for LREEs and $\leq 1.4\%$ for HREEs, except for La (4.1%) and Ce (24%) ($n = 4$, onboard blank including one re-processed and re-analyzed blank) of the average sample concentration. The average procedural lab blank

of 2% HNO₃ was ≤0.5% for all REEs, except for Ce with 4.3% (n = 25) of the average sample concentration.

3.3.4. Optimum Multiparameter Analysis (OMPA)

In order to assess the relative importance of the processes involved in oceanic geochemical REE cycling in the deep water column (≥1500 m w. d.) i.e., conservative water mass mixing/transport vs. non-conservative processes such as particle scavenging and REE release, we used optimum multiparameter analysis (OMPA). The OMPA was based on the model described in Tomczak and Large (1989), Karstensen and Tomczak (1998) and Hupe and Karstensen (2000) and used the MATLAB code of Karstensen and Tomczak (1998), openly available under <http://omp.geomar.de/node6.html>. The parameters used were potential temperature, salinity, oxygen, phosphate, nitrate, and silicate concentrations and weighted using the scheme described by Tomczak and Large (1989). We further used three water mass end-members (LCDW, UCDW, NPDW), whose end-member parameters were taken from areas north and south of our study area where deep waters enter or exit the West Pacific. The water masses were identified based on their characteristic hydrographic properties and the end-member parameters were selected from the World Ocean Circulation Experiment (WOCE, <http://www.ewoce.org>). The [Nd] end-members were taken from stations with published values close to the stations used for the hydrographic end-member parameters. Table 3.1 lists the average values of all end-member parameters used along with the respective locations and references. Nutrient data from cruise SO223T were supplemented with data from WOCE at depths where our data showed outliers towards very low concentrations most likely due to delayed sampling from the Niskin bottles at high tropical temperatures (supplementary Table S3.1).

The OMPA was limited to deep water samples (≥1500 m w. d.) along our NW-SE transect, and hence did not include shallow stations 01-02 and 15-16. We focused on the deep water column because of the difficulty of resolving subsurface and intermediate water mass end-members.

The resulting calculated conservative water mass mixing fractions of our deep water samples (see results section) were then used to calculate the dissolved [Nd] composition along our transect that is expected from conservative water mass mixing alone. The difference between the measured and modeled [Nd] hence represents the non-conservative component controlled by Nd removal or addition.

Table 3.1: Water mass end-member characteristics for each parameter along with locations and references.

water mass end-member	NPDW	UCDW	LCDW
Potential temp. (°C) ^a	2.30	2.50	0.99
Salinity ^a	34.56	34.60	34.70
Oxygen (μmol/kg) ^a	83.4	139.9	188.1
Phosphate (μmol/kg) ^a	2.80	2.53	2.29
Nitrate (μmol/kg) ^a	39.6	36.4	33.5
Silicate (μmol/kg) ^a	144.3	109.4	124.8
Location and Reference	23.83°-25.17°N/138.57°-164.98°E, WOCE P03W, P10, P13	8.91°-17.50°S/176.99°-163°W, WOCE P15S, P21W, P31	10.07°-17.50°S/176.71°-163°W, WOCE P15S, P21W, P31, GEOSECS Stations 259, 263
Nd (pmol/kg) ^b	28.0	14.2	24.7
Location and Reference	TPS24 271-1 (Piepgras and Jacobsen, 1988)	SX20 and SX22 (Amakawa et al., 2013)	SX20 and SX22 (Amakawa et al., 2013)

NPDW: North Pacific Deep Water, UCDW and LCDW: Upper and Lower Circumpolar Deep Water.

^aaverage value (n = 7-8).

^baverage value (n = 2-6).

3.4. Results

3.4.1. Dissolved REE concentrations

Data are listed in the supplementary Table S3.2 and are available on Pangaea (www.pangaea.de) under doi:10.1594/PANGAEA.871176 and the GEOTRACES data center (www.bodc.ac.uk/geotraces). Vertical full water and upper water column profiles (Figs. 3.2a, b) and sections (Figs. 3.3a-d) of dissolved praseodymium and erbium concentrations ([Pr] and [Er]) are shown as representative for LREE and HREE distributions, respectively. We do not describe the vertical profile and full water column section of middle REEs (MREE) in detail due to their intermediate behavior. The Ce profiles vary significantly due to the high analytical uncertainty (see section 3.3.2. and Behrens et al., 2016) and are therefore not discussed.

The vertical profiles show elevated [REE] at the surface compared to the subsurface (Figs. 3.2a, b). Highest surface water [REE] of all stations in this study are found at stations 01 and 02 closest to South Korea ([Pr] = 2.90 pmol/kg and 3.71 pmol/kg, [Er] = 4.13 pmol/kg and 5.24 pmol/kg, respectively, supplementary Table S3.2) (Fig. 3.2a). In the TWP, on the other hand, surface water, SPTW (120-200 m w. d., stations 17-19), and NPTW (121-142 m w. d., stations 11-14) show the lowest [REE] of our study ([Pr] = 0.57-1.21 pmol/kg, [Er] = 1.30-1.82 pmol/kg) (supplementary Table S3.2). At the equatorial stations 15 and 16, surface and subsurface [REE] are slightly elevated over those just north and south of the equator in the TWP ([Pr] = 0.91-1.45 pmol/kg, [Er] = 1.62-2.21 pmol/kg, Figs. 3.3a, c). At intermediate depths in the SKO section, LREE concentrations ([LREE]) of NPIW increase with depth, whereas low [LREE] of AAIW in the TWP section are laterally and vertically constant (Figs.

3.3b, d). Deep water [REE] increase with depth (1000-3000 m w. d.) at all stations and along the transect from south to north, with highest [REE] found in the deep North Pacific (Figs. 3.3b, d). Below 3000 m w. d., [REE] of LCDW are constant, except for near-bottom water at station 11 (93 m above the bottom) with slightly elevated [LREE], and only increase by 1.81 pmol/kg in [Pr] and 0.92 pmol/kg in [Er] from south to north (station 18 to 04) (Figs. 3.2a, b, 3b, d).

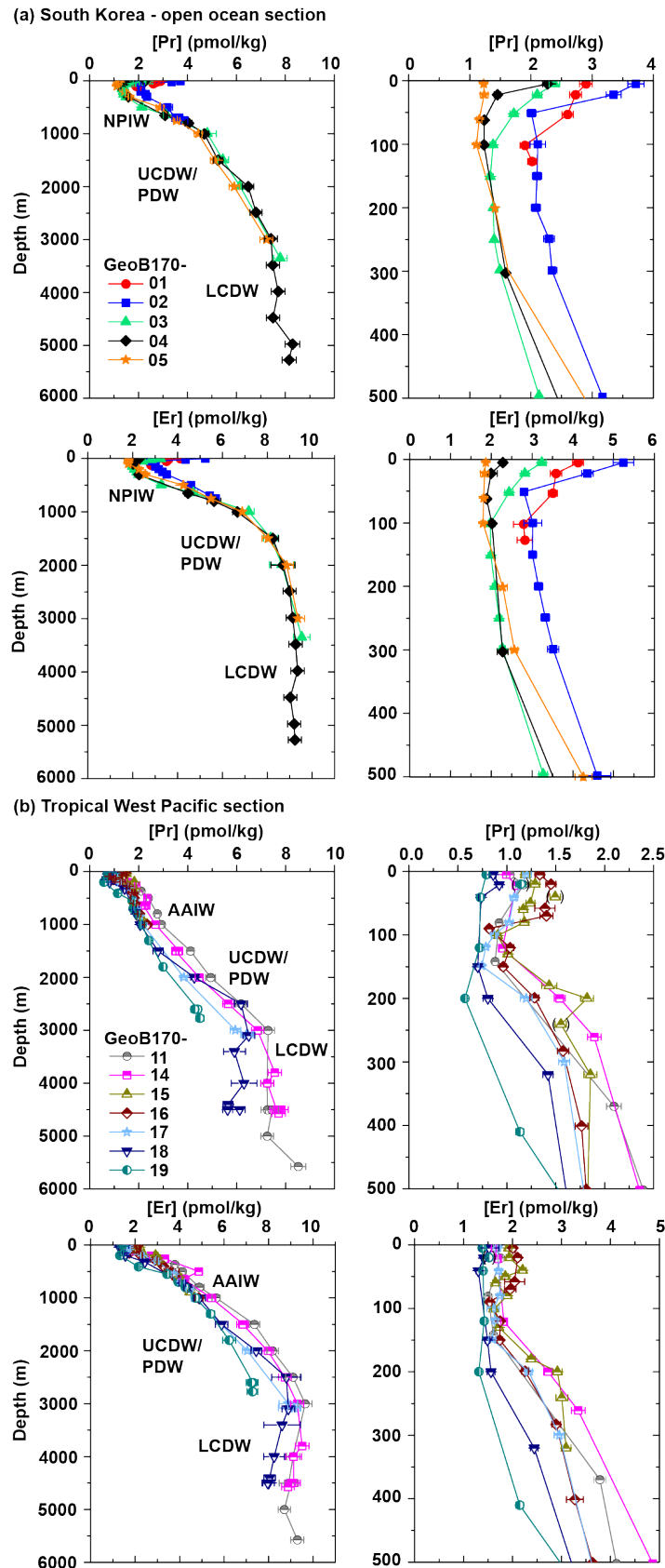


Fig. 3.2. Selected vertical full water (6000 m) and upper water column profiles (≥ 500 m) of Pr and Er concentrations (pmol/kg) representing LREEs and HREEs, respectively, from stations (a) 01-05 of the SKO, and (b) 11-19 of the TWP sections. Error bars denote 2σ SD estimated by repeated processing and analysis of GEOTRACES seawater standard SAFe 3000 m. Note that bracketed data points are flagged values and excluded from interpretation. For abbreviations of water masses see Fig. 3.1.

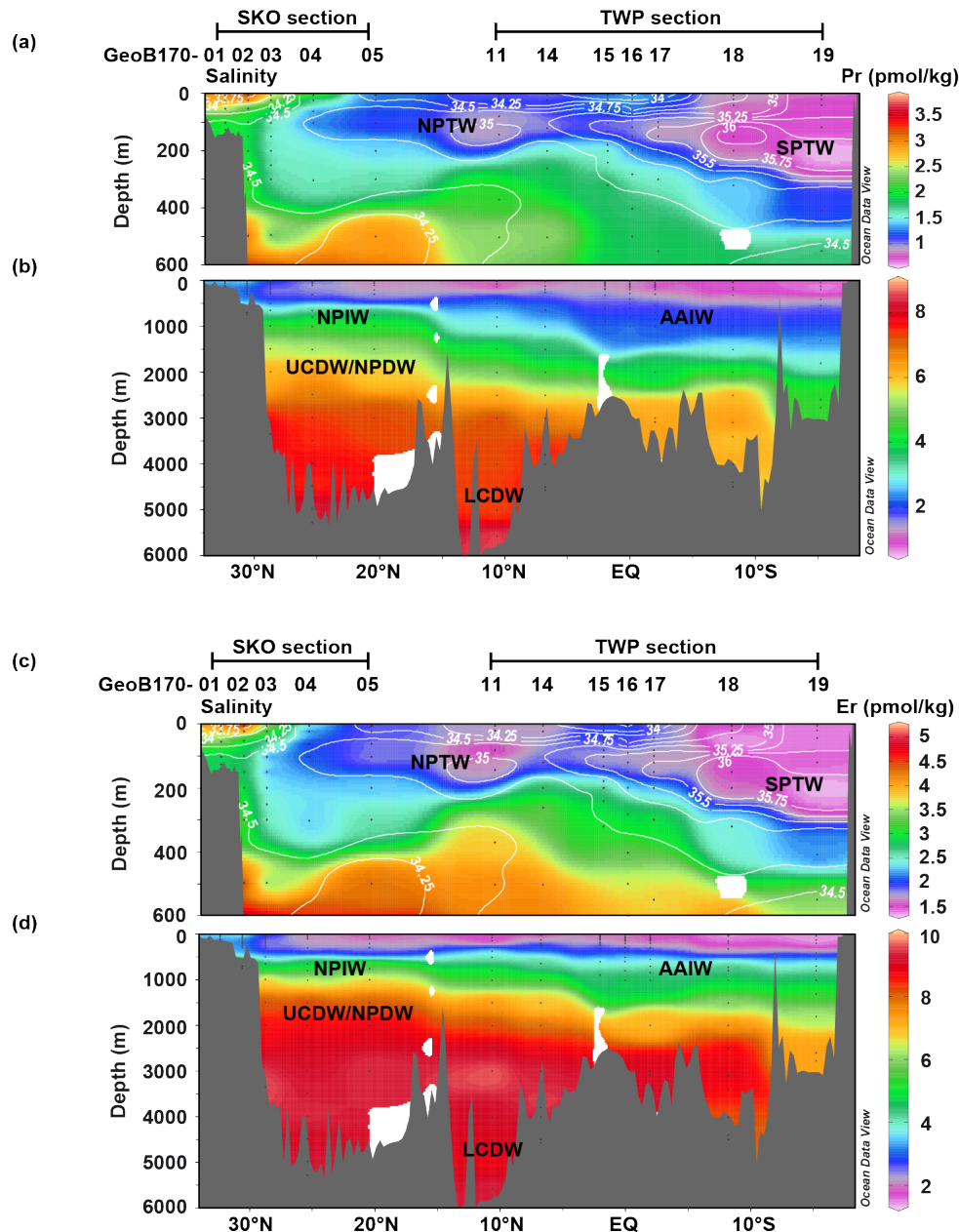


Fig. 3.3. Sections of upper water column (a, c) and full water column (b, d) showing the distribution of (a, b) Pr concentration (pmol/kg) and (c, d) Er concentration (pmol/kg) of stations from the SKO (01-05) and TWP (11-19) sections, respectively. (a, c) Salinity contours are shown in solid white (data from Behrens et al., in prep.). For abbreviations of water masses see Fig. 3.1. Sections produced with Ocean Data View (Schlitzer, 2014).

In the TWP, eastward flowing surface and subsurface currents (NECC, SC, EUC, SECC) (and the westward flowing SEC at station 19) of the equatorial zonal current system carry surface and subsurface waters that show slightly higher positive PAAS-normalized Eu anomalies ($[\text{Eu}/\text{Eu}^*]_{\text{N}} = [3 \times \text{Eu}_{\text{N}} / (2 \times \text{Sm}_{\text{N}} + \text{Tb}_{\text{N}})]$, Zhang et al., 2008) of up to 1.25 along with higher Nd isotope compositions (expressed as ϵ_{Nd}) compared to other samples of this study (Figs. 3.1a, 4a). Westward flowing subsurface currents (SEC, EIC), on the other hand, lack this elevated positive Eu anomaly (≤ 1.15) (Figs. 3.1a, 4a).

In the TWP, a depletion in heaviest REEs, expressed by elevated PAAS-normalized Er over Yb ratios $(Er/Yb)_N$, is observed in surface and subsurface (NPTW and SPTW) waters (Fig. 3.4d).

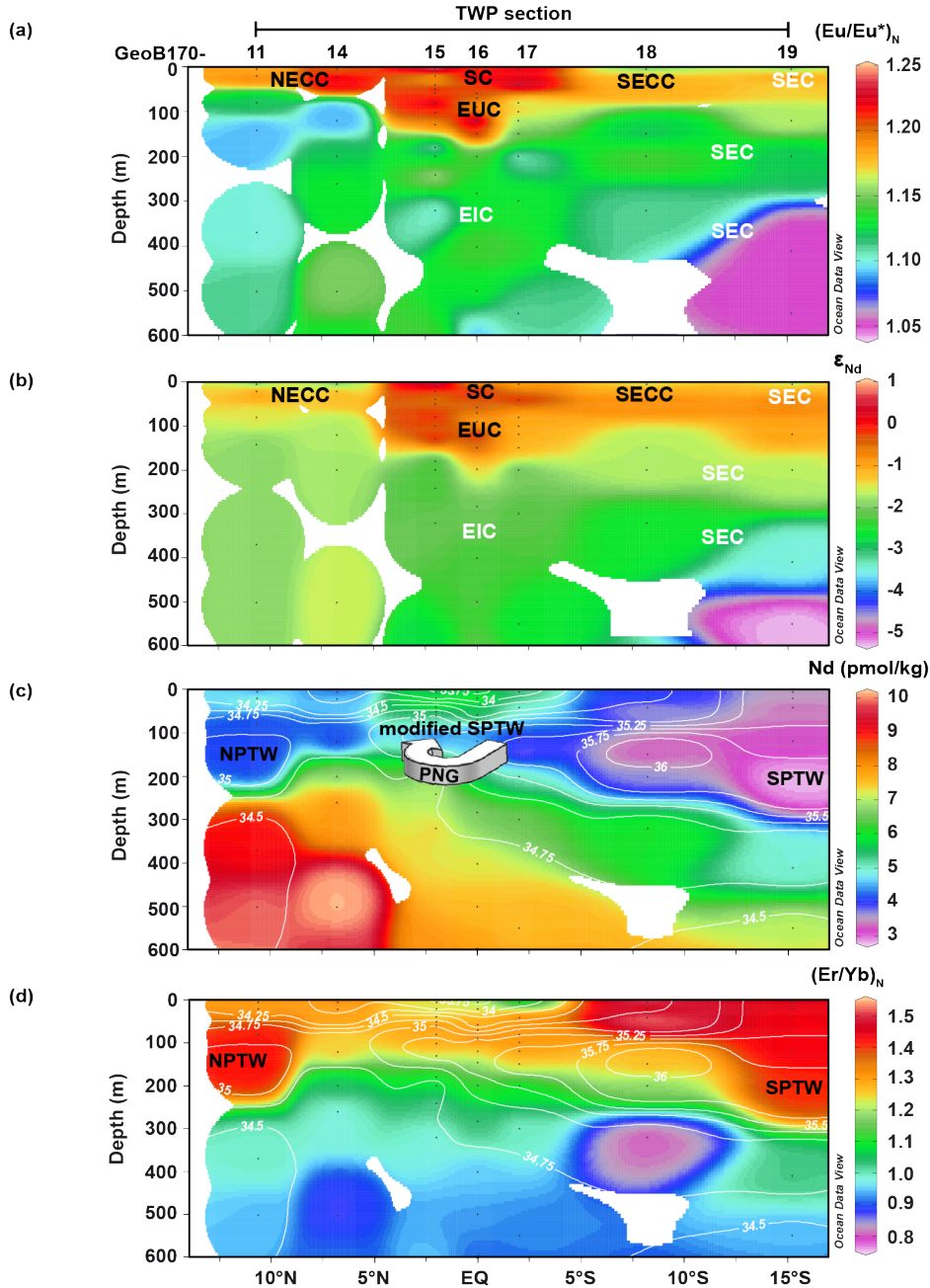


Fig. 3.4. Sections of upper water column showing the distribution of (a) PAAS-normalized Eu anomalies $(Eu/Eu^*)_N$, (b) Nd isotope ratios (expressed as ϵ_{Nd}), (c) Nd concentrations (pmol/kg), and (d) PAAS-normalized Er over Yb ratios $(Er/Yb)_N$ of stations from the TWP (11-19) section. (a, b) For abbreviations and references of surface and subsurface eastward (black) and westward (white) currents see Fig. 3.1. (c, d) Salinity contours are shown in solid white (data from Behrens et al., in prep.). Subsurface waters are North and South Pacific Tropical Water (NPTW and SPTW) and modified SPTW that is influenced by input from Papua New Guinea (PNG) along its flow path before reaching stations 15 and 16. (b, c) are modified after Behrens et al. (in prep.). Sections produced with Ocean Data View (Schlitzer, 2014).

3.4.2. Optimum Multiparameter Analysis: water mass mixing fractions

Figures 3.5a and b present the OMPA results showing the calculated water mass fractions for NPDW and LCDW, respectively. These results are consistent with hydrographic observations along our transect (Behrens et al., in prep.). The fraction of NPDW is highest (>80%) at <2000 m w. d. along the entire transect and progressively decreases with depth (Fig. 3.5a). In contrast, the fraction of LCDW is highest (>80%) below 4000 m w. d. and decreases upwards and from south to north (65% at the northernmost deep station 03 below 3000 m w. d.) (Fig. 3.5b).

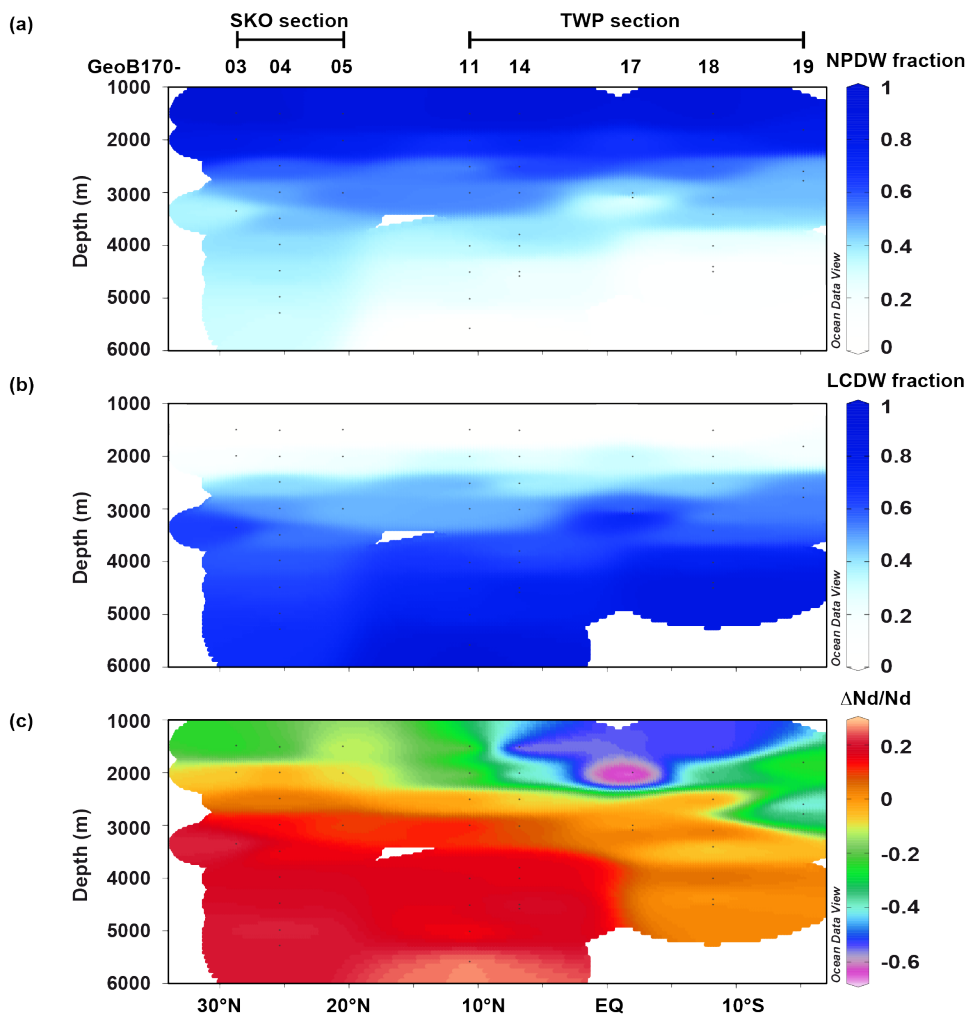


Fig. 3.5. Sections of deep water column (≥ 1500 m water depth) of stations from the SKO (03-05) and TWP (11, 14, 17-19) sections showing the calculated mixing fractions of NPDW in (a) and LCDW in (b), and (c) the contribution of ΔNd (the difference between the measured Nd concentration and the Nd concentration calculated using the OMPA results) relative to the measured Nd concentration ($\Delta\text{Nd}/\text{Nd}$). $\Delta\text{Nd}/\text{Nd}$ values around 0 represent that dissolved Nd concentrations are entirely controlled by water mass transport and mixing, whereas positive and negative values represent addition and removal of Nd, respectively. Sections produced with Ocean Data View (Schlitzer, 2014).

Figure 3.5c presents the distribution of $\Delta\text{Nd}/\text{Nd}$, where ΔNd is the difference between the measured $[\text{Nd}]$ and the calculated $[\text{Nd}]$ assuming water mass mixing only. That is, positive and negative values in Fig. 3.5c reflect the fraction of Nd addition and removal, respectively, through non-conservative processes and behavior. Values around 0, on the other hand, indicate entirely conservative behavior of dissolved $[\text{Nd}]$ i.e., a dominant control by water mass transport and mixing. At the depth of deep waters ($\sim 1500\text{-}3000$ m w. d.), our OMPA results indicate a dominance of water mass mixing ($>76\%$) on the $[\text{Nd}]$ distribution in the SKO section, and a slight dominance of Nd removal (up to 66%) over water mass mixing in the TWP section (Fig. 3.5c). At the depth of LCDW (≥ 3000 m), the OMPA results for $[\text{Nd}]$ indicate water mass transport and mixing as dominant mechanism controlling the $[\text{Nd}]$ distribution along the transect (73-100%), with some Nd addition (up to 27%) in the North Pacific (Fig. 3.5c).

3.5. Discussion

3.5.1. Conservative vs. non-conservative processes and behavior

3.5.1.1. Trace element input to the West Pacific

Highest $[\text{REE}]$ in South Korean surface waters indicate continental TE input (Fig. 3.2a). In order to identify the source of these high $[\text{REE}]$, we normalized our REE data from the SKO section to those of the surface water sample from station BO ssw-28 in the central North Pacific (Hongo et al., 2006) that can be considered to be unaffected by continental input (Greaves et al., 1989) (Fig. 3.1a). The resulting normalized REE values of surface waters at stations 01-03 show patterns enriched in LREE and MREE, with a marked increase in the HREEs ytterbium (Yb) and lutetium (Lu) (Fig. 3.6a). These patterns flatten and absolute concentrations decrease offshore, reaching normalized REE values around 1 and a nearly flat REE pattern at station 05. Available REE data of potential sources (Chinese loess, Liu et al., 1993, South Korean river water and groundwater (Jeju Island), Kim and Kim, 2014), normalized to the same surface water $[\text{REE}]$, all reveal a similar pattern of LREE and MREE enrichment (Fig. 3.6b). South Korean river water is the only source that also shows an increase in Yb and Lu seen in our surface samples, suggesting river water as an important source of REEs to the surface ocean. This is supported by low surface salinity (33.4) and unradiogenic Nd isotope compositions (expressed as ϵ_{Nd} , with ϵ_{Nd} as low as -7.3) at stations 01-02 (Behrens et al., in prep.), that are in line with input from South Korean and Chinese rivers with an unradiogenic sedimentary ϵ_{Nd} of ~ -18 to -13 (Lan et al., 1995) and $\epsilon_{\text{Nd}} \sim -11$ (Goldstein et al., 1984), respectively.

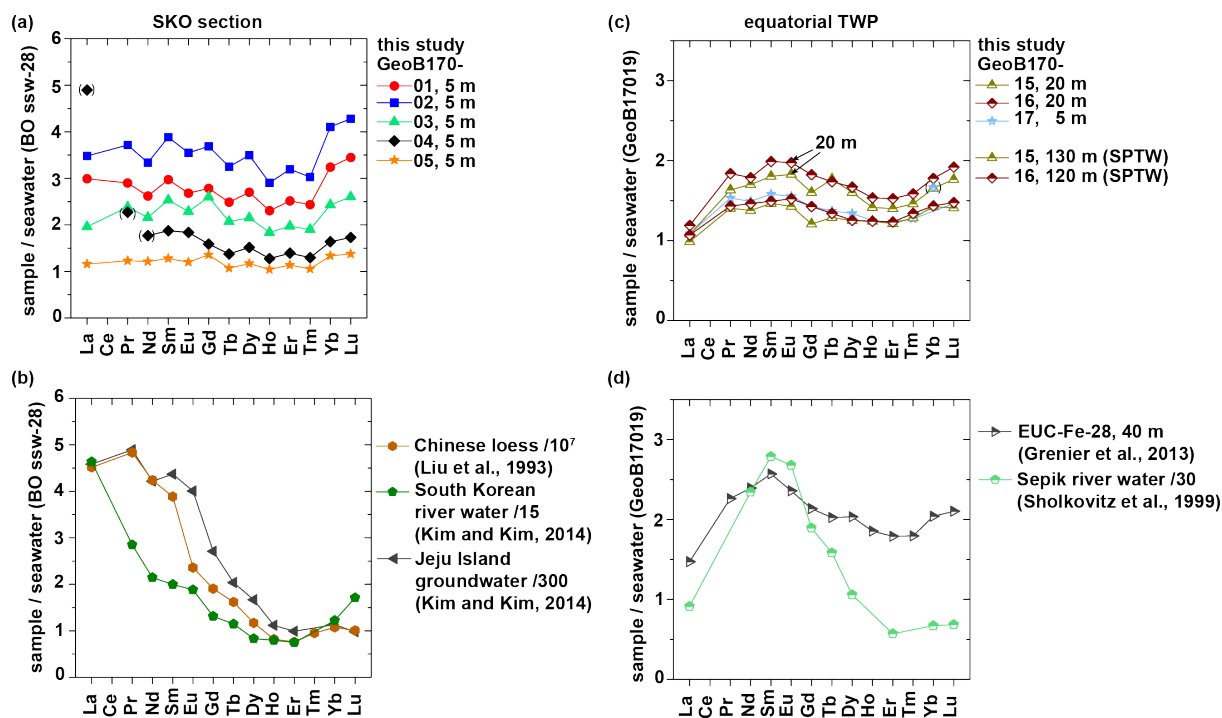


Fig. 3.6. REE patterns of (a) surface water samples of stations from the SKO (01-05) section and (c) selected surface and subsurface water samples of stations from the equatorial TWP (15-17) along with (b, d) published potential sources are plotted on linear scales. All seawater samples and potential sources are normalized to (a, b) open ocean surface water from station BO ssw-28 (Hongo et al., 2006) and (c, d) surface or subsurface (only for stations 15 and 16, 130 m and 120 m) water from station GeoB17019 (this study) (Fig. 3.1a). Published potential sources are (b) Chinese loess (Liu et al., 1993), South Korean river water and groundwater (Jeju Island) (Kim and Kim, 2014), and (d) PNG coastal surface water from station EUC-Fe-28 (Grenier et al. 2013) and Sepik river water (Sholkovitz et al., 1999) (Fig. 3.1a).

In the TWP, radiogenic ϵ_{Nd} (up to +0.7) of surface and subsurface waters was previously interpreted as reflecting TE input and/or boundary exchange at volcanic island margins such as PNG (Behrens et al., in prep.). Boundary exchange modifies the Nd isotope composition without significantly affecting Nd (and other REE) concentrations (Lacan and Jeandel, 2001, 2005). However, evidence of TE input from PNG to the TWP is given in the equatorial region based on slightly elevated surface and subsurface water (SPTW) [REE] (stations 15-17) compared to stations immediately north and south of the equator (stations 11-14 and 17-19) (Fig. 3.4c). In order to further distinguish between TE input and boundary exchange near the PNG margin, we normalized the elevated surface (5-20 m w. d.) and subsurface (SPTW, 120 and 130 m w. d.) [REE] at stations 15-17 to the [REE] of surface and subsurface water at station 19 (5 m and 120 m w. d.), which is located upstream of our equatorial stations and considered unaffected by modification (Behrens et al., in prep.). We also normalized the [REE] of PNG coastal surface water from station EUC-Fe-28 near the

mouth of the Sepik River (Grenier et al., 2013) and Sepik river water (Sholkovitz et al., 1999) (Figs. 3.1a, 3.6c, d). The normalized REE patterns reveal an MREE enrichment in surface water (stations 15-17) and SPTW (stations 15 and 16) downstream of PNG. This MREE enrichment is reminiscent of the normalized pattern of PNG coastal surface water (EUC-Fe-28) and Sepik river water (Figs. 3.6c, d). We therefore suggest active TE input from PNG into coastal surface and subsurface waters of the West Pacific, and transport within eastward flowing surface currents (SC) and the EUC towards our study area (Fig. 3.1a). Trace element sources are weathering of phosphate minerals in Sepik river water (Sholkovitz et al., 1999; Hannigan and Sholkovitz, 2001) and margin sediments (Grenier et al., 2013). Several other studies previously pointed out the importance of PNG as source of TEs, including iron, to the equatorial region (e.g., Lacan and Jeandel, 2001, Slemons et al., 2010; Radic et al., 2011; Grenier et al., 2013; Labatut et al., 2014). For example, Radic et al. (2011) and Labatut et al. (2014) used dissolved iron isotopes in equatorial West Pacific waters to suggest non-reductive dissolution of Fe from PNG margin sediments and input to surface and subsurface (EUC) waters.

3.5.1.2. Equatorial zonal trace element transport

Elevated positive PAAS-normalized Eu anomalies of surface and subsurface waters in the equatorial TWP compared to other samples of this study are indicative of REE input from the volcanic islands in the West Pacific (e.g., Behrens et al., in prep.; Grenier et al., 2013). We find Eu anomalies at stations and water depths influenced by eastward flowing surface and subsurface currents (NECC, SC, EUC, SECC), while westward currents lack this clear Eu-anomaly (except for the westward flowing SEC at station 19 due to contact with Fiji, see also Behrens et al., in prep.) (Fig. 3.4a). The elevated positive Eu anomalies in addition to the radiogenic ϵ_{Nd} signatures of the surface and subsurface waters (Behrens et al., in prep.) fingerprint the source and flow path of currents flowing eastward in the equatorial zonal current system towards the East Pacific (Figs. 3.4a, b). The REE data therefore confirm our ϵ_{Nd} results from the same stations and water depths that show a radiogenic overprint from volcanic islands, and refine previous results from this area. Our new data allow us to precisely pinpoint the eastward flowing EUC with a particularly strong and well-defined positive Eu-anomaly, enriched MREE pattern (see section 3.5.1.1.), highly radiogenic ϵ_{Nd} , and elevated [REE] at stations 15 and 16 ('modified' SPTW). These signals derive from modification at and input from PNG (see section 3.5.1.1.). Other eastward flowing currents, the NECC and

SECC, that originate from the Philippine Islands and the Solomon Islands, respectively, show a slightly less pronounced modification (Figs. 3.4a-c, 6c).

Our data therefore clearly document TE input into the West Pacific from PNG, and to a lesser extent from other volcanic islands, and eastward transport within the eastward flowing surface and subsurface currents of the tropical Pacific. The results therefore support the hypothesis of previous studies on the importance of the TWP as source region of micronutrients and other TEs to the iron-limited East Pacific (e.g., Lacan and Jeandel, 2001; Slemons et al., 2010; Radic et al., 2011; Grenier et al., 2013; Labatut et al., 2014), and highlight in detail the small-scale equatorial zonal eastward transport of TEs.

3.5.1.3. REE transport within South and North Pacific Tropical Water

In the upper 600 m w. d. of our transect, we previously highlighted the close correlation of low [Nd] with the high salinity tongue of South Pacific Tropical Water (SPTW; Behrens et al., in prep.). A similar correlation is also obvious for [Pr] and [Er] (Figs. 3.3a, c). SPTW originates in the oligotrophic South Pacific Subtropical Gyre, where [REE] at the surface are extremely low (Jeandel et al., 2013) due to almost absent terrestrial input. This tongue of high-salinity SPTW and low [REE] can be traced from station 19 towards the equator (stations 15, 16). At stations 15 and 16, slightly higher [REE] of SPTW are due to TE input from PNG (see sections 3.5.1.1. and 3.5.1.2., Fig. 3.4c). At stations 14 and 11, NPTW, the northern counterpart of SPTW, is likewise marked by high salinity and low [REE] (Behrens et al., in prep.). Our new HREE concentration ([HREE]) data, shown exemplary by [Er], also indicate a clear minimum in the SPTW and NPTW layers (Fig. 3.3c). Heavy REEs are less prone to scavenging than LREEs (e.g., Cantrell and Byrne, 1987; Byrne and Kim, 1990) and should therefore be more likely to be transported laterally without vertical modifications. Our [HREE] data therefore support our earlier suggestion of a preformed low [REE] signal that is transported into our study area by SPTW and NPTW.

Another independent feature in the REE concentration patterns, the depletion in heaviest REEs from Er to Lu, further corroborates lateral transport and origin of the low [REE] signal in the South Pacific Subtropical Gyre. The depletion in heaviest REEs, expressed in the PAAS-normalized ratio of Er over Yb ($(Er/Yb)_N$), is a widespread feature of surface waters (e.g., Hongo et al., 2006; Zhang et al., 2008; Jeandel et al., 2013; Pahnke et al., 2012; Fröllje et al., 2016) and has previously been hypothesized to trace continental input (Hongo et al., 2006; Fröllje et al., 2016). However, the South Pacific Subtropical Gyre is far remote from continental areas and receives almost no terrestrial input (e.g., cruise report

SO245, Ferdelman, 2016), yet it shows extremely strong depletion of HREEs (high $(\text{Er}/\text{Yb})_N$ ratios) down to a water depth of 170-300 m in the center of the gyre (Jeandel et al., 2013; Rehbein, in prep.). Experimental and field data have shown that HREEs (especially thulium (Tm), Yb, and Lu) are adsorbed onto bacteria cell walls (Takahashi et al., 2005; 2007), leading to a strong enrichment of these REEs in bacteria and microbial mats and a depletion in the surrounding water. We therefore suggest that the high $(\text{Er}/\text{Yb})_N$ ratios found globally in surface waters are due to microbial activity and that the especially strong Er/Yb signal in the South Pacific Subtropical Gyre may be due to the long residence time of surface waters in the gyre (e.g., Qu et al., 2013). The elevated Er/Yb signal at SPTW and NPTW depth along our section, where surface waters partly have lower Er/Yb ratios than subsurface waters (Fig. 3.4d), therefore suggests a preformed rather than local origin of the signal.

SPTW has been shown to have a transit time of ~ 2 years from its source region in the South Pacific Subtropical Gyre to the TWP (Qu et al., 2013), indicating that at least over this time period, REEs in subsurface waters in this area behave conservatively. Our full suite of [REE] therefore refines and supports our earlier notion of a laterally transported [Nd] signal by SPTW and NPTW.

3.5.1.4. Antarctic Intermediate Water and North Pacific Intermediate Water

Constant low [Nd] within AAIW along the transect has previously been related to the northward transport of preformed low [Nd] of AAIW (Behrens et al., in prep.) that is due to intense scavenging of Nd in the Southern Ocean opal belt (Stichel et al., 2012b). In contrast to AAIW, [Nd] of NPIW has been suggested to behave non-conservatively being mainly controlled by vertical Nd addition through release of Nd from sinking organic particles due to remineralization (Behrens et al., in prep.). Our new [REE] data of NPIW and AAIW support these suggestions. The increase in [REE] of NPIW with depth in the SKO section, and the low laterally and vertically constant [REE] of AAIW in the TWP section (Figs. 3.3b, d) indicate vertical release of REEs from particles at the depth of NPIW and dominant lateral advection of a preformed signal within the flow path of AAIW.

3.5.1.5. Deep to bottom waters

We previously pointed out that Nd behaves non-conservatively in deep waters (~ 1000 - 3000 m w. d.) and conservatively at the depth of LCDW (≥ 3000 m w. d.) along our transect (Behrens et al., in prep.). In order to quantify this earlier notation, we modeled the Nd distribution assuming entirely conservative behavior of [Nd] and using the water mass

fractions calculated using OMPA (Fig. 3.5). Due to a lack of REE data from the Pacific that could be used to define the end-members, we focus the following discussion on [Nd] alone.

In the northern part of the transect, deep water [Nd] (~1500-3000 m w. d.) is mainly controlled by conservative water mass mixing (>76%, Fig. 3.5c) including upwelling of deeper water from ~3000 m w. d. at stations 03-05 of the SKO section (Behrens et al., in prep.). In the TWP, the pronounced Nd removal in deep water (up to 66% at ~2000 m w. d., Fig. 3.5c) was not apparent from the measured [Nd] and other [REE] data alone (Figs. 3.3b, d). This removal may be due to enhanced scavenging of REEs near basaltic island margins of the Solomon Islands, Fiji, and Samoa (Fig. 3.1b). This is in line with an experimental study of Pearce et al. (2013), who used basaltic margin material in seawater and showed that dissolved REEs are removed from seawater by scavenging into the phosphate mineral rhabdophane. In addition, high helium concentrations in the TWP area, with a maximum at ~2000 m w. d., have been used to suggest active hydrothermal venting near the Solomon Islands and in the Tonga-Fiji region (Lupton et al., 2004, 2015; Bianchi et al., 2010), and it is known that Nd is scavenged onto Fe-Mn-oxide particles in hydrothermal plumes, leading to an [Nd] deficit compared to surrounding seawater (e.g., Klinkhammer et al., 1983; German et al., 1990; Stichel et al., 2012a). We therefore suggest that the low $\Delta\text{Nd}/\text{Nd}$ at ~2000 m w. d. may reflect enhanced scavenging in hydrothermal plumes.

Similarly to the OMPA results, deep water ϵ_{Nd} (-3.1) in the northern part of the transect is indicative of conservative behavior of ϵ_{Nd} , whereas in the TWP, deep water ϵ_{Nd} is modified towards more radiogenic values (up to -1.8) through boundary exchange at tropical volcanic island margins and by exchange with hydrothermal particles (Behrens et al., in prep.). Together with the OMPA results, the ϵ_{Nd} and [Nd] distributions within deep waters of the TWP therefore suggest that volcanic island margins and hydrothermal plumes affect both Nd isotopes and [REE] in this region.

At the depth of LCDW (≥ 3000 m w. d.), constant vertical and lateral [Nd] along the transect were previously suggested to indicate advection of [Nd], and hence conservative behavior (Behrens et al., in prep.). This is also seen in our new [REE] data (Fig. 3b, d), and the OMPA results for [Nd] support this by indicating that 73-100% of the [Nd] can be explained by conservative behavior (Fig. 3.5c). At stations 03 and 04 (~25°-28°N), the northernmost deep water stations of our transect, still show a dominance ($\geq 78\%$) of water mass transport and mixing on [Nd].

The ϵ_{Nd} of LCDW along our transect shows a non-conservative modification towards more radiogenic values (by ~ 1 ϵ_{Nd} unit) from south to north (Behrens et al., in prep.).

Together with the OMPA results, the ϵ_{Nd} and [Nd] distributions within LCDW suggest boundary exchange along the northward flow path of LCDW affecting Nd isotopes without influencing [REE]. Our results therefore demonstrate that the preformed constant [REE] are transported laterally over substantial distances (Figs. 3.7a, b), while ϵ_{Nd} is more quickly overprinted by radiogenic Nd sources. The preformed constant [REE] of LCDW along our section from station 18 to stations 04 and 03 ($\sim 8^\circ\text{S}$ to $\sim 25^\circ$ and 28°N) is also found at station TPS2471-1 (Piepgras and Jacobsen, 1992) east of our station 04, but is absent in the central North Pacific at station ALOHA near Hawaii (station KM1107-11), where an increase in LREEs at the depth of LCDW indicates the presence of PDW (Fröllje et al., 2016) (Figs. 3.1b, 3.7a, b). Minor addition of Nd within LCDW in the North Pacific (stations 03-05, 11, 14, $\sim 20\%$) suggests release of Nd from sinking particles or/and bottom sediments (e.g., Sholkovitz et al., 1989) (Fig. 3.5c). Yet, our data do not support a substantial benthic flux of REEs as suggested by Abbott et al. (2015a).

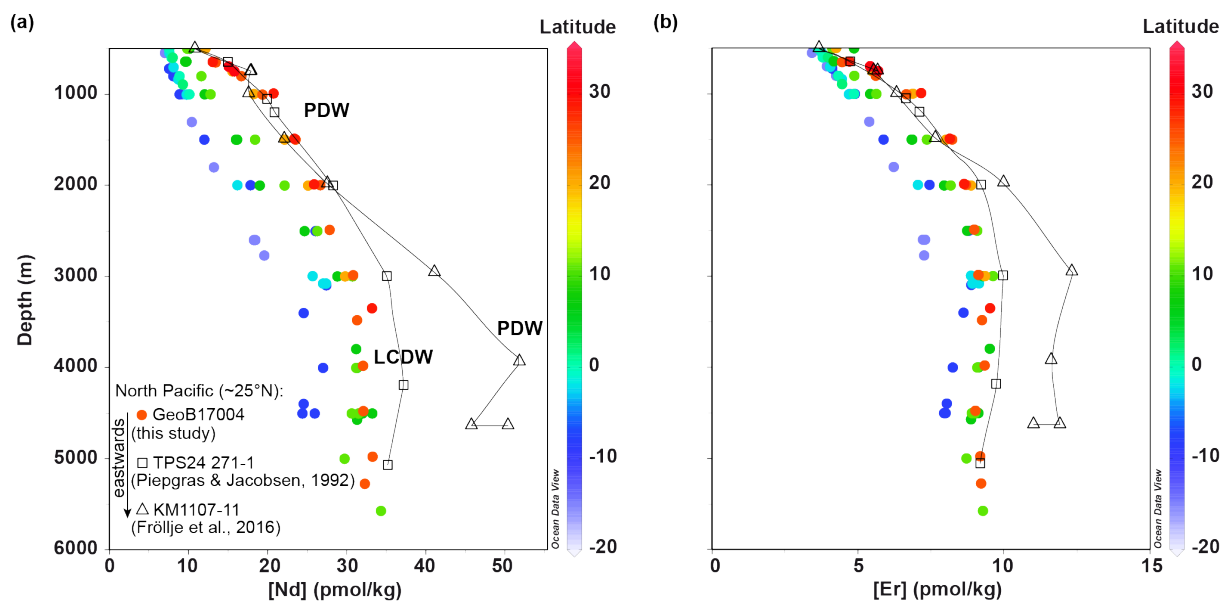


Fig. 3.7. Deep water column (a) Nd, and (b) Er concentrations (pmol/kg) for all samples of this study along the transect (color represents latitude) and published stations TPS24 271-1 (Piepgras and Jacobsen, 1992) and KM1107-11 (Fröllje et al., 2016) in the western and central North Pacific, respectively, at $\sim 25^\circ\text{N}$ (see Fig. 3.1b). For abbreviations of water masses see Fig. 3.1. Plot produced with Ocean Data View (Schlitzer, 2014).

3.6. Conclusions

This study presents dissolved seawater REE concentrations ([REE]) along a NW-SE transect in the West Pacific. Our data reveal significant continental TE input to the West Pacific near South Korea and Papua New Guinea (PNG). Our previous study using ϵ_{Nd} from the same samples also suggested input and/or modification of the seawater signal in these areas (Behrens et al., in prep.), but our new data now provide evidence for active input both near South Korea and PNG and afford clear identification of the sources. South Korean rivers are responsible for substantial REE input in the northern part of our section, while PNG river discharge and volcanic island margin sediments supply REE and modify the seawater REE composition in the tropical West Pacific. The fine-scale distribution of positive Eu anomalies that fingerprint input from the volcanic islands in the tropical West Pacific further provide detailed evidence for TE transport in the eastward flowing surface and subsurface currents of the equatorial zonal current system.

[REE] and elevated Er/Yb ratios at subsurface depth correlate with the distribution of high salinity SPTW and NPTW and are reminiscent of the surface water REE compositions in the SPTW, NPTW source regions. They hence provide evidence for a laterally transported preformed rather than local REE signal, suggesting conservative behavior of REEs even at subsurface depth in the open ocean.

The REE distributions of NPIW and AAIW indicate vertical release of REEs from particles at the depth of NPIW, and lateral transport of a preformed low-[REE] signal with AAIW.

Deep water [REE] (~1500-3000 m w. d.) in the southern part of our transect (15°S-10°N) are dominated by REE removal, likely due to scavenging at basaltic margins (the Solomon Islands, Fiji, and Samoa) and by scavenging onto Fe-Mn-oxide particles in the hydrothermal plumes located near the Solomon Islands and in the Tonga-Fiji region. In the northern part of the transect, REEs in deep waters are mainly controlled by conservative water mass mixing including upwelling of deeper water. At the depth of LCDW, preformed and vertically constant [REE] indicate lateral transport from the Southern Ocean to as far north as ~28°N in the West Pacific (up to 100% conservative behavior in the south, $\geq 78\%$ at the northernmost deep stations).

That is, the new [REE] data presented here provide additional evidence for the largely conservative behavior of REE from the subsurface to abyssal ocean in the Pacific, and for regionally and locally important REE input and modification mainly in coastal regions that

further enable tracing of small-scale REE (and other TE) transport in surface and subsurface currents in the tropical region.

3.7. Acknowledgements

We thank the scientific party, captain and crew of R/V *Sonne* cruise SO223T, particularly chief-scientist Mahyar Mohtadi. We thank all members of the Max Planck Research Group at the University of Oldenburg, especially Martina Schulz, for their help in the lab. Financial support for this study came from the German Research Foundation (DFG, PA2411/1-1), the Institute for Chemistry and Biology of the Marine Environment (ICBM), and the Max Planck Institute for Marine Microbiology.

3.8. Supplementary Tables

Table S3.1: Nutrient data from cruise SO223T (this study) supplemented with published data from WOCE (<http://www.ewoce.org>).

Sample ID	Potential temp. (°C)	Salinity	Oxygen (μmol/kg)	Phosphate (μmol/kg)	Nitrate (μmol/kg)	Silicate (μmol/kg)	Location and Reference
Station GeoB17003- (28.7163°N/131.0852°E)							
1-4	2.40	34.51	72.87	2.89	39.90	138.30	28.55°N/133.02°E, P24 Station 12
1-3	1.87	34.58	97.80	2.75	38.30	142.60	28.55°N/133.02°E, P24 Station 12
1-1	1.27	34.58	134.08	2.34	36.73	145.61	this study
Station GeoB17004- (25.3782°N/134.3756°E)							
1-11	2.36	34.52	74.73	2.87	39.80	139.90	25.73°N/134.72°E, P24 Station 20
1-10	1.83	34.59	102.27	2.72	38.00	141.60	25.73°N/134.72°E, P24 Station 20
1-9	1.53	34.63	118.99	2.63	37.20	141.60	25.73°N/134.72°E, P24 Station 20
1-8	1.37	34.64	128.25	2.58	36.50	141.30	25.73°N/134.72°E, P24 Station 20
1-7	1.28	34.65	133.81	2.52	36.00	140.30	25.73°N/134.72°E, P24 Station 20
1-6	1.23	34.66	137.22	2.52	35.90	140.00	25.73°N/134.72°E, P24 Station 20
1-5	1.21	34.66	139.70	2.51	35.90	139.80	25.73°N/134.72°E, P24 Station 20
1-4	1.20	34.66	140.34	2.53	36.00	140.00	25.73°N/134.72°E, P24 Station 20
1-1	1.20	34.66	143.97	2.52	36.00	140.00	25.73°N/134.72°E, P24 Station 20
Station GeoB17005- (20.4323°N/139.6161°E)							
1-5	2.44	34.56	86.03	2.72	37.30	139.15	20.05°N/137.02°E, PR02 Station RY8101
1-4	1.86	34.61	104.24	2.73	37.80	146.18	20.05°N/137.02°E, PR02 Station RY8101
1-1	1.40	34.65	125.93	2.61	36.30	146.99	20.05°N/137.02°E, PR02 Station RY8101
Station GeoB17011- (10.6342°N/148.9010°E)							
1-11	2.68	34.58	87.56	2.82	39.70	125.00	9.49°N/150.83°E, P04W Station 54
1-10	2.02	34.61	100.57	2.76	39.10	140.20	9.49°N/150.83°E, P04W Station 54
1-9	1.67	34.63	110.61	2.70	38.40	146.80	9.49°N/150.83°E, P04W Station 54
1-8	1.39	34.65	123.34	2.55	36.68	149.73	this study
1-7	1.17	34.67	139.90	2.49	36.10	140.35	9.49°N/150.83°E, P04W Station 54
1-5	1.08	34.67	148.42	2.44	35.50	138.84	9.49°N/150.83°E, P04W Station 54
1-4	1.03	34.68	155.26	2.40	35.00	133.40	9.49°N/150.83°E, P04W Station 54
1-1	1.01	34.68	157.69	2.43	38.00	137.35	this study
Station GeoB17014- (6.7842°N/154.1982°E)							
1-11	2.87	34.58	85.14	2.75	38.80	126.30	5.99°N/148.28°E, P10 Station 36
1-9	2.02	34.62	99.54	2.71	38.30	137.30	5.99°N/148.28°E, P10 Station 36
1-8	1.62	34.64	112.92	2.61	37.20	142.20	5.99°N/148.28°E, P10 Station 36
1-7	1.41	34.65	124.01	2.55	36.40	142.50	5.99°N/148.28°E, P10 Station 36
1-6	1.20	34.66	138.18	2.49	35.80	141.40	5.99°N/148.28°E, P10 Station 36
1-5	1.14	34.67	142.55	2.46	35.50	140.60	5.99°N/148.28°E, P10 Station 36
1-4	1.05	34.67	151.63	2.48	35.50	140.70	5.99°N/148.28°E, P10 Station 36
1-3	1.05	34.67	152.77	2.48	35.50	140.70	5.99°N/148.28°E, P10 Station 36
Station GeoB17017- (2.0021°S/161.9998°E)							
1-4	2.13	34.62	104.82	2.66	36.00	134.93	3.19°S/164.73°E, P13 Station 84
1-3	1.48	34.65	120.87	2.57	35.10	146.70	3.19°S/164.73°E, P13 Station 84
1-2	1.43	34.65	122.88	2.40	31.02	146.36	this study
Station GeoB17018- (8.2019°S/166.0826°E)							
1-9	2.67	34.58	118.50	2.62	36.90	110.26	8°S/179.01°E, P14N Station 169
1-8	1.93	34.62	120.55	2.61	36.80	118.69	8°S/179.01°E, P14N Station 169
1-7	1.59	34.64	123.03	2.59	36.60	137.70	8°S/179.01°E, P14N Station 169
1-6	1.46	34.65	126.05	2.51	35.80	138.20	8°S/179.01°E, P14N Station 169
1-5	1.34	34.66	133.41	2.49	35.50	137.80	8°S/179.01°E, P14N Station 169
1-4	1.17	34.67	146.71	2.40	34.20	136.43	8°S/179.01°E, P14N Station 169
1-3	1.14	34.67	149.05	2.30	32.90	125.60	8°S/179.01°E, P14N Station 169
1-2	1.14	34.67	148.74	2.28	32.80	124.00	8°S/179.01°E, P14N Station 169
Station GeoB17019- (15.2179°S/173.5187°E)							
1-5	2.29	34.59	131.28	2.31	37.35	115.67	this study
1-4	1.70	34.64	132.38	2.53	36.20	133.30	12.51°S/179°E, P14N Station 178
1-2	1.65	34.64	131.96	2.50	36.20	134.90	12.51°S/179°E, P14N Station 178

Table S3.2: Dissolved REE concentrations (pmol/kg), PAAS-normalized (Taylor and McLennan, 1985) Eu anomalies ($(Eu/Eu^*)_N$) and Er/Yb ratios ($(Er/Yb)_N$) for seawater samples of this study. For details on errors see doi:10.1594/PANGAEA.871176.

Sample ID	Water depth (m)	[La]	[Ce]	[Pr]	[Nd]	[Sm]	[Eu]	[Gd]	[Tb]	[Dy]	[Ho]	[Er]	[Tm]	[Yb]	[Lu]	$(Eu/Eu^*)_N^a$	$(Er/Yb)_N$
Station GeoB17001- (32.3332°N 127.4995°E; MLD: 7-8 m; bottom: 129 m)																	
1-surf	5	15.02	10.8	2.90	12.01	2.82	0.78	4.20	0.70	5.21	1.24	4.13	0.56	3.60	0.59	1.11	1.10
1-8	22	11.46	6.6	2.73	12.29	2.92	0.85*	4.95*	0.71	5.05	1.14	3.59	0.49	3.14	0.51	1.18*	1.09
1-6	53	10.43	6.0	2.60	11.09	2.79	0.78	4.25	0.67	4.76	1.10	3.51	0.48	2.92	0.49	1.14	1.15
1-4	102	8.95	5.5	1.90	7.96	1.89	0.52	3.19	0.46	3.42	0.82	2.79	0.37	2.41	0.41	1.11	1.11
1-1	127	9.00	5.6	2.02	8.15	1.89	0.53	3.12	0.48	3.44	0.87	2.82	0.40	2.47	0.40	1.11	1.09
Station GeoB17002- (30.5830°N 129.0004°E; MLD: 10-11 m; bottom: 749 m)																	
1-surf	5	17.48	10.9	3.71	15.30	3.69	1.03	5.57	0.91	6.75	1.57	5.24	0.70	4.56	0.73	1.12	1.10
1-18+19	22	14.64	8.3	3.35	14.06	3.55	0.97	5.11	0.84	5.97	1.36	4.36	0.59	3.68	0.59	1.12	1.13
1-16+17	51	7.65	5.5	2.01	8.37	2.02	0.58	3.30	0.50	3.56	0.86	2.80	0.38	2.26	0.37	1.16	1.18
1-14+15	100	10.02	5.9	2.11	9.21	2.15	0.60	3.68	0.51	3.79	0.92	3.02	0.41	2.55	0.43	1.14	1.13
1-12+13	150	9.73	5.2	2.10	8.60	2.05	0.57	3.41	0.51	3.71	0.91	3.01	0.42	2.57	0.44	1.11	1.12
1-10+11	200	10.64	4.8	2.08	9.03	2.03	0.54	3.28	0.50	3.69	0.92	3.16	0.45	2.78	0.46	1.08	1.09
1-8+9	249	12.65	4.4	2.30	9.50	2.08	0.56	3.43	0.51	3.87	0.99	3.32	0.49	2.98	0.53	1.09	1.07
1-7	299	13.83	2.5	2.34	10.15	2.04	0.59	3.57	0.52	4.00	1.03	3.52	0.52	3.29	0.58	1.14	1.02
1-6	498	19.41	2.5	3.17	13.25	2.62	0.72	4.46	0.65	5.00	1.33	4.60	0.69	4.71	0.85	1.10	0.93
1-5	696	26.0	2.5	3.51	15.11	2.93	0.83	4.58	0.68	5.78	1.54	5.43	0.82	5.46	1.02	1.17	0.95
1-4 ^b	696	26.3	2.9	3.66	15.15	3.06	0.84	5.07	0.69	5.71	1.55	5.43	0.83	5.70	1.08	1.16	0.91
1-1	748	27.1	2.8	3.87	15.81	3.08	0.87	4.79	0.70	5.90	1.60	5.70	0.87	5.65	1.05	1.18	0.97
Station GeoB17003- (28.7163°N 131.0852°E; MLD: 11-12 m; bottom: 3357 m)																	
1-surf	5	9.85	6.8	2.38	9.90	2.41	0.66	3.92	0.58	4.15	0.99	3.24	0.44	2.70	0.44	1.12	1.15
1-22+23	22	9.09	5.1	2.10	9.03	2.19	0.61	3.32	0.52	3.72	0.88	2.83	0.38	2.38	0.39	1.15	1.14
1-20+21	52	7.23	5.2	1.72	7.16	1.64	0.48	2.81	0.40	3.01	0.72	2.44	0.32	1.97	0.32	1.16	1.18
1-18+19	101	5.44	4.4	1.38	5.57	1.25	0.35	1.96	0.31	2.32	0.59	1.97	0.26	1.53	0.25	1.14	1.24
1-16+17	151	5.55	4.1	1.34	5.44	1.19	0.34	2.01	0.30	2.32	0.59	1.99	0.27	1.59	0.26	1.14	1.19
1-14+15	200	5.76	3.5	1.38	5.62	1.25	0.36	2.14	0.32	2.43	0.62	2.09	0.28	1.66	0.29	1.14	1.20
1-12+13	250	6.02	3.4	1.40	5.81	1.29	0.36	2.27	0.34	2.51	0.64	2.19	0.29	1.76	0.29	1.08	1.19
1-10+11	298	6.49	3.3	1.49	6.20	1.36	0.38	2.35	0.35	2.62	0.68	2.27	0.31	1.90	0.32	1.12	1.14
1-9	496	11.58	2.2	2.13	8.91	1.86	0.52	3.32	0.48	3.71	0.96	3.27	0.47	3.06	0.52	1.09	1.02
1-7	645	20.67	1.9	3.12	13.10	2.61	0.73	3.94	0.65	4.96	1.34	4.71	0.67	4.55	0.83	1.12	0.99
1-5	993	35.3	3.3	4.81	20.80	3.94	1.07	6.11	0.87	7.45	2.02	7.17	1.10	7.39	1.40	1.15	0.93
1-4	1490	43.9	8.9*	5.44	23.44	4.45	1.20	6.92	1.10	8.42	2.29	8.15	1.25	8.59	1.60	1.08	0.91
1-3	1988	43.0	4.1	6.14	25.88	4.87	1.37	7.75	1.16	9.06	2.40	8.65	1.32	9.31	1.75	1.15	0.89

Table S3.2 (continued)

Sample ID	Water depth (m)	[La]	[Ce]	[Pr]	[Nd]	[Sm]	[Eu]	[Gd]	[Tb]	[Dy]	[Ho]	[Er]	[Tm]	[Yb]	[Lu]	(Eu/Eu*) _N ^a	(Er/Yb) _N
1-1	3350	55.7	15.8	7.79	33.22	6.35	1.67	9.01	1.37	10.49	2.64	9.53	1.45	10.30	1.89	1.13	0.89
Station GeoB17004- (25.3782°N 134.3756°E; MLD: 27-28 m; bottom: 5339 m)																	
1-surf	5	24.6*	26.7*	2.27	8.10	1.78	0.53	2.40	0.39	2.93	0.69	2.28	0.30	1.82	0.29	1.28*	1.20
1-21+22	22	6.35	5.3	1.45	6.06	1.35	0.37	2.16	0.31	2.42	0.60	1.99	0.26	1.58	0.28	1.13	1.21
1-21+22 ^c	22	13.44*	14.5*	2.99*	12.1*	2.53*	0.72*	4.00*	0.69*	5.19*	1.36*	4.50*	0.60*	3.55*	0.57*	1.10*	1.21*
1-19+20	62	5.59	4.9	1.24	5.44	1.18	0.33	1.99	0.29	2.26	0.56	1.89	0.25	1.48	0.24	1.13	1.22
1-17+18	101	5.31	4.3	1.23	5.33	1.18	0.34	2.05	0.30	2.39	0.59	2.02	0.26	1.58	0.26	1.15	1.23
1-15+16	303	6.71	3.8	1.59	6.48	1.46	0.41	2.49	0.36	2.74	0.68	2.28	0.31	1.86	0.31	1.12	1.17
1-14	651	20.16	1.7	3.08	13.46	2.59	0.71	4.13	0.65	4.94	1.32	4.46	0.66	4.26	0.78	1.09	1.00
1-13	800	27.0	2.0	4.05	16.7	3.23	0.90	4.84	0.78	6.00	1.60	5.62	0.83	5.69	1.02	1.13	0.94
1-12	1004	34.8	4.4	4.69	19.38	3.70	0.99	5.67	0.82	6.94	1.89	6.66	1.01	6.85	1.27	1.14	0.93
1-11	1501	40.1	2.9	5.26	23.6	4.38	1.19	6.87	0.98	8.52	2.29	8.24	1.25	9.06	1.69	1.15	0.87
1-10	2000	43.5	6.1*	6.48	26.7	5.17	1.39	7.87	1.20	9.38	2.46	8.70	1.34	9.27	1.73	1.11	0.90
1-9	2487	43.7	3.1	6.80	27.89	5.35	1.47	8.01	1.23	9.83	2.49	8.99	1.37	9.92	1.80	1.14	0.87
1-8	2985	48.2	5.3	7.41	30.85	5.93	1.55	8.44	1.34	9.99	2.67	9.13	1.44	10.17	1.88	1.10	0.86
1-7	3483	48.7	4.0	7.49	31.29	6.01	1.60	9.08	1.36	10.25	2.67	9.26	1.44	10.21	1.91	1.11	0.87
1-6	3980	51.1	9.1*	7.71	32.06	6.13	1.64	8.83	1.36	10.55	2.66	9.34	1.42	10.23	1.88	1.12	0.87
1-5	4479	49.4	3.2	7.50	32.14	6.02	1.66	8.97	1.37	10.23	2.64	9.02	1.44	10.00	1.90	1.15	0.86
1-4	4977	53.3	9.7	8.29	33.29	6.42	1.66	9.15	1.38	10.33	2.70	9.19	1.45	10.15	1.88	1.11	0.87
1-1	5276	57.7	17.1	8.16	32.35	6.05	1.63	8.63	1.32	10.34	2.61	9.23	1.43	10.10	1.85	1.14	0.87
Station GeoB17005- (20.4323°N 139.6161°E; MLD: 35-36 m; bottom: 6315 m)																	
1-surf	5	5.82	4.7	1.23	5.55	1.21	0.35	2.05	0.30	2.26	0.56	1.87	0.24	1.48	0.23	1.15	1.20
1-21+22	22	5.50	3.9	1.24	5.27	1.20	0.33	2.02	0.29	2.20	0.55	1.84	0.24	1.38	0.22	1.12	1.27
1-19+20	61	4.61	4.0	1.16	4.88	1.06	0.30	1.81	0.28	2.10	0.54	1.82	0.24	1.38	0.22	1.12	1.26
1-13+14	101	5.36	4.5	1.11	4.64	1.02	0.30	1.85	0.26	2.08	0.53	1.80	0.24	1.41	0.23	1.14	1.23
1-11+12	201	6.45	3.1	1.42	5.85	1.29	0.37	2.30	0.33	2.61	0.66	2.28	0.30	1.83	0.31	1.12	1.19
1-9+10	300	8.24	2.4	1.63	6.74	1.47	0.41	2.44	0.38	3.01	0.77	2.57	0.35	2.18	0.37	1.10	1.12
1-8	500	18.58	1.6	2.88	12.16	2.34	0.63	4.05	0.60	4.55	1.21	4.26	0.60	3.84	0.71	1.06	1.06
1-7	751	26.8	2.0	3.56	15.59	2.89	0.81	4.50	0.72	5.61	1.53	5.49	0.79	5.64	1.04	1.13	0.93
1-6	998	31.3	4.7	4.44	18.30	3.59	0.98	5.61	0.80	6.75	1.89	6.88	1.05	6.82	1.29	1.15	0.96
1-5	1500	37.0	2.7	5.12	22.20	4.40	1.21	6.58	1.05	8.06	2.21	8.03	1.22	8.64	1.63	1.12	0.89
1-4	2002	41.4	2.5	5.91	25.14	4.77	1.33	7.46	1.18	8.98	2.47	8.87	1.37	9.61	1.80	1.12	0.88
1-1	3000	52.3	11.2	7.23	29.81	5.75	1.54	8.53	1.30	10.25	2.61	9.36	1.43	10.36	1.90	1.12	0.86

Table S3.2. (continued)

Sample ID	Water depth (m)	[La]	[Ce]	[Pr]	[Nd]	[Sm]	[Eu]	[Gd]	[Tb]	[Dy]	[Ho]	[Er]	[Tm]	[Yb]	[Lu]	(Eu/Eu*) ^a _N	(Er/Yb) _N
Station GeoB17011-(10.6342°N 148.9010°E; MLD: 41-42 m; bottom: 5667 m)																	
1-surf	5	5.45	4.0	1.03	4.47	1.02	0.30	1.72	0.26	2.00	0.51	1.67	0.22	1.23	0.19	1.17	1.30
1-21+22	21	5.51	2.9	1.17	4.95	1.16	0.34	1.96	0.28	2.12	0.54	1.76	0.23	1.28	0.21	1.19	1.31
1-19+20	81	4.43	2.3	0.92	4.12	0.86	0.25	1.44	0.23	1.75	0.46	1.50	0.19	1.01	0.16	1.12	1.41
1-17+18	142	4.23	2.3	0.88	4.06	0.83	0.23	1.38	0.22	1.69	0.46	1.61	0.20	1.08	0.17	1.08	1.42
1-15+16	370	14.52	1.7	2.09	9.03	1.71	0.49	2.85	0.46	3.67	1.03	3.78	0.55	3.67	0.69	1.10	0.99
1-14	502	14.90	1.6	2.39	9.89	1.94	0.55	3.51	0.51	4.11	1.14	4.13	0.63	4.18	0.78	1.11	0.94
1-13	799	17.74	1.9	2.76	11.63	2.27	0.65	3.98	0.59	4.82	1.34	4.89	0.78	5.16	1.00	1.12	0.91
1-12	1001	21.59	2.0	2.93	12.84	2.51	0.72	4.04	0.65	5.42	1.51	5.64	0.85	6.00	1.13	1.12	0.90
1-11	1500	30.1	2.9	4.11	18.39	3.46	0.97	5.52	0.88	7.31	1.98	7.36	1.12	8.40	1.55	1.11	0.84
1-10	2002	37.0	2.1	4.94	22.16	4.14	1.16	6.36	1.02	8.24	2.26	8.18	1.25	9.13	1.73	1.12	0.86
1-9	2502	43.0	3.1	6.18	26.30	5.00	1.38	7.74	1.19	9.43	2.52	9.09	1.40	9.93	1.87	1.13	0.88
1-8	3000	49.1	2.3	7.29	30.79	5.90	1.59	8.71	1.33	10.28	2.71	9.64	1.48	10.26	1.95	1.13	0.90
1-7	4002	48.2	2.8	7.24	31.22	5.78	1.54	8.77	1.33	10.16	2.61	9.10	1.43	10.02	1.88	1.10	0.87
1-6	4502	47.8	3.8	7.26	31.51	5.83	1.55	8.52	1.31	9.71	2.56	8.91	1.40	9.56	1.78	1.12	0.89
1-5 ^b	4502	45.8	3.2	7.44	30.65	5.85	1.53	8.29	1.27	9.72	2.54	9.01	1.40	9.86	1.81	1.12	0.87
1-4	5001	46.2	3.9	7.25	29.74	5.67	1.49	8.16	1.25	9.61	2.46	8.71	1.35	9.55	1.78	1.12	0.87
1-1	5574	54.0	9.2	8.52	34.32	6.67	1.73	9.31	1.44	10.77	2.72	9.29	1.45	10.13	1.87	1.11	0.88
Station GeoB17014-(6.7842°N 154.1982°E; MLD: 30-31 m; bottom: 4583 m)																	
1-surf	5	3.89	2.6	0.99	4.27	0.95	0.29	1.50	0.25	1.93	0.48	1.62	0.20	1.18	0.18	1.20	1.32
1-21+22	22	5.30	2.8	1.10	4.64	1.04	0.32	1.67	0.26	2.03	0.51	1.70	0.22	1.26	0.19	1.22	1.29
1-19+20	121	5.73	2.8	0.95	4.07	0.83	0.24	1.48	0.24	1.90	0.51	1.82	0.24	1.39	0.23	1.09	1.25
1-16+17	200	10.74	1.8	1.54	6.71	1.26	0.37	2.11	0.34	2.80	0.76	2.72	0.39	2.48	0.42	1.12	1.05
1-15	261	13.32	2.8	1.89	8.06	1.57	0.45	2.43	0.40	3.20	0.91	3.34	0.50	3.29	0.62	1.13	0.97
1-14	502	18.05	2.8	2.36	10.15	1.95	0.58	3.48	0.53	4.43	1.28	4.87	0.75*	5.30*	1.04*	1.14	0.88*
1-13	641	15.82	1.9	2.31	9.61	1.87	0.54	3.03	0.49	4.01	1.14	4.18	0.63	4.46	0.85	1.13	0.90
1-13 ^c	641	16.96	2.1	2.19	9.74	1.90	0.54	3.02	0.50	4.04	1.17	4.17	0.66	4.33	0.81	1.11	0.92
1-12	1002	20.83	1.8	2.68	12.06	2.27	0.67	3.81	0.60	5.08	1.46	5.43	0.82	5.89	1.12	1.14	0.88
1-11	1501	25.9	2.3	3.65	16.13	3.04	0.85	5.35	0.79	6.66	1.84	6.87	1.06	7.58	1.46	1.10	0.87
1-10 ^b	1501	27.6	2.5	3.50	16.07	3.03	0.88	4.98	0.78	6.62	1.83	6.84	1.06	7.43	1.41	1.15	0.88
1-9	2001	33.3	2.6	4.47	19.07	3.63	1.00	6.00	0.81	7.53	2.13	7.96	1.22	8.91	1.73	1.16	0.85
1-8	2501	43.0	2.1	5.66	24.71	4.56	1.29	7.44	1.11	9.03	2.44	8.74	1.36	9.81	1.88	1.14	0.85
1-7	3001	45.7	2.4	6.86	28.83	5.50	1.52	8.56	1.30	9.63	2.63	9.28	1.47	10.12	1.91	1.14	0.88
1-6	3800	47.2	4.1	7.56	31.21	5.84	1.59	8.77	1.34	10.29	2.67	9.51	1.45	10.39	1.89	1.13	0.88

Table S3.2 (continued)

Sample ID	Water depth (m)	[La]	[Ce]	[Pr]	[Nd]	[Sm]	[Eu]	[Gd]	[Tb]	[Dy]	[Ho]	[Er]	[Tm]	[Yb]	[Lu]	(Eu/Eu*) _N ^a	(Er/Yb) _N
1-5	4001	48.5	5.9	7.26	31.32	5.73	1.85*	8.40	1.30	10.02	2.61	9.12	1.41	10.11	1.85	1.35*	0.86
1-4	4500	48.8	7.7	7.63	32.02	5.99	1.57	8.58	1.32	10.25	3.14*	9.13	1.40	9.91	1.79	1.11	0.88
1-4 ^c	4500	52.0	10.1	7.83	33.26	5.99	1.59	8.64	1.33	10.08	2.53	9.04	1.38	9.74	1.80	1.12	0.89
1-3	4573	47.3	3.5	7.72	31.29	5.90	1.53	8.59	1.30	9.91	2.61	8.87	1.40	9.78	1.80	1.10	0.87
Station GeoB17015-(2.0046°N 157.9976°E; MLD: 19-20 m; bottom: 2695 m)																	
1-surf	5	4.81	3.6	1.19	5.42	1.20	0.38	2.02	0.31	2.40	0.56	1.92	0.25	1.48	0.23	1.25	1.24
1-23+24	20	5.63	3.6	1.29	5.94	1.35	0.41	2.11	0.36	2.55	0.59	1.93	0.25	1.51	0.25	1.18	1.22
1-21+22	40	7.78*	3.5	1.49*	6.45	1.45	0.42	2.24	0.35	2.71	0.64	2.21	0.28	1.74	0.27	1.17	1.22
1-19+20	50	6.31	4.1	1.24	5.46	1.25	0.38	2.14	0.31	2.30	0.57	1.85	0.24	1.43	0.23	1.22	1.24
1-17+18	60	18.61*	17.8*	1.17	4.97	0.98	0.31	1.63	0.26	1.98	0.50	1.66	0.21	1.14	0.18	1.20	1.38
1-15+16	80	5.35	2.1	1.18	5.06	1.12	0.35	1.69	0.28	2.18	0.54	1.89	0.24	1.43	0.22	1.23	1.27
1-13+14	101	4.34	2.2	0.91	3.95	0.86	0.27	1.42	0.23	1.79	0.47	1.62	0.21	1.20	0.19	1.21	1.30
1-11+12	130	4.74	2.3	1.01	4.42	0.99	0.30	1.50	0.25	1.94	0.52	1.72	0.23	1.35	0.21	1.19	1.22
1-9+10	180	9.33	3.4	1.43	5.92	1.22	0.34	2.04	0.32	2.57	0.68	2.38	0.33	2.08	0.36	1.09	1.09
1-7+8	200	16.16*	6.5*	1.82	7.54	1.50	0.43	2.57	0.38	3.11	0.83	2.92	0.42	2.62	0.47	1.12	1.06
1-5+6	241	11.28	3.5	1.55*	7.12	1.36	0.40	2.24	0.36	2.96	0.80	3.01	0.45	2.87	0.51	1.15	1.00
1-3+4	320	20.95*	10.3*	1.85	7.38	1.42	0.40	2.41	0.37	3.04	0.85	3.09	0.46	3.05	0.57	1.10	0.97
1-2	602	13.19	1.7	1.82	8.02	1.54	0.45	2.53	0.42	3.53	1.01	3.98	0.59	4.03	0.72	1.13	0.94
1-1	893	15.14	1.8	2.13	9.31	1.82	0.54	3.22	0.50	4.09	1.18	4.47	0.70	4.79	0.90	1.14	0.89
Station GeoB17016-(0.0001°N 160.0003°E; MLD: 16-17 m; bottom: 2837 m)																	
1-surf	5	4.71	3.6	1.34	5.69	1.34	0.40	2.28	0.33	2.52	0.62	2.01	0.27	1.59	0.26	1.21	1.21
1-23+24	20	6.21	4.2	1.45	6.23	1.48	0.44	2.41	0.36	2.66	0.64	2.10	0.27	1.63	0.27	1.22	1.24
1-21+22	58	5.71	4.1	1.39	5.86	1.39	0.41	2.30	0.34	2.51	0.61	2.04	0.26	1.54	0.25	1.21	1.27
1-19+20	70	16.25*	10.9*	1.40	5.82	1.29	0.38	2.00	0.32	2.35	0.57	1.95	0.25	1.44	0.23	1.20	1.30
1-17+18	90	5.84	3.4	0.82	3.71	0.77	0.24	1.34	0.21	1.68	0.46	1.53	0.20	1.08	0.18	1.18	1.36
1-15+16	120	5.14	2.7	1.03	4.69	1.01	0.32	1.77	0.26	1.95	0.52	1.75	0.24	1.36	0.22	1.25	1.23
1-13+14	150	5.25	2.6	0.96	4.43	0.93	0.29	1.54	0.24	1.86	0.51	1.74	0.24	1.41	0.24	1.21	1.18
1-11+12	199	7.67	2.3	1.28	5.50	1.18	0.34	1.90	0.29	2.35	0.63	2.26	0.31	1.94	0.35	1.14	1.11
1-9+10	283	8.83	1.7	1.57	6.71	1.34	0.39	2.30	0.35	2.81	0.78	2.89	0.41	2.66	0.48	1.13	1.04
1-7+8	401	17.51*	5.3*	1.76	7.26	1.45	0.43	2.54	0.39	3.18	0.90	3.27	0.50	3.30	0.60	1.13	0.95
1-5+6	501	11.47	1.5	1.81	7.56	1.53	0.44	2.68	0.40	3.38	0.96	3.64	0.54	3.73	0.71	1.12	0.93
1-3+4	599	12.82	2.0	1.84	7.86	1.54	0.44	2.70	0.42	3.42	1.03	3.79	0.60	4.00	0.76	1.09	0.91
1-2	799	14.66	2.0	2.03	8.88	1.71	0.51	3.06	0.47	3.97	1.14	4.33	0.68	4.63	0.89	1.13	0.90

Table S3.2. (continued)

Sample ID	Water depth (m)	[La]	[Ce]	[Pr]	[Nd]	[Sm]	[Eu]	[Gd]	[Tb]	[Dy]	[Ho]	[Er]	[Tm]	[Yb]	[Lu]	(Eu/Eu*) _N ^a	(Er/Yb) _N
1-1	1003	18.05	2.8	2.36	10.15	1.95	0.58	3.48	0.53	4.43	1.28	4.87	0.75	5.30	1.04	1.14	0.88
Station GeoB17017- (2.0021°S 161.9998°E; MLD: 11-12 m; bottom: 3162 m)																	
1-surf	5	5.68	4.9	1.21	5.20	1.18	0.35	1.89	0.28	2.14	0.52	1.70	0.22	1.52	0.20	1.21	1.07
1-23+24	41	5.41	3.4	1.07	4.80	1.09	0.34	1.92	0.27	2.07	0.52	1.72	0.22	1.24	0.20	1.23	1.33
1-21+22	80	5.28	2.1	1.02	4.56	1.00	0.30	1.72	0.27	1.98	0.54	1.74	0.23	1.28	0.21	1.15	1.31
1-19+20	100	5.62	2.5	0.87	3.92	0.79	0.24	1.40	0.21	1.73	0.46	1.60	0.21	1.17	0.20	1.17	1.31
1-17+18	119	4.55	1.5	0.79	3.75	0.78	0.24	1.39	0.22	1.72	0.49	1.64	0.22	1.20	0.21	1.15	1.31
1-15+16	149	5.06	2.3	0.74	3.49	0.67	0.21	1.21	0.20	1.62	0.46	1.58	0.22	1.20	0.21	1.14	1.26
1-13+14	200	7.11	1.8	1.20	5.14	0.99	0.28	1.77	0.27	2.20	0.61	2.33	0.32	2.09	0.37	1.10	1.07
1-11+12	300	9.28	1.7	1.59	6.57	1.34	0.38	2.27	0.34	2.90	0.81	2.96	0.43	2.88	0.53	1.12	0.98
1-9+10	550	11.76	1.5	1.83	7.59	1.51	0.43	2.65	0.41	3.42	1.00	3.76	0.58	3.92	0.75	1.11	0.92
1-7+8	701	12.73	1.6	1.89	8.15	1.59	0.46	2.91	0.44	3.56	1.05	4.06	0.61	4.23	0.80	1.10	0.92
1-6	840	13.97	1.8	2.06	8.72	1.72	0.51	3.10	0.47	4.01	1.15	4.45	0.68	4.73	0.91	1.13	0.90
1-5	1004	15.42	2.0	2.17	9.81	1.96	0.55	3.44	0.52	4.22	1.27	4.70	0.76	5.24	0.98	1.08	0.86
1-4	2000	35.6	10.3*	3.84	16.22	2.89	0.83	5.00	0.71	6.63	1.89	7.05	1.13	7.86	1.51	1.16	0.86
1-3	2998	42.5	2.4	5.95	25.73	4.84	1.32	7.71	1.18	9.08	2.49	8.88	1.40	9.85	1.87	1.10	0.86
1-2	3082	43.9	4.3	6.39	27.4	5.13	1.37	7.79	1.21	9.19	2.53	8.92	1.42	9.74	1.84	1.10	0.88
1-1 ^b	3082	45.1	4.0	6.46	27.0	5.14	1.40	7.66	1.18	9.34	2.50	9.16	1.39	10.04	1.90	1.13	0.87
Station GeoB17018- (8.2019°S 166.0826°E; MLD: 43-44 m; bottom: 4623 m)																	
1-surf	5	4.11	2.6	0.86	3.91	0.88	0.26	1.46	0.24	1.72	0.45	1.52	0.18	0.96	0.15	1.14	1.51
1-23+24	21	5.97	3.2	0.92	4.18	0.88	0.26	1.41	0.23	1.71	0.44	1.41	0.18	0.95	0.15	1.17	1.42
1-21+22	41	4.01	1.8	0.74	3.52	0.71	0.22	1.19	0.20	1.53	0.40	1.30	0.16	0.81	0.12	1.18	1.53
1-19+20	150	3.89	1.4	0.70	3.17	0.67	0.20	1.17	0.19	1.54	0.45	1.49	0.20	1.12	0.19	1.11	1.27
1-17+18	200	4.72	1.9	0.81	3.66	0.70	0.21	1.47	0.19	1.63	0.44	1.56	0.21	1.27	0.20	1.13	1.18
1-15+16	320	9.44	3.6	1.42	6.05	1.10	0.30	1.86	0.27	2.26	0.65	2.44	0.35	2.94	0.44	1.10	0.79
1-13+14	720	12.66	1.3	1.82	7.57	1.44	0.42	2.74	0.42	3.66	1.06	4.13	0.64	4.39	0.84	1.07	0.90
1-11+12	800	13.60	1.4	1.89	8.10	1.54	0.46	2.75	0.44	3.88	1.13	4.33	0.67	4.76	0.92	1.11	0.87
1-10	1002	15.04	1.5	2.06	8.92	1.71	0.50	3.21	0.48	4.24	1.25	4.90	0.75	5.25	1.02	1.09	0.89
1-9	1502	21.76	1.2	2.79	12.00	2.14	0.65	3.74	0.56	5.29	1.53	5.88	0.92	6.67	1.28	1.19	0.84
1-8	2000	31.7	2.2	4.27	17.89	3.47	0.95	5.64	0.77	7.12	2.03	7.45	1.16	8.28	1.59	1.16	0.86
1-7	2501	42.2	4.4	6.18	26.1	5.07	1.38	7.78	1.22	9.19	2.57	8.80	1.38	9.53	1.78	1.11	0.88
1-6	3100	51.0*	6.5	6.50	27.42	5.29	1.45	7.94	1.19	9.51	2.47	8.89	1.37	9.57	1.84	1.15	0.89
1-5	3403	41.0	3.1	5.91	24.6	4.75	1.29	7.33	1.14	8.84	2.42	8.61	1.36	9.48	1.80	1.11	0.87
1-4	4002	43.7	9.2*	6.30	27.00	4.77	1.29	7.43	1.07	8.35	2.26	8.25	1.22	8.95	1.67	1.14	0.88

Table S3.2 (continued)

Sample ID	Water depth (m)	[La]	[Ce]	[Pr]	[Nd]	[Sm]	[Eu]	[Gd]	[Tb]	[Dy]	[Ho]	[Er]	[Tm]	[Yb]	[Lu]	(Eu/Eu*) _N ^a	(Er/Yb) _N
1-3	4400	40.9	2.5	5.65	24.59	4.43	1.23	7.10	1.09	8.31	2.28	8.05	1.28	8.88	1.69	1.12	0.87
1-2	4500	42.4	6.5*	6.13	26.0	4.67	1.25	7.19	1.11	8.28	2.26	8.00	1.27	8.99	1.69	1.10	0.85
1-1 ^b	4500	42.6	2.7	5.63	24.41	4.44	1.19	6.96	1.04	8.46	2.24	7.96	1.25	8.79	1.71	1.10	0.87
Station GeoB17019- (15.2179°S 173.5187°E; MLD: 103 m; bottom: 2784 m)																	
1-surf	5	5.22	4.2	0.79	3.49	0.75	0.23	1.32	0.21	1.59	0.42	1.38	0.17	0.92	0.14	1.15	1.44
1-22+23	20	13.02*	9.8*	1.14*	4.67*	0.94*	0.28*	1.36	0.23	1.76*	0.45	1.52*	0.19	1.05*	0.16	1.19*	1.38*
1-20+21	41	4.01	1.7	0.73	3.34	0.69	0.22	1.23	0.20	1.53	0.42	1.40	0.18	0.93	0.15	1.17	1.43
1-18+19	120	4.81	3.3	0.72	3.21	0.68	0.21	1.24	0.19	1.56	0.42	1.42	0.18	0.95	0.15	1.16	1.43
1-16+17	200	3.42	1.5	0.57	2.77	0.53	0.16	0.97	0.16	1.34	0.38	1.31	0.17	0.89	0.15	1.12	1.41
1-14+15	410	7.63	2.1	1.13	4.91	0.90	0.24	1.56	0.24	2.04	0.58	2.15	0.30	2.01	0.34	1.04	1.02
1-12+13	550	11.65	3.6	1.73	7.05	1.32	0.36	2.16	0.37	3.13	0.91	3.43	0.52	3.48	0.66	1.04	0.94
1-10+11	700	13.39	1.2	1.77	7.96	1.47	0.42	2.74	0.41	3.62	1.05	3.94	0.61	4.22	0.82	1.07	0.89
1-8+9	800	15.99	2.3	1.95	8.55	1.58	0.45	2.79	0.45	3.86	1.12	4.26	0.68	4.56	0.84	1.07	0.89
1-7	1002	16.08	1.3	2.13	9.30	1.74	0.50	3.34	0.50	4.24	1.28	4.72	0.77	5.33	1.05	1.06	0.85
1-6	1302	17.59	1.1	2.41	10.47	1.94	0.56	3.62	0.56	4.80	1.41	5.39	0.86	6.05	1.16	1.07	0.85
1-5	1802	25.0	1.8	2.99	13.25	2.34	0.70	4.17	0.60	5.67	1.60	6.22	0.96	6.81	1.28	1.18	0.87
1-4	2600	32.6	1.3	4.40	18.48	3.45	0.98	5.72	0.76	7.09	2.01	7.30	1.13	8.22	1.59	1.20	0.85
1-3 ^b	2600	32.0	1.5	4.29	18.33	3.41	0.97	5.53	0.80	7.02	2.01	7.23	1.15	8.16	1.53	1.18	0.85
1-2	2772	39.2	7.6	4.50	19.61	3.49	1.00	5.60	0.88	7.29	2.00	7.27	1.13	8.32	1.53	1.14	0.84

MLD: mixed layer depth related to 0.125 kg/m³ density offset from surface (Miller, 1976).^aEu anomaly calculated as (Eu/Eu*)_N = 3×Eu_N/(2×Sm_N+Tb_N) (e.g., Zhang et al., 2008).^btotal procedural replicate.^cre-processed and re-analyzed.*questionable/suspect data (Quality Flag Scheme after IODE, for details see http://www.iode.org/index.php?option=com_oce&task=viewDocumentRecord&docID=10762).

4. Rapid and precise analysis of rare earth elements in small volumes of seawater - Method and intercomparison

Melanie K. Behrens^a, Jesse Muratli^b, Catherine Pradoux^c, Yingzhe Wu^d, Philipp Böning^a,
Hans-Jürgen Brumsack^e, Steven L. Goldstein^d, Brian Haley^b, Catherine Jeandel^c, Ronja
Paffrath^a, Leopoldo D. Pena^f, Bernhard Schnetger^e, Katharina Pahnke^a

manuscript published in

Marine Chemistry 186, 110-120, doi.10.1016/j.marchem.2016.08.006 (2016)

^aMax Planck Research Group for Marine Isotope Geochemistry, Institute for Chemistry and Biology of the Marine Environment (ICBM), University of Oldenburg, Carl-von-Ossietzky-Str. 9-11, 26129 Oldenburg, Germany

^bCollege of Earth, Ocean and Atmospheric Sciences, Oregon State University, 104 CEOAS Administration Building, Corvallis, Oregon, USA

^cLaboratoire d'Etudes en Géophysique et Océanographie Spatiale (LEGOS), Université de Toulouse (CNRS/CNES/UPS/IRD), Observatoire Midi-Pyrénées, 14 Avenue Edouard Belin, 31400, Toulouse, France

^dLamont-Doherty Earth Observatory and Department of Earth and Environmental Sciences, Columbia University, 61 Rt. 9W, Palisades, NY 10964, USA

^eInstitute for Chemistry and Biology of the Marine Environment (ICBM), University of Oldenburg, Carl-von-Ossietzky-Str. 9-11, 26129 Oldenburg, Germany

^fDepartment of Earth and Ocean Dynamics, University of Barcelona, Martí Franquès s/n, 08028 Barcelona, Spain

Highlights

- Robust and rapid preconcentration of REE using the seaFAST system in offline mode
- Accurate and precise isotope dilution ICP-MS method
- Intercomparison provides first Pacific seawater REE reference standard
- International intercomparison of Pacific seawater REE for the GEOTRACES program

Abstract

Rare earth elements are used as tracers for oceanic trace element cycling. However, the low (picomolar level) dissolved REE concentrations and time-consuming methods have so far hindered their extensive use in marine studies. This study reports the first application of the automated seaFAST-pico system (Elemental Scientific Inc.) in offline mode and using multi-element isotope dilution inductively coupled plasma-mass spectrometry (ID ICP-MS) for the robust and rapid pre-concentration, purification, and analysis of dissolved REEs from small volumes of seawater (11-12 mL). Accuracy of our new method is checked with replicates of GEOTRACES intercalibration seawater from BATS (North Atlantic) at 15 m and 2000 m water depths. Our results show excellent agreement (within the analytical uncertainty, 2σ SD) with the published intercalibrated values from the GEOTRACES intercalibration study. Replicates of GEOTRACES intercalibration seawater from SAFe at 3000 m water depth (North Pacific) indicate a procedural long-term error of $\leq 3.9\%$ 2σ RSD for all REEs, except for Ce and Gd. An international intercomparison from 4 labs using SAFe 3000 m seawater aliquots, 2 of which also use the seaFAST-pico system in offline mode, and different pre-concentration, purification, and analytical methods shows excellent agreement between REE concentrations within 7% (2σ RSD) (except for Ce 71%, Gd 14%, Lu 12%). This is comparable to the agreement obtained for the BATS 15 m and 2000 m samples by six different labs for the international GEOTRACES intercalibration study (van de Flierdt et al., 2012). The REE intercomparison values of SAFe 3000 m (i.e., the average of the values from the 4 labs) in this study agree within the analytical uncertainties (2σ SD) with published REE values of deep seawater from nearby stations. Our international intercomparison provides the first REE intercomparison values for the GEOTRACES intercalibration station SAFe at 3000 m, and establishes the first reference seawater REE values for quality control of future REE studies in the Pacific Ocean as SAFe will remain a GEOTRACES baseline, and hence intercalibration station, for cruises in the North Pacific. Our method is easy to adopt and enables the extensive use of REEs, thereby opening the way to build a global seawater REE dataset.

4.1. Introduction

Rare earth elements exist predominantly in the trivalent oxidation state. Only Eu and Ce can be reduced to Eu(II) and oxidized to Ce(IV) depending on the redox conditions. A systematic chemical property of REEs is the decrease in ionic radii with increasing atomic number, which leads to an increase in the strength of complexation by carbonate ions from LREEs to heavy HREEs in seawater that makes heavies more soluble. Light REEs are therefore preferentially scavenged by particles, resulting in a characteristic shale-normalized fractionation pattern in seawater with a HREE over LREE enrichment (e.g., Cantrell and Byrne, 1987; Elderfield, 1988; Byrne and Kim, 1990; Quinn et al., 2006; Schijf et al., 2015). Differences and changes in shale-normalized REE patterns in seawater have been used as diagnostic tool to trace and characterize 1) marine geochemical processes (e.g. scavenging, remineralization, redox changes), 2) sources of trace elements to the ocean, 3) anthropogenic pollution, and 4) different water masses (e.g., Alibo and Nozaki, 1999; Elderfield, 1988; Hongo et al., 2007; Jeandel et al., 2013; Kim and Kim, 2011; Kulaksiz and Bau, 2011; Lacan and Jeandel, 2001; Shaw et al., 2003; Sholkovitz et al., 1994; Zhang and Nozaki, 1996).

The wide potential for the application of REEs in marine, coastal, and estuarine environments as well as the lack of understanding of oceanic trace element cycling has led to increased interest in applying seawater REE analyses. As a result, REEs are part of the international GEOTRACES program (e.g., Grenier et al., 2013; Hathorne et al., 2015; Jeandel et al., 2013). However, extensive use of REEs as tracers in the ocean has been hindered by major difficulties: 1) the low (picomolar level) concentration of REEs in seawater that requires sample pre-concentration, 2) the high salt matrix interferences that require sample purification, 3) the potential fractionation of REEs during the chemical procedures, 4) the high analytical precision required to resolve small changes in the fractionation among REEs, and 5) the oxide interferences (Ba on Eu, and LREEs on HREEs).

In previous approaches, dissolved REEs have been pre-concentrated and purified using liquid-phase or solid-phase extractions (e.g., magnesium or iron co-precipitation, chelating and ion-exchange resins) and analyzed by either instrumental neutron activation, thermal ionization mass spectrometry, inductively coupled plasma-atomic emission spectrometry, or inductively coupled plasma-mass spectrometry (Hatje et al., 2014; Shaw et al., 2003; Zheng et al., 2015 and references therein). However, these methods have important limitations due either the requirement of large sample volumes (up to ~20 L), the inability to analyze mono-isotopic REEs, low precision, or time-consuming procedures (e.g., de Baar et

al., 1985; Greaves et al., 1989). Recently, Hathorne et al. (2012, 2015) presented a method using the commercially available seaFAST system (Elemental Scientific Inc. Omaha, Nebraska, USA) that allows automated, rapid pre-concentration and purification of all REEs directly from small volumes of seawater (7 mL and 11 mL, respectively). In both cases, the authors used the online pre-concentration system directly connected to an ICP-MS. This allows for the immediate determination of REE concentrations yielding average precisions of 12% (2σ RSD) for a 7 mL seawater sample (South Atlantic, 59°N, 0°E, 2000 m) (Hathorne et al., 2012) and 8.4%, 12%, and 5.0% (2σ RSD) for an 11 mL seawater sample (BATS, 31°40'N, 64°10'W, 15 m and 2000 m; Station 113, 52°59.80'S, 0°02.00'E, 1000 m), respectively (Hathorne et al., 2015).

In this study, we present the method at ICBM (Institute for Chemistry and Biology of the Marine Environment), University of Oldenburg, that uses the seaFAST-pico system in offline pre-concentration mode, that is, the pre-concentrated REE fractions are collected into sample vials prior to analysis. We choose the offline operation for the following reasons: 1) the automated pre-concentration can be run over night independent of an ICP-MS, saving argon gas and operator time, and 2) the samples can be analyzed with a constant signal instead of an elution peak signal, allowing several measurement passes and, if required, re-analyses, thereby increasing analytical precision significantly. The disadvantages are the lack of immediate assessment of the elemental concentrations, lower signal intensities for the same sample volume compared to time-resolved analysis at the highest elution peak signal (e.g., Hathorne et al., 2012), and the potential of slightly higher total procedural blanks due to an additional dilution step.

In the first part of this manuscript, we outline the details of our procedure using the seaFAST system in offline mode and provide a robust and rapid method for the pre-concentration and purification of REEs from small sample volumes (11-12 mL). For analyses, we use the advantages of both multi-element ID ICP-MS and a desolvating sample introduction system for precise and accurate analysis of REE concentrations (presented as pmol/kg). In the second part of this manuscript, we provide an international intercomparison by four labs of dissolved REE concentrations on sample aliquots from North Pacific station SAFe from 3000 m water depth. Lab 1 is ICBM, Lab 2 is LDEO (Lamont Doherty Earth Observatory), Columbia University, Lab 3 is CEOAS (College of Earth, Ocean and Atmospheric Sciences), Oregon State University, and Lab 4 is LEGOS (Laboratoire d'Etudes en Géophysique et Océanographie Spatiale), University of Toulouse. Both LDEO and CEOAS also use the seaFAST-pico system in offline mode, and we outline the small

differences in procedure. These results further validate our new method and provide the first REE intercomparison values for a GEOTRACES intercalibration station in the North Pacific, based on averaging the average values from the four labs. So far, there is no widely available GEOTRACES seawater standard for REE concentrations from the Pacific. The GEOTRACES intercalibration samples BATS 15 m and 2000 m from the North Atlantic are nearly depleted already, and the SAFe sample is a possible alternative.

4.2. Materials and procedures

4.2.1. Sample locations and onboard procedure

We used seawater collected during two GEOTRACES intercalibration cruises at stations BATS (31°40'N, 64°10'W, 15 m, 2000 m water depth) in the North Atlantic (R/V *Knorr*, KN193-6, June-July 2008) and SAFe (30°N, 140°W, 3000 m water depth) in the North Pacific (R/V *Knorr*, KN195-8, May 2009). The shipboard sampling procedures are described in detail in Pahnke et al. (2012) and van de Flierdt et al. (2012). Briefly, the surface water was sampled using a trace-metal clean towed sampling system (GeoFish) (Bruland et al., 2005), while deep waters were collected from multiple casts using trace-metal clean GO-FLO bottles (General Oceanics) (Cutter and Bruland, 2012; van de Flierdt et al., 2012). Seawater samples were filtered through 0.2 µm pore size Osmonics (Memtrex) cartridge filters, transferred into large tanks through Teflon tubing, acidified to $\text{pH} \leq 2$, mixed overnight, and subsampled into acid-cleaned HDPE or LDPE bottles. The participants of this intercomparison study received aliquots directly from the intercalibration cruise in 2009 (e.g., van de Flierdt et al., 2012) or we provided them with an aliquot from our subsample in acid-cleaned HDPE bottles.

4.2.2. Lab 1: Offline seaFAST pre-concentration of REEs and multi-element ID ICP-MS

4.2.2.1. Pre-concentration of REEs from seawater

The pre-concentration method of this study (Lab 1, ICBM) is described in detail in the following and summarized in Table 4.1. Dilutions were prepared with high purity water (18.2 MΩ cm). Chemicals used were of high purity (ammonium hydroxide, ultra-quality Carl Roth) and ultra-high purity (nitric acid, glacial acetic acid, optima quality Fisher Chemical). The required buffer solution was prepared using 157 mL high purity water, 140 mL glacial acetic acid, and 203 mL 20% ammonium hydroxide. The pH of the buffer solution (6.0 ± 0.2) was adjusted by adding small amounts of either glacial acetic acid or ammonium hydroxide.

Dilutions were prepared with high purity water (18.2 MΩ cm). Chemicals used were of high purity (ammonium hydroxide, ultra-quality Carl Roth) and ultra-high purity (nitric

acid, glacial acetic acid, optima quality Fisher Chemical). The required buffer solution was prepared using 157 mL high purity water, 140 mL glacial acetic acid, and 203 mL 20% ammonium hydroxide. The pH of the buffer solution (6.0 ± 0.2) was adjusted by adding small amounts of either glacial acetic acid or ammonium hydroxide. A 1.5 N HNO₃ was used as eluting acid, and a 2% HNO₃ was used as rinse solution for the autosampler probe.

The seaFAST-pico system used here for the automated pre-concentration of REEs from seawater consists of an autosampler with 120 positions for sample and elution vials each, clean enclosure, and ultra-low particulate air filter, a pre-concentration and clean-up column with PFA (perfluoroalkoxy) housing and PTFE (polytetrafluoroethylene) frits, and triple 6-port valves with PFA rotors and CTFE (chlorotrifluoroethylene) stators that regulate the pre-concentration process. All solutions were pumped through PFA tubing using one 12 mL CTFE/PTFE and three 3 mL quartz/PFA SYRIX syringe pumps (S400V syringe pump module). The pre-concentration and clean-up columns were packed with 200 µL of a chelating resin consisting of ethylenediaminetriacetic acid and iminodiacetic acid functional groups to pre-concentrate trace elements from seawater while anions and alkali and alkaline earth cations pass through the resin (<http://www.icpms.com/pdf/seaFAST-seawater-analysis.pdf>). For our purposes, a 10 mL PFA sample loop was used that required an initial sample volume of 11-12 mL. The offline pre-concentration and elution of REEs on the seaFAST for 11-12 mL of seawater took ~15 min per sample and the separations were run automatically overnight.

Table 4.1: Summary of methodologies used in this study (Lab 1) and by the three participating labs.

Lab	Sample Volume	Spike	Pre-concentration Method	Quantification Method	Instrument
1	11-12 mL	multi-element REE spike	offline seaFAST-pico system	isotope dilution	Thermo Finnigan ELEMENT 2 ICP-MS
2	10 mL	multi-element REE spike	offline seaFAST-pico system	isotope dilution	VG PQ ExCell ICP-MS
3	20 mL		offline seaFAST-pico system	external standards	Thermo Xseries-II ICP-MS
4	500 mL	¹⁵⁰ Nd, ¹⁷² Yb, Indium, Rhenium	Fe co-precipitation with 0.5 g Fe; 2 mL of Biorad AG1X8 anion exchange resin, 100-200 µm mesh-size	isotope dilution coupled with internal and external standards	Agilent 7500 ICP-MS

Lab 1: Institute for Chemistry and Biology of the Marine Environment (ICBM), University of Oldenburg.

Lab 2: Lamont-Doherty Earth Observatory (LDEO), Columbia University.

Lab 3: College of Earth, Ocean and Atmospheric Sciences (CEOAS), Oregon State University.

Lab 4: Laboratoire d'Etudes en Géophysique et Océanographie Spatiale (LEGOS), University of Toulouse.

Prior to pre-concentration on the seaFAST, we weighed 11-12 mL of each seawater sample ($\text{pH} \leq 2$) into 13 mL Teflon tubes and spiked it with a multi-element REE spike to obtain a value of $^{145}\text{Nd}/^{143}\text{Nd}$ of 6 (Table 4.2).

Table 4.2: Isotope concentrations and natural isotope abundances of the diluted spike solution (DKM3) together with isotope ratios of spike-sample mix and error magnification factor (EMF) used for SAFe 3000 m in this study (Lab 1).

Element	Isotope 1	Isotope 2	[Isotope 1] _{sp} (pmol/g)	[Isotope 2] _{sp} (pmol/g)	[Isotope 1] _{nat}	[Isotope 2] _{nat}	Ideal ratio*	EMF of ideal ratio	Range of measured ratio	EMF of measured ratio
La	139	138	0.322	0.023	0.9991	0.0009				
Ce	142	140	6.016	0.526	0.1107	0.8848	1.2	1.23	5.3-7.3	1.89-2.78
Nd	145	143	3.700	0.031	0.0830	0.1218	9.0	1.16	6.0-7.6	1.16-1.18
Sm	149	147	1.992	0.008	0.1380	0.1500	15.6	1.13	12.9-16.4	1.13
Eu	153	151	0.575	0.033	0.5223	0.4777	4.4	1.67	4.3-5.2	1.67-1.69
Gd	155	157	1.125	0.015	0.1473	0.1568	8.3	1.26	5.2-6.5	1.27-1.30
Dy	161	163	1.179	0.019	0.1888	0.2497	6.9	1.25	3.3-4.0	1.30-1.35
Er	167	166	0.570	0.018	0.2294	0.3341	4.6	1.35	1.8-2.1	1.56-1.68
Yb	171	174	0.628	0.006	0.1431	0.3184	6.6	1.15	1.7-2.0	1.31-1.38
Lu	176	175	0.013	0.005	0.0259	0.9741				

[Isotope 1]_{sp} and [Isotope 2]_{sp}: concentrations of isotopes 1 and 2 in the diluted spike.

[Isotope 1]_{nat} and [Isotope 2]_{nat}: natural fractional abundances of isotopes 1 and 2.

Note that La and Lu were treated as mono-isotopic elements (see text).

*ideal isotope ratio of spike-sample mix:
$$\sqrt{\frac{[\text{Isotope 1}]_{\text{sp}} \times [\text{Isotope 1}]_{\text{nat}}}{[\text{Isotope 2}]_{\text{sp}} \times [\text{Isotope 2}]_{\text{nat}}}}$$

The spike was diluted from a pre-mixed REE spike stock solution (prepared by Gilbert N. Hanson of SUNY Stony Brook and called DKM) by 1:24,130 (DKM3) to a concentration of 3.7 pmol/g for ^{145}Nd , and recalibrated by ICP-MS against the AMES Nd standard using reverse isotope dilution. Details on the spike solution (DKM3) including the isotope concentrations and the natural isotope abundances are reported in Table 4.2. The volume of spike that was added to a seawater sample was optimized for each sample aiming at a low error magnification factor while not compromising the counting statistics and thus analytical precision. We allowed equilibration of the sample-spike mixture for at least 48 hours. The spiked samples were arranged in the seaFAST autosampler for automated pre-concentration. The seaFAST procedure was as follows: Prior to each sample pre-concentration, the buffer solution was passed through the clean-up column to reduce possible trace metal impurities in the buffer, and used to precondition the pre-concentration column for 60 s at 0.2 mL/min. The sample was vacuum-loaded into a 10 mL PFA sample loop, then cleaned buffer (at 0.7 mL/min) and high purity water (at 2.5 mL/min) were added to ensure a pH of 6, before the mixture was passed through the pre-concentration column (at 0.5 mL/min). The column was

then rinsed with 4.8 mL of the buffer solution-high purity water mix to wash out the seawater matrix (at 0.5 mL/min buffer, 2.5 mL/min water). The REEs were eluted with 200 μL and 300 μL of 1.5 N HNO_3 in reverse direction at a flow rate of 0.2 mL/min and 0.5 mL/min, respectively, and collected in pre-cleaned PFA micro vials.

Following each sample processing, the pre-concentration column was cleaned with 4.5 mL of the elution acid (1.5 N HNO_3) and conditioned with a buffer solution-high purity water mix in preparation for the next sample. During each session, at least three total procedural blanks of 2% HNO_3 were processed and subsequently spiked with a diluted multi-element REE spike (1:1,518,843, DKM2) for quantification. The samples were diluted to 1.2 mL with high purity water manually in preparation for analysis by ICP-MS. BATS seawater from 15 m (11 and 22 mL) and 2000 m (11 mL) were processed as described above, except for sample volumes of 22 mL, which were loaded into a 10 mL PFA sample loop (11 mL were loaded twice). Each sample was then manually diluted with high purity water to ~ 0.7 - 0.9 mL. In order to analyze all samples at similar final REE concentrations, we targeted a concentration range of 280-380 pmol/kg for Nd and adjusted the initial loaded sample volume or manually diluted the final sample volume accordingly.

The small differences in the seaFAST offline pre-concentration method of Lab 1 compared to those of Labs 2 and 3 (LDEO and CEOAS; see supplementary material) are due to the different quantification methods applied by the labs (e.g., external standard calibration, isotope dilution) and the required final sample volume. Lab 2 eluted the REEs in three steps each of 100 μL of 1.6 N HNO_3 and Lab 3 used a sample volume of ~ 20 mL (instead of 10 mL) that was loaded in two steps using a 10 mL PFA sample loop and REEs were eluted with 200 μL of 1.5 N HNO_3 . Other than Labs 1 and 2, Lab 3 (CEOAS) used five external calibration standards of increasing concentrations (instead of a multi-element spike) for quantification. These external calibration standards were adjusted to a pH of ~ 1.6 by adding ammonium hydroxide in order to increase column buffering and passed through the seaFAST column the same way as the samples.

4.2.2.2. REE determination by ID ICP-MS

Lab 1 (ICBM) used a Thermo Finnigan ELEMENT 2 ICP-MS for REE concentration measurements at the ICBM, University of Oldenburg. The instrument was coupled to an autosampler (CETAC ASX-100) and a desolvation introduction system (CETAC Aridus 2) that was used with a nitrogen-argon gas mixture to enhance sensitivity and to minimize oxide formation to a negligible level (e.g., Grenier et al., 2013; Rousseau et al., 2013). The ICP-MS

was operated at low resolution in counting mode and the guard electrode was switched off. We optimized the instrument for sensitivity daily while aspirating a 100 ng/L tune solution of Ba, Ce, and Lu. Two mixed REE standard solutions (solution 1: Ba, La, Ce, Pr, Tb, Er, and Yb, and solution 2: Nd, Sm, Eu, Gd, and Dy) were measured to assess the formation of LREE oxides that interfere with HREEs, and of Ba oxides that interfere with Eu. We found negligible oxide interferences and monitored the long-term stability of the oxide formation with the above mentioned 100 ng/L tune solution. Typical count rates for 100 ng/L ^{140}Ce were 500 000. As analyzed samples rarely contain Ba due to the above described purification procedure, and given the low oxide formation rates for Ba and LREEs (always 0.01-0.03% for Ce and Ba), no oxide interference corrections of any element had to be applied. All necessary masses between 137 and 177 were scanned in ESCAN (electro scan) mode that required a single magnet jump at mass 158 in order to scan the entire mass range. The sample time for every mass was 0.02 s, except for isotopes with lower signal intensities: ^{159}Tb , ^{165}Ho , ^{166}Er , ^{167}Er , ^{169}Tm , ^{175}Lu (0.04 s) and ^{147}Sm , ^{151}Eu , ^{153}Eu (0.06 s). The longer sampling time improved the precision significantly. The total measurement time of 2 min 39 s consisted of 3 runs of 4 passes and allowed for low sample volume and hence higher concentrated samples providing higher signal intensities thereby optimizing the precision. The instrument operating conditions are reported in Table 4.3.

Table 4.3: Instrument operating conditions for the Thermo Finnigan ELEMENT 2 ICP-MS at the ICBM.

Instrument	Operating Conditions
Equipment	
nebulizer	PFA micro-flow pumped at 0.1 mL/min
CETAC Aridus 2	sweep gas: 2-6 L/min, nitrogen gas: 3-6 mL/min
spray chamber	heated PFA spray chamber
sample and skimmer cones	Nickel
Parameters	
nebulizer/auxiliary/cooling gas flows (L/min)	~0.80 ^a /1.40/13
RF power (W)	1250
detection mode	counting
sample time (s)	0.02s, except: ^{147}Sm , ^{151}Eu , ^{153}Eu = 0.06s, ^{159}Tb , ^{165}Ho , ^{166}Er , ^{167}Er , ^{169}Tm , ^{175}Lu = 0.04s
mass window	40
samples/peak	40
resolution	low

^aoptimized for each measurement session.

We used a standard solution with seawater-like relative REE concentrations in 2% HNO₃ (REE Coral Sea standard, Zheng et al., 2015, provided by Gideon Henderson, University of Oxford) as an external standard. We analyzed the standard both unspiked and spiked at each session at similar signal intensities as the pre-concentrated samples, except for Ce (~5 times higher in the standard). The unspiked REE Coral Sea standard was analyzed after every third sample and used for sensitivity correction of the mono-isotopic elements as well as for monitoring and correction of instrumental mass bias. The results of the spiked REE Coral Sea standard were used to assess the overall analytical long-term precision (see results and discussion section).

The GEOTRACES intercalibration seawater samples from BATS at 15 m and 2000 m that were characterized previously with respect to their REE concentrations (van de Flierdt et al., 2012), were used as external standards and to check the accuracy of our method. Seawater samples from BATS were measured at similar signal intensities as the samples.

Details on the analyzed isotopes in our ID ICP-MS method that was modified from Jones (2010) and Pahnke et al. (2012) are presented in Table 4.4.

Table 4.4: Isotopes analyzed at the ICBM.

Element	Isotope 1	Isotope 2	Comments
Ba	137		to monitor Ba-oxide formation (interference with ¹⁵³ Eu)
La	139		ID element treated as mono-isotopic element
Ce	140	142	ID element; isobaric interference correction of ¹⁴² Nd on ¹⁴² Ce
Pr	141		mono-isotopic element
Nd	143	145	ID element
Sm	147	149	ID element
Eu	151	153	ID element
Gd	155	157	for instrumental mass bias correction of ¹⁵⁵ Gd/ ¹⁵⁷ Gd
Gd	158		magnet jump
Tb	159		mono-isotopic element
Dy	161	163	ID element
Ho	165		mono-isotopic element
Er	166	167	ID element
Tm	169		mono-isotopic element
Yb	171	174	ID element
Lu	175		ID element treated as mono-isotopic element
Hf	177		to monitor any isobaric interference of ¹⁷⁴ Hf on ¹⁷⁴ Yb

We measured a 2% nitric acid instrumental blank before each sample and standard. Raw count rates of each measured mass for samples and standards were first corrected for

these instrumental blanks. The ID element concentrations of the samples were calculated by using ID equations as illustrated by equation (4.1) using Nd as an example:

$$[\text{Nd}]_{\text{smpI}} = \left(\frac{RI_{\text{sp}} - R_{\text{mix}}}{R_{\text{mix}} - RI_{\text{true}}} \right) \times [\text{Nd}]_{\text{sp}} \times \frac{m_{\text{sp}}}{m_{\text{smpI}}} \times \frac{M_{\text{Nd}}}{A_{\text{Nd}}} \quad (4.1)$$

Abbreviations sp and smpI stand for spike and sample, respectively.

RI_{sp} : isotope ratio of $^{143}\text{Nd}/^{145}\text{Nd}$ in the spike

R_{mix} : isotope ratio of $^{143}\text{Nd}/^{145}\text{Nd}$ in the sample/spike mixture

RI_{true} : natural isotope ratio of $^{143}\text{Nd}/^{145}\text{Nd}$

$[\text{Nd}]_{\text{sp}}$: concentration of ^{145}Nd in the spike (mol/g)

m_{sp} and m_{smpI} : weighted masses of spike and sample (g)

M_{Nd} : natural atomic mass of Nd (g/mol)

A_{Nd} : natural relative abundance of ^{145}Nd

Cerium and ytterbium, both required for ID calculations (^{142}Ce and ^{174}Yb), have isobaric interferences from ^{142}Nd and ^{174}Hf , respectively. Before applying the ID equation (4.1) to Ce, ^{142}Ce was corrected for isobaric interference of ^{142}Nd in the sample and the spike:

$$^{142}\text{Ce} = (^{142}\text{Ce} + ^{142}\text{Nd})_{\text{M}} - \left(\frac{^{143}\text{Nd}_{\text{M-sp}}}{R2_{\text{true}}} + \frac{^{143}\text{Nd}_{\text{sp}}}{R2_{\text{sp}}} \right) \quad (4.2)$$

Abbreviation M stands for measured counts.

$(^{142}\text{Ce} + ^{142}\text{Nd})_{\text{M}}$: total measured counts on mass 142

$^{143}\text{Nd}_{\text{M-sp}}$: measured spike-subtracted counts on mass 143

$R2_{\text{true}}$: natural isotope ratio of $^{143}\text{Nd}/^{142}\text{Nd}$

$^{143}\text{Nd}_{\text{sp}}$: measured counts on ^{143}Nd in the spike

$R2_{\text{sp}}$: isotope ratio of $^{143}\text{Nd}/^{142}\text{Nd}$ in the spike (0.5968)

Spike-subtraction from measured counts on ^{143}Nd was done following equation (4.3):

$$^{143}\text{Nd}_{\text{M-sp}} = ^{143}\text{Nd}_{\text{M}} - \left(\frac{RI_{\text{true}} \times ^{145}\text{Nd}_{\text{M}} - ^{143}\text{Nd}_{\text{M}}}{\left(\frac{RI_{\text{true}}}{RI_{\text{sp}}} - 1 \right)} \right) \quad (4.3)$$

$^{143}\text{Nd}_{\text{M}}$: total measured counts on mass 143

$^{145}\text{Nd}_{\text{M}}$: total measured counts on mass 145

RI_{true} : natural isotope ratio of $^{143}\text{Nd}/^{145}\text{Nd}$

RI_{sp} : isotope ratio of $^{143}\text{Nd}/^{145}\text{Nd}$ in the spike

Measured counts on ^{143}Nd in the spike were calculated by subtracting the measured spike-subtracted counts on mass 143 from the total measured counts on mass 143.

No isobaric interference correction was necessary for ^{174}Yb , as ^{174}Hf (monitored by ^{177}Hf) was negligible in our samples.

Instrumental mass bias was determined on the unspiked REE Coral Sea standard and was typically $\leq 1\%$ per amu for REEs, except for Gd. Instrumental mass bias corrections for Gd used the exponential law on the measured $^{155}\text{Gd}/^{157}\text{Gd}$ ratio, assuming a natural ratio of $^{155}\text{Gd}/^{157}\text{Gd} = 0.9394$ before the application of the ID equation. A reference isotope (^{147}Sm) was used as an internal standard to quantify the mono-isotopic elements (^{141}Pr , ^{159}Tb , ^{165}Ho , ^{169}Tm) based on the instrument's sensitivity response for these elements in the unspiked REE Coral Sea standard, defined as the number of counts per concentration in the standard. The concentration of the mono-isotopic elements was then calculated using the internal standard concentration of ^{147}Sm and multiplying with the ratio of the sensitivity of ^{147}Sm to that of the respective mono-isotopic element and vice versa for the measured sample counts.

Lanthanum and lutetium, both ID elements (^{138}La , ^{176}Lu), have isobaric interferences with ^{138}Ba and ^{138}Ce , and with ^{176}Yb and ^{176}Hf , respectively. Due to these interferences and the low abundance of ^{138}La (0.09%) and ^{176}Lu (2.59%), quantification used ^{139}La and ^{175}Lu that were spike-subtracted and treated as mono-isotopic elements.

4.2.3. Pre-concentration methods and mass spectrometry of labs participating in the intercomparison

Each lab used its own preferred method for pre-concentration of REEs from seawater and mass spectrometric analysis. These methods, including that of Lab 1 (ICBM) are summarized in Table 4.1. The methods of Labs 2-4 are described in the supplementary material.

4.3. Results and discussion

4.3.1. Lab 1: Offline seaFAST pre-concentration of REEs and multi-element ID ICP-MS

4.3.1.1. Blanks and detection limit

Lab 1 measured and subtracted instrumental blank solutions of 2% nitric acid that accounted for $\leq 0.8\%$ of the measured sample and standard intensities for REEs, except for two standards with a blank signal of 1.1-1.2% for Nd and three standards with a blank signal of 1.1% for Tb (see Materials and procedures section). The average total procedural blank of

2% nitric acid ($n = 25$) was $\leq 0.2\%$ of each REE concentration of the SAFe 3000 m analyses, except for Ce, which varied significantly and ranged from 1.6% up to 18% (Table 4.5).

The detection limit of our analytical method for REEs, based on three times the standard deviation of the total procedural blanks ($n = 25$) following Zheng et al. (2015), ranged between 0.002 pmol/kg for Tm and 0.4 pmol/kg for Ce (Table 4.5), and was similar to those reported by Zheng et al. (2015).

Table 4.5: Average total procedural blank ($n = 25$) and detection limit for all REEs (Lab 1).

Element	Average Blank (pmol/kg)	Detection Limit (pmol/kg) ^a
La	0.1	0.2
Ce ^b	0.2	0.4
Pr	0.02	0.04
Nd	0.06	0.1
Sm	0.01	0.03
Eu	0.002	0.008
Gd	0.01	0.03
Tb	0.001	0.003
Dy	0.01	0.02
Ho	0.001	0.01
Er	0.002	0.02
Tm	0.0004	0.002
Yb	0.002	0.01
Lu	0.0002	0.01

^athree times the standard deviation of the total procedural blanks.

^bmax blank: 0.6 pmol/kg, min blank: 0.1 pmol/kg.

4.3.1.2. Accuracy and precision

The accuracy of our method was checked with repeated processing and analysis of GEOTRACES intercalibration seawater from BATS 15 m ($n = 5$) and 2000 m ($n = 5$) and SAFe 3000 m ($n = 16$, Nd only) and comparison to the intercalibration values, published by van de Flierdt et al. (2012) for BATS 15 m and 2000 m ($n = 12-26$) and Pahnke et al. (2012) for SAFe 3000 m ($n = 2$, Nd only). Our results for BATS 15 m and 2000 m together with the published intercalibration values are reported in Table 4.6.

The precision of our REE concentration measurements for BATS 15 m was $\leq 8.8\%$ for LREEs and $\leq 3.9\%$ for HREEs, except for Ce (11.3%) and Gd (5.1%) (2σ RSD, $n = 5$, Table 4.6, average precision excluding Ce: 3.5%). The precision of BATS 2000 m analyses was $\leq 4.6\%$ for LREEs and $\leq 3.7\%$ for HREEs, except for Ce (26%) and Gd (6.8%) (2σ RSD, $n = 5$) (Table 4.6, average precision excluding Ce: 3.5%). The internal errors of BATS 15 m and

2000 m analyses were lower than the reported precisions for LREEs and HREEs, except for two samples (4.7% and 12.4% for Nd, 2σ RSD). Our mean REE concentrations from BATS (15 m, 2000 m) ($n = 5$ for each depth) are well within the confidence interval (15% and 12%, respectively, 2σ RSD) of the published intercalibration values (van de Flierdt et al., 2012), with maximum relative deviations of 6.6% for all REEs (Table 4.6, Figs. 4.1a, b). Moreover, our results are close to the published data of Rousseau et al. (2013) deviating by $\leq 6.2\%$ for all REEs except for La (9.4%, BATS 15 m) and Tb (7.6%, BATS 2000 m).

Table 4.6: Dissolved REE concentrations (pmol/kg) of this study (Lab 1) compared to GEOTRACES intercalibration samples at BATS 15 m and 2000 m.

	La	Ce	Pr	Nd	Sm	Eu	Gd	Tb	Dy	Ho	Er	Tm	Yb	Lu
BATS, 15 m (KN193-6-Nd-601)														
this study (n = 5)	14.1	11.9	3.30	13.98	3.20	0.86	4.84	0.81	5.91	1.45	4.83	0.69	4.24	0.69
2σ SD (pmol/kg)	1.2	1.3	0.25	0.44	0.07	0.02	0.25	0.01	0.23	0.04	0.11	0.02	0.11	0.01
2σ RSD%	8.8	11.3	7.6	3.1	2.1	2.3	5.1	1.1	3.9	2.7	2.3	2.4	2.5	1.2
GEOTRACES mean value^a	14.7	12.0	3.12	14.1	3.21	0.89	4.83	0.79	5.90	1.49	4.80	0.70	4.16	0.67
2σ SD (pmol/kg)	2.2	2.7	0.37	1.2	0.36	0.10	0.55	0.08	0.53	0.13	0.43	0.06	0.51	0.09
2σ RSD%	15.0	23	11.8	8.8	11.2	11.8	11.4	10.7	8.9	9.0	8.9	9.0	12.3	13.8
BATS, 2000 m (KN193-6-Nd-401)														
this study (n = 5)	22.9	5.0	4.15	13.98	3.38	0.85	4.71	0.79	5.80	1.46	5.00	0.74	4.83	0.84
2σ SD (pmol/kg)	1.0	1.3	0.04	0.80	0.10	0.03	0.32	0.03	0.19	0.05	0.17	0.02	0.09	0.02
2σ RSD%	4.3	26	0.9	4.6	2.9	4.1	6.8	3.7	3.3	3.6	3.3	2.7	1.8	2.8
GEOTRACES mean value^a	23.6	5.1	4.03	17.3	3.45	0.91	4.84	0.79	5.80	1.52	5.04	0.75	4.76	0.81
2σ SD (pmol/kg)	2.8	2.3	0.36	1.2	0.34	0.10	0.53	0.07	0.38	0.09	0.25	0.05	0.25	0.04
2σ RSD%	11.8	44	8.9	7.0	9.8	11.2	10.9	9.5	6.5	5.9	5.0	6.4	5.3	4.6

^adata from van de Flierdt et al. (2012).

The precision of our REE concentration measurements for BATS 15 m was $\leq 8.8\%$ for LREEs and $\leq 3.9\%$ for HREEs, except for Ce (11.3%) and Gd (5.1%) (2σ RSD, $n = 5$, Table 4.6, average precision excluding Ce: 3.5%). The precision of BATS 2000 m analyses was $\leq 4.6\%$ for LREEs and $\leq 3.7\%$ for HREEs, except for Ce (26%) and Gd (6.8%) (2σ RSD, $n = 5$) (Table 4.6, average precision excluding Ce: 3.5%). The internal errors of BATS 15 m and 2000 m analyses were lower than the reported precisions for LREEs and HREEs, except for two samples (4.7% and 12.4% for Nd, 2σ RSD). Our mean REE concentrations from BATS (15 m, 2000 m) ($n = 5$ for each depth) are well within the confidence interval (15% and 12%, respectively, 2σ RSD) of the published intercalibration values (van de Flierdt et al., 2012), with maximum relative deviations of 6.6% for all REEs (Table 4.6, Figs. 4.1a, b). Moreover,

our results are close to the published data of Rousseau et al. (2013) deviating by $\leq 6.2\%$ for all REEs except for La (9.4%, BATS 15 m) and Tb (7.6%, BATS 2000 m).

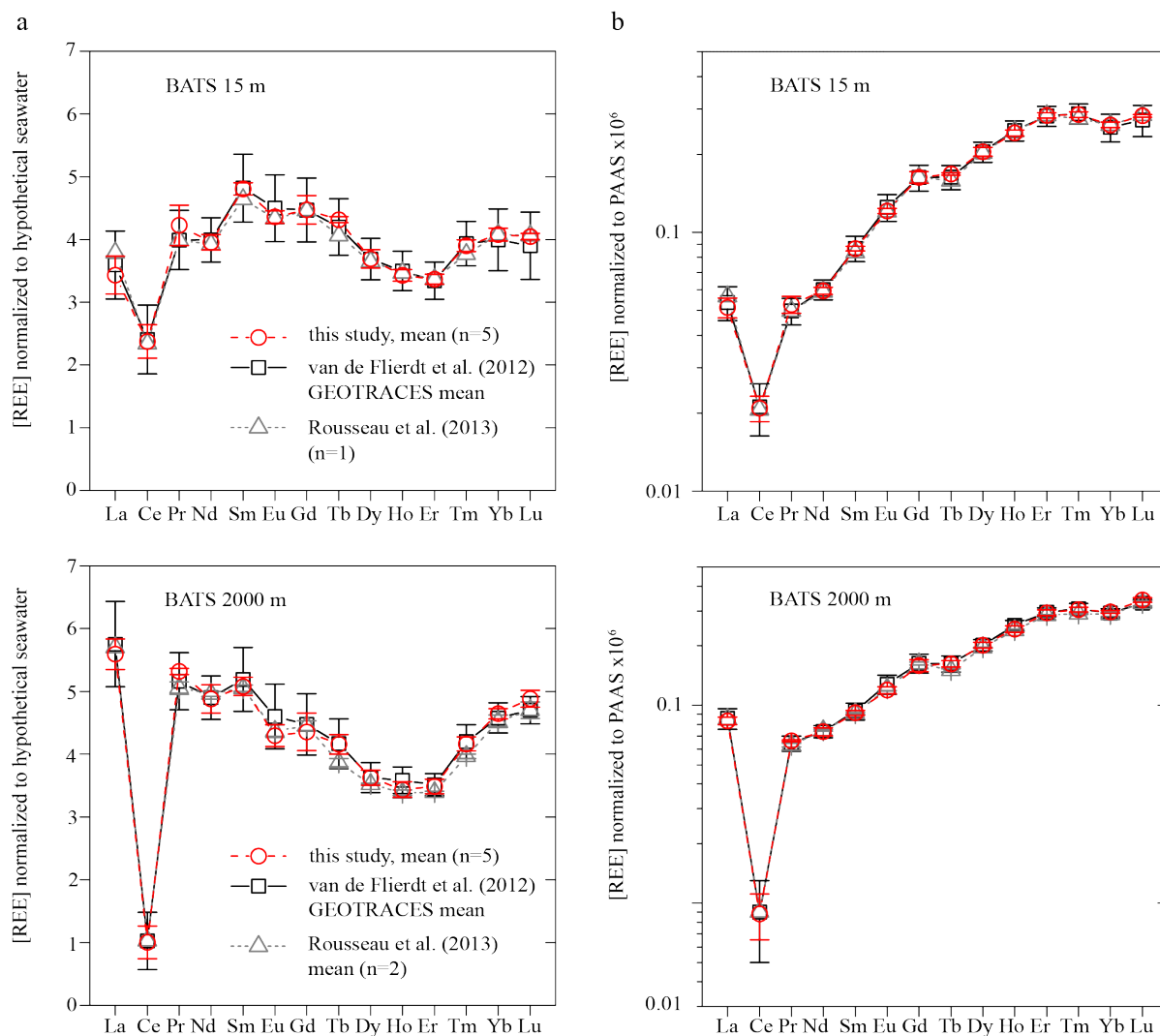


Fig. 4.1. Average dissolved REE concentrations of seawater at BATS 15 m and 2000 m measured in this study in comparison with published GEOTRACES mean REE intercalibration values (van de Flierdt et al., 2012) and published mean REE values from Rousseau et al. (2013). (a) REE concentrations normalized to hypothetical seawater after van de Flierdt et al. (2012). (b) REE concentrations normalized to PAAS (Taylor and McLennan, 1985). Error bars denote $\pm 2\sigma$ SD. Rousseau et al. (2013) reported no error bars for BATS 15 m and for La and Ce at BATS 2000 m.

The long-term precision of our method is demonstrated by multiple runs of the spiked REE Coral Sea standard ($n = 18$) and replicates of SAFe 3000 m ($n = 16$), respectively. The analytical long-term precision of the spiked REE Coral Sea standard that was measured at similar signal intensities as the pre-concentrated samples (except for Ce: ~ 5 times higher in standard), was $\leq 5.7\%$ for all REEs, except for Gd with 7.7% (2σ RSD, $n = 18$, average precision: 4.4%). The internal errors (counting errors) of the spiked REE Coral Sea standard

analyses were $\leq 7.0\%$ for all REEs, except for three samples (7.2-11%, 2σ RSD). The long-term precision of SAFe 3000 m measurements was $\leq 3.9\%$ for all REEs, except for Ce (39%) and Gd (6.2%) (2σ RSD, $n = 16$, Table 4.7, average precision excluding Ce: 3.4%). The internal errors of SAFe 3000 m analyses were lower than or in the range of the reported long-term precision, except for some REEs in six samples (6.2-11%, 2σ RSD, Supplementary Table S4.1). Our measured Nd concentration of SAFe 3000 m (46.4 ± 1.1 pmol/kg, 2σ SD, a relative deviation of 4.5%) is in good agreement with published Nd concentrations from samples taken on the same cruise at the same station and depth (44.4 ± 1.0 pmol/kg, 2σ SD, and 44.4 ± 2.5 pmol/kg, 2σ SE) analyzed so far only for Nd concentrations by two other labs (Pahnke et al., 2012). Our long-term precision of $\leq 3.9\%$ (2σ RSD, $n = 16$) is similar to that of Zheng et al. (2015) ($\sim 6\%$, 2σ RSD, $n = 37$) for an in-house seawater standard (SWC-2). However, we used a sample volume of 11-12 mL, while Zheng et al. (2015) used 100 mL of seawater, indicating a major advancement in sample volume required for the analysis of REEs in seawater.

Our precision of Ce obtained from SAFe 3000 m (39% 2σ RSD, 4.5 pmol/kg Ce) is much lower than the one we obtained using the higher concentrated seawater standards BATS 15 m (11.3% 2σ RSD, 11.9 pmol/kg Ce) and BATS 2000 m (26% 2σ RSD, 5.0 pmol/kg Ce). The internal precision of Ce measurements of SAFe 3000 m (typically $\leq 5.3\%$ 2σ RSD) suggests that Ce can be measured with high precision even in low concentration samples. Therefore, given the highly variable blank levels for Ce and the strongly depleted Ce concentration in the deep Pacific relative to average continental material, we suggest that variable Ce contamination during sample processing is likely contributing to the low precision of Ce in this study. We can exclude acid impurities, insufficiently cleaned vials, and referential retention of Ce on the seaFAST column, as all these possibilities were tested and found to have negligible blank concentrations.

4.3.2. Blanks and precision of participating labs

All the labs (except Lab 3, CEOAS) corrected the sample raw counts for instrumental blanks of 1-3% nitric acid that were usually $< 1\%$ of the signal intensities of the sample. Total procedural blanks of 1% or 2% nitric acid represented $\leq 0.9\%$ ($n = 5$, Lab 2, LDEO) or $\leq 1.1\%$ ($n = 2$, Lab 3) or $\leq 0.06\%$ ($n = 12$, Lab 4, LEGOS) of the measured sample intensities for REEs, except for Ce. Total procedural blanks for Ce were higher and/or more variable than for other REEs (Lab 2: $\leq 1.7\%$, Lab 3: $\leq 1.1\%$ and 11.6%, Lab 4: 3%). Labs 2 and 4 subtracted the total procedural blanks for REEs.

Long-term precision data reported for REE concentrations in Table 4.7 are based on replicates of BATS 2000 m (Lab 2, $n = 14$), an in-house deep seawater standard (Lab 3, NBP195 1097 m, $n = 12$), and a combination of standard solutions, replicates of SAFe 3000 m, and other in-house seawater samples (Lab 4, $n = 30$).

For Lab 2, the seaFAST system has recently come online and these are the first published analyses using it.

For SAFe 3000 m, precision of Ce (Lab 2: 9.9%, Lab 3: 86%, and Lab 4: 5.9%) was worse than average precision of the other REEs (Lab 2: 2.5%, Lab 3: 6.3%, and Lab 4: 2.0%, 2σ RSD, $n = 5-6$, Table 4.7).

Similar to the results from our new method discussed above, all participating labs measured higher and/or more variable blanks for Ce, and observed much lower precision for the low Ce concentrations of SAFe 3000 m. This supports the suggestion that variable Ce contamination during sample processing of low concentrated samples is likely contributing to the precision of the Ce analyses, as the effect on Ce is significant, but negligible for other REEs. As Lab 3 reported no Ce oxide formation rates for this study (only typical oxide formation rates, without correcting for it, see supplementary material), the low precision of Ce (86%) might be also related to this issue. Further details on the analytical methods and results of each individual lab are provided in the supplementary material.

4.3.3. Dissolved REE concentrations at SAFe 3000 m (North Pacific): intercomparison

Detailed results of REE concentrations of SAFe 3000 m from this study (Lab 1, $n = 16$) and the participating labs (Labs 2-4, $n = 5-6$) are presented in the Supplementary Tables S4.1 and S4.2, respectively. The average REE concentrations and precision reported by each lab, and the average values for SAFe 3000 m from the 4 labs (the “REE intercomparison values”) are presented in Table 4.7. Figures 4.2a and b show the average REE patterns of SAFe 3000 m from each lab normalized to hypothetical seawater (van de Fliedrt et al., 2012) and Post-Archean Australian Shale (PAAS) (Taylor and McLennan, 1985), respectively. The plotted errors are the long-term precision of each lab as reported in Table 4.7. The long-term and internal precisions are typically 2-3 times higher for labs using ID ICP-MS methods (Labs 1, 2, and 4) compared to the one using an external standard calibration method (Lab 3) (Figs. 4.2 c, d). The REE concentrations all agree within 7%, except for Ce with 71%, Gd with 14% and Lu with 12% (2σ RSD, Table 4.7). This overall agreement between the 4 labs for SAFe 3000 m is comparable to the agreement reported for BATS 15 m (15%, for all REEs, except for Ce with 23%) and BATS 2000 m (12% for all REEs, except for Ce with

44%) by six different labs for the international GEOTRACES intercalibration study (van de Flierdt et al., 2012). In both studies, Ce presents the biggest challenge. Given the lower Ce concentration at SAFe 3000 m (3.8 pmol/kg Ce) compared to BATS 15 m and 2000 m (12 pmol/kg and 5.1 pmol/kg Ce, respectively), it is not surprising that the precision of the Ce intercomparison value from SAFe 3000 m is lowest. The large spread of measured Ce concentrations is probably partly due to the higher and more variable blanks for Ce compared to the other REEs (≤ 1.1 -18% this study, 4-10% van de Flierdt et al., 2012) in combination with low Ce concentrations.

Table 4.7: Intercomparison of dissolved REE concentrations (pmol/kg) of SAFe 3000 m.

	La	Ce	Pr	Nd	Sm	Eu	Gd	Tb	Dy	Ho	Er	Tm	Yb	Lu
SAFe, 3000 m														
Lab 1 (ICBM) KNR 195-8-Nd 2191														
average (n = 16)	64.2	4.5	10.83	46.4	9.12	2.41	13.40	2.02	14.91	3.74	12.76	1.97	13.80	2.53
2 σ SD (pmol/kg)	2.5	1.7	0.39	1.1	0.21	0.06	0.83	0.06	0.53	0.15	0.41	0.07	0.39	0.10
long-term 2 σ RSD% (n = 16) ^a	3.9	39	3.6	2.4	2.3	2.4	6.2	2.8	3.6	3.9	3.2	3.5	2.9	3.8
Lab 2 (LDEO) KN 195-8-Th 2210														
average (n = 5)	63.2	2.35	10.07	43.9	8.72	2.28	11.49	1.90	14.29	3.69	12.51	1.87	13.37	2.25
2 σ SD (pmol/kg)	1.8	0.23	0.14	0.68	0.20	0.10	0.61	0.04	0.48	0.05	0.39	0.03	0.27	0.02
2 σ RSD%	2.9	9.9	1.4	1.5	2.3	4.3	5.3	1.9	3.4	1.4	3.1	1.8	2.0	1.0
long-term 2 σ RSD% (n = 14) ^b	5.1	3.4	1.7	2.8	4.0	5.5	5.9	4.7	4.4	2.3	4.8	3.3	4.6	4.3
Lab 3 (CEOAS) KNR 195-8-Nd 2191														
average (n = 6)	67.7	5.4	10.16	46.0	8.97	2.36	12.50	1.94	14.70	3.79	12.70	1.95	13.20	2.52
2 σ SD (pmol/kg)	4.1	4.6	0.74	3.1	0.56	0.16	0.82	0.10	0.80	0.29	0.71	0.14	0.72	0.15
2 σ RSD%	6.0	86	7.3	6.8	6.3	6.9	6.6	5.2	5.5	7.7	5.6	7.3	5.4	5.8
long-term 2 σ RSD% (n = 12) ^c	6.8	6.7	6.7	6.2	6.6	8.4	7.9	4.9	8.2	8.3	7.5	8.8	8.6	7.6
Lab 4 (LEGOS) KNR195-8-REE-2183														
average (n = 6)	66.3	3.06	10.25	47.30	9.08	2.40	13.25	1.96	14.71	3.75	12.87	1.92	13.38	2.34
2 σ SD (pmol/kg)	1.6	0.18	0.23	0.68	0.21	0.06	0.22	0.04	0.26	0.06	0.30	0.02	0.31	0.06
2 σ RSD%	2.4	5.9	2.2	1.4	2.3	2.6	1.7	2.0	1.7	1.6	2.3	1.2	2.3	2.5
long-term 2 σ RSD% (n = 30) ^d	3.0	5.0	3.5	2.0	3.5	4.0	3.5	3.0	2.0	3.0	3.0	6.0	2.5	3.0
Intercomparison value (n = 4)														
2 σ SD (pmol/kg)	4.1	2.7	0.7	2.9	0.4	0.1	1.7	0.1	0.5	0.1	0.3	0.1	0.5	0.3
2 σ RSD%	6.2	71	6.7	6.3	4.1	5.1	14	5.2	3.6	2.1	2.4	4.7	3.8	12

^aprecision based on replicates of SAFe 3000 m.^bprecision based on replicates of BATS 2000 m.^cprecision based on in-house deep seawater sample NBP95 (1097 m, Bransfield Strait).^dprecision based on multiple runs of standard solutions, replicates of SAFe 3000 m, and other in-house seawater samples.

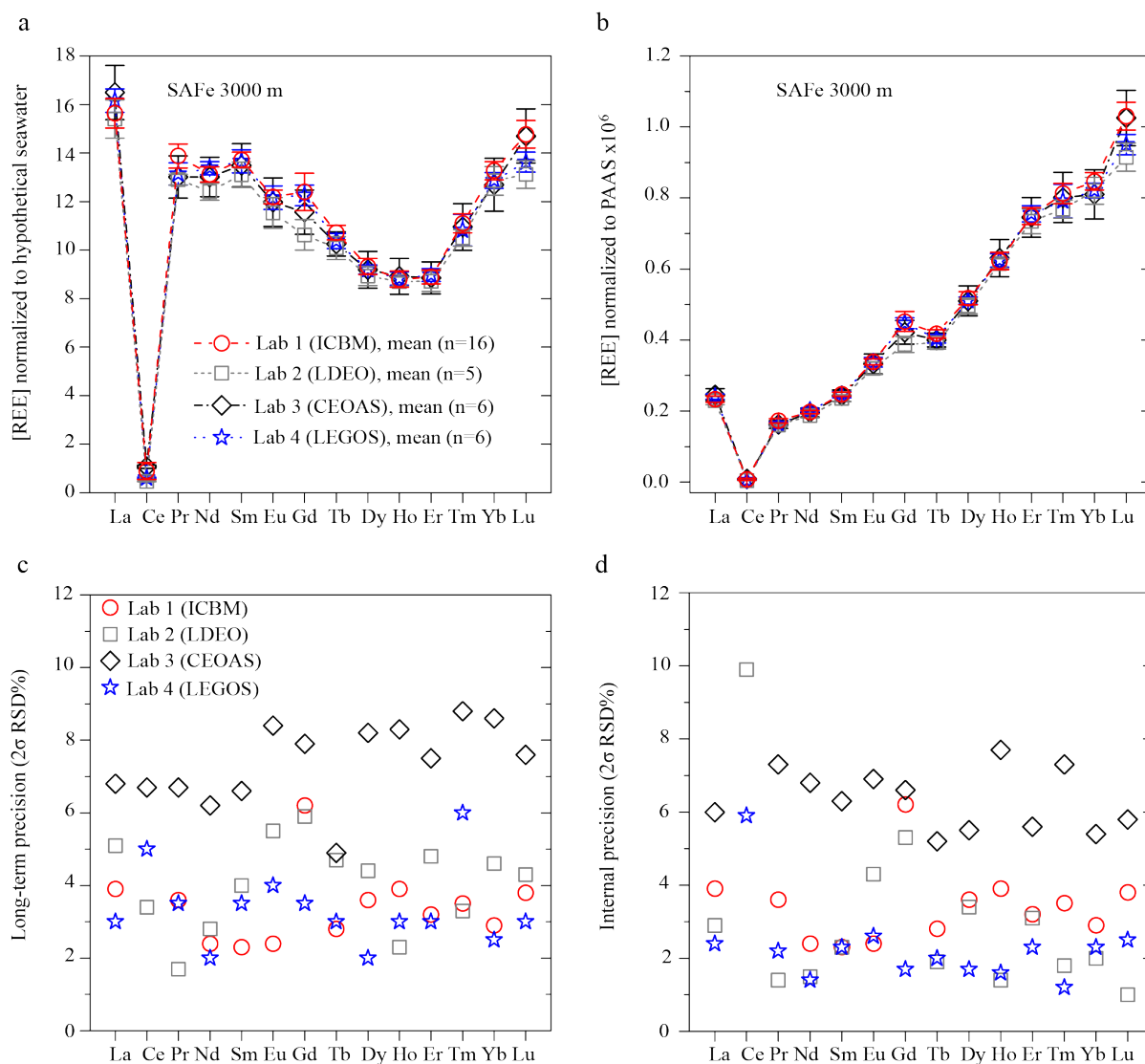


Fig. 4.2. Average dissolved REE concentrations of SAFe 3000 m along with long-term and internal precisions (2σ RSD%) reported for this study (Labs 1–4). (a) REE concentrations normalized to hypothetical seawater (La: 4.1 pmol/kg, Ce: 5.0 pmol/kg, Pr: 0.78 pmol/kg, Nd: 3.54 pmol/kg, Sm: 0.67 pmol/kg, Eu: 0.20 pmol/kg, Gd: 1.08 pmol/kg, Tb: 0.19 pmol/kg, Dy: 1.60 pmol/kg, Ho: 0.42 pmol/kg, Er: 1.43 pmol/kg, Tm: 0.18 pmol/kg, Yb: 1.04 pmol/kg, Lu: 0.17 pmol/kg) after van de Flierdt et al. (2012). (b) REE concentrations normalized to PAAS (Taylor and McLennan, 1985). (a–b) Error bars denote $\pm 2\sigma$ SD calculated from the long-term precision of each lab as reported in Table 4.7. (c) Long-term precision (precision of Ce is omitted for Lab 1) and (d) internal precision (precision of Ce is omitted for Labs 1 and 3) of each lab as reported in Table 4.7.

In our study, the slightly lower precisions of Gd (14%) and Lu (12%) compared to the other REE results mainly from the lower concentrations of these elements measured by Lab 2. The precision of the shale-normalized REE patterns of the labs is better than that of the absolute concentrations for most REEs, which is shown by normalizing the REE results to the same Nd concentration (46.4 pmol/kg Nd of Lab 1, Table 4.7) and comparing the deviations (Figs. 4.3 a-d). This may result from slight errors in the spike concentrations (e.g., due to evaporation).

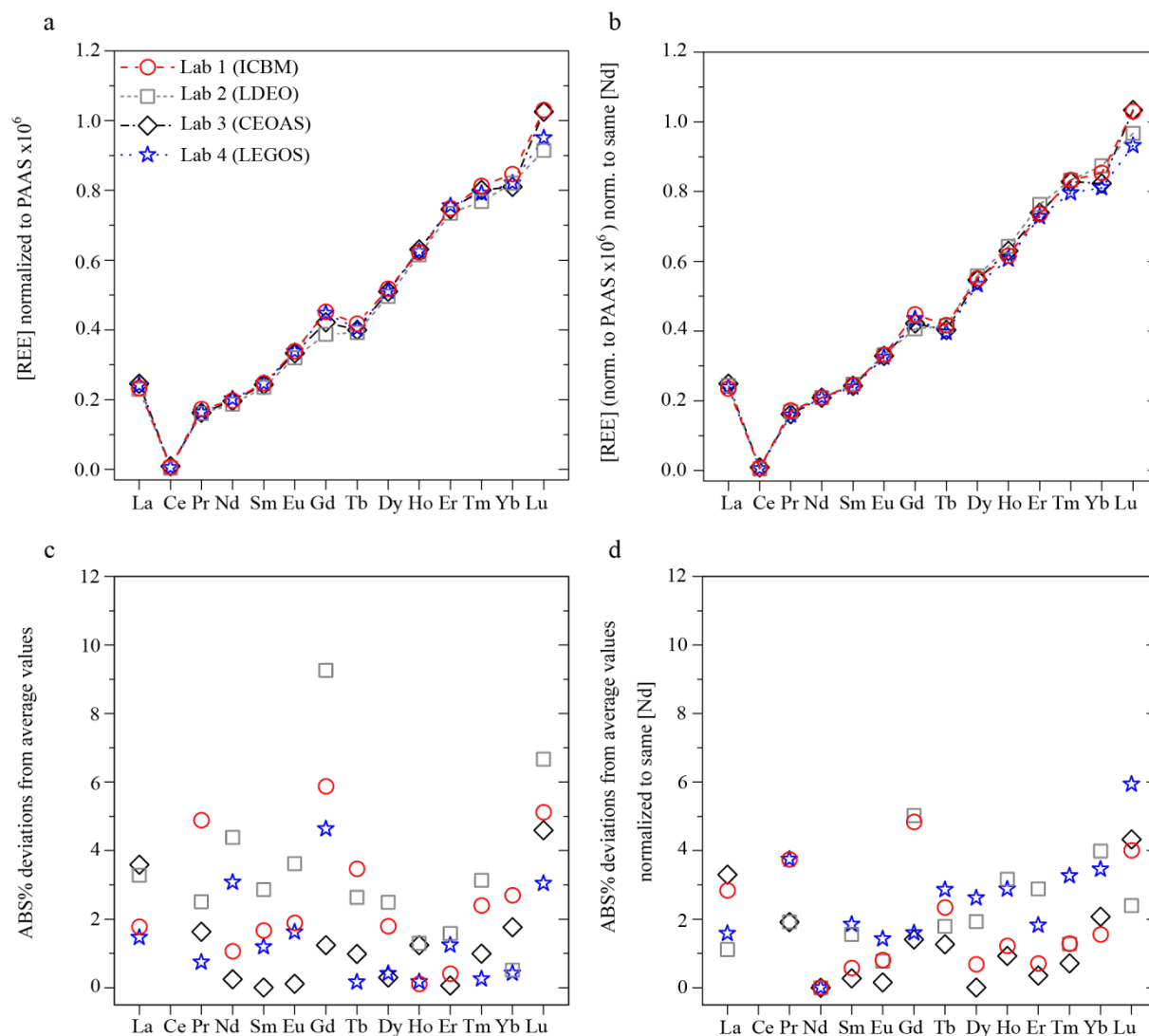


Fig. 4.3. (a) REE concentrations normalized to PAAS (Taylor and McLennan, 1985). (b) PAAS-normalized REE concentrations normalized to the same Nd concentration (46.4 pmol/kg Nd of Lab 1, Table 7). (c) Absolute (ABS) deviations (%) from average values (omitting Ce). (d) Absolute deviations (%) from average values normalized to same Nd concentration (omitting Ce).

Published data for SAFe 3000 m are so far only available from two other labs for Nd (44.4 ± 1.0 pmol/kg, 2σ SD, and 44.4 ± 2.5 pmol/kg, 2σ SE, Pahnke et al., 2012). These results agree well with the Nd intercomparison value of this study (45.9 ± 2.9 pmol/kg, 2σ SD, relative deviation of 3.4%).

Compared to REE analyses using the seaFAST method in online mode with reported average precisions of 8.4%, 12%, and 5% (2σ RSD) for BATS 15 m, 2000 m, and Station 113 1000 m, respectively (Hathorne et al., 2015), our offline method achieved slightly higher average precisions for REEs (3.5% for BATS 15 m and 2000 m, respectively, 3.4% for SAFe 3000 m, excluding Ce, 2σ RSD). Similarly, Labs 2 and 3 that also used the seaFAST in offline mode, reported average precisions of 4.1% and 7.4% (2σ RSD) for REEs based on

BATS 2000 m and in-house seawater NBP95 1097 m, respectively. A possible reason for the slightly lower average precisions reported by Lab 3 and Hathorne et al. (2015) compared to those of Labs 1 and 2 is the use of different quantification methods using external standard calibration and ID ICP-MS, respectively.

The REE intercomparison concentrations of station SAFe (30°N, 140°W) at 3000 m reported for this study agree within the uncertainties (2σ SD) with published REE concentrations of deep water at nearby stations VERTEX II (18°N, 108°W, 3000 m, de Baar et al., 1985) and TPS24-76-1 (24°15.0'N, 159°15.6'W, 4621 m, Piepgras and Jacobsen, 1992) and show similar PAAS-normalized REE patterns (Figs. 4.4a, b). The consistency of REE data between stations SAFe and TPS24-76-1 demonstrates the ability of our method to provide reliable marine REE concentrations and further validates the results from the intercomparison.

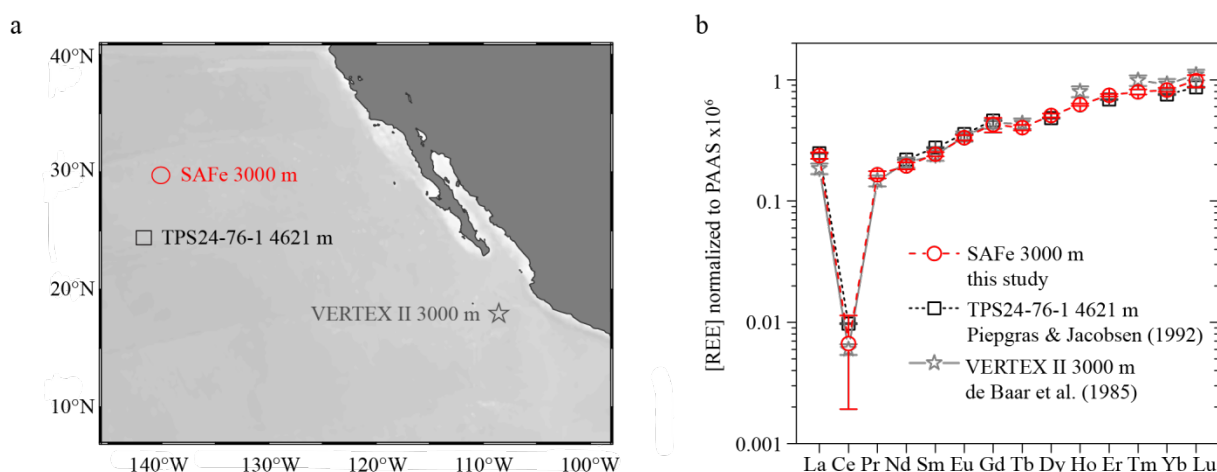


Fig. 4.4. (a) Map showing location of deep water sampling stations SAFe 3000 m (this study), VERTEX II 3000 m (de Baar et al., 1985) and TPS24-76-1 4621 m (Piepgras and Jacobsen, 1992). (b) REE concentrations of SAFe 3000 m (intercomparison values, this study) compared to published REE values of nearby stations VERTEX II 3000 m and TPS24-76-1 4621 m (de Baar et al., 1985 and Piepgras and Jacobsen, 1992), normalized to PAAS (Taylor and McLennan, 1985). Error bars denote $\pm 2\sigma$ SD. Map produced with Ocean Data View (Schlitzer, 2014).

4.4. Conclusions

This study presents a rapid and robust pre-concentration and purification method for REEs from small volumes of seawater (11-12 mL) by applying the seaFAST-pico system (Elemental Scientific Inc.) in offline mode for the first time. We provide an accurate and precise multi-element ID ICP-MS method for routine REE analyses. The accuracy of our method was assessed by repeated processing and analysis of GEOTRACES intercalibration seawater from BATS at 15 m and 2000 m. Our average REE concentrations are within the 2σ

RSD confidence interval of published intercalibration values for these samples (15% and 12%, van de Flierdt et al., 2012), deviating by only 6.6% from those values.

In addition, an international intercomparison using seawater from SAFE at 3000 m (North Pacific) with three other labs applying different sample volumes and methods demonstrates the applicability of our method for high-precision measurements of dissolved REE concentrations. Overall, the REE concentrations of SAFE 3000 m are in very good agreement between all labs, reproducing (2σ RSD) within 7% for all REEs (4.1-0.1 pmol/kg, 2σ SD), except for Ce (71%, 2.7 pmol/kg, 2σ SD), Gd (14%, 1.7 pmol/kg, 2σ SD), and Lu (12%, 0.3 pmol/kg, 2σ SD). The lower precision of Ce compared to the other REEs is most likely due to more variable and higher blank contributions to the low Ce concentration in the deep Pacific sample.

The described method can be easily adopted by other labs as the seaFAST system is commercially available, and enables the extensive use of REEs in high-resolution sampling and measurement campaigns such as the GEOTRACES program. In addition, our international intercomparison exercise provides the first intercomparison values for dissolved REE concentrations in the North Pacific from the GEOTRACES intercalibration station SAFE from 3000 m water depth, and establishes this station and depth as a seawater reference for REE concentrations in the Pacific as SAFE will remain a baseline, and hence intercalibration station, for cruises in the North Pacific.

4.5. Acknowledgements

We thank the scientific parties, the chief scientists, the captain and crew of the two GEOTRACES intercalibration cruises on the R/V *Knorr* (KN193-6, KN195-8) for providing the seawater intercalibration samples used in this study. We thank Gideon Henderson for providing the REE Coral Sea standard, the members of the Max Planck Research Group for Marine Isotope Geochemistry, especially Martina Schulz for their help in the lab. Financial support for this study came from the Institute for Chemistry and Biology of the Marine Environment (ICBM), the Max Planck Institute for Marine Microbiology, and the German Research Foundation (DFG, PA2411/1-1). LP acknowledges support from the Ramón y Cajal program (MINECO, Spain). The LDEO analyses were funded by a US National Science Foundation grant (OCE12-60514 to SLG and LP). This is LDEO contribution number 8052.

4.6. Supplementary material

4.6.1. Pre-concentration methods and mass spectrometry of participating labs

4.6.1.1. Lab 2, LDEO, Columbia University: Offline seaFAST pre-concentration and multi-element isotope dilution ICP-MS

The dilutions were prepared from high purity water (18.2 MΩ cm). The 1.6 N HNO₃ elution acid was made from concentrated high purity nitric acid (Optima quality, Fisher Chemical). The buffer solution (pH = 6.0 ± 0.2) was prepared by using 834 mL of high purity water, 70 mL of 17.5 N high purity glacial acetic acid (Optima quality, Fisher Chemical), and 96 mL of high purity 11.4 N ammonium hydroxide (Optima quality, Fisher Chemical). The REEs were pre-concentrated from seawater samples by applying the offline ESI seaFAST-pico system with the same automated steps as at ICBM (see the section on Pre-concentration of REEs from seawater in the main text). Unlike Lab 1, Lab 2 eluted the REEs in three steps each of 100 μL of 1.6 N HNO₃ at an initial flow rate of 0.1 mL/min and a final flow rate of 0.5 mL/min. Like Lab 1, quantification used the DKM multi-element REE spike. A VG PQ ExCell quadrupole ICP-MS at LDEO was used for the measurements. The instrument was coupled to a desolvation introduction system (CETAC Aridus) that minimized oxide formation. The instrument was optimized for sensitivity and operated in pulse counting mode. The oxide formation rate (<1% for Ce) was checked by using a 100 ng/L Ce tune solution. Instrumental blanks for 3% HNO₃ that represented <1% of the measured sample intensities for REEs were subtracted from the sample raw counts. The data were reduced using the same basic isotope dilution equations as described for Lab 1. In contrast to Lab 1, Lab 2 corrected all REEs for oxide formation and mass fractionation.

To measure the total procedural blank, Lab 2 processed 10 mL of 1% HNO₃ through the seaFAST the same way as the samples. At least 5 procedural blanks were processed during each seaFAST session. Sample intensities were corrected by subtracting the procedural blank using $I_{\text{meas}} = I_{\text{raw}} - I_{\text{procedural_blk}}$, where I_{raw} is the raw intensity of the sample, $I_{\text{procedural_blk}}$ is the intensity of the procedural blank and I_{meas} is the intensity after procedural blank correction.

To correct for oxide formation, Lab 2 did oxide calibration analysis by measuring masses of M and MO in pure, single element solutions of Ba and REEs. This analysis was only needed once. The oxide calibration value is expressed as the ratio of $\frac{MO_{\text{Ical}}}{M_{\text{Ical}}}$, where M_{Ical} is

the intensity of mass M and $^{MO}I_{cal}$ is the intensity of mass MO measured during the calibration. For an unknown sample, the oxide interference for any mass M is calculated with $^{MO}I_{int} = \frac{^{MO}I_{cal}}{M_{I_{cal}}} \times M_{I_{meas}}$, where $M_{I_{meas}}$ is the measured intensity for any mass and $^{MO}I_{int}$ is the intensity of its oxide interference.

The oxide calibration values are not constant and need to be adjusted each time REEs are measured. Therefore, Lab 2 analyzed $^{157}\text{PrO}/^{141}\text{Pr}$ ratio of a 100 ng/L Pr solution during each session of REE measurement to get the correction factor $C = \frac{\left(\frac{^{157}\text{PrO}}{^{141}\text{Pr}}\right)_{today}}{\left(\frac{^{157}\text{PrO}}{^{141}\text{Pr}}\right)_{cal}}$, where $\left(\frac{^{157}\text{PrO}}{^{141}\text{Pr}}\right)_{cal}$ was measured during the oxide calibration analysis and $\left(\frac{^{157}\text{PrO}}{^{141}\text{Pr}}\right)_{today}$ was measured each time Lab 2 analyzed REEs. Then the oxide interference is expressed as $^{MO}I_{int} = C \times \frac{^{MO}I_{cal}}{M_{I_{cal}}} \times M_{I_{meas}}$. The final true intensity without oxide interference is calculated as $^{MO}I_{Ox_cor} = ^{MO}I_{meas} - C \times \frac{^{MO}I_{cal}}{M_{I_{cal}}} \times M_{I_{meas}}$.

Lab 2 used the exponential law $R_C = R_m \times \left(\frac{m_i}{m_j}\right)^\beta$ to correct for mass fractionation, where R_C is the mass fractionation corrected isotope ratio in the sample, R_m is the measured isotope ratio in the sample, m_i is the atomic mass of numerator spike isotope, usually the one enriched in the spike, m_j is the atomic mass of reference isotope. To calculate β , Lab 2 prepared a mass bias solution in which each REE has concentration of 100 ng/L and measured it during each REE measurement session. β is expressed as $\beta = \frac{\text{Ln}\left(\frac{R_n}{R_{mb}}\right)}{\text{Ln}\left(\frac{m_i}{m_j}\right)}$, where R_n is the ratio in natural samples, R_{mb} is the measured ratio in the mass bias solution.

The precision determined from replicates of SAFe 3000 m was $\leq 4.3\%$ for LREEs and $\leq 3.4\%$ for HREEs, except for Ce (9.9%) and Gd (5.3%) (2σ RSD, $n = 5$). The internal errors (2σ RSD) of REE concentration measurements for individual SAFe 3000 m analyses were lower than or around the same value as the reported precision, except for Eu ($\leq 7.5\%$) and Tb ($\leq 5.4\%$) in two samples, and for Ho (4.7%) and Lu (4.9%) in one sample (Supplementary Table S4.2).

4.6.1.2. Lab 3, CEOAS, Oregon State University: Offline seaFAST pre-concentration and external standards for REE quantification

All dilutions were prepared by using high purity water (18.2 M Ω cm). The 1.5 N elution acid was prepared from sub-boiled distilled nitric acid. The buffer solution was prepared by mixing trace metal purity glacial acetic acid and ammonium hydroxide (both $\geq 99.99\%$, Sigma Aldrich) with high purity water. The REEs were pre-concentrated from seawater by using the offline seaFAST-pico system with the same automated pre-concentration steps as described for Lab 1 (see the section on Pre-concentration of REEs from seawater in the main text). Unlike Labs 1 and 2, Lab 3 used a sample volume of ~ 20 mL (instead of 10 mL) that was loaded in two steps onto a 10 mL PFA sample loop and eluted the REEs with 200 μ L of 1.5 N HNO₃ (instead of 500 μ L). Other than Labs 1 and 2, Lab 3 used five external calibration standards of increasing concentrations (instead of a multi-element spike) for quantification. The external calibration standards were prepared by weight from primary REE solutions and mixed to approximate a seawater REE pattern. These external calibration standards were passed along with two total procedural blanks through the seaFAST column the same way as the samples. The samples were processed and analyzed in three sessions together with external calibration standards and total procedural blanks. The intercalibration sample from SAFe 3000 m was processed and analyzed twice in the first session (KNR 195-8-Nd 2191_lab3_run1-2, Supplementary Table S4.2), and once in the second session (KNR 195-8-Nd 2191_lab3_run3, Supplementary Table S4.2) along with external calibration standards in 1% HNO₃ and a total procedural blank of sub-boiled distilled 1% HNO₃. In the third session, the SAFe sample was processed and analyzed three times (KNR 195-8-Nd 2191_lab3_run4-6, Supplementary Table S4.2) along with external calibration standards and a total procedural blank that were both adjusted to a pH of ~ 1.6 by adding ammonium hydroxide in order to increase column buffering. During the third pre-concentration session, a consistency REE standard prepared from reagent-grade salts to approximate seawater composition was processed throughout the day and used to calculate an evaporation correction factor. The REE concentrations were obtained using a Thermo Xseries-II ICP-MS at the CEOAS, Oregon State University. The instrument was operated in pulse counting mode and optimized for sensitivity of indium by using a 1 μ g/L tune solution (Co, In, Ce, U). The oxide formation rate (typically 1.5-2% Ce) was not determined for the three analytical sessions. The measured counts of REEs for the total procedural blanks (n = 2) were $\leq 1.1\%$ of the counts in SAFe 3000 m, except for Ce (11.6%) in the pH-adjusted total procedural blank that was measured in the third session. For the third session, repeated analyses of the consistency REE standard were

corrected to the initial replicate and regressed against the sample number as a proxy for time. This regression provided a correction for sample evaporation. A response rate (i.e. corrected counts/(pmol/kg)) was calculated by using the known concentrations of the external calibration standards. Sample concentrations were then determined by using this response rate. The long-term precision of REE concentration analyses, checked with repeated processing and analysis of in-house deep seawater sample NBP95 (1097 m, Bransfield Strait), was $\leq 8.4\%$ for LREEs and $\leq 8.8\%$ for HREEs (2σ RSD, $n = 12$). The precision of REE concentration analyses of SAFe 3000 m replicates was $\leq 7.3\%$ for LREEs and $\leq 7.7\%$ for HREEs, except for Ce (86%) (2σ RSD, $n = 6$). The internal errors (2σ RSD) were lower than or in the range of the reported precision, except for La (7.8%), Gd (8.0%) and Tb (6.5%) in two samples (Supplementary Table S4.2). Internal errors were determined from the 2σ RSD of all runs of SAFe 3000 m for each session, except for the second session, where only one replicate was pre-concentrated. For this session, the standard error of the calibration standard regression was calculated and used.

4.6.1.3. Lab 4, LEGOS, University of Toulouse: Iron hydroxide co-precipitation and two-element isotope spike coupled with internal and external standards

All chemicals used were of ultra-pure quality. Each seawater aliquot (500 mL, pH = 2) was weighed, spiked with ^{150}Nd and ^{172}Yb , and left for equilibration for three days. The REEs were then pre-concentrated using iron hydroxide co-precipitation: we added purified FeCl_3 in 0.1 N HCl to the sample and used ammonium hydroxide to raise the pH to 7-8. The REE-Fe precipitate was centrifuged, extracted, and dissolved in 1 mL of 6 N HCl. The sample was loaded on a column with 2 mL of an AG1X8 100-200 μm mesh-size resin in order to remove iron and seawater matrix. We eluted the sample with 4 mL of 6 N HCl, evaporated, and dissolved it again in 0.4 mL of 0.32 N HNO_3 . Indium and rhenium each at 0.4 $\mu\text{g/L}$ were added as internal standards to all samples. The REEs were quantified using external calibration standards prepared from mixed REE solutions of seawater-like concentrations in the range of 3 and 30 mg/L for Nd as example. An Agilent 7500 ICP-MS was used for REE concentration measurements at LEGOS, University of Toulouse. Details of the REE pre-concentration procedure and the ICP-MS method can be found in Lacan and Jeandel (2001). Briefly, an isotope spike enriched in ^{150}Nd and ^{172}Yb was used to calculate the concentrations of Nd and Yb by isotope dilution. All other REEs were determined by external calibration, while internal standards (indium and rhenium) were used for sensitivity drift corrections. The recovery of the chemistry extraction (average values: 91% and 94% for Nd and Yb,

respectively) was calculated by comparing the concentrations achieved by isotope dilution to the values derived from external calibration standards. The other REEs were then corrected for this recovery (Lacan and Jeandel, 2001). Instrumental blank solutions of 2% nitric acid that represented $\leq 0.2\%$ of the analyzed sample intensities for REEs ($< 0.07\%$ for La, Pr, Nd, Sm, and HREEs) were measured and subtracted. Total procedural blank solutions of 2% nitric acid were doped with indium and rhenium each at 400 ng/L and processed the same way as the samples through the whole chemical extraction. The total procedural blanks were redissolved in 2% nitric acid ($n = 12$) and accounted $\leq 0.06\%$ of the sample signals for all REEs, except for Ce (3%). The total procedural blanks were subtracted for REEs. A combination of standard solutions (e.g., Geostandard SLRS5), replicates of SAFe 3000 m, and other in-house seawater samples achieved a long-term precision of $\leq 4.0\%$ for LREEs and $\leq 3.5\%$ for HREEs, except for Ce with 5.0% and Tb with 6.0% (2σ RSD, $n = 30$). The precision of REE concentration measurements determined for SAFe 3000 m was $\leq 2.6\%$ for all REEs, except for Ce with 5.9% (2σ RSD, $n = 6$). The internal errors (2σ RSD) of REE concentration measurements for SAFe 3000 m were lower than or in the range of the reported long-term precision (Supplementary Table S4.2).

4.6.2. Supplementary Tables

Table S4.1: Dissolved REE concentrations (pmol/kg) of SAFe 3000 m analyzed at ICBM.

	La	Ce	Pr	Nd	Sm	Eu	Gd	Tb	Dy	Ho	Er	Tm	Yb	Lu	2 σ^a														
SAFE, 3000 m (KNR 195-8-Nd 2191)																													
Lab 1																													
run_1	64.6	5.9	2.1	10.80	1.9	46.6	2.7	9.18	3.7	2.40	2.0	12.67	4.5	1.97	2.0	15.04	0.6	3.65	1.9	12.66	1.1	1.95	1.9	13.92	3.6	2.54	1.0		
run_2	65.6	2.5	5.4	2.2	10.81	1.4	46.1	2.1	9.01	3.1	2.41	3.4	12.98	4.3	2.02	2.1	15.06	2.6	3.83	3.1	12.82	2.5	1.96	2.0	13.88	3.1	2.53	0.9	
run_3	65.8	2.7	5.0	2.4	11.07	2.0	47.2	3.0	9.13	0.7	2.44	1.5	13.48	1.8	2.03	3.7	14.76	3.8	3.79	0.6	12.58	3.2	2.02	3.4	13.75	3.7	2.53	3.3	
run_4	65.3	2.9	3.9	7.3	10.73	2.3	47.1	10.8	9.01	3.1	2.42	0.5	13.27	6.6	2.02	3.9	14.79	5.9	3.74	2.7	12.55	2.0	1.98	3.6	13.57	4.8	2.57	3.3	
run_5	63.1	0.9	4.1	1.9	10.86	2.7	46.2	4.0	9.13	3.4	2.42	3.5	12.96	4.2	2.06	3.5	14.87	2.5	3.71	3.3	13.20	2.1	1.96	2.3	13.59	6.5	2.50	2.3	
run_6	64.1	2.0	4.2	1.8	10.59	1.1	46.6	2.2	9.12	4.9	2.42	2.1	13.21	5.2	2.01	2.2	15.29	0.7	3.69	4.2	12.88	3.0	1.96	1.1	13.83	3.5	2.53	1.4	
run_7	65.4	0.5	4.7	1.4	11.21	1.2	46.6	4.2	9.42	2.4	2.39	3.1	13.78	6.8	2.06	1.7	15.49	3.0	3.84	3.0	12.90	2.4	2.02	1.8	14.12	3.1	2.58	3.3	
run_8	65.1	1.3	3.6	5.1	10.69	2.5	46.4	2.2	9.18	3.3	2.45	3.0	13.09	6.3	2.02	3.5	14.51	3.3	3.75	1.3	12.51	1.3	1.97	3.9	13.47	1.3	2.49	2.7	
run_9	63.5	3.9	6.5	5.3	11.14	5.5	46.1	6.9	9.02	4.5	2.40	4.7	13.25	5.9	1.99	3.9	14.82	3.7	3.75	3.1	12.75	2.9	1.95	3.4	13.85	5.4	2.58	3.4	
run_10	62.2	1.1	4.8	2.9	11.00	3.3	46.3	2.0	9.19	1.2	2.40	5.8	13.71	6.0	2.00	2.2	14.81	1.1	3.67	1.9	12.86	1.5	1.91	4.2	13.90	1.6	2.55	2.0	
run_11	64.3	3.1	4.2	2.5	10.76	0.7	45.5	3.5	9.13	2.4	2.42	2.2	14.34	3.2	2.03	3.6	14.55	4.4	3.82	1.7	12.66	3.3	2.00	1.7	14.13	2.8	2.61	5.0	
run_12	64.4	1.4	3.3	4.0	10.52	1.3	46.4	2.8	9.01	1.2	2.42	3.0	13.88	2.9	2.08	2.5	14.62	2.1	3.84	1.3	12.41	1.4	2.02	1.6	13.64	2.3	2.60	3.6	
run_13	62.8	4.7	3.5	7.0	10.92	8.4	45.9	6.9	9.12	8.2	2.35	7.4	13.14	4.6	2.05	4.1	14.89	5.2	3.76	7.3	13.05	5.2	2.01	8.9	13.93	3.7	2.45	5.0	
run_14	65.4	5.5	4.1	8.1	10.63	7.2	47.2	9.3	9.03	8.5	2.44	7.7	13.6	8.8	1.99	7.1	15.1	6.7	3.60	6.2	12.7	8.0	1.91	4.4	13.6	7.7	2.51	6.2	
run_15	62.4	1.0	4.0	2.0	10.86	1.0	46.2	1.4	9.10	2.0	2.36	1.6	13.64	1.8	2.02	2.8	15.19	3.7	3.67	2.7	12.86	0.7	1.98	2.8	14.00	2.1	2.46	0.9	
run_16	62.6	2.4	4.4	3.5	10.74	2.5	45.3	6.9	9.21	1.8	2.36	1.9	13.47	2.9	2.02	2.8	14.85	3.2	3.69	2.4	12.83	2.5	1.95	2.4	13.65	2.6	2.48	0.5	
average (n =16)	64.2	4.5	10.83	46.4	9.12	2.41	13.40	2.02	14.91	3.74	12.76	1.97	13.80	2.53															
2 σ SD (pmol/kg)	2.5	1.7	0.39	1.1	0.21	0.06	0.83	0.06	0.53	0.15	0.41	0.07	0.39	0.10															
2 σ RSD%	3.9	39	3.6	2.4	2.3	2.4	6.2	2.8	3.6	3.9	3.2	3.5	2.9	3.8															

^ainternal 2 σ RSD%.

Table S4.2: Dissolved REE concentrations (pmol/kg) of SAFe 3000 m analyzed by the participating labs.

	La	2 σ^a	Ce	2 σ^a	Pr	2 σ^a	Nd	2 σ^a	Sm	2 σ^a	Eu	2 σ^a	Gd	2 σ^a	Tb	2 σ^a	Dy	2 σ^a	Ho	2 σ^a	Er	2 σ^a	Tm	2 σ^a	Yb	2 σ^a	Lu	2 σ^a			
SAFe, 3000 m																															
Lab 2 (LDEO) KN 195-8-Th 2210																															
run_1	64.7	3.3	2.44	2.4	10.02	1.7	43.66	1.5	8.60	2.4	2.23	6.7	11.97	2.1	1.90	0.8	14.06	2.4	3.67	4.7	12.65	1.5	1.85	3.9	13.45	3.3	2.24	3.2			
run_2	63.1	0.9	2.36	3.1	9.99	1.7	43.99	1.3	8.83	1.1	2.34	2.0	11.18	1.0	1.92	3.6	14.16	0.9	3.66	0.8	12.38	2.3	1.85	4.1	13.19	2.2	2.26	2.9			
run_3	63.0	1.4	2.16	0.6	10.06	1.9	43.73	1.1	8.81	2.8	2.26	2.7	11.56	1.9	1.92	4.1	14.47	1.5	3.71	2.8	12.23	1.5	1.89	3.5	13.31	0.8	2.24	4.3			
run_4	62.3	1.4	2.34	2.0	10.09	2.1	43.58	1.1	8.69	2.1	2.23	7.5	11.38	2.4	1.90	5.4	14.13	2.8	3.71	3.2	12.69	2.1	1.87	4.0	13.37	1.7	2.26	1.3			
run_5	62.8	2.0	2.46	3.2	10.18	3.6	44.42	1.5	8.66	1.0	2.32	3.8	11.35	1.5	1.88	4.4	14.61	3.0	3.71	1.5	12.60	1.5	1.88	2.5	13.55	3.5	2.24	4.9			
average (n = 5)	63.2		2.35		10.07		43.9		8.72		2.28		11.49		1.90		14.29		3.69		12.51		1.87		13.37		2.25				
2 σ SD (pmol/kg)	1.8		0.23		0.14		0.68		0.20		0.10		0.61		0.04		0.48		0.05		0.39		0.03		0.27		0.02				
2 σ RSD%	2.9		9.9		1.4		1.5		2.3		4.3		5.3		1.9		3.4		1.4		3.1		1.8		2.0		1.0				
Lab 3 (CEOAS) KNR 195-8-Nd 2191																															
run_1	70.2	7.8	3.2	9.8	10.18	4.9	46.6	4.4	9.37	5.1	2.41	5.4	13.0	8.0	1.97	6.5	15.05	5.1	3.86	5.6	12.74	3.1	2.00	6.7	13.41	3.7	2.47	1.6			
run_2	66.4	7.8	3.0	9.8	9.83	4.9	45.2	4.4	9.04	5.1	2.32	5.4	12.3	8.0	1.89	6.5	14.51	5.1	3.71	5.6	12.47	3.1	1.91	6.7	13.06	3.7	2.50	1.6			
run_3	65.1	2.0	3.6	6.4	9.61	3.5	43.4	2.2	8.60	0.2	2.23	5.7	11.90	1.5	1.86	1.7	13.99	1.2	3.54	2.4	12.1	3.1	1.82	3.0	12.53	0.9	2.41	0.8			
run_4	70.0	4.9	7.7	5.4	10.60	2.6	47.6	3.6	9.09	4.9	2.46	4.2	12.82	4.2	1.95	1.8	14.94	2.1	3.94	4.3	13.10	2.2	1.99	1.2	13.39	1.0	2.58	0.5			
run_5	67.7	4.9	7.4	5.4	10.39	2.6	47.3	3.6	9.05	4.9	2.36	4.2	12.31	4.2	1.98	1.8	14.70	2.1	3.78	4.3	12.82	2.2	1.97	1.2	13.48	1.0	2.59	0.5			
run_6	66.7	4.9	7.3	5.4	10.35	2.6	46.0	3.6	8.69	4.9	2.40	4.2	12.67	4.2	1.95	1.8	14.99	2.1	3.88	4.3	12.96	2.2	1.99	1.2	13.35	1.0	2.57	0.5			
average (n = 6)	67.7		5.4		10.16		46.0		8.97		2.36		12.50		1.94		14.70		3.79		12.70		1.95		13.20		2.52				
2 σ SD (pmol/kg)	4.1		4.6		0.74		3.1		0.56		0.16		0.82		0.10		0.80		0.29		0.71		0.14		0.72		0.15				
2 σ RSD%	6.0		86		7.3		6.8		6.3		6.9		6.6		5.2		5.5		7.7		5.6		7.3		5.4		5.8				
Lab 4 (LEGOS) KNR195-8-REE-2183																															
run_1	66.1	1.8	3.21	2.2	10.19	1.8	47.25	1.8	9.06	1.9	2.39	2.6	13.33	2.6	1.96	2.2	14.66	2.2	3.78	2.2	12.87	2.0	1.93	2.3	13.59	2.0	2.36	2.2			
run_2	65.9	1.8	2.97	1.9	10.21	1.7	47.36	2.0	9.15	2.2	2.38	2.3	13.20	2.1	1.96	2.1	14.73	2.1	3.74	2.3	12.95	2.3	1.93	2.0	13.45	1.9	2.35	1.8			
run_3	65.9	1.7	2.98	1.7	10.24	1.8	47.03	1.8	8.95	2.0	2.39	2.1	13.20	1.9	1.94	2.0	14.79	2.0	3.72	2.0	12.78	2.1	1.90	2.1	13.22	2.0	2.30	1.8			
run_4	65.5	1.9	3.03	2.2	10.12	1.6	46.86	1.8	8.98	2.3	2.37	2.3	13.20	2.6	1.96	1.7	14.69	2.1	3.73	2.2	12.82	2.2	1.92	2.9	13.46	1.9	2.37	2.0			
run_5	67.7	1.6	3.11	1.8	10.45	1.6	47.83	1.8	9.23	2.4	2.46	2.6	13.43	1.7	1.99	1.8	14.89	1.8	3.78	1.6	13.12	1.7	1.93	1.7	13.41	1.9	2.34	1.7			
run_6	66.8	1.3	3.06	1.4	10.31	1.2	47.46	1.3	9.10	2.2	2.41	2.3	13.12	1.8	1.94	2.0	14.51	1.8	3.71	2.0	12.68	1.8	1.91	2.0	13.18	2.2	2.30	1.8			
average (n = 6)	66.3		3.06		10.25		47.30		9.08		2.40		13.25		1.96		14.71		3.75		12.87		1.92		13.38		2.34				
2 σ SD (pmol/kg)	1.6		0.18		0.23		0.68		0.21		0.06		0.22		0.04		0.26		0.06		0.30		0.02		0.31		0.06				
2 σ RSD%	2.4		5.9		2.2		1.4		2.3		2.6		1.7		2.0		1.7		1.6		2.3		1.2		2.3		2.3				

^ainternal 2 σ RSD%.

5. Conclusions and perspectives

5.1. Major Conclusions

This thesis presented dissolved seawater ϵ_{Nd} and [REE] from twelve stations along a NW-SE transect in the West Pacific (R/V *Sonne* cruise SO223T, GEOTRACES Process Study GPpr04) at unprecedented vertical and spatial resolution for this area. This high-resolution transect allows to exploit the high potential of Nd isotopes in combination with [Nd], as well as of the full suite of [REE] as tracers of sources and processes that control their distributions in the West Pacific (chapters 2 and 3). Additionally, a new robust and rapid REE method was developed and an international intercomparison on seawater [REE] was conducted in order to open the way for a fast growing high-quality global ocean REE dataset (chapter 4). Consequently, the overarching goal of this thesis was to add to the understanding of the controls on Nd isotope and REE (and of potentially other TE) distributions in the West Pacific, and the ocean in general. In the following, the major conclusions of this thesis are summarized:

Coastal input near South Korea and volcanic islands in the tropical West Pacific

The ϵ_{Nd} and [REE] data reveal sources of continental input near South Korea and volcanic islands in the TWP. Unradiogenic ϵ_{Nd} (-7.3), elevated [Nd] (15.30 pmol/kg), and low salinity of South Korean coastal waters clearly indicate local input to the surface of the East China Sea via freshwater discharge of South Korean and Chinese rivers. In the TWP, radiogenic ϵ_{Nd} (-2.0 to +0.7), positive Eu anomalies (1.15-1.25), and enriched MREE patterns of surface and subsurface waters, all characteristics for basaltic sources, fingerprint local modification at and input from Papua New Guinea (PNG), and to a lesser extent from the Philippines and Solomon Islands.

Trace element input to the tropical West Pacific and small-scale eastward transport within equatorial zonal currents

In the TWP, the fine-scale distribution of ϵ_{Nd} and [REE] that indicate local imprints and input from volcanic islands into surface and subsurface waters (see section above) further allows detailed tracing of the origin and small-scale circulation of the equatorial zonal current system, and further provides evidence for TE transport within eastward flowing equatorial zonal currents. The results therefore support the hypothesis of previous studies on the crucial role of the TWP as source region of micronutrients and other TEs to the HNLC area of the

East Pacific (e.g., Lacan and Jeandel, 2001; Slemons et al., 2010; Radic et al., 2011; Grenier et al., 2013; Labatut et al., 2014), and highlight in detail the small-scale equatorial zonal eastward transport.

Dominant conservative behavior of REEs and dominant non-conservative behavior of ϵ_{Nd} in the West Pacific

The data provide evidence for the largely conservative behavior of REEs in subsurface to bottom waters, reflecting lateral water mass transport and mixing, whereas strong non-conservative behavior of ϵ_{Nd} in the West Pacific is due to boundary exchange at the surrounding volcanic island margins.

The results point out the high potential of [REE] as lateral water mass tracer in the Pacific, even at subsurface depth. The strong correlation of high-salinity with low-[REE] and elevated Er/Yb ratios of SPTW deciphers advection of preformed low [REE] from its formation region in the oligotrophic South Pacific Subtropical Gyre to the TWP, and hence explains the low subsurface [REE] previously found in this area. Similarly, at the depth of AAIW and LCDW, preformed and vertically constant [REE] indicate lateral transport from the Southern Ocean to as far north as 10°N and 28°N in the West Pacific, respectively. In contrast, when AAIW and LCDW enter the TWP, the ϵ_{Nd} values of these water masses are more radiogenic than in the Southern Ocean by up to 3.1 and 4.4 ϵ_{Nd} units, and further increase towards the north by up to 3.7 and ~ 1 ϵ_{Nd} units, respectively, suggesting boundary exchange with basaltic island margins. In the TWP, deep water (~ 1500 - 3000 m) both [REE] and ϵ_{Nd} data provide evidence for enhanced scavenging of REEs and isotopic exchange of Nd near volcanic island margins and within deep hydrothermal plumes located at ~ 2000 m water depth in this region.

In summary, constant preformed [REE] are transported laterally over substantial distances in the Pacific, while ϵ_{Nd} signatures of these water masses are more quickly modified by radiogenic sources, except within WNPCW, NPIW, and UCDW/PDW in the Northwest Pacific, where ϵ_{Nd} can be used as quasi-conservative water mass tracer.

New rapid and precise REE method and first reference seawater REE standard in the Pacific open the way to build a global high-quality seawater REE dataset

The study in chapter 4 presents a new rapid and precise method for dissolved seawater [REE] (picomolar level) and an international intercomparison by four labs of [REE] in seawater from the GEOTRACES intercalibration station SAFE 3000 m. For the first time, the

method used the automated seaFAST-pico system in offline mode and multi-element ID ICP-MS for the robust and rapid pre-concentration, purification, and analysis of dissolved [REE] from small volumes of seawater (11-12 mL). The accuracy of this new method was checked by multiple repeated processing and analysis of GEOTRACES intercalibration seawater from BATS at 15 m and 2000 m. The [REE] results on replicates of GEOTRACES intercalibration seawater from SAFe 3000 m further point out a procedural long-term precision of $\leq 3.9\%$ (2σ RSD) for all REEs, except for Ce and Gd.

The international intercomparison from four labs using SAFe 3000 m seawater aliquots indicates excellent agreement between [REE] within 7% (except for Ce 71%, Gd 14%, Lu 12%, 2σ RSD), and thus provides the first reference seawater REE standard in the Pacific for quality control of future marine REE studies. The method is easy to adopt, enables the extensive use of REEs, and ultimately opens the way for a fast growing and high-quality global ocean REE dataset.

5.2. Perspectives

As a next step, the results presented in this thesis can be supplemented by future studies. Chapters 2 and 3 of this thesis pointed out the importance of the TWP as the source region of micronutrients and other TEs for the tropical East Pacific HNLC area. Consequently, changes in the western tropical Pacific TE input and zonal current system can therefore have a significant impact on ecosystems in the East, and hence on the nourishment of people depending on marine fishery (Séférian et al., 2014). Although many recent studies were focused on the upper oceanic circulation of the tropical Pacific, its complex zonal current system particularly that below 400 m water depth including recently discovered mid-depth currents/jets (Cravatte et al., 2012), is still not completely resolved, while even less is known about their geochemical composition. The crucial role of the equatorial current system in supplying the East Pacific with micronutrients derived from the West Pacific highlights the importance for a detailed geochemical and oceanographic understanding of these currents near their origin and potential inter-annual variability of supplied material from the West Pacific source area. As the project in this thesis (chapters 2 and 3) provided high-resolution vertical Nd isotope and [REE] profiles, but with limited spatial coverage, this and previous studies did not resolve the role of the mid-depth currents/jets and the inter-annual variability of TE supply and current transport in any spatial or vertical detail. Therefore, I collected high-resolution vertical surface and surface to deep water samples for dissolved Nd isotopes and [REE] at 14 stations in the western tropical Pacific during the oceanographic-geochemical

R/V *L'Atalante* cruise CASSIOPEE within a French-German collaboration (GEOTRACES compliant data, GPc05). This detailed study is based on an integrated approach using geochemical and physical oceanographic data and will provide the means to solve the enigma posed by recently discovered mid-depth currents/jets (Cravatte et al., 2012) with respect to their origin, spatial extent, geochemical composition, dynamics and temporal variability, and hence their potential as conduits of micronutrients to the HNLC area of the tropical East Pacific.

The sparse dissolved seawater ϵ_{Nd} and REE dataset in the Pacific will further be extended by another collaborative and follow-up study (GEOTRACES compliant data, GPc04, R/V *Sonne* cruise SO225) that will add to the understanding of seawater ϵ_{Nd} and REE cycling in the equatorial central Pacific. Therefore, I analyzed high-resolution vertical full water column profiles of dissolved ϵ_{Nd} at three stations located near the Manihiki Plateau, which is a large igneous province. The new ϵ_{Nd} data will clarify whether local imprints from the Manihiki Plateau itself or from adjacent volcanic islands (e.g., Samoa) influence surface to deep water ϵ_{Nd} , in particular that of LCDW in this region. Additionally, the ϵ_{Nd} data will verify if a radiogenic ϵ_{Nd} imprint on equatorial central Pacific surface to mid-depth waters trace their eastward flow within the zonal currents and possibly within the recently discovered mid-depth currents/jets (Cravatte et al., 2012).

Concerning the REE data of this thesis (chapter 3), an interesting investigation is to examine in detail how mid-depth waters in the TWP (stations 11-19) inherit their distinctly low Dy/Er ratio, and whether this ratio may have the potential as a powerful tracer of lateral water mass transport (Zhang and Nozaki, 1996; Osborne et al., 2015). Osborne et al. (2015) suggested that the distinctly low Dy/Er ratio found at mid-depth in the tropical Atlantic may trace the flow path of AAIW, although these authors left the process that leads to the low Dy/Er signal unexplained. Therefore, the major goal of a follow-up study is to understand the process that posed the low Dy/Er signal in the TWP, and thus exploiting its potential as lateral water mass tracer.

Yet, the data of this thesis do not support a substantial benthic flux of REEs to Pacific deep waters as suggested by Abbott et al. (2015a), however, this has to be tested in other oceanic regions. Therefore, an interesting future investigation would be a detailed assessment of the impact of benthic fluxes on dissolved seawater ϵ_{Nd} and [REE] distributions in the Pacific, and on a global scale.

As the data of this thesis provide evidence for both enhanced scavenging and isotopic exchange of Nd in hydrothermal plumes, another promising aspect would be to measure

dissolved and particulate ϵ_{Nd} and [REE] within hydrothermal fluids and the surrounding seawater in different oceanic regions and geological settings. The data would then enable to estimate and model the local and global deep water REE budgets, and define the potentially crucial role of hydrothermal plumes on dissolved seawater ϵ_{Nd} and [REE] distributions.

Finally, the analysis of both dissolved and particulate ϵ_{Nd} and [REE] along transects is an important next step in order to define the role of marine particles on their dissolved distributions in the global ocean, and in marine biogeochemical processes in general. So far, this has been hindered by the large sample volumes required for the analysis of suspended particulate ϵ_{Nd} and [REE], however, the application of in-situ pumps, which allow large volume filtration, opens the way for accurate sampling of particles (Bishop et al., 2012).

6. References

- Abbott, A. N., Haley, B. A., McManus, J., Reimers, C. E. (2015a) The sedimentary flux of dissolved rare earth elements to the ocean. *Geochim. Cosmochim. Acta* **154**, 186-200.
- Abbott, A. N., Haley, B. A., McManus, J. (2015b) Bottoms up: Sedimentary control of the deep North Pacific Ocean's ϵ_{Nd} signature. *Geology* **43**(11), 1035-1038.
- Alibo, D. S., Nozaki, Y. (1999) Rare earth elements in seawater: particle association, shale-normalization, and Ce oxidation. *Geochim. Cosmochim. Acta* **63**, 363-372.
- Amakawa, H., Alibo, D. S., Nozaki, Y. (2004b) Nd concentration and isotopic composition distributions in surface waters of Northwest Pacific Ocean and its adjacent seas. *Geochem. J.* **38**, 493-504.
- Amakawa, H., Nozaki, Y., Alibo, D. S., Zhang, J., Fukugawa, K., Nagai, H. (2004a) Neodymium isotopic variations in Northwest Pacific water. *Geochim. Cosmochim. Acta* **68**, 715-727.
- Amakawa, H., Sasaki, K., Ebihara, M. (2009) Nd isotopic composition in the central North Pacific. *Geochim. Cosmochim. Acta* **73**, 4705-4719.
- Amakawa, H., Tazoe, H., Obata, H., Gamo, T., Sano, Y., Shen, C. C. (2013) Neodymium isotopic composition and concentration in the Southwest Pacific Ocean. *Geochem. J.* **47**, 409-422.
- Andersson, P. S., Porcelli, D., Frank, M., Bjork, G., Dahlqvist, R., Gustafsson, O. (2008) Neodymium isotopes in seawater from the Barents Sea and Fram Strait Arctic-Atlantic gateways. *Geochim. Cosmochim. Acta* **72**, 2854-2867.
- Arsouze, T., Dutay, J.-C., Lacan, F., Jeandel, C. (2007) Modeling the neodymium isotopic composition with a global ocean circulation model. *Chem. Geol.* **239**, 165-177.
- Arsouze, T., Dutay, J.-C., Lacan, F., Jeandel C. (2009) Reconstructing the Nd oceanic cycle using a coupled dynamical -biogeochemical model. *Biogeosciences* **6**, 2829-2846.
- Barber, R. T., Sanderson, M. P., Lindley, S. T., Chai, F., Newton, J., Trees, C. C., Foley, D. G., Chavez, F. P. (1996) Primary productivity and its regulation in the equatorial Pacific during and following the 1991-92 El Niño. *Deep Sea Res. II* **43**, 933-970.
- Basak, C., Pahnke, K., Frank, M., Lamy, F., Gersonde, R. (2015) Neodymium isotopic characterization of Ross Sea Bottom Water and its advection through the southern South Pacific. *Earth Planet. Sci. Lett.* **419**, 211-221.

- Beardsley, R. C., Limeburner, R., Yu, H., Cannon, G. A. (1985) Discharge of the Changjiang (Yangtze River) into the East China Sea. *Cont. Shelf Res.* **4**, 57-76.
- Behrens, M. K., Muratli, J., Pradoux, C., Wu, Y., Böning, P., Brumsack, H.-J., Goldstein, S. L., Haley, B., Jeandel, C., Paffrath, R., Pena, L. D., Schnetger, B., Pahnke, K. (2016) Rapid and precise analysis of rare earth elements in small volumes of seawater - Method and intercomparison. *Mar. Chem.* **186**, 110-120.
- Behrens, M. K., Pahnke, K., Schnetger, B., Brumsack, H.-J. (in prep.) Sources and processes affecting the distribution of dissolved Nd isotopes and concentrations in the West Pacific.
- Bianchi, D., Sarmiento, J. L., Gnanadesikan, A., Key, R. M., Schlosser, P., Newton, R. (2010) Low helium flux from the mantle inferred from simulations of oceanic helium isotope data. *Earth Planet. Sci. Lett.* **297**, 379-386.
- Bingham, F. M. (1992) Formation and spreading of Subtropical Mode Water in the North Pacific. *J. Geophys. Res. Oceans* **97**, 11177-11189.
- Bingham, F. M., Lukas, R. (1995) The distribution of Intermediate Water in the western equatorial Pacific during January-February 1986. *Deep-Sea Res. I* **42**, 1545-1573.
- Bishop, J. K. B., Lam, P. J., Wood, T. J. (2012) Getting good particles: accurate sampling of particles by large volume in-situ filtration. *Limnol. Oceanogr. Methods* **10**, 681-710.
- Bostock, H. C., Opdyke, B. N., Williams, M. J. M. (2010) Characterising the intermediate depth waters of the Pacific Ocean using delta C-13 and other geochemical tracers. *Deep-Sea Res. I* **57**, 847-859.
- Broecker, W. S., Peng, T. H. (1982) *Tracers in the Sea*. Eldigio Press, Palisades, New York.
- Bruland, K. W., Franks, R. P., Knauer, G. A., Martin, J. H. (1979) Sampling and analytical methods for the determination of copper, cadmium, zinc and nickel in seawater. *Anal. Chim. Acta* **105**, 233-245.
- Bruland, K. W., Lohan, M. C. (2003) *Controls of trace metals in seawater*. In: *Treatise on Geochemistry: The Oceans and Marine Geochemistry* (ed. Elderfield, H.). Elsevier, Amsterdam, pp. 23-47.
- Bruland, K. W., Rue, E. L., Smith, G. J., DiTullio, G. R. (2005) Iron, macronutrients and diatom blooms in the Peru upwelling regime: brown and blue waters of Peru. *Mar. Chem.* **93** (2-4), 81-103.
- Byrne, R. H., Kim, K.-H. (1990) Rare earth element scavenging in seawater. *Geochim. Cosmochim. Acta* **54**, 2645-2656.

- Callahan, J. E. (1972) Structure and circulation of deep-water in Antarctic. *Deep-Sea Res.* **19**, 563-575.
- Cannon, G. A. (1966) Tropical waters in the western Pacific Ocean, August-September 1957. *Deep-Sea Res.* **13**, 1139-1148.
- Cantrell, K. J., Byrne, R. H. (1987) Rare earth element complexation by carbonate and oxalate ions. *Geochim. Cosmochim. Acta* **51**, 597-605.
- Carter, P., Vance, D., Hillenbrand, C. D., Smith, J. A., Shoosmith, D. R. (2012) The neodymium isotopic composition of waters masses in the eastern Pacific sector of the Southern Ocean. *Geochim. Cosmochim. Acta* **79**, 41-59.
- Chang, P. H., Isobe, A. (2003) A numerical study on the Changjiang diluted water in the Yellow and East China Seas. *J. Geophys. Res. Oceans* **108**, 1-17.
- Chester, R., Jickells, T. (2012) *Trace elements in the Oceans*. In: Marine Geochemistry, John Wiley & Sons, Ltd, Chichester, UK.
- Coale, K. H., Johnson, K. S., Fitzwater, S. E., Gordon, R. M., Tanner, S., Chavez, F. P., Ferioli, L., Sakamoto, C., Rogers, P., Millero, F., Steinberg, P., Nightingale, P., Cooper, D., Cochlan, W. P., Landry, M. R., Constantinou, J., Rollwagen, G., Trasvina, A., Kudela, R. (1996) A massive phytoplankton bloom induced by an ecosystem-scale iron fertilization experiment in the equatorial Pacific Ocean. *Nature* **383**, 495-501.
- Cravatte, S., Kessler, W. S., Marin, F. (2012) Intermediate zonal jets in the tropical Pacific Ocean observed by argo floats. *J. Phys. Oceanogr.* **42**, 1475-1485.
- Cutter, G. A., Bruland, K. W. (2012) Rapid and noncontaminating sampling system for trace elements in global ocean surveys. *Limnol. Oceanogr. Methods* **10**, 425-436.
- Dagg, M., Benner, R., Lohrenz, S., Lawrence, D. (2004) Transformation of dissolved and particulate materials on continental shelves influenced by large rivers: plume processes. *Cont. Shelf Res.* **24**, 833-858.
- de Baar, H. J. W., Bacon, M. P., Brewer, P. G., Bruland, K. W. (1985) Rare earth elements in the Pacific and Atlantic Oceans. *Geochim. Cosmochim. Acta* **49** (9), 1943-1959.
- Elderfield, H. (1988) The oceanic chemistry of the rare earth elements. *Philos. Trans. R. Soc. Lond. Ser. A* **325**, 105-126.
- Elderfield, H., Greaves, M. J. (1982) The rare earth elements in seawater. *Nature* **296**, 214-219.

- Elemental Scientific (2014). *SeaFAST automating seawater analysis*. Nebraska, USA, <http://www.icpms.com/pdf/seaFAST-seawater-analysis.pdf> (accessed 03/01/2016).
- Ferdelman, T. G. (2016) *Cruise report SO245 - UltraPac: Process oriented biogeochemical, microbiological and ecological investigations of the ultraoligotrophic South Pacific Gyre (R/V Sonne, 12/17–01/18, Antofagasta, Chile to Wellington, New Zealand)*. Max Planck Institute for Marine Microbiology, Bremen.
- Fine, R. A., Lukas, R., Bingham, F. M., Warner, M. J., Gammon, R. H. (1994) The western equatorial Pacific - a water mass crossroads. *J. Geophys. Res. Oceans* **99**, 25063-25080.
- Firing, E., Wijffels, S. E., Hacker, P. (1998) Equatorial subthermocline currents across the Pacific. *J. Geophys. Res. Oceans* **103**, 21413-21423.
- Fitzsimmons, J. N., Jenkins, W. J., Boyle, E. A. (2014) Distal transport of dissolved hydrothermal iron in the deep South Pacific Ocean. *Proc. Natl. Acad. Sci. U.S.A.* **111**(47), 16654-16661.
- Frank, M. (2002) Radiogenic isotopes: Tracers of past ocean circulation and erosional input. *Rev. Geophys.* **40**(1), 1-38.
- Frank, M. (2011) Chemical twins, separated. *Nature Geoscience* **4**, 220-221.
- Fröllje, H., Pahnke, K., Schnetger, B., Brumsack, H.-J., Dulai, H., Fitzsimmons, J. N. (2016) Hawaiian imprint on dissolved Nd and Ra isotopes and rare earth elements in the central North Pacific: Local survey and seasonal variability. *Geochim. Cosmochim. Acta* **189**, 110-131.
- Garabato, A. C. N., Heywood, K. J., Stevens, D. P. (2002) Modification and pathways of Southern Ocean deep waters in the Scotia Sea. *Deep-Sea Res. Part I* **49**, 681-705.
- German, C. R., Klinkhammer, G. P., Edmond, J. M., Mitra, A., Elderfield, H. (1990) Hydrothermal scavenging of rare earth elements in the ocean. *Nature* **345**, 516–518.
- Goldstein, S. L., Onions, R. K., Hamilton, P. J. (1984) A Sm-Nd isotopic study of atmospheric dusts and particulates from major river systems. *Earth Planet. Sci. Lett.* **70**, 221-236.
- Goldstein, S. L., Hemming, S. R. (2003) *Long-lived isotopic tracers in oceanography, paleoceanography, and ice-sheet dynamics*. In: *Treatise on Geochemistry: The Oceans and Marine Geochemistry* (ed. Elderfield, H.). Elsevier, New York, pp. 453-489.
- Gordon, A. L. (1986) Interocean exchange of thermocline water. *J. Geophys. Res. Oceans* **91**, 5037-5046.

- Grasse, P., Stichel, T., Stumpf, R., Stramma, L., Frank, M. (2012) The distribution of neodymium isotopes and concentrations in the Eastern Equatorial Pacific: Water mass advection versus particle exchange. *Earth Planet. Sci. Lett.* **353**, 198-207.
- Greaves, M. J., Elderfield, H., Klinkhammer, G. P. (1989) Determination of the rare earth elements in natural waters by isotope dilution mass spectrometry. *Anal. Chim. Acta* **218**, 265-280.
- Greaves, M. J., Elderfield, H., Sholkovitz, E. R. (1999) Aeolian sources of rare earth elements to the Western Pacific Ocean. *Mar. Chem.* **68**, 31-38.
- Grenier, M., Cravatte, S., Blanke, B., Menkes, C., Koch-Larrouy, A., Durand, F., Melet, A., Jeandel, C. (2011) From the western boundary currents to the Pacific Equatorial Undercurrent: Modeled pathways and water mass evolutions. *J. Geophys. Res. Oceans* **116**, C12044.
- Grenier M., Jeandel C., Lacan, F., Vance, D., Venchiarutti, C., Cros, A., Cravatte, S. (2013) From the subtropics to the central equatorial Pacific Ocean: Neodymium isotopic composition and rare earth element concentration variations. *J. Geophys. Res. Oceans* **118**, 592-618.
- Haley, B. A., Klinkhammer, G. P., McManus, J. (2004) Rare earth elements in pore waters of marine sediments. *Geochim. Cosmochim. Acta* **68**, 1265-1279.
- Haley, B. A., Frank, M., Hathorne, E., Pisias, N. (2014) Biogeochemical implications from dissolved rare earth element and Nd isotope distributions in the Gulf of Alaska. *Geochim. Cosmochim. Acta* **126**, 455-474.
- Hannigan, R. E., Sholkovitz, E. R. (2001) The development of middle rare earth element enrichments in freshwaters: weathering of phosphate minerals. *Chem. Geol.* **175**, 495-508.
- Hara, Y., Obata, H., Doi, T., Hongo, Y., Gamo, T., Takeda, S., Tsuda, A. (2009) Rare earth elements in seawater during an iron-induced phytoplankton bloom of the western subarctic Pacific (SEEDS-II). *Deep-Sea Res. II Top. Stud. Oceanogr.* **56** (26), 2839-2851.
- Hathorne, E. C., Haley, B., Stichel, T., Grasse, P., Zieringer, M., Frank, M. (2012) Online pre-concentration ICP-MS analysis of rare earth elements in seawater. *Geochem. Geophys. Geosyst.* **13** (1), Q01020.
- Hathorne, E. C., Stichel, T., Bruck, B., Frank, M. (2015) Rare earth element distribution in the Atlantic sector of the Southern Ocean: The balance between particle scavenging and vertical supply. *Mar. Chem.* **177**, 157-171.

- Hatje, V., Bruland, K. W., Flegal, A. R. (2014) Determination of rare earth elements after pre-concentration using NOBIAS-chelate PA-1 (R) resin: method development and application in the San Francisco Bay plume. *Mar. Chem.* **160**, 34-41.
- Hawco, N. J., Ohnemus, D. C., Resing, J. A., Twining, B. S., Saito, M. A. (2016) A dissolved cobalt plume in the oxygen minimum zone of the eastern tropical South Pacific. *Biogeosciences* **13**, 5697-5717.
- SCOR Working Group: Henderson, G. M., Anderson, R. F., Adkins, J., Andersson, P., Boyle, E. A., Cutter, G., de Baar, H., Eisenhauer, A., Frank, M., Francois, R., Orians, K., Gamo, T., German, C., Jenkins, W., Moffett, J., Jeandel, C., Jickells, T., Krishnaswami, S., Mackey, D., Masque, P., Measures, C. I., Moore, J. K., Oschlies, A., Pollard, R., van der Loeff, M. R. D., Schlitzer, R., Sharma, M., von Damm, K., Zhang, J. (2007) GEOTRACES - An international study of the global marine biogeochemical cycles of trace elements and their isotopes. *Chem. Erde-Geochem.* **67**, 85-131.
- Hongo, Y., Obata, H., Alibo, D. S., Nozaki, Y. (2006) Spatial variations of rare earth elements in North Pacific surface water. *J. Oceanogr.* **62**, 441-455.
- Hongo, Y., Obata, H., Gamo, T., Nakaseama, M., Ishibashi, J., Konno, U., Saegusa, S., Ohkubo, S., Tsunogai, U. (2007) Rare earth elements in the hydrothermal system at Okinawa Trough back-arc basin. *Geochem. J.* **41**, 1-15.
- Hoshika, A., Tanimoto, T., Mishima, Y., Iseki, K., Okamura, K. (2003) Variation of turbidity and particle transport in the bottom layer of the East China Sea. *Deep-Sea Res. Part II* **50**, 443-455.
- Hupe, A., Karstensen, J. (2000) Redfield stoichiometry in Arabian Sea subsurface waters. *Glob. Biogeochem. Cycles* **14**, 357-372.
- Isobe, A. (1999) On the origin of the Tsushima Warm Current and its seasonality. *Cont. Shelf Res.* **19**, 117-133.
- Jacobsen, S. B., Wasserburg, G. J. (1980) Sm-Nd isotopic evolution of chondrites. *Earth Planet. Sci. Lett.* **50**, 139-155.
- Jeandel, C., Thouron, D., Fieux, M. (1998) Concentrations and isotopic compositions of neodymium in the eastern Indian Ocean and Indonesian straits. *Geochim. Cosmochim. Acta* **62**, 2597-2607.
- Jeandel, C., Arsouze, T., Lacan, F., Techine, P., Dutay, J.-C. (2007) Isotopic Nd compositions and concentrations of the lithogenic inputs into the ocean: A compilation, with an emphasis on the margins. *Chem. Geol.* **239**, 156-164.

- Jeandel, C., Delattre, H., Grenier, M., Pradoux, C., Lacan, F. (2013) Rare earth element concentrations and Nd isotopes in the Southeast Pacific Ocean. *Geochem. Geophys. Geosyst.* **14**, 328-341.
- Johannesson, K. H., Burdige, D. J. (2007) Balancing the global oceanic neodymium budget: Evaluating the role of groundwater. *Earth Planet. Sci. Lett.* **253**, 129-142.
- Johnson, G. C., Toole, J. M. (1993) Flow of deep and bottom waters in the Pacific at 10°N. *Deep-Sea Res. Part I* **40**, 371-394.
- Jones, K. M. (2010) An evaluation of radiogenic isotopes as tracers of ocean circulation and sediment transport: modeling, seawater, and sediment studies, Department of Earth and Environmental Sciences. Columbia University, New York, PhD thesis, pp. 253.
- Kaneko, I., Takatsuki, Y., Kamiya, H. (2001) Circulation of intermediate and deep waters in the Philippine Sea. *J. Oceanogr.* **57**, 397-420.
- Karstensen, J., Tomczak, M. (1998) Age determination of mixed water masses using CFC and oxygen data. *J. Geophys. Res. Oceans* **103**, 18599-18609.
- Kashino, Y., Aoyama, M., Kawano, T., Hendiarti, N., Syaefudin, Anantasena, Y., Muneyama, K., Watanabe, H. (1996) The water masses between Mindanao and New Guinea. *J. Geophys. Res. Oceans* **101**, 12391-12400.
- Kawabe, M., Fujio, S., Yanagimoto, D. (2003) Deep-water circulation at low latitudes in the western North Pacific. *Deep-Sea Res. Part I* **50**, 631-656.
- Kawabe, M., Fujio, S., Yanagimoto, D., Tanaka, K. (2009) Water masses and currents of deep circulation southwest of the Shatsky Rise in the western North Pacific. *Deep-Sea Res. Part I* **56**, 1675-1687.
- Kawabe, M., Fujio, S. (2010) Pacific ocean circulation based on observation. *J. Oceanogr.* **66**, 389-403.
- Kawano, T., Fukasawa, M., Kouketsu, S., Uchida, H., Doi, T., Kaneko, I., Aoyama, M., Schneider, W. (2006) Bottom water warming along the pathway of lower circumpolar deep water in the Pacific Ocean. *Geophys. Res. Lett.* **33**, L23613.
- Kim, I., Kim, G. (2011) Large fluxes of rare earth elements through submarine groundwater discharge (SGD) from a volcanic island, Jeju, Korea. *Mar. Chem.* **127**, 12-19.
- Kim, I., Kim, G. (2014) Submarine groundwater discharge as a main source of rare earth elements in coastal waters. *Mar. Chem.* **160**, 11-17.

- Klinkhammer, G., Elderfield, H., Hudson, A. (1983) Rare earth elements in seawater near hydrothermal vents. *Nature* **305**, 185-188.
- Kulaksiz, S., Bau, M. (2011) Anthropogenic gadolinium as a microcontaminant in tap water used as drinking water in urban areas and megacities. *Appl. Geochem.* **26**, 1877-1885.
- Labatut, M., Lacan, F., Pradoux, C., Chmeleff, J., Radic, A., Murray, J. W., Poitrasson, F., Johansen, A. M., Thil, F. (2014) Iron sources and dissolved-particulate interactions in the seawater of the Western Equatorial Pacific, iron isotope perspectives. *Glob. Biogeochem. Cycle* **28**, 1044-1065.
- Lacan, F., Jeandel, C. (2001) Tracing Papua New Guinea imprint on the central equatorial Pacific Ocean using neodymium isotopic compositions and rare earth element patterns. *Earth Planet. Sci. Lett.* **186**, 497-512.
- Lacan, F., Jeandel, C. (2005) Neodymium isotopes as a new tool for quantifying exchange fluxes at the continent-ocean interface. *Earth Planet. Sci. Lett.* **232**, 245-257.
- Lambelet, M., van de Fliedert, T., Crocket, K., Rehkamper, M., Kreissig, K., Coles, B., Rijkenberg, M. J. A., Gerringa, L. J. A., de Baar, H. J. W., Steinfeldt, R. (2016) Neodymium isotopic composition and concentration in the western North Atlantic Ocean: Results from the GEOTRACES GA02 section. *Geochim. Cosmochim. Acta* **177**, 1-29.
- Lan, C. Y., Lee, T., Zhou, X. H., Kwon, S. T. (1995) Nd isotopic study of precambrian basement of South Korea - evidence for early archean crust. *Geology* **23**, 249-252.
- Liu, C. Q., Masuda, A., Okada, A., Yabuki, S., Zhang, J., Fan, Z. L. (1993) A geochemical study of loess and desert sand in northern China - implications for continental crust weathering and composition. *Chem. Geol.* **106**, 359-374.
- Lukas, R., Firing, E., Hacker, P., Richardson, P. L., Collins, C. A., Fine, R., Gammon, R. (1991) Observations of the Mindanao Current during the Western Equatorial Pacific-Ocean Circulation Study. *J. Geophys. Res. Oceans* **96**, 7089-7104.
- Lupton, J. E., Pyle, D. G., Jenkins, W. J., Greene, R., Evans, L. (2004) Evidence for an extensive hydrothermal plume in the Tonga-Fiji region of the South Pacific. *Geochem. Geophys. Geosyst.* **5**, Q01003.
- Lupton, J., Rubin, K. H., Arculus, R., Lilley, M., Butterfield, D., Resing, J., Baker, E., Embley, R. (2015) Helium isotope, C/He-3, and Ba-Nb-Ti signatures in the northern Lau Basin: Distinguishing arc, back-arc, and hotspot affinities. *Geochem. Geophys. Geosyst.* **16**, 1133-1155.

- Macdonald, A. M., Mecking, S., Robbins, P. E., Toole, J. M., Johnson, G. C., Talley, L., Cook, M., Wijffels, S. E. (2009) The WOCE-era 3-D Pacific Ocean circulation and heat budget. *Prog. Oceanogr.* **82**, 281-325.
- Masuzawa, J. (1969) Subtropical Mode Water. *Deep-Sea Res.* **16**, 463-472.
- McCartney, M. S. (1982) The subtropical recirculation of Mode Waters. *J. Mar. Res.* **40**, 427-464.
- McTaggart, K. E., Johnson, G. C., Johnson, M. C., Delahoyde, F. M., Swift, J. H. (2010) *Notes on CTD/O₂ data acquisition and processing using Sea-Bird hardware and software (as available)*. In: GO-SHIP repeat hydrography manual: A collection of expert reports and guidelines (eds. Hood, E. M., Sabine, C. L., Sloyan, B. M.), Version 1, IOCCP Rep. 14, ICPO Publ. Ser. 134, 10 pp.
- Measures, C., Hatta, M., Fitzsimmons, J., Morton, P. (2015) Dissolved Al in the zonal N Atlantic section of the US GEOTRACES 2010/2011 cruises and the importance of hydrothermal inputs. *Deep-Sea Res. Part II Top. Stud. Oceanogr.* **116**, 176–186.
- Miller, J. R. (1976) The salinity effect in a mixed layer ocean model. *J. Phys. Oceanogr.* **6**, 29-35.
- Milliman, J. D., Meade, R. H. (1983) World-wide delivery of river sediment to the oceans. *J. Geol.* **91**, 1-21.
- Moffett, J. W. (1990) Microbially mediated cerium oxidation in seawater. *Nature* **345**, 421-423.
- Molina-Kescher, M., Frank, M., Hathorne, E. (2014) South Pacific dissolved Nd isotope compositions and rare earth element distributions: water mass mixing versus biogeochemical cycling. *Geochim. Cosmochim. Acta* **127**, 171-189.
- Morel, F. M. M., Milligan, A. J., Saito, M. A. (2003) *Marine bioinorganic chemistry: the role of trace metals in the oceanic cycles of major nutrients*. In: Treatise on Geochemistry: The Oceans and Marine Geochemistry (ed. Elderfield, H.). Elsevier, Oxford, pp. 113-143.
- Nakamura, H. (1996) A pycnostad on the bottom of the ventilated portion in the central subtropical North Pacific: Its distribution and formation. *J. Oceanogr.* **52**, 171-188.
- Nitani, H. (1972) *Beginning of the Kuroshio*. In: Kuroshio, its physical aspects (eds. Stommel, H., Yoshida, K.). Univ. of Tokyo Press, Tokyo, pp. 129-163.

- Nozaki, Y. (2001) *Rare earth elements and their isotopes*. In: Encyclopedia of Ocean Sciences (eds. Steele, J. H., Thorpe, S. A., Turekian, K. K.) Academic, London, pp. 2354-2366.
- O'Connor, B. M., Fine, R. A., Olson, D. B. (2005) A global comparison of subtropical underwater formation rates. *Deep-Sea Res. Part I* **52**, 1569-1590.
- O'Nions, R. K., Hamilton, P. J., Evensen, N. M. (1977) Variations in $^{143}\text{Nd}/^{144}\text{Nd}$ and $^{87}\text{Sr}/^{86}\text{Sr}$ ratios in oceanic basalts. *Earth Planet. Sci. Lett.* **34**, 13-22.
- Orsi, A. H., Whitworth, T., Nowlin, W. D. (1995) On the meridional extent and fronts of the Antarctic Circumpolar Current. *Deep-Sea Res. Part I* **42**, 641-673.
- Osborne, A. H., Haley, B. A., Hathorne, E. C., Fogel, S., Frank, M. (2014) Neodymium isotopes and concentrations in Caribbean seawater: Tracing water mass mixing and continental input in a semi-enclosed ocean basin. *Earth Planet. Sci. Lett.* **406**, 174-186.
- Osborne, A. H., Haley, B. A., Hathorne, E. C., Plancherel, Y., Frank M. (2015) Rare earth element distribution in Caribbean seawater: Continental inputs versus lateral transport of distinct REE compositions in subsurface water masses. *Mar. Chem.* **177**, 172-183.
- Pahnke, K., Goldstein, S. L., Hemming, S. R. (2008) Abrupt changes in Antarctic Intermediate Water circulation over the past 25,000 years. *Nature Geoscience* **1**, 870-874.
- Pahnke, K., van de Flierdt, T., Jones, K. M., Lambelet, M., Hemming, S. R., Goldstein, S. L. (2012) GEOTRACES intercalibration of neodymium isotopes and rare earth element concentrations in seawater and suspended particles. Part 2: Systematic tests and baseline profiles. *Limnol. Oceanogr. Methods* **10**, 252-269.
- Park, S. C., Chu, K. S. (1991) *Dispersal patterns of river-derived fine-grained sediments on the inner shelf of Korea Strait*. In: Oceanography of Asian Marginal Sea (ed. Takano, K.). Oceanogr. Ser. 54, Elsevier, Amsterdam, pp. 231-240.
- Pearce, C. R., Jones, M. T., Oelkers, E. H., Pradoux, C., Jeandel, C. (2013) The effect of particulate dissolution on the neodymium (Nd) isotope and Rare Earth Element (REE) composition of seawater. *Earth Planet. Sci. Lett.* **369**, 138-147.
- Pickard, G. L., Emery, W. J. (1990) *Descriptive Physical Oceanography: An Introduction*. Elsevier, Boston.
- Piegras, D. J., Wasserburg, G. J. (1980) Neodymium isotopic variations in seawater. *Earth Planet. Sci. Lett.* **50**, 128-138.

- Piepgras, D. J., Wasserburg, G. J. (1987) Rare earth element transport in the western North Atlantic inferred from Nd isotopic observations. *Geochim. Cosmochim. Acta* **51**, 1257-1271.
- Piepgras, D. J., Jacobsen, S. B. (1988) The isotopic composition of neodymium in the North Pacific. *Geochim. Cosmochim. Acta* **52**, 1373-1381.
- Piepgras, D. J., Jacobsen, S. B. (1992) The behaviour of rare earth elements in seawater - precise determination of variations in the North Pacific water column. *Geochim. Cosmochim. Acta* **56**, 1851-1862.
- Pin, C., Zalduegui, J. F. S. (1997) Sequential separation of light rare-earth elements, thorium and uranium by miniaturized extraction chromatography: Application to isotopic analyses of silicate rocks. *Anal. Chim. Acta* **339**, 79-89.
- Qu, T. D., Mitsudera, H., Yamagata, T. (1998) On the western boundary currents in the Philippine Sea. *J. Geophys. Res. Oceans* **103**, 7537-7548.
- Qu, T. D., Mitsudera, H., Yamagata, T. (1999) A climatology of the circulation and water mass distribution near the Philippine coast. *J. Phys. Oceanogr.* **29**, 1488-1505.
- Qu, T. D., Lindstrom, E. J. (2002) A climatological interpretation of the circulation in the Western South Pacific. *J. Phys. Oceanogr.* **32**, 2492-2508.
- Qu, T. D., Lindstrom, E. J. (2004) Northward intrusion of Antarctic intermediate water in the western Pacific. *J. Phys. Oceanogr.* **34**, 2104-2118.
- Qu, T. D., Gao, S., Fukumori, I., Fine, R. A., Lindstrom, E. J. (2009) Origin and pathway of equatorial 13°C water in the Pacific identified by a simulated passive tracer and its adjoint. *J. Phys. Oceanogr.* **39**, 1836-1853.
- Qu, T. D., Gao, S., Fine, R. A. (2013) Subduction of South Pacific Tropical Water and its equatorward pathways as shown by a simulated passive tracer. *J. Phys. Oceanogr.* **43**, 1551-1565.
- Quinn, K. A., Byrne, R. H., Schijf, J. (2006) Sorption of yttrium and rare earth elements by amorphous ferric hydroxide: Influence of solution complexation with carbonate. *Geochim. Cosmochim. Acta* **70**, 4151-4165.
- Radic, A., Lacan, F., Murray, J. W. (2011) Iron isotopes in the seawater of the equatorial Pacific Ocean: New constraints for the oceanic iron cycle. *Earth Planet. Sci. Lett.* **306**, 1-10.

- Rehbein, M. (in prep.) Rare earth elements in the subtropical South Pacific. Master Thesis, University of Oldenburg.
- Reid, J. L. (1959) Evidence of a South Equatorial Countercurrent in the Pacific Ocean. *Nature* **184**, 209-210.
- Reid, J. L. (1965) *Intermediate waters of the Pacific Ocean*. Johns Hopkins Press, Baltimore.
- Reid, J. L. (1997) On the total geostrophic circulation of the Pacific Ocean: flow patterns, tracers, and transports. *Prog. Oceanogr.* **39**, 263-352.
- Rempfer, J., Stocker, T. F., Joos, F., Dutay, J.-C., Siddall, M. (2011) Modelling Nd-isotopes with a coarse resolution ocean circulation model: Sensitivities to model parameters and source/sink distributions. *Geochim. Cosmochim. Acta* **75**, 5927-5950.
- Resing, J. A., Sedwick, P. N., German, C. R., Jenkins, W. J., Moffett, J. W., Sohst, B. M., Tagliabue, A. (2015) Basin-scale transport of hydrothermal dissolved metals across the South Pacific Ocean. *Nature* **523**, 200-206.
- Rickli, J., Frank, M., Halliday, A. N. (2009) The hafnium-neodymium isotopic composition of Atlantic seawater. *Earth Planet. Sci. Lett.* **280**, 118-127.
- Rickli, J., Gutjahr, M., Vance, D., Fischer-Goedde, M., Hillenbrand, C. D., Kuhn, G. (2014) Neodymium and hafnium boundary contributions to seawater along the West Antarctic continental margin. *Earth Planet. Sci. Lett.* **394**, 99-110.
- Rousseau, T. C. C., Sonke, J. E., Chmeleff, J., Candaudap, F., Lacan, F., Boaventura, G., Seyler, P., Jeandel, C. (2013) Rare earth element analysis in natural waters by multiple isotope dilution - sector field ICP-MS. *J. Anal. At. Spectrom.* **28** (4), 573-584.
- Rousseau, T. C. C., Sonke, J. E., Chmeleff, J., van Beek, P., Souhaut, M., Boaventura, G., Seyler, P., Jeandel, C. (2015) Rapid neodymium release to marine waters from lithogenic sediments in the Amazon estuary. *Nat. Commun.* **6**, 7592.
- Rowe, G. D., Firing, E., Johnson, G. C. (2000) Pacific equatorial subsurface countercurrent velocity, transport, and potential vorticity. *J. Phys. Oceanogr.* **30**, 1172-1187.
- Ryan, J. P., Ueki, I., Chao, Y., Zhang, H. C., Polito, P. S., Chavez, F. P. (2006) Western Pacific modulation of large phytoplankton blooms in the central and eastern equatorial Pacific. *J. Geophys. Res. Biogeosci.* **111**, G02013.
- Schijf, J., Christenson, E.A., Byrne, R.H. (2015) YREE scavenging in seawater: a new look at an old model. *Mar. Chem.* **177**, 460-471.

- Schlitzer R. (2014) *Ocean Data View*, <http://odv.awi.de>.
- Schnetger, B., Lehnert, C. (2014) Determination of nitrate plus nitrite in small volume marine water samples using vanadium(III)chloride as a reduction agent. *Mar. Chem.* **160**, 91-98.
- Séférian, R., Bopp, L., Gehlen, M., Swingedouw, Mignot, D. J., Guilyardi, E., Servonnat, J., (2014) Multiyear predictability of tropical marine productivity. *Proc. Natl. Acad. Sci.* **111** (32), 11646-11651.
- Semeniuk, D. M, Bundy, R. M., Posacka, A. M., Robert, M., Barbeau, K. A., Maldonado, M. T. (2016) Using ⁶⁷Cu to Study the Biogeochemical Cycling of Copper in the Northeast Subarctic Pacific Ocean. *Front. Mar. Sci.* **3**, 1-19.
- Shabani, M. B., Akagi, T., Masuda, A. (1992) Preconcentration of trace rare-earth elements in seawater by complexation with bis(2-ethylhexyl) hydrogen phosphate and 2-ethylhexyl dihydrogen phosphate adsorbed on a C18 cartridge and determination by inductively coupled plasma mass-spectrometry. *Anal. Chem.* **64**, 737-743.
- Shaw, T. J., Duncan, T., Schnetger, B. (2003) A pre-concentration/matrix reduction method for the analysis of rare earth elements in seawater and groundwaters by isotope dilution ICPMS. *Anal. Chem.* **75**, 3396-3403.
- Shimizu, H., Tachikawa, K., Masuda, A., Nozaki, Y. (1994) Cerium and neodymium isotope ratios and REE patterns in seawater from the North Pacific Ocean. *Geochim. Cosmochim. Acta* **58** (1), 323-333.
- Sholkovitz, E. R., Piepgras, D. J., Jacobsen, S. B. (1989) The pore water chemistry of rare earth elements in Buzzards Bay sediments. *Geochim. Cosmochim. Acta* **53**, 2847-2856.
- Sholkovitz, E. R., Landing, W. M., Lewis, B. L. (1994) Ocean particle chemistry - the fractionation of rare earth elements between suspended particles and seawater. *Geochim. Cosmochim. Acta* **58**, 1567-1579.
- Sholkovitz, E. R., Elderfield, H., Szymczak, R., Casey, K. (1999) Island weathering: river sources of rare earth elements to the Western Pacific Ocean. *Mar. Chem.* **68**, 39-57.
- Siddall, M., Khatiwala, S., van de Flierdt, T., Jones, K., Goldstein, S. L., Hemming, S., Anderson, R. F. (2008) Towards explaining the Nd paradox using reversible scavenging in an ocean general circulation model. *Earth Planet. Sci. Lett.* **274**, 448-461.
- Singh, S. P., Singh, S. K., Goswami, V., Bhushan, R., Rai, V. K. (2012) Spatial distribution of dissolved neodymium and ϵ_{Nd} in the Bay of Bengal: Role of particulate matter and mixing of water masses. *Geochim. Cosmochim. Acta* **94**, 38-56.

- Slemons, L. O., Murray, J. W., Resing, J., Paul, B., Dutrieux, P. (2010) Western Pacific coastal sources of iron, manganese, and aluminum to the Equatorial Undercurrent. *Glob. Biogeochem. Cycles* **24**, GB3024.
- Sloyan, B. M., Rintoul, S. R. (2001) Circulation, renewal, and modification of Antarctic mode and intermediate water. *J. Phys. Oceanogr.* **31**, 1005-1030.
- Stichel, T., Frank, M., Rickli, J., Haley B. A. (2012b) The hafnium and neodymium isotope composition of seawater in the Atlantic sector of the Southern Ocean. *Earth Planet. Sci. Lett.* **317**, 282-294.
- Stichel, T., Pahnke, K., Goldstein, S. L., Hartman, A. E., Scher, H. (2012a) The geochemistry of seawater neodymium isotopes in the TAG hydrothermal plume at the Mid Atlantic Ridge, Abstract OS41A-1690 Presented at 2012 Fall Meeting. AGU, San Francisco, Calif., 3-7 Dec.
- Stichel, T., Hartman, A. E., Duggan, B., Goldstein, S. L., Scher, H., Pahnke, K. (2015) Separating biogeochemical cycling of neodymium from water mass mixing in the Eastern North Atlantic. *Earth Planet. Sci. Lett.* **412**, 245-260.
- Stramma, L., Johnson, G. C., Firing, E., Schmidtko, S. (2010) Eastern Pacific oxygen minimum zones: Supply paths and multidecadal changes. *J. Geophys. Res. Oceans* **115**, C09011.
- Suga, T., Kato, A., Hanawa, K. (2000) North Pacific Tropical Water: its climatology and temporal changes associated with the climate regime shift in the 1970s. *Prog. Oceanogr.* **47**, 223-256.
- Suga, T., Motoki, K., Aoki, Y., Macdonald, A. M. (2004) The North Pacific climatology of winter mixed layer and mode waters. *J. Phys. Oceanogr.* **34**, 3-22.
- Sverdrup, H. U., Johnson, M. W., Fleming, R. H. (1942) *The Oceans: Their Physics, Chemistry, and General Biology*. Prentice Hall, New York.
- Takahashi, Y., Chatellier, X., Hattori, K. H., Kato, K., Fortin, D. (2005) Adsorption of rare earth elements onto bacterial cell walls and its implication for REE sorption onto natural microbial mats. *Chem. Geol.* **219**, 53-67.
- Takahashi, Y., Hirata, T., Shimizu, H., Ozaki, T., Fortin, D. (2007) A rare earth element signature of bacteria in natural waters? *Chem. Geol.* **244**, 569-583.
- Tachikawa, K., Athias, V., Jeandel, C. (2003) Neodymium budget in the modern ocean and paleo-oceanographic implications. *J. Geophys. Res. Oceans* **108**, 3254.

- Talley, L. D. (1993) Distribution and formation of North Pacific Intermediate Water. *J. Phys. Oceanogr.* **23**, 517-537.
- Talley, L. D. (1999) *Some aspects of ocean heat transport by the shallow, intermediate and deep overturning circulations*. In: Mechanisms of Global Climate Change at Millennial Time Scales (eds. Clark, U., Webb, S., Keigwin, D.). Geophys. Monogr. Ser. Vol. 112, AGU, Washington D. C., pp. 1-22.
- Talley, L. D. (2008) Freshwater transport estimates and the global overturning circulation: Shallow, deep and throughflow components. *Prog. Oceanogr.* **78**, 257-303.
- Talley, L. D., Pickard, G. E., Emery, W. J., Swift, J. H. (2011) *Descriptive Physical Oceanography: An Introduction*. Elsevier, Burlington, MA.
- Tanaka, M., Shimizu, H., Masuda, A. (1990) Features of the heavy rare earth elements in seawater. *Geochem. J.* **24**, 39-46.
- Tanaka, T., Togashi, S., Kamioka, H., Amakawa, H., Kagami, H., Hamamoto, T., Yuhara, M., Orihashi, Y., Yoneda, S., Shimizu, H., Kunimaru, T., Takahashi, K., Yanagi, T., Nakano, T., Fujimaki, H., Shinjo, R., Asahara, Y., Tanimizu, M., Dragusanu, C. (2000) JNdi-1: a neodymium isotopic reference in consistency with LaJolla neodymium. *Chem. Geol.* **168**, 279-281.
- Taylor, S. R., McLennan, S. M. (1985) *The Continental Crust, Its Composition and Evolution: An Examination of the Geochemical Record Preserved in Sedimentary Rocks*. Blackwell, Oxford.
- Tian, R. C., Hu, F. X., Martin, J. M. (1993) Summer nutrient fronts in the Changjiang (Yantze River) estuary. *Estuar. Coast. Shelf Sci.* **37**, 27-41.
- Tomczak, M., Large, D. G. B. (1989) Optimum multiparameter analysis of mixing in the thermocline of the eastern Indian Ocean. *J. Geophys. Res. Oceans* **94**, 16141-16149.
- Tomczak, M. G., Godfrey J. S. (1994) *Regional Oceanography: An Introduction*. Pergamon, Oxford.
- Tomczak, M. G., Godfrey, J. S. (2003) *Regional Oceanography: An Introduction*. 2nd improved edition. Daya Publishing House, Delhi.
- Tsuchiya, M. (1981) The origin of the Pacific equatorial 13°C water. *J. Phys. Oceanogr.* **11**, 794-812.
- Tsuchiya, M., Lukas, R., Fine, R. A., Firing, E., Lindstrom, E. (1989) Source waters of the Pacific Equatorial Undercurrent. *Prog. Oceanogr.* **23**, 101-147.

- Tsuchiya, M. (1991) Flow path of the Antarctic Intermediate Water in the western equatorial South-Pacific Ocean. *Deep-Sea Res. Part A* **38**, S273-S279.
- van de Flierdt, T., Pahnke, K., Amakawa, H., Andersson, P., Basak, C., Coles, B., Colin, C., Crocket, K., Frank, M., Frank, N., Goldstein, S. L., Goswami, V., Haley, B. A., Hathorne, E. C., Hemming, S. R., Henderson, G. M., Jeandel, C., Jones, K., Kreissig, K., Lacan, F., Lambelet, M., Martin, E. E., Newkirk, D. R., Obata, H., Pena L., Piotrowski, A. M., Pradoux, C., Scher, H. D., Schöberg, H., Singh, S. K., Stichel, T., Tazoe, H., Vance, D., Yang, J. (2012) GEOTRACES intercalibration of neodymium isotopes and rare earth element concentrations in seawater and suspended particles. Part 1: reproducibility of results for the international intercomparison. *Limnol. Oceanogr. Methods* **10**, 234-251.
- Vance, D., Thirlwall, M. (2002) An assessment of mass discrimination in MC-ICPMS using Nd isotopes. *Chem. Geol.* **185**, 227-240.
- Vance, D., Scrivner, A. E., Beney, P., Staubwasser, M., Henderson, G. M., Slowey, N. C. (2004) The use of foraminifera as a record of the past neodymium isotope composition of seawater. *Paleoceanography* **19**, PA2009.
- Wang, Z.-L., Yamada, M. (2007) Geochemistry of dissolved rare earth elements in the Equatorial Pacific Ocean. *Environ. Geol.* **52** (4), 779-787.
- Whitworth, T., Orsi, A. H., Kim, S.-J., Nowlin, W. D. (1998) *Water masses and mixing near the antarctic slope front*. In: *Ocean, Ice and Atmosphere: Interactions at the Antarctic Continental Margin* (eds. Jacobs, S. S., Weiss, R. F.). Antarctic Research Ser. Vol. 75, AGU, Washington D. C., pp. 1-27.
- Wu, Q., Colin, C., Liu, Z., Douville, E., Dubois-Dauphin, Q., Frank, N. (2015) New insights into hydrological exchange between the South China Sea and the Western Pacific Ocean based on the Nd isotopic composition of seawater. *Deep-Sea Res. II* **122**, 25-40.
- Wyrtki, K., Kilonsky, B. (1984) Mean water and current structure during the Hawaii-to-Tahiti Shuttle Experiment. *J. Phys. Oceanogr.* **14**, 242-254.
- Yang, J., Haley, B. (2016) The profile of the rare earth elements in the Canada Basin, Arctic Ocean. *Geochem. Geophys. Geosy.* **17**, 3241-3253.
- Yasuda, I., Okuda, K., Shimizu, Y. (1996) Distribution and modification of north Pacific intermediate water in the Kuroshio-Oyashio interfrontal zone. *J. Phys. Oceanogr.* **26**, 448-465.
- Yasuda, I. (2004) North Pacific intermediate water: Progress in SAGE (SubArctic Gyre Experiment) and related projects. *J. Oceanogr.* **60**, 385-395.

- You, Y. Z., Suginoara, N., Fukasawa, M., Yasuda, I., Kaneko, I., Yoritaka, H., Kawamiya, M. (2000) Roles of the Okhotsk Sea and Gulf of Alaska in forming the North Pacific Intermediate Water. *J. Geophys. Res. Oceans* **105**, 3253-3280.
- You, Y. Z., Suginoara, N., Fukasawa, M., Yoritaka, H., Mizuno, K., Kashino, Y., Hartoyo, D. (2003) Transport of North Pacific Intermediate Water across Japanese WOCE sections. *J. Geophys. Res. Oceans* **108**, 3196.
- Zenk, W., Siedler, G., Ishida, A., Holfort, E., Kashino, Y., Kuroda, Y., Miyama, T., Muller, T. J. (2005) Pathways and variability of the Antarctic Intermediate Water in the western equatorial Pacific Ocean. *Prog. Oceanogr.* **67**, 245-281.
- Zhang, J., Nozaki, Y. (1996) Rare earth elements and yttrium in seawater: ICP-MS determinations in the East Caroline, Coral Sea, and South Fiji basins of the western South Pacific Ocean. *Geochim. Cosmochim. Acta* **60**, 4631-4644.
- Zhang, J., Nozaki, Y. (1998) Behavior of rare earth elements in seawater at the ocean margin: A study along the slopes of Sagami and Nankai Troughs near Japan. *Geochim. Cosmochim. Acta* **62**, 1307-1317.
- Zhang, Y., Lacan, F., Jeandel, C. (2008) Dissolved rare earth elements tracing lithogenic inputs over the Kerguelen Plateau (Southern Ocean). *Deep-Sea Res. II* **55**, 638-652.
- Zheng, X. Y., Yang, J. J., Henderson, G. M. (2015) A robust procedure for high-precision determination of rare earth element concentrations in seawater. *Geostand. Geoanal. Res.* **39** (3), 277-292.
- Zheng, X. Y., Plancherel, Y., Saito, M. A., Scott, P. M., Henderson, G. M. (2016) Rare earth elements (REEs) in the tropical South Atlantic and quantitative deconvolution of their non-conservative behavior. *Geochim. Cosmochim. Acta* **177**, 217-237.
- Zimmermann, B., Porcelli, D., Frank, M., Rickli, J., Lee, D.-C., Halliday, A. N. (2009) The hafnium isotope composition of Pacific Ocean water. *Geochim. Cosmochim. Acta* **73**, 91-101.

7. Data handling

Data are submitted to the online database Pangaea (www.pangaea.de) and are password protected until publication of the manuscripts:

Chapter 2: data will be available for download under doi:10.1594/PANGAEA.869418

Chapter 3: data will be available for download under doi:10.1594/PANGAEA.871176

In addition, data of chapters 2 and 3 (GEOTRACES Process Study GPpr04, cruise SO223T) will be published in the GEOTRACES Intermediate Data Product 2017 (IDP2017) and will be available under the GEOTRACES International Data Assembly Centre (GDAC) (<http://www.bodc.ac.uk/geotraces/>).

Acknowledgements

At first, I thank Dr. Katharina Pahnke for giving me the great opportunity to work on this research project in the Max Planck Research Group for Marine Isotope Geochemistry, and for the kind and excellent supervision. Thank you for giving me the chance to participate on two awesome research cruises, to attend international conferences, and to work with international scientists.

I further thank Prof. Dr. Thorsten Dittmar for reviewing this thesis and Prof. Dr. Hans-Jürgen Brumsack for agreeing to be part of my doctorate committee.

Thanks to Dr. Bernhard Schnetger and Dr. Philipp Böning for their technical assistance and helpful discussions on setting up the REE method on the ICP-MS. Prof. Dr. Gideon Henderson is acknowledged for providing the REE Coral Sea standard.

Many thanks for the good collaboration and effort of all my co-authors who participated in the international intercomparison study.

I also thank all the current and former members of the Max Planck Research Group for Marine Isotope Geochemistry for their help in the lab, the great working atmosphere, and many helpful discussions. Susanne Wendeling and Elke Hoxka are acknowledged for helping me with administrative work.

Thanks as well to the members of the Microbiogeochemistry Group, especially to Eleonore Gründken and Carola Lehnert for their help in the lab.

Further, I thank the scientific parties, captains and crews of R/V *Sonne* cruise SO223T and R/V *L'Atalante* cruise CASSIOPEE. In particular, I thank the chief scientists Dr. Mahyar Mohtadi (cruise SO223T) and Prof. Dr. Frederic Marin (cruise CASSIOPEE) for their support. I also thank Prof. Dr. Catherine Jeandel, Prof. Dr. Frederic Marin, and Dr. Sophie Cravatte for giving me the chance to participate on the CASSIOPEE cruise, and Catherine Pradoux for the good collaboration concerning the packing for this cruise.

Finally, I thank my family and Thomas for their enormous support, understanding, and interest in my work.

Curriculum vitae

Name: Melanie K. Behrens
Date of birth: Dec. 03, 1985
Place of birth: Lahr, Germany

Education

Since 09/2012 PhD student in the Max Planck Research Group for Marine Isotope Geochemistry at the Institute for Chemistry and Biology of the Marine Environment (ICBM), Carl von Ossietzky University Oldenburg

2011 Diploma in Mineralogy, Rheinische Friedrich-Wilhelms University Bonn

2007 Pre-diploma in Geosciences, Eberhard Karls University Tübingen

Publications

Behrens, M.K., Muratli, J., Pradoux, C., Wu, Y., Böning, P., Brumsack, H.-J., Goldstein, S.L., Haley, B., Jeandel, C., Paffrath, R., Pena, L.D., Schnetger, B., Pahnke, K. (2016). Rapid and precise analysis of rare earth elements in small volumes of seawater - method and intercomparison. *Marine Chemistry*, 186, 110-120.

Luguet, A., **Behrens, M.**, Pearson, D.G., König, S., Herwartz, D. (2015). Significance of the whole rock Re-Os ages in cryptically and modally metasomatised cratonic peridotites: Constraints from HSE-Se-Te systematics. *Geochimica et Cosmochimica Acta* 164, 441-463.

Presentations

2016

Behrens, M.K., Pahnke, K., Schnetger, B., Brumsack, H.-J. (2016). A detailed picture of trace element input and equatorial transport to the iron-limited tropical East Pacific from Nd isotopes and REE in the West Pacific. Dissertations Symposium in Chemical Oceanography, DISCO XXV, October 9-14, Honolulu, Hawaii, USA (invited oral presentation)

Behrens, M.K., Pahnke, K., Schnetger, B., Brumsack, H.-J. (2016). Rare earth element cycling in the West Pacific - method and application. Goldschmidt Conference, June 26-July 1, Yokohama, Japan (oral presentation)

2015

Behrens, M.K., Pahnke, K., Schnetger, B., Brumsack, H.-J. (2015). Trace element inputs to the upper West Pacific from Nd isotopes and rare earth elements. AGU Fall Meeting, December 14-18, San Francisco, USA (poster, won Outstanding Student Paper Award)

Behrens, M., Pahnke, K. (2015). Neodym-Isotope und Seltene Erden-Verteilungen im Westpazifik. Status seminar on ocean research with R/V *Sonne*, February 12-13, University of Bremen, Germany (invited oral presentation)

2014

Behrens, M., Pahnke, K. (2014). Neodymium isotope distribution in the West Pacific between South Korea and Fiji. Ocean Sciences Meeting, February 23-28, Honolulu, Hawaii, USA (poster)

2013

Pahnke, K., **Behrens, M.**, Goldstein, S.L., Hemming, S.R. (2013). Holocene and last glacial maximum ϵ_{Nd} distribution in the Atlantic. 11th International Conference on Paleoceanography, September 1-6, Barcelona-Sitges, Spain (poster)

2011

Luguet, A., **Behrens, M.**, Herwartz, D., Pearson, D.G. (2011). Re-Os and Lu-Hf dating in Letlhakane peridotite xenoliths (Botswana). Goldschmidt Conference, August 14-20, Prague, Czech Republic (oral presentation)

2010

Behrens, M., Luguet, A., Herwartz, D., Pearson, D.G. (2010). Lu-Hf and Re-Os isotopic systematics in highly metasomatised mantle: A case study in Letlhakane peridotite xenoliths, Botswana. - 88th DMG (Deutsche Mineralogische Gesellschaft / German Mineralogical Society) meeting, September 19-22, Münster, Germany (poster)

Cruises

2015 CASSIOPEE Pacific cruise (R/V *L'Atalante*), New Caledonia

2012 TransGeoBioOc Pacific cruise (R/V *Sonne*), South Korea-Fiji

Erklärung

Hiermit versichere ich, dass ich die Arbeit unter Befolgung der Leitlinien guter wissenschaftlicher Praxis der Carl von Ossietzky Universität selbstständig verfasst habe und nur die angegebenen Hilfsmittel benutzt habe. Zusätzlich erkläre ich, dass diese Dissertation weder in ihrer Gesamtheit noch in Teilen einer anderen wissenschaftlichen Hochschule zur Begutachtung in einem Promotionsverfahren vorliegt oder vorgelegen hat. Teile dieser Arbeit sind wie angegeben veröffentlicht oder in Vorbereitung für die Veröffentlichung. Zusätzlich erkläre ich, dass im Zusammenhang mit dem Promotionsvorhaben keine kommerziellen Vermittlungs- oder Beratungsdienste in Anspruch genommen worden sind.

Oldenburg, im Februar 2017

Melanie K. Behrens